

DEPARTMENT OF BIOMEDICAL ENGINEERING
UNIVERSITY OF STRATHCLYDE, GLASGOW, UK

Metal Microneedle Arrays for Transdermal Drug Delivery

MOHAMMAD REZA SALAMATI

A thesis presented in fulfilment of the requirements for the degree of

Doctor of Engineering

September 2018

Copyright Statement

'This thesis is the result of the author's original research. It has been composed by the author and has not been previously submitted for examination which has led to the award of a degree'.

'The copyright of this thesis belongs to the author under the terms of the United Kingdom Copyright Acts as qualified by University of Strathclyde Regulation 3.50. Due acknowledgement must always be made of the use of any material contained in, or derived from, this thesis.'

Signed:

Date:

Dedication

*This thesis is dedicated to my inspiring parents and brothers
(Ali, Lida, Alireza and Hamid)
without whom none of my successes would have been possible*

Acknowledgement

This thesis owes its existence to the generous assistance, guidance and support of a great number of individuals.

Sincere gratitude, in particular, is owed to the director of studies Dr Andrzej Rosochowski, to whom the writer is deeply indebted for his patient guidance, open door policy and invaluable ideas, criticisms and comments, throughout the course of this investigation, which provided much of the inspiration behind this work.

The writer is deeply grateful to all those who at various stages of the study contributed greatly towards technical aspects and overall accomplishment of the objectives of this study: Mr Jawad Qarni for sharing his technical knowledge throughout the course of this research. Mr Bob Smith and Mr Graeme Scott of Pascoe Engineering Ltd for fabricating various components for the experimental equipment used in this project. Samuel Bigot of Cardiff University for providing technical expertise in Micro manufacturing and Dr Agostino Murata for his expert advice on ultrasonic assisted forming.

Appreciation is also due to the numerous other people: Dr Richard Black, Dr Giribaskar Sivaswamy, Dr Malgorzata Rosochowska, Sonia Boczkal, and all the staff at the Biomedical Engineering and DMEM departments at University of Strathclyde for their support and assistance in this research project.

The writer wishes to express his gratitude to Engineering and Physical Sciences Research Council (EPSRC) who generously provided funding that facilitated conditions under which the commencement and accomplishment of this study was made possible.

The writer is most appreciative for the patience and understanding of, and the sacrifices made by, his family (parents: Ali and Lida, brothers: Alireza, and Hamidreza) in furtherance of this study.

Thanks are also given to the writer's grandparents: Qorbanali and Homa, Yahya and Zahra and other relatives, whose names would not be possible to list here, whom provided constant encouragement and moral support from afar.

Finally, a word of thanks to my friends: Russell Black, Ajitpal Dhillon, Amir Daneshvar and Arthur Yip, Barry Hunter, Danial Kahani, David Cunningham, Dino Bertolaccini, Drew Irvine, Duncan Lindsay, Kowk Bon Tang, Ramin Mofidi, Saber Khayatzaeh, Saeed Tamimi, for their understanding and moral support during the course of the studies.

Abstract

Microneedles have now been produced from ceramics, metals and polymers. The general properties of ceramics suggest the needles would be resistant to compression but fragile under shear forces. Polymers have a low Young's modulus, therefore, could deform before puncturing the skin. Metals have been used in hypodermic needles for a long time. They are strong enough to break the skin barrier but mass producing micro components from metal is often very expensive, therefore, using conventional manufacturing methods, it might not be the best material of choice for a product that requires to be made in the billions annually. For metals to be considered as a viable material for microneedles, it is necessary to propose a new manufacturing method that is suitable for low value high volume produced micro component.

Ultrafine-grain Al1050 has been created using Incremental equal channel angular pressing. The finer grain structure should allow for smaller detail to be produced as well as being stronger. Experimentally it has been shown that allying ultrasonic to the backward extrusion process can reduce the forming force by about 20 percent while increasing the height of the microneedles by 80 percent. Using UFG material results in greater needle height uniformity across the billet. It was also found that applying gold to the surface of the billet improves the formability of the needles.

Table of Contents

Copyright Statement	ii
Dedication	iii
Acknowledgement	iv
Abstract	v
Table of Contents	vi
List of Figures	xi
List of Tables	xviii
1. INTRODUCTION	1
1.1. BACKGROUND	1
1.2. THESIS STRUCTURE	2
2. LITERATURE REVIEW	4
2.1. INTRODUCTION	4
2.2. SKIN: FUNCTION AND ANATOMY	4
2.2.1. Hypodermis	6
2.2.2. Dermis	6
2.2.3. Epidermis	7
2.2.3.1. Stratum Basale	7
2.2.3.2. Stratum Spinosum.....	8
2.2.3.3. Stratum Granulosum.....	8
2.2.3.4. Stratum Lucidum.....	8
2.2.3.5. Stratum Corneum.....	9
2.3. DRUG ABSORPTION THROUGH THE SKIN	10
2.4. CURRENT DRUG DELIVERY METHODS	12
2.4.1. Oral Route	12
2.4.2. Hypodermic Needles Route	12
2.4.3. Transdermal Route	13
2.5. OVERCOMING THE NATURAL BIOLOGICAL BARRIER.....	14

2.5.1.	Transdermal Drug Delivery	14
2.5.2.	Formulation-Based Methods	15
2.5.2.1.	Prodrugs	15
2.5.2.2.	Excipients	16
2.5.2.3.	Super Saturation	16
2.5.2.4.	Chemical Penetration Enhancers	17
2.5.3.	Device Based Methods.....	18
2.5.3.1.	Ultrasonic Devices.....	19
2.5.3.2.	Thermal and Optical Devices	20
2.5.3.3.	Electrical Devices.....	21
2.6.	MICRONEEDLES	23
2.6.1.	Patient acceptance and safety	25
2.6.2.	Advantages of Microneedles	27
2.6.3.	Microneedle Types.....	28
2.6.3.1.	Solid Microneedles.....	30
2.6.3.2.	Drug-coated Microneedles	31
2.6.3.3.	Biodegradable Microneedles	32
2.6.3.4.	Hollow Microneedles	33
2.6.4.	Materials and Manufacturing Methods	35
2.6.5.	Microforming	37
2.6.6.	The Microforming System	38
2.6.6.1.	Size Effect.....	39
2.6.7.	Lubrication	43
2.6.8.	Vibration-Assisted Microextrusion	44
2.6.8.1.	Ultrasonic – Background	48
2.6.8.2.	Methods of generating ultrasonic vibrations	48
2.6.8.3.	Magnetostrictive Transducer	49
2.6.8.4.	Piezoelectric Transducer	49
2.6.8.5.	Transducer Selection.....	50
2.6.8.6.	Ultrasonic Assisted Metal Forming	51
2.6.8.7.	Acoustoplastic Effect.....	52
2.6.8.8.	Ultrasonic Oscillations Force Reduction	53
2.7.	GRAIN REFINEMENT	55
2.7.1.	Severe Plastic Deformation Processes:	55
2.7.2.	Equal Channel Angular pressing (ECAP) or Extrusion (ECAE)	57
2.7.3.	Incremental ECAP process.....	60
2.8.	SUMMARY	61
3.	MATERIALS AND METHODS	62
3.1.	ALUMINIUM	62

3.1.1.	Classification of Aluminium Alloys.....	62
3.2.	ALUMINIUM 1050	63
3.2.1.	Aluminium biocompatibility	65
3.2.2.	Choice of Material.....	65
3.3.	SURFACE ROUGHNESS MEASUREMENT	66
3.3.1.	Stylus Instrument	66
3.3.2.	Focus Variation Instrument.....	67
3.4.	HARDNESS TESTING	70
3.4.1.	Vickers Micro Hardness Testing.....	70
3.4.2.	Sample Mounting.....	72
3.5.	FRICTION.....	74
3.5.1.	Grease and Oil.....	75
3.5.2.	Molybdenum Disulphide.....	76
3.5.3.	Graphite.....	78
3.6.	CONVERSION COATING	79
3.7.	GOLD SPUTTER DEPOSITION	81
3.8.	TENSILE TESTING	83
3.9.	CONFIGURATIONS OF IECAP RIGS	85
3.9.1.	IECAP COMPONENTS	86
3.10.	Backward Extrusion Rig.....	91
3.10.1.	Backward Extrusion	91
3.11.	ULTRASONIC EQUIPMENT.....	104
3.11.1.	Ultrasonic Generator and Control Circuit	104
3.11.2.	Ultrasonic Transducer	105
3.11.3.	Ultrasonic Booster.....	106
3.11.4.	Sonotrode	106
3.12.	PUNCH AND DIE FABRICATION	106
3.12.1.	Punch Material	107
3.12.2.	Single Pin Punch Fabrication	107
3.12.3.	Microneedle cavity punch fabrication.....	108
3.12.4.	Die Fabrication.....	109
3.13.	SUMMARY	110

4.	RESULTS AND DISCUSSION.....	112
4.1.	INTRODUCTION.....	112
4.2.	PART A: EFFECT OF CHANNEL ANGLE ON THE MATERIAL FLOW, HARDNESS DISTRIBUTION AND PROCESS FORCES DURING INCREMENTAL ECAP OF AL-1050 BILLETS.....	115
4.2.1.	IECAP Process.....	115
4.2.2.	Experimental Setup.....	117
4.2.3.	First Pass Experiments.....	118
4.2.4.	Finite Element Simulation.....	122
4.2.5.	First Pass Channel and Pusher Configuration Results.....	123
4.2.6.	Material Flow.....	124
4.2.7.	Strain Distribution.....	125
4.2.8.	Thermal Effects.....	126
4.2.9.	Hardness Measurement.....	127
4.2.10.	Microstructure.....	129
4.2.11.	Conclusion for the First Pass Various Geometry.....	131
4.3.	PART B: MULTI PASS EXPERIMENTS.....	133
4.3.1.	Effects of Load during Multi Step IECAP.....	134
4.3.2.	Hardness Evolution during Multi Pass IECAP.....	137
4.3.3.	Tensile Testing.....	142
4.3.4.	Microstructure analysis.....	145
4.3.5.	Microstructure Grain Size Refinement.....	146
4.3.6.	Conclusions.....	148
4.4.	PART C: METAL FORMING EXPERIMENTS.....	152
4.4.1.	Billet Surface Conditions.....	152
4.4.2.	Single Pin Punch.....	154
4.4.3.	Single Pin Experimental Results.....	156
4.4.4.	Single Pin Coarse Grain Experiments.....	158
4.4.5.	Single Pin Ultra Fine Grain (UFG) Experiments.....	161
4.4.6.	Ultrasonic Assisted Single Pin Forming.....	163
4.4.7.	Micro punch.....	171
4.4.8.	Micro forming experiments.....	172
4.4.8.1.	Grease lubricant.....	173
4.4.8.2.	Coarse Grain Billet Surface Coating Conditions.....	174
4.4.8.3.	Ultra-Fine Grain Billet Surface Coating Conditions.....	175

4.4.9.	Comparing the Gold Coating Surfaces against the Different Grain Size Billets	176
4.4.9.1.	Application of Ultrasonic Oscillation on CG Billets	178
4.4.9.2.	Application of Ultrasonic Oscillation on UFG Billets	179
4.4.10.	Role of Ultrasonic assisted forming on needle height when billets with grain sizes are used.....	179
4.4.10.1.	Needle Height	180
4.4.10.2.	Forming Force	182
4.4.11.	Conclusion.....	182
4.5.	PART D: USING FEA IN ASSESSING BACKWARD EXTRUSION OF MULTIPLE MICRO-PINS	184
4.5.1.	FE Model.....	184
4.5.2.	Results	187
4.5.2.1.	PIN Geometry.....	187
4.5.2.2.	Friction	188
4.5.2.3.	PIN Density and Central PIN Removal.....	188
4.5.2.4.	Grain Size	190
4.5.2.5.	Pin Height Uniformity	191
4.5.3.	Conclusions	193
5.	FINAL CONCLUSIONS AND RECOMMENDATIONS FOR FUTURE WORKS	196
5.1.	CONCLUSIONS	196
5.2.	RECOMMENDATIONS FOR FUTURE WORKS.....	198
	APPENDIX A:	199
	REFERENCES.....	201

List of Figures

Figure 2.1:	Human skin cross-section diagram showing the three main layers that build up the skin. Adapted from: http://owh.adam.com/pages/guide/reftext/html/skin_sys_fin.html.....	5
Figure 2.2:	Yearly increase in microneedle related publications. Adapted from Kim et al. 2012.	25
Figure 2.3:	Section A illustrates four main types of microneedles: solid, coated, dissolving and hollow microneedles. Section B illustrates the drug delivery methods: Poke and patch, Coat and poke, poke and release, poke and flow. Kim et al. 2012.	29
Figure 2.4:	Solid microneedles have been made from a variety of materials Adopted from Kim et al. 2012.....	31
Figure 2.5:	Coated microneedles that have been presented in the literature. Adopted from Kim et al. 2012.....	32
Figure 2.6:	Biodegradable microneedles presented in the literature. Adopted from Kim et al. 2012.	33
Figure 2.7:	Hollow microneedles presented in the literature. Adopted from Kim Y., 2012.	34
Figure 2.8:	Factors associated with microforming. (Engel & Eckstein 2002).	39
Figure 2.9:	Size effect related issues in micro forming process (Fu & Chan 2013).....	40
Figure 2.10:	The proportional number of the surface grains to the internal grains. Deng et al 2011.....	41
Figure 2.11:	Schematic diagram showing the evolution of surface topography during forming under liquid lubrication conditions. Deng et al. 2011.....	44
Figure 2.12:	Schematic diagram of A- ultrasonic forward-rod extrusion, B-ultrasonic double cup backward extrusion, C- combination of the ultrasonic forward-rod-backward-cup extrusion process and forward-rod and backward-cup processes (Bunget & Ngaile 2011).	47
Figure 2.13:	Common frequency ranges for various ultrasonic processes.....	48
Figure 2.14:	Blaha and Langenecker observed the first Acousto-Plastic Effect. Blaha and Langenecker, 1955.....	51
Figure 2.15:	The acoustoplastic effect reported by Kirchner et al, 1984. Adapted from Kirchner et al, 1984.....	52
Figure 2.16:	Illustration comparing large grain and small grain for filling a small “V” notch. Adapted from Saotome et al. 1998	55
Figure 2.17:	Schematic diagram of an ECAE operation – die, tool, billet and workpiece. Adapter from Sklenicka et al. 2012.	57
Figure 2.18:	Left: Deformation behaviour of a cubic element during a single pass in ECAE Right: Shearing behaviour of a cubic element with the increase in number of passes during different processing routes of ECAE. Left: (Furukawa et al. 2001), Right: (Furukawa et al. 1998).	59

Figure 2.19:	<i>Schematic showing the Dies and punch in the Incremental ECAP process. A=Die, B=Pusher and C=Punch. Adopted from Rosochowski and Olejnik 2011.</i>	60
Figure 3.1:	<i>Equilibrium Microstructure of the Aluminium 1050 Alloy.....</i>	65
Figure 3.2:	<i>Alicona Infinite Focus and the schematic diagram of a typical focus variation instrument: (1) CCD sensor, (2) lenses, (3) white light source, (4) semi-transparent mirror, (5) objective lens with limited depth of field, (6) sample, (7) vertical movement with driving unit, (8) contrast curve calculated from the local window, (9) light rays from the white light source, (10) optional analyser, (11) optional polariser and (12) optional ring light. Adapted from Leach 2011.</i>	69
Figure 3.3:	<i>The complete Zwick ZHVμ micro hardness tester shown on the right. On the left a schematic of the Vickers hardness testing method. Adapted from Zwick ZHVμ micro hardness tester user manual.....</i>	72
Figure 3.4:	<i>Castable Mounting Equipment: (1) Vacuum pump, (2) air filtration chamber, (3) vacuum chamber, (4) vacuum pressure indicator, (5) motorised base for rotating specimens, (6) EpoThin 2 resin and hardener mixed and ready for pouring, (7) casting moulds.....</i>	74
Figure 3.5:	<i>Crystal structure of MoS₂. Each sulphur atom is equidistant from three molybdenum atoms. Each molybdenum atom is also equidistant from six sulphur atoms. Each molybdenum atom is at the centre of right angled prism that has sulphur atoms in each of its six corners. Adapted from Lansdown, 1999.</i>	77
Figure 3.6:	<i>The flat structure of graphite is clearly visible under a scanning electron microscope. Crystal structure of graphite. Each carbon atom is bonded to three other surrounding carbon atoms. The flat rings of carbon atoms are bonded into the hexagonal structures. The layers are then held together using weak Van der Waals bonds. Adopted from Eagle Graphite website (www.eaglegraphite.com/portfolio-posts/graphite-flakes-sem-showing-some-sideways).....</i>	79
Figure 3.7:	<i>Steps required for calcium aluminate conversion coating. A schematic showing conversion coating layer and the lubrication layers.</i>	81
Figure 3.8:	<i>Agar scientific MB7341 auto sputter coater and the sputtering process ..</i>	83
Figure 3.9:	<i>True stress Vs. true strain curve showing the difference between the behaviour of pure aluminium and pure copper. Djavanroodi et al, 2012.</i>	85
Figure 3.10:	<i>Zwick Roell Z150 and a drawing of the micro tensile test samples.....</i>	85
Figure 3.11:	<i>The 1000kN hydraulic press setup used to IECAP process pairs of billets. A – shows the press setup in the laboratory. B – a schematic of the various elements of the IECAP press. HA= Hydraulic actuator, SV= Servo valve, LVDT= Linear variable differential transformer, NI= National Instruments module, MC= Motor controller, M= Electric motor, SJ= Screw jack, LC= Load cell, P= Punch, TC= Temperature controller, Die=Die setup, Cubus= Software</i>	88
Figure 3.12:	<i>Other hardware used for the IECAP rig. A- the black hydraulic storage tanks and pump, the blue chiller. B- rig's electrical components control</i>	

	<i>and safety box. C- 4 National instruments modules used to control and record rig movement. D- manual control hand controller.</i>	<i>89</i>
Figure 3.13:	<i>IECAP custom virtual instrument front panel.....</i>	<i>91</i>
Figure 3.14:	<i>An illustration of the five steps in the backward extrusion process and the four main elements: punch, die, billet, ejection pin.....</i>	<i>92</i>
Figure 3.15:	<i>Available equipment. A- 250kN hydraulic press, B- some components that were salvaged and reused from a previous setup upper and lower shoes are visible as well as the guide pins and the ball bearings, C- the metal C section and extenders that could be used to transfer the hydraulic actuator displacement and force into the top shoe.</i>	<i>94</i>
Figure 3.16:	<i>A: CAD model of the microforming backward extrusion rig. The yellow component is the target for the eddy current non-contact displacement sensor and the red component is the sensor holder. The red circles indicating the bolt and block components used during the setup phase of the tooling. B: Some of the main sections of the rig. Blue arrows- extenders, Yellow arrows- ultrasonic transducer and amplitude booster, purple arrows top shoe and other top half of the rig components, green arrow- bottom shoe and rig bottom half components.</i>	<i>96</i>
Figure 3.17:	<i>Nylon rings used in the top and bottom of the rig to isolate the vibrating components of the rig from the rest of the rig. The ejector pin can also be seen in the centre of the bottom half of the rig.</i>	<i>97</i>
Figure 3. 18:	<i>1- Top shoe, 2- top shoe coupling, 3- Ultrasonic sonotrode, 4- Sonotrode to top shoe coupling coupling. (B) 5- Punch holder, 6- Punch, 7- Target disk. (C) 8- Bottom shoe, 9- Bottom shoe coupling, 10- Bottom die holder to bottom shoe coupling coupling, 11- Bottom die holder (D) 12- Billet, 13- Die, 14- Die Disk, 15- Ejector pin. Red arrows also showing the diameter of the punch 4.95mm and the diameter of the die 5mm</i>	<i>98</i>
Figure 3.19:	<i>A - The components of the rig before assembly and testing. B - Fully assembled rig inside the 250kN hydraulic press.</i>	<i>100</i>
Figure 3. 20	<i>Micro Epsilon UI eddy current non-contact sensor specifications.....</i>	<i>101</i>
Figure 3.21:	<i>The custom made virtual instrument used to capture the data from the eddy current sensor, actuator LVDT, and load cell. A- the LabVIEW system diagram for the virtual instrument. B- the front panel of the custom virtual instrument.....</i>	<i>103</i>
Figure 3.22	<i>A) the custom made ultrasonic control is shown. A dial for controlling the amplitude is located in the middle of the control facing. Seven segment displays are used to display the frequency of the oscillation. B) the internal electronics of the control box after repairs had been carried out.</i>	<i>105</i>
Figure 3.23:	<i>The fully assembled ultrasonic generator consisting of transducer, booster, and sonotrode that was used for the ultrasonic experiments. ...</i>	<i>105</i>
Figure 3.24:	<i>A- the copper electrode used for the sink EDM manufacture of the single pin punch. B- the fully fabricated single pin punch. C- single pin punch sectioned in half so the profile of the cavity can be verified.....</i>	<i>108</i>
Figure 3.25:	<i>A- the sacrificial blank that was used for calibrating the laser in the DMG Mori Lasertech 40. A series of conical holes can be seen on the perimeter</i>	

of the blank. B- the microneedle punch with an array of micro conical cavities. The cavity dimensions are shown. Cavities are 1mm apart..... 109

Figure 4.1:	<i>Schematic of IECAP process (A=Die, B=Pusher and C=Punch) Rosochowski and Olejnik 2011..... 116</i>
Figure 4.2:	<i>Relative movement of punch and pusher tools during the IECAP process. Stage 1 – feed stage. Stage 2 – deformation stage. 117</i>
Figure 4.3:	<i>The punch and split die design for A $\phi=90^\circ$ IECAP die and B $\phi=120^\circ$ IECAP die..... 118</i>
Figure 4.4:	<i>A – the initial microstructure of the Al1050 material using SEM. B – The grain boundaries determined by software to calculate grain size. 119</i>
Figure 4.5:	<i>Pair of billets after cleaning. Represents the shape of the billets after 50% processing with A – $\phi=90^\circ$ and B – $\phi=120^\circ$..... 120</i>
Figure 4.6:	<i>Deformation and feeding force recordings for A – $\phi=90^\circ$ and B – $\phi=120^\circ$. The punch force is shown in red and the pusher force is shown in blue.121</i>
Figure 4.7:	<i>FE analysis model for channel intersection angles of A – $\phi=90^\circ$ and B – $\phi=120^\circ$ IECAP process. The billets are shown in green, the channel in light grey and the pusher and punch are shown in dark grey..... 123</i>
Figure 4.8:	<i>Influence of channel intersection angle ϕ on the material flow A – $\phi=90^\circ$ and B – $\phi=120^\circ$..... 124</i>
Figure 4.9:	<i>Evolution of equivalent plastic strain distribution at 15%, 30%, 50% and 90% processed state for (a) $\phi=90^\circ$ and (b) $\phi=120^\circ$..... 126</i>
Figure 4.10:	<i>Temperature distribution in tools and billet at 25%, 50% and 90% IECAP processed billets A – 90° and B – 120° configuration 127</i>
Figure 4.11	<i>(a)Schematic showing the plane where hardness measurements were made. (b) Hardness maps from regions of the processed billets in inlet and exit channel of incremental ECAP dies having two different die corner angles..... 129</i>
Figure 4.12:	<i>SEM examination of the microstructure of billets during first pass A – $\phi=90^\circ$ and B – $\phi=120^\circ$ IECAP with the corresponding grain boundary that were determined by software to calculate grain size..... 131</i>
Figure 4.13:	<i>The feeding force and deformation force recordings for IECAP passes 1 to 8. 135</i>
Figure 4.14:	<i>Graph showing the peak loads recorded for the punch and pusher during the IECAP of Al1050 from pass 1 to pass 8. 136</i>
Figure 4.15:	<i>Micro hardness measurement along the flow plain for partially processed billets after IECAP passes of $\phi=90^\circ$ at 1, 2, 3, 4, 6, 8 and $\phi=120^\circ$ first pass. 138</i>
Figure 4.16:	<i>Hardening results of billets after passing through the plastic shear zone for passes 1, 2, 3, 4, 6, 8. The green line represents the centre of the billet and the location of the hardness measurements. The blue dot (starting point of hardness results shown in graph), is located 10mm from the centre of the shear zone in the vertical axis and the red dot (ending point of hardness results shown in graph), is located 10mm from the centre of the shear zone in the horizontal axis..... 139</i>

Figure 4.17:	<i>The partial billets were cut into 3 cross sections and hardness of the sections were investigated. The regions of interest from the billets were the input channel, shear zone and the output channel. The cut path of the three sections for the billets are shown in the top schematic.</i>	141
Figure 4.18:	<i>Various stages of IECAPing a pair of Al1050 billets.</i>	142
Figure 4.19:	<i>True stress-true strain curves of samples from billets before and after IECAP process. Specimens were created from pass 0, 1, 2, 3, 4, 6 and 8 billets.....</i>	144
Figure 4.20:	<i>Inverse pole figure maps showing the deformation characteristics of aluminium matrix of Al1050 billets before and after I-ECAP process(a) as received sample, (b) after 1st pass,(c)after 2nd pass and (d)after 4th pass.</i>	146
Figure 4.21:	<i>Bright field TEM micrographs showing the deformation characteristics of aluminium matrix in AA1050 alloy billet subjected I-ECAP process after (a) one pass, (b) two passes, (c) six passes and (d) eight passes. Corresponding Selected area diffraction patterns (SADP) are given as inserts.</i>	147
Figure 4.22:	<i>Billet surface roughness analysis for a variety of condition. A- Surface after wire EDM cutting. B- Surface conversion coating. C- Surface after grinding with P2500 emery paper. D- Surface after sandblasting.....</i>	153
Figure 4.23:	<i>Copper electrode used to produce the single pin punch. A- Electrode surface used for surface roughness quantification. 1 to 5 represent the areas of interest for roughness analysis. B- The copper electrode. C- Close look at the tip of the electrode.....</i>	154
Figure 4.24:	<i>Examination of the inner surface of the punch after sink EDM and spark drill production. A) Sectioned single pin punch counted in polymer. B) Side view of the inner cavity of the punch. C) Bottom view of the conical cavity of the punch. D) Locations of interest for surface roughness measurements.....</i>	156
Figure 4.25:	<i>Graph showing the reading from (top) the eddy current non-contact sensor, (middle) force recorded by the load cell, (bottom) voltage signal captured from the non-contact sensor during an ultrasonic assessed forming trial. Voltage signal shows a 0.1 fluctuation, which represents the 0.01mm amplitude of the punch under excitation.</i>	157
Figure 4.26:	<i>The press force and the pin height were recorded for each pin. A and B show the location of surface roughness measurements for each pin.</i>	158
Figure 4.27:	<i>Effect of the combination of surface conditions and lubrications is examined against the formed pin heights.</i>	159
Figure 4.28:	<i>Effect of the combination of surface conditions and lubrications is examined against the required forming force.....</i>	160
Figure 4.29:	<i>Using UFG to form single pin under a variety of lubrication conditions.</i>	161
Figure 4.30:	<i>Comparison drawn between the effects of the two grain sizes on pin height and press force.</i>	162
Figure 4.31:	<i>The effects of punch displacement speed on the press force and pin height under 2 different billet grain sizes.</i>	163

<i>Figure 4.32:</i>	<i>Effects of ultrasonic assisted backwards extrusion on CG Al1050. Press force and pin height are investigated with respect to lubrication condition.</i>	<i>164</i>
<i>Figure 4.33:</i>	<i>Effects of ultrasonic assisted backwards extrusion on CG Al1050. Press force and pin height are investigated with respect to lubrication condition</i>	<i>165</i>
<i>Figure 4.34:</i>	<i>The effects of punch displacement length while ultrasonic oscillations were induced on the press force and pin height under two different billet grain sizes.</i>	<i>166</i>
<i>Figure 4.35:</i>	<i>The effects of punch displacement speed while ultrasonic oscillations were induced on the press force and pin height under two different billet grain sizes.</i>	<i>167</i>
<i>Figure 4.36:</i>	<i>Comparing press force for pins that were created with different grain sizes and with/without ultrasonic assistance during various lubrication conditions.</i>	<i>168</i>
<i>Figure 4.37:</i>	<i>Comparing pin heights for pins that were created with different grain sizes and with/without ultrasonic assistance during various lubrication conditions.</i>	<i>169</i>
<i>Figure 4.38:</i>	<i>EBSD of a single pin. Pin conditions – CG billet, no ultrasonic oscillations, grease lubrication.</i>	<i>170</i>
<i>Figure 4.39:</i>	<i>Punch with micro conical cavities created by laser ablation. A- the completely fabricated punch. B the surface of the punch.</i>	<i>171</i>
<i>Figure 4.40:</i>	<i>Surface height fluctuation for the micro needle punch.</i>	<i>172</i>
<i>Figure 4.41:</i>	<i>Effect of grain size on surface topography when grease was used as a lubricant to coat the billet subjected to micro-forming: (A) GC and (B) UFG. Note that there is no ultrasonic excitation added to the punch, ...</i>	<i>174</i>
<i>Figure 4.42:</i>	<i>Effect of using CG billets. Coating conditions compared against the needle height distribution.</i>	<i>175</i>
<i>Figure 4.43:</i>	<i>Effect of using UFG billets. Surface conditions compared against the needle height distribution.</i>	<i>176</i>
<i>Figure 4.44:</i>	<i>Microneedle heights achieved when billets were coated in gold. Two grain sizes were investigated and compared.</i>	<i>177</i>
<i>Figure 4.45:</i>	<i>The surface profile of gold coated microneedles on the billet. Two grain sizes compared. A- CG, B-UFG.</i>	<i>177</i>
<i>Figure 4.46:</i>	<i>Ultrasonic assisted backward extrusion of microneedles using CG billets with different surface conditions and lubricants.</i>	<i>178</i>
<i>Figure 4.47:</i>	<i>Ultrasonic assisted backward extrusion of microneedles using UFG billets with different surface conditions.</i>	<i>179</i>
<i>Figure 4.48:</i>	<i>Effect of ultrasonic oscillation assisted forming on needle height of CG and UFG billets.</i>	<i>180</i>
<i>Figure 4.49:</i>	<i>Formed microneedle.</i>	<i>181</i>
<i>Figure 4.50:</i>	<i>Gold coated billet with fully formed microneedles. A- image with mm scale bar. B- scanned surface of the billet.</i>	<i>183</i>

Figure 4.51	<i>Top (Left): Process/tool configuration, Top (right) pin geometry and (Bottom) forming and adaptive meshing.....</i>	185
Figure 4.52:	<i>A-D pins arranged in a square array. E-H pins arranged in a hexagonal array.</i>	186
Figure 4.53:	<i>Effect of the pin angle 90°- A on the extrusion load required to form a scaled-up single CG Al1050 pin friction condition used for simulations friction factor 0.15.</i>	187
Figure 4.54:	<i>The effect of friction conditions on the load required to extrude a square (SQ) array of UFG Al1050 pins with spacing of 0.5mm.</i>	188
Figure 4.55:	<i>Removing the central pin in a 0.5mm spaced square array (case A-B) and 0.5mm spaced hexagonal array (C-D). Backward extruded micro pins on Al1050 billet.</i>	189
Figure 4.56:	<i>The effect of friction conditions on formability of CG Al1050 pins laid out in a hexagonal array without a central pin with a spacing of 0.75mm... </i>	189
Figure 4.57:	<i>Effect of pin density and central pin removal in square (SQ) and hexagonal (HEX) pin arrays on the extrusion load for CG Al1050</i>	190
Figure 4.58:	<i>Comparing the effects of grain size on the forming load for different pin density and layout on Al1050 billet friction condition used for simulations friction factor 0.15</i>	191
Figure 4.59:	<i>Cross-sections through the centre of a billet extruded into a square array of 0.5mm spaced micro pins. A) UFG in frictionless conditions, B) UFG with friction factor = 0.15, C) CG with friction factor = 0.15, D) UFG with friction factor = 0.8, E) UFG with friction factor = 0.15 and central pin removed.</i>	192
Figure 4.60:	<i>UFG material formed into an array of micro pins using lubrication (friction factor = 0.15); process was stopped when the central outer pin reached a height of 0.3mm.</i>	193

List of Tables

<i>Table 3.1:</i>	<i>Chemical Composition of the 1050 Alloy BS EN 573-3: 2009.....</i>	<i>64</i>
<i>Table 3.2:</i>	<i>Typical Mechanical Properties of the 1050 Alloy.....</i>	<i>64</i>
<i>Table 4.1:</i>	<i>Surface roughness after a variety of conditions.</i>	<i>154</i>
<i>Table 4.2:</i>	<i>Roughness measurement along the copper electrode surface.....</i>	<i>155</i>
<i>Table 4.3:</i>	<i>Roughness measurement along the inner surface of the punch.....</i>	<i>155</i>
<i>Table 4.4:</i>	<i>A combination of billet surfaces and lubrications tested. The load, pin height and surface roughness in two locations is presented in this table.</i>	<i>159</i>
<i>Table 4.5</i>	<i>Experimental plan for microneedle array cavity punch. Also includes the extrusion force recorded from the experiments.</i>	<i>173</i>
<i>Table 4.6:</i>	<i>Details of the micro pin layouts shown in Figure 4.52.....</i>	<i>186</i>

1. INTRODUCTION

1.1. BACKGROUND

The pharmaceutical industry is an ever evolving field with progressive adaption to new technologies and solutions. With the advancement in technology, the last few decades have seen a rapid development in potent, hydrophilic, large molecular weight compounds such as proteins and peptides (Amsden & Goosen 1995). Prior to invention of the modern hollow hypodermic needles as we know today – invented by Scottish inventor Alexander Wood, in 1853 (Hingson & Hughes 1947), but contributions have been made by various inventors (Schwidetzky & Rutherford 1944) – most therapeutics were inhaled or ingested. Oral delivery of medication requires the passing through the stomach, intestinal track and into the liver. Inhalation requires the small particles to pass through the thin barrier in the lungs and into the blood stream. This degradation can reduce the potency and alter the active compounds in the drugs.

From rudimental observation it was thought the skin was impervious to the penetration of chemical compounds. Skin is the largest organ in the human body and carries out several vital functions. A study in 1919 by Smith (Donnelly et al. 2012) found the outer layer of the skin to be the main barrier to the external environment. With the creation of the hypodermic needle, it was possible to break through this barrier and introduce compounds directly into the body. In doing so, the doctor would be purposefully damaging several layers of the patient’s tissue in a localised area, but this was seen as a small price to pay for the delivery of the medication. The patient’s skin would then repair the damage that was caused by the health professional.

In 1998 Henry et al used the skin itself as the site for drug delivery rather than just a barrier that needed to be overcome. Manufacturing methods for small needles had yet to catch-up with this idea, but the progress in the semiconductor manufacturing industry allowed for the production of microneedles. Henry introduced the “microneedle patch” in 1998 and since then there has been an explosion of research in this field.

Ever since introduction of the concept of using microneedles for the purpose of drug delivery, an influx of interest and research have been developed on the subject. Various materials have been examined and a variety of methods have been developed in order to mass produce the microneedles.

The main objective of this research is to develop a manufacturing method that is capable of producing an array of small metal microneedles that could be used for transdermal drug delivery. In order to develop a full understanding of the issues involved in the development of microneedles for transdermal delivery, it is necessary to examine the problem systematically and build an understanding of the requirements. It is also critical to identify the methods by which other research groups and the medical industry are using to overcome the skin barrier.

1.2. THESIS STRUCTURE

Chapter two [Literature Review] starts with reviewing human skin's function, anatomy and the methods of drug delivery through the skin. Current transdermal drug delivery methods and ways of overcoming the natural biological barrier are then studied. The concept of microneedles and various issues surrounding usage of microneedles from patents point of view is then reviewed. The types of microneedles, materials and manufacturing methods currently used for the production of these microneedles are then investigated. The various aspects of microforming are investigated with specially attention to the effects of small grain size in metals. Finally, various issues surrounding grain refinement and advanced technical processes currently used in industry for microforming that could be used in microneedles production, have been investigated.

Chapter three [Materials and Methods] investigates the available options of material and their suitability for this study, the methods of microforming metals for the purpose of this research. Aluminium 1050 has been selected as the choice of material for this study. Various aspects and issues relating to the selected material including surface roughness measurement, hardness testing is then investigated in detail. Technical issues and practical methods relevant to micro-forming process such as: friction, conversion coating, gold sputter deposition, tensile testing are studied in detail. Following investigation of various manufacturing methods, it was decided that

extrusion would be the best method for producing low cost microneedles. In order to run tests, a rig has been designed that would allow backward extrusion experiments to be conducted. Ultrasonic equipment, punch, and die fabrication methods were used in the process of conducting experimentations.

Chapter four [Results and Discussion] presents various experiments that were conducted for the purpose of this research. It is organised in four parts. In part (a) the effect of shear angle on the material flow and hardness distribution during incremental ECAP of Al1050 billets are presented. In part (b) multi-pass experiments are examined, analysed and discussed. Effects of load during multi-step IECAP, hardness evolution during multi pass IECAP, tensile testing, and visualising grain size refinement were investigated. In part (c) outcome of using FE analysis in assessing backward extrusion of multiple micro-pins is discussed. In part (d) experiments were conducted assessing the effects of lubrication condition, grain size and ultrasonic oscillation assisted microforming are presented and discussed.

Final conclusions and recommendations for future works are presented in chapter five. It is concluded that ultrasonic oscillation assisted gold coated billets produce the tallest microneedles with significantly less forming force when compared to other conditions. It is suggested that the next step would be for bio-compatible materials are used in the forming process to produce microneedles that could be used for transdermal drug delivery.

2. LITERATURE REVIEW

2.1. INTRODUCTION

Microneedles have now been produced from ceramics, metals and polymers. The general properties of ceramics suggest the needles would be resistant to compression but fragile under shear forces. Polymers have a low young's modulus, therefore, could deform before puncturing the skin. Metals have been used in hypodermic needles for a long time. They are strong enough to break the skin barrier but mass producing micro components from metal can be expensive (unless component can be manufactured from sheet; allowing sheet metal forming tooling to be used), therefore, using conventional manufacturing methods, it might not be the best material of choice for a product that requires to be made in the billions annually. For metals to be considered as a viable material for microneedles, it is necessary to propose a new manufacturing method that is suitable for low value high volume produced micro component.

Prior to proposing a solution, it is necessary to examine the problem more closely to develop an understanding of the requirements that need to be satisfied. It is also critical to identify the methods by which other research groups and the industry are using to overcome the skin barrier. The following sections will examine the properties of skin and identify its key features making it effective against exogenous material such as chemicals, pathogens etc.

2.2. SKIN: FUNCTION AND ANATOMY

Skin is a vital organ of the human body. It has been reported as the heaviest and largest organ with a weight of about 16 percent of body mass and covering 1.8m² (Gawkrodger 2008). At first glance it appears homogenous and simple but human skin serves several different functions and is, therefore, very complex. It forms a protective casing that separates the external environment from the internal body components by connecting to digestive, respiratory and urogenital tracks. The most obvious role of the skin is functioning as a physical barrier protecting the body's internals from the surroundings (Barry 1983). The way this main function is achieved, as well as its numerous other less obvious functions, makes it a very interesting organ to study. Some of these functions are as following:

- Prevention of the loss of vital endogenous material such as water (Brown et al. 2006) - In humans' water accounts for approximately 70 percent of body weight.
- The subcutaneous adipose tissue prevents harm from mechanical shock.
- Internal temperature regulation by controlled water loss through sweating.
- Metabolism and synthesis of lipid soluble secosteroid. In 1982 Maclaughlin, et al showed that in the presence of sunlight, skin was able to produce previtamin D3 (cholecalciferol) by means of photosynthesising of cholesterol precursor.
- Also a great shield against electricity, radiation, various chemicals, burns and dangerous microorganisms.
- The subcutaneous adipose tissue acts as heat insulation and as an energy store for heat production (Cinti 2005).
- Disposal of waste chemicals such as urea using glandular secretion (Barry 1983).
- Perception of pain, heat and pressure via the imbedded receptors.

To achieve all its many functions, skin is considered to be a composite of three distinct layers as shown in Figure 2.1.

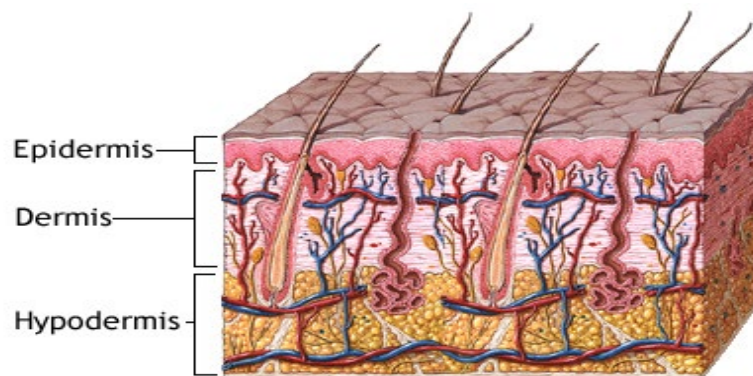


Figure 2.1: *Human skin cross-section diagram showing the three main layers that build up the skin.*
 Adapted from: http://owh.adam.com/pages/guide/reftext/html/skin_sys_fin.html

- A) The hypodermis - also referred to as the subcutaneous, is the bottom layer of the skin and contains fatty tissue.

- B) The middle layer of the skin sandwich is the dermis. This layer comprises of connective tissue.
- C) The outermost layer is the epidermis. This layer is avascular and stratified (Kermici et al. 1977).

By studying each layer of the skin anatomy at depth, it is possible to understand the mechanisms by which the skin achieves those previously stated capabilities. We are most interested in barriers to drug delivery, therefore, will be examining skin layers from that viewpoint.

2.2.1. Hypodermis

The Hypodermis (hypo derived from Greek meaning under) is the fatty fibrous layer residing on the bottom layer of skin. This layer provides impact cushioning and thermal insulation to the body through the use of interlaced collagen fibres and stored lipids. This subcutaneous fat can be found in most regions of the body and can be used as a form of energy when required (Barry 1983). This layer provides the links necessary for the upper layer of the skin to the underlying components of the body. This layer also contains blood vessels, white blood cells, lymphatic components, hair follicles roots and the glandular part of some sweat glands.

2.2.2. Dermis

The dermis can be three to five mm thick (Barry 1983) and is composed of a meshed matrix of predominantly collagen and elastin. The collagen and elastin provide the strength and the elasticity required for this tissue. This tough supportive layer connects the epidermis and hypodermis (Gawkrödger 2008). (Barry 1983) reported this layer accounting for most of the bulk of the skin. The collagen matrix also holds blood vessels, lymphatic components and nerves. The dermis can be further subdivided into two layers. The lower layer known as the reticular and the upper as the papillary. The papillary is only one hundred to two hundred microns thick and is attached to the bottom layer of the epidermis (Scheuplein and Blank, 1971).

2.2.3. Epidermis

The outermost layer of the skin is called the epidermis (epi derived from Greek meaning over). Gawkrödger describes this layer as a stratified squamous epithelium. This multi layered shield is the first line of defence from the outside environment. The thickness of this layer can vary from a few hundredth of a millimetre to almost one millimetre depending on factors such as race, sex, age and anatomical region (Prausnitz, Mitragotri, et al. 2004). Ninety percent of this layer is formed from keratinocytes (McGrath, 2004). This type of cell differs from most other cells in the body because they come from the basale layer and travel upwards towards the surface of the skin. During this maturation and migration, they change from cuboid shaped, metabolically active cells to flat, dead, keratinized cells (Barry 1983). There are distinct features through the depth of the epidermis, therefore it is possible to further subdivide this into 4 layers. The four stages of maturation of keratinocytes are stratum (stratum from the Latin meaning layer) basale that is connected to the dermic, followed by the stratum spinosum, then then stratum granulosum and finally the topmost layer of the epidermis being the stratum corneum (Gawkrödger 2008).

2.2.3.1. Stratum Basale

The layer that separates the dermis and the epidermis is known as the stratum basale. Undifferentiated keratinocytes stem cells can be found here. To balance the loss of the cells in the upper part of the epidermis, these undifferentiated cells undergo constant mitosis; therefore, the epidermis maintains a constant thickness (Eckert 1989). These cells are cuboidal in shape and lack the morphological and biochemical markers that other cells in the upper layer of the epidermis resemble. Under a microscope it is possible to distinguish between the basale cell and the basale lamina. The stem cells are attached to the basale lamina which in turn connects to the dermis. Other structures that can also be observed are hemidesmosomes and desmosomes.

Stratum basale also contains dendritic cell, melanocytes and Merkel cells. Dendritic cells such as Langerhans cells are very important antigen-presenting cells. They are able to capture and process foreign antigens. They quickly surround foreign material and process them into immunogenic peptides. Langerhans cells are able to migrate to lymphatic nodes and present the processed peptides on their surface to other cells such

as T lymphocytes of the immune system (Stoitzner et al. 2010). The inflammatory response of the body can activate these cells. To achieve a systemic immune response these cells that normally reside within the epidermis travel towards the lymphatic system of the dermis. They then travel to local lymph nodes and achieve a systemic immune response (Kripke et al. 1990).

2.2.3.2. Stratum Spinosum

The Stratum spinosum sometimes referred to as the prickly layer (Barry 1983) due to its appearance is located above the stratum basale. It is constructed of several layers of keratinocytes that are joined together by desmosomes (Obland 1958). These intercellular bridges are bundles of filaments that are made from pre-keratin. This junction maintains the structure of the epidermis but allows oxygen and other nutrients within the tissue fluid to pass through the spaces between connected cells.

2.2.3.3. Stratum Granulosum

In most parts of the body the stratum granulosum is the layer below the stratum corneum. The stratum granulosum is the region between living and dead cells. This layer is named after the keratohyalin granules that is found in this layer (Eckert 1989). This region contains three to five layers of cells that contain deteriorated organelles. The cytoplasm is abundant with lamellated granules and keratohyalin granules. The granules contain profilaggrin which aids the accumulation of keratin filaments. Profilaggrin is a precursor to a protein called filaggrin. The filaggrin protein binds to the keratin fibres (Markova et al. 1993).

2.2.3.4. Stratum Lucidum

In some regions of the body there is an additional layer called stratum lucidum. This name has been derived from the Latin word lucidus which means clear due to translucent appearance under an optical microscope. This layer can be found in the areas of the body where the skin is thickest e.g. sole of the foot and palm of the hand (Narayan 2009). The cells in this region are dead and flattened with some keratohyalin protein amongst the cells.

2.2.3.5. Stratum Corneum

The top layer of epidermis is the stratum corneum. It can be 20-30 cell layers thick. It is composed of 20-30 flattened, hard protein envelopes and keratin. This keratinized dead cell region contains no nerves or blood vessels. The stratum corneum is 10-20 μ m thick (Prausnitz, Mitragotri, et al. 2004) and can vary depending on factors such as race, sex, age and anatomical region. The extracellular space surrounding the cells contains lipids. This layer is continuously replenished with the cells that migrated upwards from the bottom layer of the epidermis the stratum basale. In 1971 Scheuplein and Blank described this complex process of polymerisation and dehydration of the inner cell material, which resulted in the shrunken, protein filled, and dead cells (Scheuplein & Blank 1971).

As the keratinocytes migrate upwards towards the surface, they lose seventy percent of their water content. As keratinocyte progresses up through the epidermis, it is transformed at the stratum granulosum into a nonviable corneocyte. They are then shed in the epidermal turnover process. The transformation of the keratinocyte into corneocyte involves the loss of the cell organelles such as the nucleus and cytoplasm, formation of the tough outer structure, accumulation of keratin proteins and release of lipids into extracellular spaces. By dry weight corneocyte is comprised of about eighty percent keratin protein. Corneocytes polyhedrons are 0.3 μ m thick with a diameter of 30 μ m (Lindberg & Forslind 2003). These corneocytes are adapted to provide the protective shield required for the body but are dislodged from the stratum corneum during the natural shedding of the outer layer of the skin (Eckert 1989), which is referred to as desquamation.

The way the stratum corneum is constructed has been said to play an important role in the shield function of the epidermis (Potts & Francoeur 1991). The brick and mortar construction of the corneocyte and lipid assembly (Elias 1981) provides a difficult water permeability pathway. This composite membrane is said to be a thousand times less permeable than other bio-membranes in the body (Potts & Francoeur 1991). Although this barrier is highly impermeable, it is permeable to a select group of lipophilic compounds that can diffuse across the skin (Brown et al. 2006).

The stratum corneum has a density of one and a half grams per cubic centimetre (Barry 1983) and gives the epidermis its mechanical strength. This strength can also be attributed to the overlapping cell construction. This thin laminate layer consists of 15 to 20 percent water with 20 and 40 percent lipids and keratinised proteins respectively (Anderson & Cassidy 1973).

Once the anatomy of the skin is known and the function of each layer and sublayer is understood it is possible to look into the factors that affect drug delivery.

2.3. DRUG ABSORPTION THROUGH THE SKIN

Although skin was thought to be impervious to exogenous substances there are now a wide spectrum of research showing this not to be the case. As previously discussed the stratum corneum is not metabolically active and no functioning transportation system exists. It is possible to passively diffuse some drugs through the skin using the conventional cutaneous delivery system (Scheuplein & Blank 1971). Molecules smaller than 500 Dalton (Da) can pass through the skin barrier (Brown et al. 2006). The infiltration of small hydrophilic molecules in the lipid lamella of the stratum corneum is controlled by the rate of partition. The permeation of small hydrophobic molecules in the watery environment of the viable epidermis through the stratum corneum is controlled by the rate of partition. The amount of penetration for drugs decreases significantly as their molecular size increases beyond 500Da (Brown et al. 2006).

Various equations have been proposed to describe this passive transdermal drug absorption. Fick's law of diffusion can be adapted to describe the rate of permeation across the stratum corneum. Hadgraft and Lane proposed the following equation (Hadgraft & Lane 2006):

$$J = \frac{KD(C_{app} - C_{rec})}{h}$$

- Where J - the steady state flux per unit area
- K - the partition of the permeant between the applied compound to the skin. Therefore, this is the likelihood of the permeant leaving its vehicle and enter the stratum corneum.

- D - the coefficient of diffusion
- C_{app} - the applied concentration of the permeant vehicle
- C_{rec} - the concentration in the body
- h - the diffusion path length of the lipid lamina

Williams and Barry described K as the octanol / water partition coefficient K_{oct} or $\log P$. As described before the greater the lipophilic of the molecule, the easier it will partition into the stratum corneum's lipid construction. The increase in lipophilic can be described as a greater $\log P$ value. The following equation can be used to describe the permeability coefficient K_p (Williams & Barry 2004).

$$K_p = PD/h$$

Potts and Guy observed a relationship between permeability coefficient, $\log P$ and molecular weight (MW). They proposed the following equation (Potts & Guy 1992):

$$-6.3 + 0.71 \log K_{oct} - 0.0061 MW = \log K_p (cm/sec)$$

Therefore, it is possible that an increase in molecular weight will result in a reduction in $\log K_p$ (Comer & Tam 2001). Potts and Guy also went further and described molecular volume MV increasing with a reduction in $\log K_p$. The relationship between the coefficient of diffusion and molecular weight is exponential so it is possible to see a reduction in the permeability of large molecules is limited by their size. Increasing molecular weight decreases the permeability coefficient by decreasing the coefficient of diffusion.

It is possible to simplify the steady state flux equation when performing in vitro transdermal diffusion studies because the applied concentration of the permeant vehicle is much larger than the concentration in the body (Hadgraft & Lane 2006).

$$J = K_p C_{app}$$

When the applied concentration of the permeant vehicle equals the solubility limit of the drug in the applied formulation the maximum flux can be obtained.

It was shown that disrupting the stratum corneum can lead to increased permeability. (Scheuplein 1976) showed it was possible to increase passive transdermal drug delivery by applying an adhesive tape to the surface of the stratum corneum. Theoretically, it is possible to increase the efficiency of drug delivery, thus, increasing the size of the molecules of the drug that can pass into the skin by disrupting the stratum corneum.

2.4. CURRENT DRUG DELIVERY METHODS

With the advancement in drug discovery over the last 100 years has come new and improved drug delivery methods that allow the drugs to keep their potency.

2.4.1. Oral Route

The oral route has remained the conventional route for drug delivery due to requiring no training for administration, ease of administration, convenience, pain free association (Park et al. 2005). Pills, capsules and tablets are cost effective and can be used for a wide range of medicines. Thanks to its many advantages, the oral route remains the delivery route for most drugs.

Many factors can alter the effectiveness of drugs when administered orally. Drugs that are administered through the oral, pass through the digestive tract and get metabolised and degraded in the highly acidic environment of the gastrointestinal fluid. This is then followed by enzymatic metabolism in the hepatic first pass of the liver (Benet et al. 1996). Circulation of blood from the small intestine into the liver via the portal vein is referred to as portal circulation. Going through this complex system can inevitably result in the variability in the level of systemic response to the activity component of the drug. Foods ingested by the patient as well as the other components in the tablet's preparation can affect the effectiveness of absorption of oral drugs into the body.

2.4.2. Hypodermic Needles Route

Cutaneous drug delivery is an interesting drug delivery route for proteins, hormones, peptides, nucleic acids, antibodies and vaccines as the enzymes in the digestive tract and the liver degrade these compounds (Brown et al. 2006) when administered orally. Hypodermic needles are used to deliver large molecules and molecules that are made

inactive when administered orally. This method avoids the complexities of the gastrointestinal tract but requires administration by a medical professional (Davis et al. 2004). Breaking the protective skin barrier causes pain and can introduce an infection into the body.

One of the main advantages of hypodermic needles is the ability to deliver the drug to the required region of the body without systemic distribution. This method delivers the full dose of the drug in a short period of time which can result in irritation and potential toxic effects. In an effort to reduce this possibility, the potency of drugs is often reduced. To prevent the initial high dosage and decay of the therapeutic it is often necessary to re-administer the drug to the patient over time. Both oral delivery and hypodermic needle route can require several dosages to maintain an effective active component level of the therapeutic in the body. There are some prolonged release formulations available to overcome these challenges (Park et al. 2005). With the limitations described above there could be a potential for a self-administering, minimally invasive drug delivery method that could deliver a range of macromolecule therapeutics (Sullivan et al. 2008).

2.4.3. Transdermal Route

A range of transdermal drug delivery patches exist that can overcome the previous limitations of hypodermic needles and pills. New formulations can allow controlled release of some therapeutic substances from transdermal patches into the network of capillaries. Molecule degradation would not take place in this route as the gastrointestinal tract and liver would be bypassed (Prausnitz 2001). As stated previously, the architecture and material in the stratum corneum makes it very difficult for hydrophilic molecules and molecules with a molecular weight larger than 500Da to pass through healthy skin (Sullivan et al. 2008). Therefore, other methods are required to increase the permeability of the skin (Li & Soar 2008). Transdermal drug delivery presents an appealing yet challenging unconventional drug delivery site with many advantages and limitations. The Ideal drug delivery device would be capable of delivering hydrophilic and biological macromolecules into the skin while being self-administering and while minimising patient pain and the chances of infection.

The following section will look into the traditional and novel methods of sub-cutaneous drug delivery.

2.5. OVERCOMING THE NATURAL BIOLOGICAL BARRIER

Several barriers in the body restrict delivery of medicaments to the required location with the required rate. These barriers are the gastrointestinal tract and the greater mucosal membrane (Lichtenberger 1987), skin (Scheuplein & Blank 1971) as well as the blood- brain barrier (Syková & Nicholson 2008) and cell membrane (Whitehead et al. 2009). Unfortunately, these barriers also treat therapeutic drugs as foreign chemicals and pathogens, therefore, restrict their pathway into the body.

Over the last few decades the methods for easing the transportation of the medicaments into the body has received significant attention. There are two main categories of methods that increase the possibility of improving drug delivery. These are: device based and formulation based methods. The formulation-based methods utilise penetration enhancers and carriers as well as making use of prodrugs and inactive vehicles such as excipients. The device-based method utilises a physical product that disrupts the protection barrier and allows the medicament to pass into the body. Device based methods often require a power source to achieve their functionality, but are able to control the quantity and rate of delivery of the therapeutic substance. The requirement for a power source often drives the cost up for device-based products.

Some of the current solutions for overcoming the skin barrier of the body will be looked at in the following section.

2.5.1. *Transdermal Drug Delivery*

To complete the drug absorption process and pass into the lower viable tissue of the body, medicaments can take three routes.

- Intercellular route – diffusing through the intercellular lipids,
- Transcellular route – diffusing through the coenocytes,
- Shunt route (transappendageal) – through the sweat glands and / or hair follicles.

The route used for transdermal drug delivery depends on several factors such as the drug molecules chemical and physical properties, permeation aids applied to the skin and anatomical region where the drug is being applied. Altering the chemical or physical properties of molecules can denature them and cause them to become ineffective, thus may not be a possible option for many medicaments. Drug application site must be chosen carefully. As discussed earlier, the stratum corneum is the main barrier to transdermal drug delivery due to its properties. The thickness of this layer also varies with many factors, therefore, some sites on the body would be more suitable and simpler for transdermal drugs to overcome. Permeation aids can facilitate drug absorption by disrupting the body's natural barrier.

When referring to transdermal drug delivery it is important to distinguish this from dermal or topical delivery. The phrase transdermal drug delivery is used when medicaments are delivered across healthy and unbroken skin into the systemic circulation where they will offer their therapeutic effect. Percutaneous absorption is used to describe the process by which this is achieved. Topical formulation is intended to be applied to damaged, broken or diseased skin. Their therapeutic compound is intended to target sites in the skin and not the percutaneous absorption (Brown et al. 2006).

2.5.2. *Formulation-Based Methods*

The formulation-based method for cutaneous drug delivery can be achieved through several different methods. The conventional and most straightforward way would be to mix the therapeutic with gels, ointments and creams and applying them to the surface of the skin. Other method would be using passive patches to deliver the therapeutic. Some of these methods increase the permeability of the skin but others utilise thermodynamic activity to increase drug diffusion force (Brown et al. 2006). The section above briefly described some of these methods but the following section will look at each method in greater detail.

2.5.2.1. Prodrugs

This method involves a lot of chemistry and requires the attachment of lipophilic sections onto the hydrophilic drug molecule (Bundgaard 1992). Often using covalent

bonds to join the moiety, it is possible to ease the movement of the drug through the lipophilic stratum corneum and into the viable tissue. Once in the epidemic, the lipophilic moiety is severed from the molecule by enzymes, allowing the drug to become active (Amsden & Goosen 1995). This also leads to one of the main drawbacks of this formulation-based method. The enzymatic process by which these prodrugs become active can vary depending on the patient. There is also a limit on the molecular size that can be used with this method. As discussed earlier the larger the size of the molecule the less permeable it becomes.

Even with these limitations it has been demonstrated that by using this method it would be possible to considerably increase the permeability of large molecules such as hormones that are released by thyrotropin (Møss & Bundgaard 1990) as well as smaller molecule 5-fluorouracil (SASAKI et al. 1990). Another advantage of using prodrugs is the ability of the added lipophilic section of the compound that maintains the functionality of the initial molecule in the blood stream prior to it reaching the site of action (Møss & Bundgaard 1990).

2.5.2.2. Excipients

Inactive vehicles such as excipients in the form of liposomes and its derivatives are used to aid drug delivery to the skin. Initially they were used to target specific organs (Weinstein et al. 1979) but were later used for the administration of topical medicaments to the skin (Mezei & Gulasekharam 1980). Liposomes in the form of cholesterol and phospholipids form layers around the active molecule and allow it to pass into the skin (Barry 2001). There is then a build-up of the active molecule in the epidermis which can have a localised affect (Mezei & Gulasekharam 1980).

2.5.2.3. Super Saturation

This method raises the activity a therapeutic compound above its solubility limit, therefore, increasing the penetration of the medicament without disrupting the stratum corneum lipids (Billett et al. 1997). The main drawback of this method is the instability of many compounds as they crystallise out of solution and become non-absorbent (Billett et al. 1997). Therefore, it is only suitable for a small collection of compounds unless further development is undertaken. Billetta reported a linear increase of the flow

of piroxicam with the increase in saturation (Billetta et al. 1994). There are some patents - such as US 5906830 A (Farinas et al. 1999) - associated with this drug delivery enhancement method.

2.5.2.4. Chemical Penetration Enhancers

This is a very effective method of drug delivery through the skin barrier. As our understanding of skin and its make-up has improved it has allowed researchers to propose and investigate several different penetration enhancers. Over the last two decades more than 10 classes of penetration enhancers have been described. These are fatty amines, acids, esters and salts of fatty acids, as well as surfactants such as anionic, cationic, non-ionic and dipolar (Karande et al. 2005). The mechanism by which these penetration enhancers work can be one of or a combination of the following mechanisms (Barry 1983):

- Interacting with intercellular protein,
- Disrupting the lipids in the stratum corneum,
- Improving the divisibility of the active drug, solvent or co-enhancer into the stratum corneum.

Fatty acid enhancers increase the fluidity of lipid protein section of the stratum corneum, whereas solvent swelling or protein conformal change is used for polar pathway alteration (Pathan & Setty 2009). The skin's laminate structure can also be altered by some chemical penetration enhancers by acting on the polar and non-polar pathways (Pathan & Setty 2009).

These alterations to the skin's structure often lead to the main disadvantage of using such penetration enhancers. Irritation of the skin area is often reported due to the complex chemical behaviour of this method. Hydrogen bonds play an important role in the maintenance of the skin's proteins in its required locations. Polar interaction can alter the ratio of hydrogen bonds in the skin structure, which can lead to skin degradation and irritation (Karande et al. 2005). To further explore this field Williams and Barry conducted a comprehensive review and undertook a wider review of compounds, sites and methods of action (Williams & Barry 2004).

In addition to the formulation-based methods there is also a device based method for enhancing transdermal drug delivery. The following section will examine some of these devices and the method by which they achieve their functionality.

2.5.3. Device Based Methods

Formulation based methods have shown the possibility of passively delivering medicaments across the skin but suffer from some limitations. As previously stated molecules with a molecular weight of over 500Da find it very difficult to pass through the stratum corneum (Bos & Meinardi 2000). With recent advances in drug discovery and molecular engineering it has become necessary to deliver molecules with a weight significantly greater than 500Da (Brown et al. 2006). To overcome this barrier many new devices and methods have been developed (Mitragotri & Lahann 2012) over the last two decades. These active devices usually require an external power source to function and either drive the molecules through the skin or disrupt the skin to allow the molecules to pass through with less hindrance (Brown et al. 2006). There are several advantages of using the device-based method but one of the main advantage is the ability to control dosage delivery. There are several effective devices that can be placed on the skin or on the mucosal membrane for direct drug delivery (Arora et al. 2008).

There are five main categories of device based transdermal drug delivery enhancers. They are broadly categorised by the technology that drives their functionality. These are:

- Ultrasonic devices (Mitragotri 2005)
- Thermal and optical devices (Singh et al. 2010)
- Electrical field devices (Prausnitz 1997)
- High pressure devices (Mitragotri 2006)
- Microneedles (Prausnitz 2004)

Each of these devices have been designed to disrupt the skin barrier temporarily to allow the macromolecules of medicaments to pass into the body. Each of these categories will be explored in greater detail to understand how these devices achieve their enhanced functionality and drug delivery capabilities.

2.5.3.1. Ultrasonic Devices

Often referred to as acoustic ablation, phonophoresis, sonophoresis or sonoporation; refer to the use of high frequency sound to deliver molecules into cells and tissue. Phoresis is derived from Greek word meaning the movement of something by using a proxy. In this case, the proxy being used is high frequency sound. A wide spectrum of frequencies (20KHz to 16MHz) have been used for sonophoresis. Normally humans have a hearing range of 20Hz to 20KHz (Møller 2012), but this can reduce with age. Frequencies greater than the human hearing frequency of 20KHz are referred to as ultrasound.

Ultrasonic have been used to aid drug delivery through the skin since the middle of the 20th century (Mitragotri & Lahann 2012). In tissue these ultrasonic waves induce movement of water molecules which causes a pressure gradient to develop. For transdermal drug delivery of macromolecule porpoises (Amsden & Goosen 1995), sonophoresis must act on the stratum corneum. The rapid alteration can cause small cavities to form in the lipid region of the stratum corneum, thus enhancing the skins permeability (Paliwal & Mitragotri 2006). They can also reduce the boundary layer thickness by mixing, cause fluid to flow more easily and elevate temperature (Kost 1993). Experiments conducted by Bommannan et al. demonstrated the possibility of pushing water-soluble material into the skin. Bommannan et al. also showed that it was possible to enhance the penetration of small molecular weight compound such as salicylic acid (Bommannan et al. 1992). Lower frequency ultrasound (20KHz to 100KHz) has been shown to be more effective at delivering high molecular weight compounds (Mitragotri et al. 1995).

Several ultrasonic devices are currently being used clinically. They operate at frequencies between 1MHz to 3MHz, and are often used for enhancing the delivery of anti-inflammatories and steroids during physiotherapy (Lavon & Kost 2004). There are also devices that operate at the lower ultrasonic frequencies for the delivery of lidocaine (Kim et al. 2012). As well as increasing the drug delivery into the skin, ultrasonic have also been used to deliver medicaments into the brain passed the blood brain barrier (Mesiwala et al. 2002). Another area where ultrasonic is making great advancement is in clot destruction (Doomernik et al. 2011). Not only can ultrasonic

devices break the clot mechanically but they also drive the clot-busting drug deep into the clot allowing quicker destruction.

There are disadvantages to using this method. Intense and localised ultrasonic energy can damage vesicles and rupture cells in the body (May et al. 2002). The patient can also be harmed further due to the increased intensity and duration of exposure; the temperature of the surrounding tissue can increase significantly (Lavon & Kost 2004), which can lead to tissue breakdown and other complications.

2.5.3.2. Thermal and Optical Devices

This method is another example of multi-disciplinary solution for a medical problem. Thermal devices specifically target the stratum corneum layer of the skin. They achieve their function by selectively removing the top layer of skin while leaving the deeper tissue undamaged and cool (Bramson et al. 2003). This is achieved by carefully controlling the temperature and power duration of the device (Singh et al. 2010). Careful control over the depth of removal is extremely important because the nerves that react to pain reside in the dermis layer underneath stratum corneum.

Related to this method is the radio frequency method. Using electrodes - arranged in an array - it is possible to achieve selective localised destruction of the stratum corneum using radio frequencies. These radio waves cause the stratum corneum to heat up quickly and disintegrate. Birchall et al showed that it is possible to use radio frequencies to create micro channels in the skin which could then be used to allow cutaneous gene expression of plasmid DNA (Birchall et al. 2006).

The obvious technique that comes to mind when researching selective thermal removal would be lasers. As well as for other industries, lasers have been developed to aid drug delivery into the body. Lasers are used to deliver light energy into the stratum corneum. This rapid delivery of energy causes the water in the stratum corneum to rapidly evaporate which causes micro channels to form. Laser devices using erbium doped yttrium aluminium garnet that can increase the permeability of skin have been made small enough to be hand held and portable (Kalluri & Banga 2011). As with all laser devices, it is necessary to take precautions and be properly trained prior to contact with the patient.

2.5.3.3. Electrical Devices

Broadly speaking there are two main types of drug delivery devices that use electricity as their main mode of delivery. These are electroporation and iontophoresis. The methods by which these devices achieve their functionality is different, therefore, will be explored individually.

2.5.3.3.1. *Electroporation*

Electroporation devices apply high voltage pulses to the surface of the skin for short periods of time. The pulses of voltages used can range from 100 to a few hundred volts lasting a few microseconds to milliseconds (Prausnitz et al. 1993). These pulses induce temporary movement in the skin cells (Brown et al. 2006). The increase in the permeability of the skin surface can be attributed to the temporary pores that are created (Weaver et al. 1999). This method has been demonstrated to be effective for both small molecular weight (Prausnitz et al. 1993), (Banga & Prausnitz 1998) and large molecular weight (Guy et al. 1987) compounds. As well as voltage and time other factors such as the number of pulses, the rate of delivery of the pulses and the wave form of the pulse being applied (Banga et al. 1999).

There are, however, some drawbacks attributed to using this method. It has been found that the pulses used in electroporation can induce involuntary muscle contraction (Escobar-Chávez et al. 2009) as well as mild erythema (Prausnitz, Allen, et al. 2004), and oedema (Prausnitz et al. 1993). Due to these side-effects electroporation is not usually used on patient's skin but it has been shown to be very effective in delivering drugs into tumours and cells (Heller et al. 2005).

2.5.3.3.2. *Iontophoresis*

Where electroporation method is mostly focused on voltage control, iontophoresis is predominantly based on current control (Kalia et al. 2004). In iontophoresis, currents less than 500 mA per cm² are used to transport charged molecules across the skin barrier (Guy et al. 2000). The electrical potential that is applied to the skin surface causes the charged particles to be repelled into the tissue. The medicaments used with this method are often topically applied then iontophoresis is used to enhance the permeation (Y. Wang et al. 1993).

As well as the charged molecules, iontophoresis can also be used for neutral molecules (Sieg et al. 2004). The mechanisms by which the molecules pass through the barrier are electro-osmosis (uncharged), electrorepulsion (charged), electroperturbation (charged and uncharged) (Brown et al. 2006) as well as trans-follicular (Guy et al. 2000). The charge to mass ratio becomes important in iontophoresis. Ideally, the molecule will have a high charge to mass ratio, allowing greater tissue penetration enhancement. The side effects of iontophoresis can be mild erythema (Prausnitz, Mitragotri, et al. 2004) and possible irreversible cell damage (Burnette & Ongpipattanakul 1988).

By generating current in the system it is possible to transport compounds into the skin. The greater the current generated, the more ions are transported. The effectiveness of iontophoresis is also dependant on the ionic mobility, polarity and the valency of the medicament. Compounds such as dexamethasone (Lark & Gangarosa 1990), insulin (Langkjær et al. 1998) and lidocaine (Spierings et al. 2008) have been tested with iontophoresis devices. Therefore, it is possible to use iontophoresis on a range of compounds with varying molecular weights. It has also been clinically used with pilocarpine for the identification of cystic fibrosis (Brown et al. 2006). Iontophoresis can also remove glucose from the body, allowing the monitoring of diabetic people (Tamada et al. 1999).

2.5.3.3.3. High Pressure Devices

High pressure devices provide interesting solutions to the transdermal drug delivery problem. Instead of increasing the permeability of the skin and then applying the medicaments, high pressure devices use the particles themselves to drive through the skin and reach the subdermal tissue (Schramm & Mitragotri 2002). There are two main types of high-pressure devices. The liquid micro jet device and the powder jet device. As for a liquid micro jet device the medicament cartridge is liquid filled (Mitragotri 2006), the powder jet device is filled with a powder form of the drug (Kendall et al. 2004). High-speed devices usually have three main sections; a section holding the medicament, holes with a diameter of a few hundred microns that the medicament can pass through and a method for inducing acceleration in the holding section then the operator triggers it. Compressed air or springs can be used to accelerate the

medicaments through the holes towards the skin (Mitragotri 2006). The small particles can travel at speeds of 200 meters per second towards the surface of the skin. The momentum gained allows them to penetrate the stratum corneum and go into viable tissue.

This also leads to the main drawbacks of such devices. With drug particles traveling that fast it is inevitable that some patients would report pain. The sudden impact of the medicaments onto the skin also leads to localised bruising (Jackson et al. 2001). In response the patient complains. In order to improve clinical adaption, several control measures have been proposed. Some of the proposed improvement measures are: variable velocity injection (Stachowiak et al. 2009), real-time controller (Taberner et al. 2012) and pulsed micro jet injection (Arora et al. 2007).

There are several advantages for using high-pressure devices. The key advantage is the ability to use current formulations of proven medicaments, therefore no alteration needs to be made to the drug and the pharmaceutical company incurs no additional cost. There have already been several examples of immunisation studies being carried out with current vaccines using liquid micro jet devices. In 2003 Weniger reported on immunisation against cholera, hepatitis B, influenza, measles, polio and smallpox using liquid micro jet devices (Weniger 2003).

Another advantage of high-pressure devices is not requiring additional power. Unlike most of the other active drug delivery devices discussed previously, high-pressure devices can be small and very portable. The spring can be reset or a compressed gas reservoir replaced (Weniger 2003). This simplifies the clinical use of these devices and allows them to be used in more remote locations.

2.6. MICRONEEDLES

Microneedles (MNs) are a simple concept, evolved from hypodermic needle roots. Microneedle devices are usually an array of and short needles designed to penetrate the skin. The concept of microneedles was first introduced by Gerstel and Place in 1976 (Gerstel & Place 1976). However, it was not until 1998 that this could be realised. In 1998 a paper by Henry et al showed the world that it was possible to produced microneedle (Henry et al. 1998). Due to the advancement of new micro manufacturing

methods, thanks to the semiconductor industry, it was possible to produce precision protrusions small, strong and sharp enough to be used as needles.

Hypodermic needles have been used for over one hundred years and have proven to be effective drug delivery devices. Transdermal patches are common sight now, often being used for nicotine delivery for those who wish to quit smoking. Nicotine has a molecular weight of 162 Da (Prausnitz 2004), therefore, can pass through the stratum corneum and into the capillaries. Microneedles are a hybrid solution combining the effectiveness of hypodermic needles with the ease of use of transdermal patches (Sullivan et al. 2008). By producing small channels in the stratum corneum barrier with microneedles, it is possible to increase the permeability of the skin, allowing larger molecules to pass through (Wu et al. 2008). Similar to transdermal patches, microneedles require no external power supply unlike other active devices.

Microneedles have demonstrated benefits over the hypodermic needle and the interest in them has rapidly increased. This is demonstrated by the increase in review papers and patent applications (Vandervoort & Ludwig 2008) during the last two decades. In 2012 Kim et al graphically presented the increased number of publications on the subject of microneedles (Kim et al. 2012), which can be seen in Figure 2.2.

Hypodermic needles are one of the most widely used medical devices today for the administration of drugs and vaccines. Over fifteen billion hypodermic needles are used annually around the world (Hauri et al. 2004), even though trypanophobia – a fear of needles – affects at least one in ten people (Hamilton 1995).

Microneedles are seen as minimally invasive, as they are short enough to minimise contact with the nerves present in the dermis, therefore no pain being perceived by the patient. MNs can be used in an array to increase the permeability of the skin. In a recent study (Gill & Prausnitz 2008) have demonstrated that increasing the number of needles by a factor of ten, doubles the pain score whereas tripling the length of the needle increases the pain score by a factor of seven. Using an array of MNs, it is possible to increase the skins permeability without causing pain or blood loss to the patient.

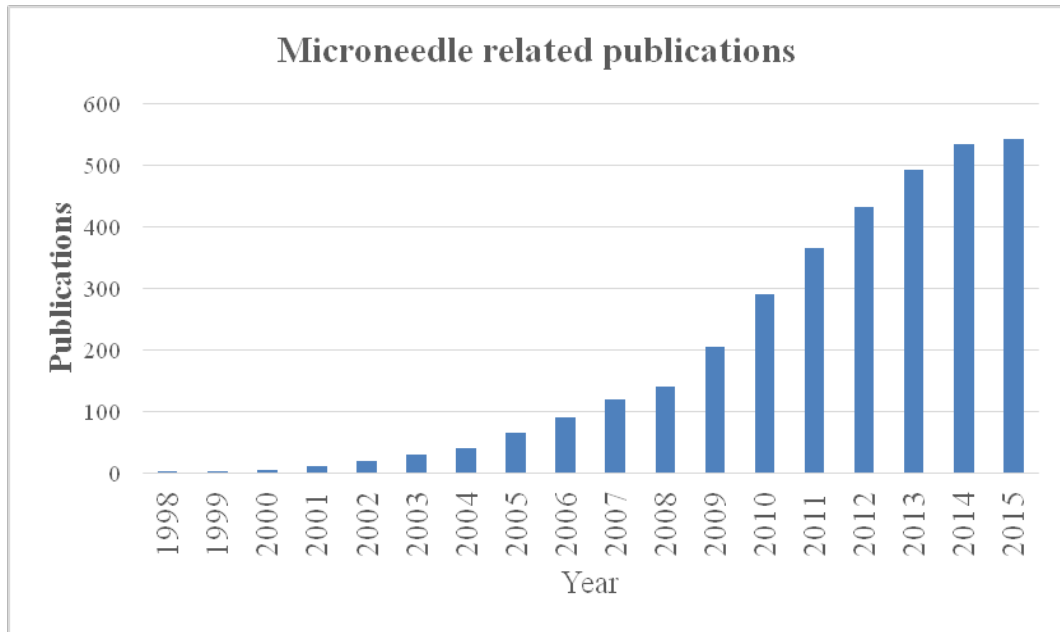


Figure 2.2: *Yearly increase in microneedle related publications. Adapted from Kim et al. 2012.*

2.6.1. Patient acceptance and safety

Microneedles are seen positively in comparison to hypodermic needle injections by patients and healthcare workers (Birchall et al. 2011). The perceived benefits were the possibility of self-administration but with a reduction in the risk of infections, tissue damage and pain. The disadvantages of such a device could be the increased cost, reduced accuracy and reliability of drug delivery and the increased chances of misuse. In a recent influenza vaccination survey Arnou, et al have reported that people preferred microneedles over hypodermic injection; mostly due to the smaller needle size, as well as the increased immunogenicity of intradermal vaccination (Arnou et al. 2011). The survey showed that vaccination rates would also increase.

These psychological findings are very interesting. For microneedles to succeed and to increase their uptake, it is important to look into the reasoning behind this. Many studies were conducted on factors such as pain, recovery and the risk of patient infection. These will be examined in the following section.

Pain – one of the main reasons for Patients considering microneedles favourably is because they are perceived as minimally invasive. Kaushik et al conducted a study to examine the perception of pain associated with microneedles (Kaushik et al. 2001).

The study found that it was more painful to be injected with a 26-gauge hypodermic needle than an array of 400 microneedles with a length of 150 μm . A later study by Gill et al found that length and the number of microneedles greatly affected pain score, but microneedle thickness and tip angle had weak effects (Gill & Prausnitz 2008). All microneedles studied induced significantly less pain than the hypodermic needle control. Publications such as Bal (Bal et al. 2008) and Haq (Haq et al. 2009) show microneedles shorter than 400 μm are painless, but Haq et al move further to suggest that a single microneedle with a length of 1mm was not painful (Haq et al. 2009). Hollow microneedles have been reported to cause some minor pain during insertion and injection. Pain can also be induced due to the force required to break the stratum corneum, therefore, it is important to examine the forces required to insert microneedles into the skin.

Insertion and fracture force – needles used in microneedle drug delivery should be sharp and strong enough to resist fracture and deformation during insertion, as well as being capable of withstanding the lateral forces induced by the elasticity of the skin. Davis et al have compared the forces required to break hollow microneedles with the skin insertion force (Davis et al. 2003). The skin insertion force was dependent on the tip area and was measured to be 0.1-3.0N. One of the findings of the author was that the force was not linked to the needle being hollow or solid. Wall thickness also played no part in the amount of insertion force, but plays an important role in fracture force. The fracture force is independent of tip radius but can be influenced by wall angle. The fracture forces recorded are 0.5-6N, which agree with Kim's findings (Kim et al. 2012). A strong microneedle will have a small tip radius and a large wall thickness.

Recovery- after microneedles' removal, small holes remain in the skin. The duration of these channels remaining open is very important. The channels remaining open for a long time will increase the chances of infection but short durations will result in poor topical drug delivery. In 2008, Wermeling et al studied the kinetics of pore resealing after microneedling. When the skin barrier was not hindered it could recover in 2 hours but when the recovery process was obstructed it could remain open for up to 40 hours (Gupta et al. 2011). It is also possible to increase this opening time to 7 days by applying recovery inhibitors such as diclofenac sodium (S. L. Banks et al. 2011).

Infection risk – the holes remaining open following microneedle insertion can be a gateway for pathogens to enter the body and leading to infection. As discussed previously, the skin has a large number of defence cells to protect it from exogenous pathogens (Kupper & Fuhlbrigge 2004). Hutin et al showed that the holes left after sterilised hypodermic needle use pose little threat to infection (Hutin et al. 2003). Donnelly et al went further and specifically examined microbial penetration post microneedle use (Donnelly et al. 2009). When compared to hypodermic needles, it was found that less microbial penetration occurred after microneedle use.

2.6.2. Advantages of Microneedles

As described previously, there are also a large number of capillaries in the dermis. Microneedles also avoid these capillaries, therefore, causing no bleeding to the patient. By penetrating the skin and coming into close contact with the capillaries, it is possible for microneedles to deliver medicaments that will then be absorbed into and distributed by the vascular system (Lv et al. 2006). As well as these advantages, there are additional benefits to using microneedles for transdermal drug delivery. These are briefly reviewed in the following:

Minimised skin and tissue damage – microneedles pierce the skin deep enough to allow drug delivery but they are short enough to avoid further unnecessary tissue damage.

Can be self-applied – microneedle application can be as straight forwards as applying a plaster and no medical training is necessary. This can be advantageous to patients and medical professionals.

Antibody response can be achieved quickly – Langerhans cells and other antigens reside within the skin as the body's main line of defence

Local anaesthetic delivery – only delivering anaesthetic effects to the region required rather than to the whole body.

Reduced vaccination dosage – smaller dosage of vaccine is needed to obtain/achieve an immunological response from the body.

Gradual diffusion can be achieved – traditional drug delivery methods such as hypodermic needling and oral have a toxic peak concentration immediately after administration. To combat this, it is often necessary to use low concentration and repeat the administrations once the body breaks down the drug. Microneedles can provide a controllable drug concentration delivery by gradual diffusion through the skin and into the body. In the event of re-dosing being necessary, a lower dosing frequency can be required with microneedles. They can be kept into the skin for a duration of time ranging from seconds up to months. When no longer required the microneedle patch can also be easily removed.

Hollow microneedles can be used for fluid extraction – small amounts of blood and other bodily fluids can be extracted for analysis within the devices that is attached to the microneedles. It has been proposed that diabetes patients can have their blood glucose levels monitored prior to insulin delivery to ensure optimum dosing levels, which can then be delivered with the same microneedles.

Targeted skin section therapy – benefits to the skin appearance have been shown post microneedling. It is possible to use microneedles for a range of cosmetic purposes. They can be used to reduce the appearance of uneven skin, scars and wrinkles. As well as increase hair growth to reduce alopecia.

2.6.3. Microneedle Types

Microneedles (MNs) are developed specifically for their intended use. There are different designs and configurations of microneedles available. There are four main types of microneedle devices:

Solid MNs – these are mostly used to induce porosity in the skin prior to medicament application.

Coated MNs – drug coated solid microneedles are used to deliver medicaments as they are inserted into the skin.

Biodegradable MNs – these are made from dissolvable material mixed with the drug. The material starts to break down once inserted into the body, in doing so releasing the medicaments.

Hollow MNs – these are functionally similar to hypodermic needles and inject the medicament into the patient after insertion.

The availability of the various types of microneedles has resulted in five types of microneedle mediated drug delivery techniques. These transdermal drug delivery methods are:

- Dip and scrape
- Poke and patch
- Coat and poke
- Poke and release
- Poke and flow

The method by which they achieve their drug delivery capabilities differs and can be seen in Figure 2.3.

Various materials and manufacturing methods are used to produce these microneedles. These different microneedles and their manufacturing methods will be examined in the following section.

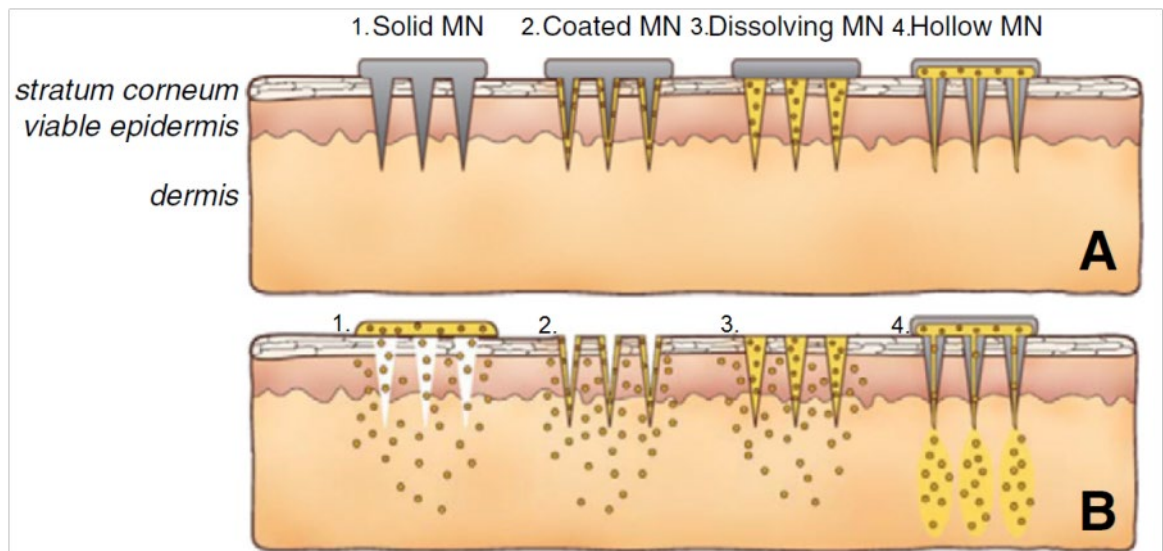


Figure 2.3: Section A illustrates four main types of microneedles: solid, coated, dissolving and hollow microneedles. Section B illustrates the drug delivery methods: Poke and patch, Coat and poke, poke and release, poke and flow. Kim et al. 2012.

2.6.3.1. Solid Microneedles

The first study on microneedles was conducted by Henry et al on solid microneedles (Henry et al. 1998). They tried to determine whether microneedles could be used to increase transdermal drug delivery. The solid microneedles were embedded in cadaver skin, causing the permeability of calcein to significantly increase.

Solid microneedles can be used for different drug delivery methods that share some similarities. These two methods are dip and scrape and poke and patch. They are similar in the fact that they both use solid microneedles but differ in the way the drug is applied to the patient.

Dip and scrape method – as the name suggests the solid microneedles are dipped into a liquid solution of the drug. They are then scraped repeatedly across the skin. The medicaments pass into the viable tissue through the small abrasions created by the scraping of the stratum corneum. Dip and scrape has been used to vaccinate against anthrax (Mikszta et al. 2005) hepatitis B (Mikszta et al. 2002), Japanese encephalitis (Dean et al. 2005), and rabies (Laurent et al. 2010).

Poke and patch method – this is the oldest and the most often described solid microneedle method found in the literature. An array of solid microneedles is depressed onto skin, resulting in micro channels being formed in the stratum corneum (Kalluri et al. 2011). Following the removal of the array, a path containing the drug suspended in cream, lotion or gel is applied (Gupta et al. 2011). The medicament diffuses through the channels created by the initial “poke” step and into tissue. They can be used for either local effect on the site of insertion or for systemic treatment via the capillaries and the immune response system.

Once these small channels have been created in the stratum corneum, they will automatically seal in a few hours. If required they can be kept open for up to a day (S. Banks et al. 2011) so no repeat poking or scraping will be required.

Various solid microneedles have been made and can be found in the literature. Kim et al. gathered several of these and presented them in their paper (Kim et al. 2012). Figure 2.4 shows some of these.

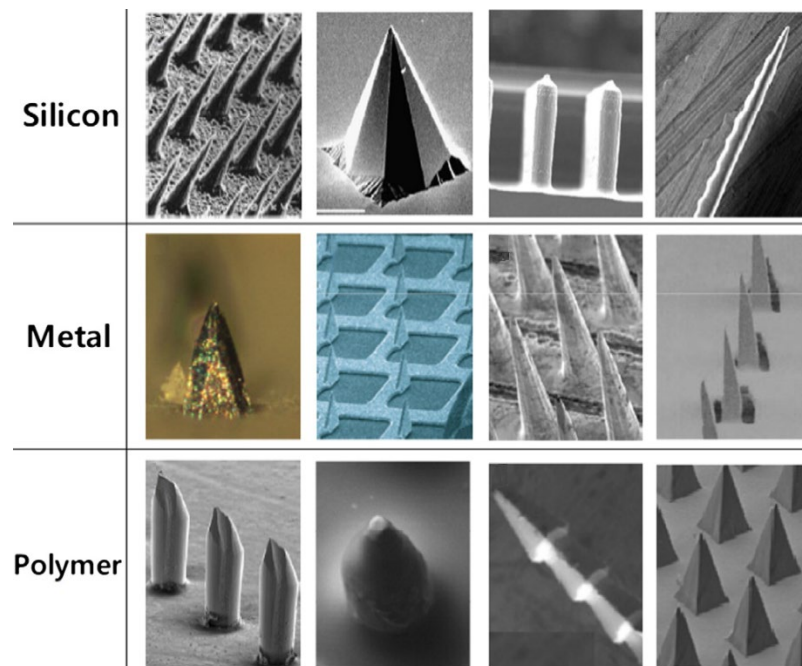


Figure 2.4: *Solid microneedles have been made from a variety of materials
Adopted from Kim et al. 2012.*

2.6.3.2. Drug-coated Microneedles

Matriano et al, examined the use of microneedles for the delivery of a model protein antigen (Matriano et al. 2002). They coated model protein antigen onto the needle surface and examined their effectiveness. Those microneedles were prepared with a dry-film coating of antigen. Using a high-velocity injector, the coated solid microneedles were then inserted into the skin of hairless guinea pigs. This drug delivery method was then referred to as coat and poke.

Coat and Poke method – during the manufacturing of these solid microneedles, they are pre-coated with the drug in a water-soluble formulation. These pre-coated microneedles can then be inserted into tissue. Similar to the method used by Matriano et al in 2002, high velocity injector can be used to facilitate better insertion. The microneedles are then left in the skin for a few minutes to allow dissolving of the coating; from the surface of the microneedles into the skin.

Various coated microneedles have been made and can be found in the literature. Kim et al. gathered several of these and presented them in their paper (Kim et al. 2012). Figure 2.5 shows some of these.

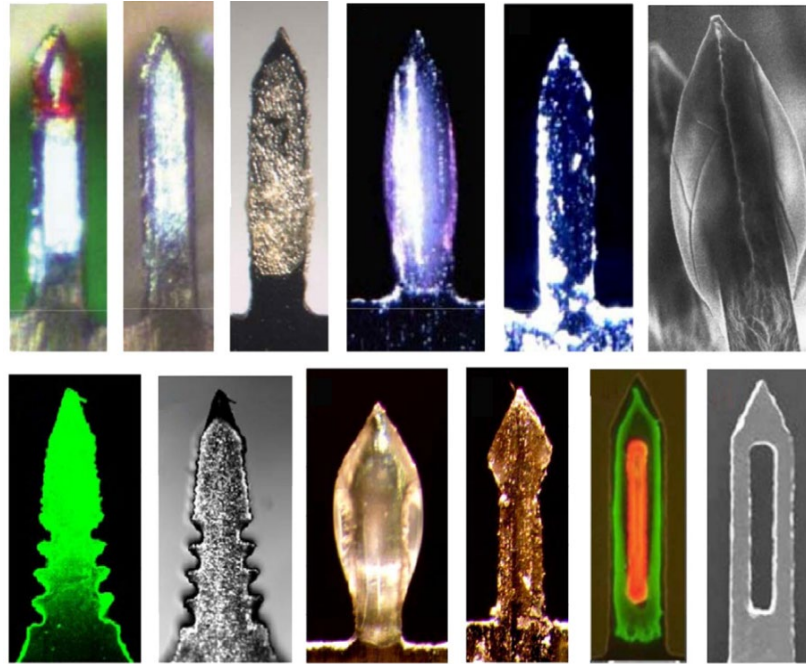


Figure 2.5: Coated microneedles that have been presented in the literature. Adopted from Kim et al. 2012.

2.6.3.3. Biodegradable Microneedles

Unlike the other types of microneedles described above, biodegradable microneedles are designed to leave behind no biohazardous sharp wastes (Prausnitz et al. 2009). They are constructed from sugars and water-soluble polymers that can be dissolved once inserted into skin (Zhu et al. 2016). The method is called poke and release.

Poke and release - fabrication from biodegradable materials, that are also biocompatible, allows this type of microneedle to be inserted into the skin and be left behind. They can be made from cellulose, hyaluronic acid, polymers and other materials (Park et al. 2016). The other advantage of having microneedles manufactured from biodegradable and biocompatible materials is not having to worry about needle stick injury and fractured needles reaming in the body. Since they dissolve into the body it is possible to load needles with drugs and allow the natural dissolving action to release the medicament into the body. By mixing the medicament into the microneedle, it is possible to enhance the stability of the drugs (Park et al. 2016). The rate of release can be controlled by adjusting the dissolving rate of the microneedles.

Various biodegradable microneedles have been made and can be found in the literature. Kim et al. gathered several of these and presented them in their paper (Kim et al. 2012). Figure 2.6 shows some of these.



Figure 2.6: *Biodegradable microneedles presented in the literature. Adopted from Kim et al. 2012.*

2.6.3.4. Hollow Microneedles

Hollow microneedles are very similar to solid microneedles but differ in one very important way. They contain a bore through the needle; allowing the transportation of drugs through this channel and into the skin. Hollow microneedles also allow for blood and other bodily fluids to be extracted. This method of drug delivery is called poke and flow.

Poke and Flow – using hollow microneedles it is possible to deliver drugs through slow diffusion or pressure-driven flow for rapid rates of delivery (Gupta et al. 2011). Once the needles are inserted into the skin then the fluid flows into the body. Rapid rates of delivery are one of the main advantages of hollow micro needles. Pressure can be used to inject the drug quickly into the body, therefore, achieving a quick altering the bloods medicament concentration level. Variable diffusion rate can also be achieved when required. By altering and controlling the pressure it is possible to precisely control diffusion rates of drugs into patients. There are various examples of pressure controlling devices used with hollow microneedles. These can be as simple

as springs (Burton et al. 2011) to complicated piezoelectric motors and micro-fluid pumps (Ali & Nagib 2011), (Ashraf et al. 2010).

Fluid extraction – as discussed previously, hollow microneedles can be used to deliver drugs and extract bodily fluid. Advances in technology have resulted in very small quantities of blood being required for biochemistry testing. There are several publications showing the hollow microneedles being used to extract Nano litres of blood for blood glucose level testing (Wang et al. 2005), (Gattiker et al. 2005), (Li et al. 2009).

Various hollow microneedles have been made and can be found in the literature. Kim et al gathered several of these and presented them in their paper. Figure 2.7 shows some of these (Kim et al. 2012).

To meet the requirements of the various microneedle types and drug delivery methods a range of materials and manufacturing methods have been used. There is a strong relation between the material choice, manufacturing technique, geometry and the intended use. The material and the manufacturing methods used to produce microneedles is explored in the following section.

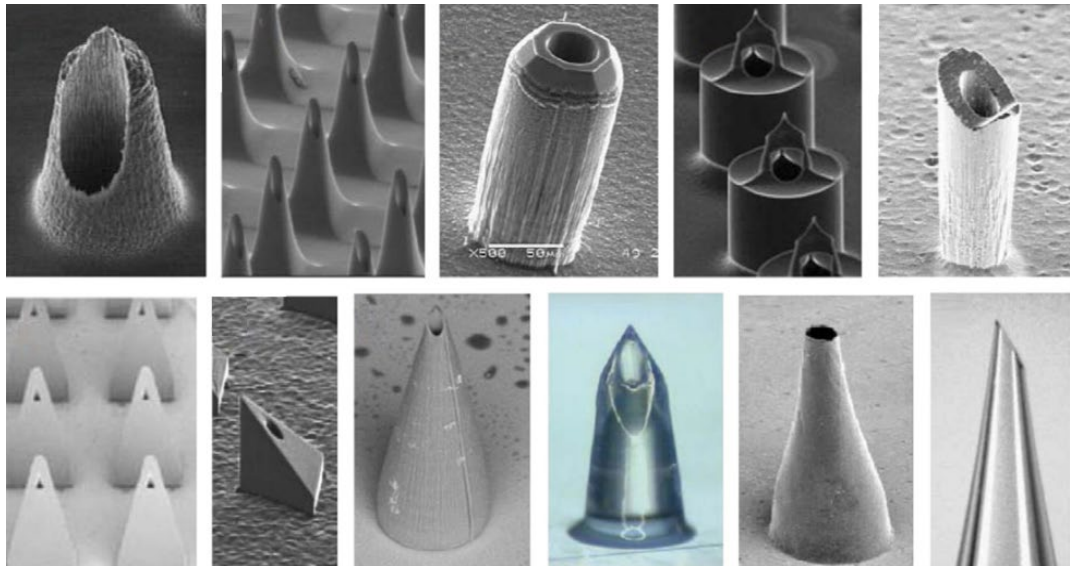


Figure 2.7: *Hollow microneedles presented in the literature. Adopted from Kim Y., 2012.*

2.6.4. *Materials and Manufacturing Methods*

Microneedles can be made from a range of ever increasing materials. Ceramics, metals and polymers have been used to produce microneedles destined for transdermal drug delivery. Several different manufacturing techniques have been demonstrated to have the capability of producing MN arrays. Manufacturing techniques such as surface and bulk-micromachining (Lin & Pisano 1999); (Gardeniers et al. 2002), reactive ion etching microfabrication (Henry et al. 1998); (Griss & Stemme 2002); (Trautmann et al. 2003), polysilicon micro-moulding (Zahn et al. 2000), chemical isotropic etching (Stoeber & Liepmann 2000); (Shikida et al. 2004), injection moulding, followed by laser drilling (Trichur et al. 2002) can be used to produce MN arrays. Each material has its own manufacturing methods associated with it.

Ceramics – can be used for producing solid, coated and hollow microneedles, but not for biodegradable microneedles. Excellent performance can be expected under loading conditions but shear forces could cause the brittle material to brake and imbed itself into skin. Careful geometry selection can increase shear force resistance.

A simple fabrication technique such as micro moulding can be used to create small ceramic protrusions. Ceramic slurries can be poured into silicone polymer (polydimethylsiloxane, PDMS) moulds then sintered (Bystrova & Luttge 2011). Other more complicated manufacturing methods involving lasers, lithography and photosensitive polymer–ceramic hybrids have also been used (Ovsianikov et al. 2007). In 1998 Henry et al used silicon to produce the first microneedles. They used techniques that were initially developed for the production of Micro Electro-Mechanical Systems (MEMS) and silicon chips. The methods that have been described utilise the dry etching process, which is based on reactive ion etching with a chromium mask. Solid microneedles can also be formed using anisotropic wet etching process that uses alkaline solutions (Wilke et al. 2005).

Wet etching process can be cheaper than dry etching, but there will be geometrical limitations restricted to anisotropic etching along crystal planes by the etchant (Chen et al. 2010). Ji et al overcame the limitations of wet etching through combining isotropic dry etching and anisotropic wet etching (Ji et al. 2006).

Metals – used to produce solid, coated and hollow microneedles. Metals can maintain their shape during skin insertion and can withstand some shear forces without breakage. Other advantages of metals are biocompatibility and ease of sterilisation. Laser cutting (Yuzhakov 2010), laser removal (Omatsu et al. 2010), electroplating (Choi et al. 2010) and wet etching (Matriano et al. 2002) have been used to produce metal microneedles. It is possible to use both sheet and bulk material to make metal microneedles. Small “V”s can be cut into sheets of stainless steel and titanium then bent to an angle of 90° to form the microneedles. Stainless steel and titanium were chosen because of their biocompatibility. Micro moulding techniques have also been used to produce aluminium microneedles (Matteucci et al. 2009).

Polymers - received significant interest recently due to its biocompatibility and dissolvability properties. Moulds have been made using photolithography and light curable polymers. These moulds can then be used to mass produce other microneedles. A polymer known as SU-8 is often used in conjunction with ultraviolet light to make small structures. SU-8 is an epoxy-based photoresist. The exposed part solidifies and the unexposed part is washed away therefore it is referred to as a negative photoresist. Using rotation and glass lenses it was possible to create tapered microneedles. There are various examples of SU-8 being used to create polymer microneedles (Yoon et al. 2006) and (Park et al. 2007).

Poly methyl methacrylate (PMMA) has also been used to make polymer microneedles. Producing these needles requires the material to be exposed to deep X-rays lithography (Sugiyama et al. 2004). This technique is known as Lithographie, Galvanoformung und Abformung (LIGA). Translated to English it means Lithography, Electroforming (electroplating) and Moulding which is explanatory to the forming process (Han et al. 2007). These methods can be used to produce needles that are a few millimetres in height with a narrow base.

Micro moulding techniques can also be used with thermos plastic to produce solid polycarbonate microneedles (Han et al. 2007). For poke and release drug delivery, water-soluble and biodegradable polymers with the drug mixed into the polymer have been produced using the moulding technique. Once these needles enter the skin, they

start to break down and dissolve into the tissue. As they dissolve the medicament is released into the body.

Currently MNs are mostly manufactured from polymers and ceramics but these materials have their drawbacks. Polymers have a low Young's modulus and an aspect ratio of 12:1 can be achieved (Park & Prausnitz 2010). Ceramics are known to be very brittle and can break during insertion into the patient, therefore, metals should be considered. The properties of metals are more suitable for MNs as they have a higher Young's modulus than polymers but are less brittle than ceramics. Rosochowska, et al. have demonstrated that it was possible to fabricate metal micro pins using backward extrusion (Rosochowska et al. 2010).

2.6.5. Microforming

Everything appears to be getting smaller these days. As the drive for achieving ever so smaller components increases so does the need for manufacturing methods to adapt. Although the components are getting smaller, the service demands are still similar to those of the previous macro components, therefore, material selection is critical. Due to the well documented properties of metals, the demand for metal micro components has increased. The electronics and medical devices industries are examples of clients that are driving the miniaturisation technology requirements.

As previously discussed there are various manufacturing methods that can be used to produce micro components. Large scale production with high accuracy can be achieved by lithographic technologies such as LIGA-processes but the available materials are limited and component costs are high (Gillner et al. 2000). Most of the manufacturing methods have been adapted from the electronics and semiconductor industry but there are also shaping and forming methods available in the conventional forming domain. Precision turning and milling can still be found in some components for luxury watches, but these are often produced in very small numbers and produced at very high cost, therefore, not suitable for low value high volume products.

One such manufacturing method that could be suitable for low value high volume components is microforming. Microforming is the method of producing metal parts

with at least two dimensions measuring under one millimetre (Fu & Chan 2013). This method can achieve small dimensions, close tolerance requirements and at high production rates. By using a single die, it is possible to lower production costs of the components (Hanada et al. 2003).

The microforming process appears simple and straight forward at first sight but decreasing the size of a component past a certain point presents its own challenges. Conventional forming knowledge and material behaviour cannot be applied due to several reasons. It is important to examine different aspects of microforming prior to initiating production. An in-depth analysis of microforming must be carried out to understand the microforming process, its challenges and methods of overcoming those challenges.

2.6.6. *The Microforming System*

Since the microforming process shares many similarities to conventional forming methods, four main considerations can be made. These considerations are Material, process, tool and machinery. These aspects will be examined from the viewpoint of microforming.

Material –material behaviour changes as the size of the component decreases past a certain point. This is due to the “size effects”. The size effect is connected to the billet size, shape, microstructure, surface topography as well as the lubrication usage. As the forming process is scaled down, those factors remain unchanged, therefore, leading to a different metal flow behaviour (Messner et al. 1994).

Process – scale reduction influences the process. The forming force, the spring back scatter the friction results are all affected.

Tools – manufacturing the tools required for microforming can be challenging. The tools required for microforming are often very small and have very good surface finish as well as having very close tolerances. New manufacturing methods have been developed that can overcome these difficulties. Photolithography and anisotropic etching techniques (Saotome & Iwazaki 2001), electric discharge machining (EDM) (Engel & Eckstein 2002) and micro EDM (Uhlmann et al. 2005).

Machinery – challenges linked to machines or equipment grow with size reduction. Manufacturing micro components requires micro-handling equipment. Accurate manipulation of small components is critical to achieving good components. Inaccuracies deemed negligible for macro components can be critical for micro components. These clearances can influence the accuracy of the parts that are produced. Due to the small contact area and weight of the components, it can be difficult to grip small components. Often the parts do not separate from a gripper by themselves due to adhesion forces. Sanchez-Salmeron et al presented various problems and solution associated with micro handling (Sanchez-Salmeron et al. 2005). Engel and Eckstein discussed factors affecting micro formed components (Engel & Eckstein 2002) as illustrated in Figure 2.8 .

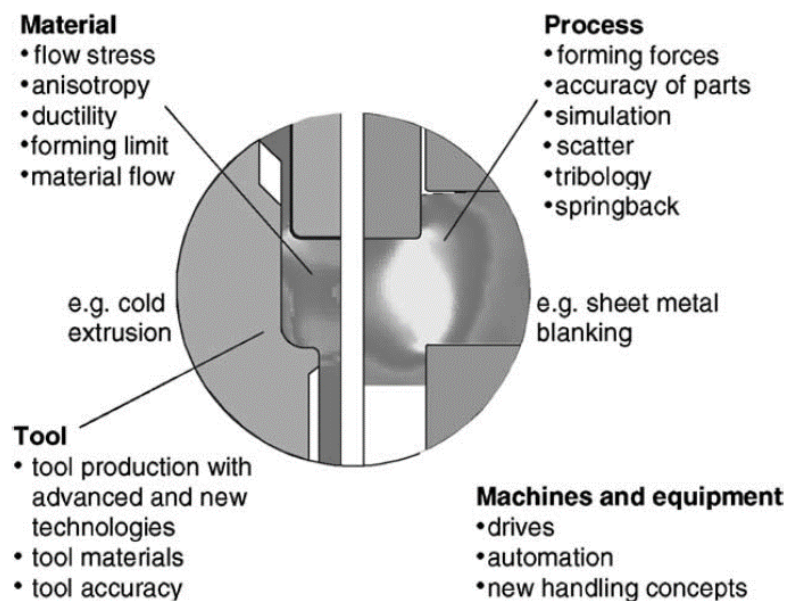


Figure 2.8: Factors associated with microforming. (Engel & Eckstein 2002).

2.6.6.1. Size Effect

As mentioned previously the size effect could play an important role in several aspects of microforming, therefore, will be discussed in greater depth.

The size effects can be relevant to all forming processes because it affects critical parameters; friction and material behaviour. A variety of tests (tensile, upsetting, air bending and punching (Geiger et al. 1997), have been used to determine the influence

of size reduction. These tests have shown that flow stresses decreased as the part size decreased. In 2013 Fu and Chan provided a diagram that illustrated the size effect related issues in micro forming processes and can be seen in Figure 2.9 (Fu & Chan 2013).

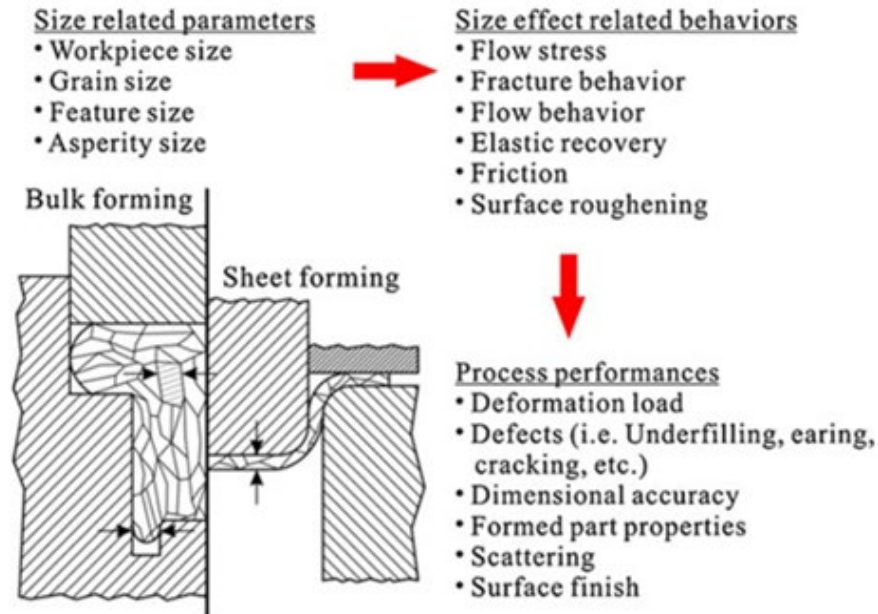


Figure 2.9: Size effect related issues in micro forming process (Fu & Chan 2013)

The ‘Surface Layer Model’ has been used to explain the reduction in the measured flow stress. In this model the material is not considered as a homogeneous continuum due to the ratio of grain size to billet dimensions. In a micro billet, the proportional number of grains representing the surface layer compared to the inner grains becomes high. As a result of size reduction the ratio of surface grains to volume grains increases as shown in Figure 2.10.

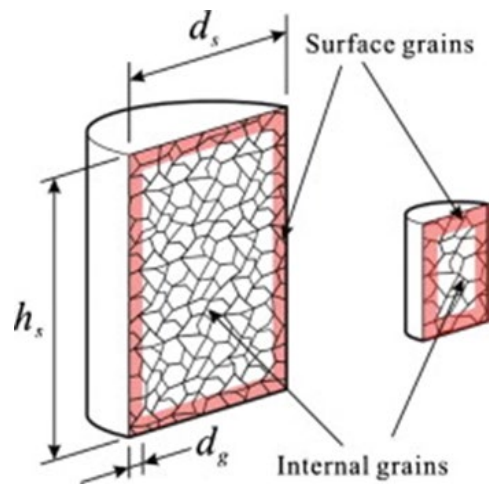


Figure 2.10: *The proportional number of the surface grains to the internal grains. Deng et al 2011.*

As a result of size reduction the ratio of surface grains to volume grains increases. The outer grains are constrained on less sides than the inner grains that are constrained on all sides. During the plastic deformation process, the surface grains behave differently than the inner grains due to lower constraint forces in the surface area therefore, the flow stress will be lower (Geiger et al. 1997). There are also other behavioural changes during microforming due to the size effect. These are explained in following:

Flow stress - increases with grain size as illustrated in (Chan et al. 2011) and decreases with the reduction of component size (Diehl et al. 2010). Flow stress the stress value derived from the load–displacement data measured during the mechanical testing.

Fracture – takes place through the localised shearing in the individual grain (Fu and Chan, 2011). Fracture strain increases with the reduction in component size during upsetting of bulk metal (Chan et al. 2012).

Flow behaviour – Flow behaviour means flow of workpiece/billet material under the influence of applied load. Material flow behaviour is also depends on the pre-deformation history of the starting materials where the billets are prepared. Non uniform flow causes the uneven filling of the die geometry. This worsens as the component size decreases and the grain size increases (Eichenhueller et al. 2007).

Elastic recovery – If a material is taken beyond the yield point and the applied stress is then removed, the material ends up with a permanent strain which is called as plastic deformation. The amount of elastic strain that material will take before reaching the yield point is called elastic strain recovery. Degree of elastic recovery is related to modulus of elasticity of the material. An increase in spring back is observed when the ratio of component thickness to grain size decreases (Liu et al. 2011).

Surface roughening – the measured roughness value to component size ratio increases with larger grain sizes and smaller component sizes (Chan et al. 2012).

Repeatability – due to less grains being available in the component the individual properties of the grain can become an important factor. Each grain has different properties therefore a variation in the material properties can be expected. The variation in the material properties increases with the reduction in component size and increased grain size (Diehl et al. 2010).

Mechanical property of the final component – It depends mainly on the size, shape of the fine grains formed and also on the nature of grain boundaries generated in the matrix as a results of severe plastic deformation occurring in SPD methods (Rosochowski et al. 2007),

Frictional – Based on the principle of lubricant entrapment in the asperities between the forming tool and billet, two types of lubricant modes expected in the case of lubricants used in metal forming process namely: closed lubricant pockets and open lubricant pockets. In the case of closed lubricant pocket formation, lubricant may not be able to escape due to the pressure imposed by the forming load that leads to development of hydrostatic pressure. This causes the lubricant to bear the applied load. In the case of open lubricant pocket formation, the lubricant can escape and may not be able to support the transmission of applied load (Vollertsen 2013). The ratio of open lubricant pocket increases with the reduced component size, which results in an increase in the interfacial friction between the tool and the component (Engel 2006).

2.6.7. Lubrication

As lubrication is a key factor in all forming processes, it is important to have a good understanding of the need for lubricants and the method of achieving their function. Not using lubrication or using the wrong lubrication will result in components that are not fully formed and have a rough surface finish. It can also result in adhesion and galling (Taureza et al. 2014). Understanding the frictional behaviour during the microforming processes will allow accurate components to be produced that also have the required reduced surface roughness.

The profile of the component surface is often referred to as the topography. This is due to the peaks and valleys that can be observed when high magnification is used.

The component to be formed has a certain surface topography and so has the forming tool. It is possible to quantify amount of variation in the surface topography by using the roughness value. Various roughness factors are available such as average roughness and maximum and minimum heights. It is also important to distinguish roughness from changes in surface profile. Secondary surface treatments are often used to smoothen the surface roughness of a new forming tool as tool surface roughness can have a detrimental effect on the surface finish of the components.

As well as conventional lubricants such as oil and grease, there are also less common methods such as conversion coating. In conventional lubrication methods such as the one shown in Figure 2. 11, prior to the tool coming in contact with the component surface, a layer of lubricant is applied. Initially some lubricant flows into the valleys and is trapped by the peaks. Once the tool comes into contact with the component, some lubricant is trapped in the roughness valleys. This trapped lubrication is referred to as closed lubricant pockets (CLPs). Fluids are non-compressible, therefore, these CLPs cause a hydrostatic pressure to be generated and some of the forming load acts onto the lubricant. With CLPs the material can slide along the tooling surface with low friction. It is also possible to squeeze the lubrication out of the roughness valleys. This is referred to as open lubrication pockets (OLPs). In OLPs, the peaks come into contact with the tool, therefore, share the deformation load. This results in these peaks to flatten and become the real contact areas (RCAs). As the RCA increases so does the

interfacial friction. As the compression continues, the material starts to flow outwards and the component to tooling interface area increases (Deng et al. 2011).

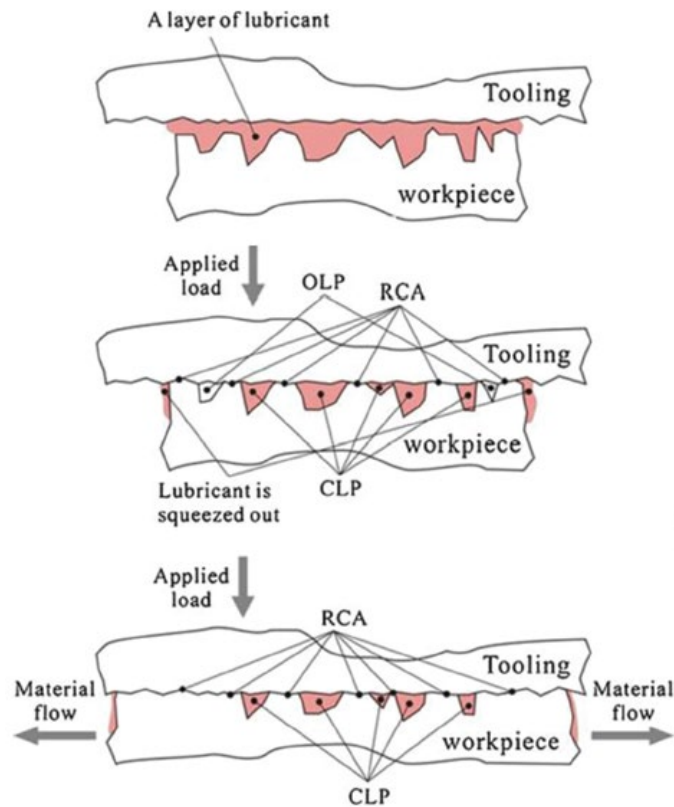


Figure 2.11: *Schematic diagram showing the evolution of surface topography during forming under liquid lubrication conditions. Deng et al. 2011.*

Double cup extrusion tests are often used to determine the impacts of size effect and lubrication (Vollertsen et al. 2004). Lubricants cannot be held efficiently in the area near the perimeter of the contact surface, therefore, RCA forms and the interfacial friction increases. Some authors (Tiesler 2002), (Engel 2006), suggest the size of OLP region does not change with component size and others (Deng et al. 2011) found the variation of OLP rim thickness is not proportional to the variation of specimen size. These were based on tests carried out on the compression of different scaled copper cylinders.

2.6.8. *Vibration-Assisted Microextrusion*

Small component sizes require good dimensional accuracy and reduced surface roughness. Tight dimensional accuracies and low surface roughness can be achieved

when high contact pressures are used with relatively large movement at the component to tool interface (Presz & Rosochowski 2006). High contact pressures can also lead to galling (Presz & Andersen 2007). As the component size decreases the appearance of galling can increase because of the worsening state of lubrication (Tiesler 2002). To prompt the uptake of microforming as a viable manufacturing method for small components it is necessary to minimise the likelihood of galling and other unwanted surface imperfections. Several research groups have investigated the use of vibration of the tool to overcome challenges of microforming.

Using vibration, it has been reported that a reduction in the forming force has been recorded as well as the improvement in the surface finish. Industrial usage of vibration forming is very limited due to the high energy cost as well as the added cost of implementing this method into existing heavy dies. These limitations would be less significant when vibrations are applied to microforming as the dies are usually smaller, therefore, lighter and less powerful vibration devices would be required. Vibration forming might not be economically viable for the large component forming sector but the advantages that it presents would make it an ideal candidate for microforming components.

Vibration has been applied in various processes, such as deep drawing (Jimma et al. 1998), extrusion (Mousavi et al. 2007) and upsetting (Hung et al. 2007). Mousavi investigated conventional forward extrusion and applied ultrasonic. The die was stationary while the billet was extruded into the die opening. Mousavi concluded that the extrusion force and the stress required for material to flow would be reduced by applying the ultrasonic vibrations if the extrusion speed was below the critical speed based on the results of the investigation. Mousavi also reported that applying the ultrasonic vibrations had no significant effect on the equivalent plastic strain of the material. A larger reduction in average extrusion force was obtained by either reducing the extrusion speed or increasing the amplitude of vibrations (Mousavi et al. 2007).

This reduced interfacial friction between the tool and the component and the flow stress resulting in greater formability and surface finish. Subsonic vibrations can also be used to reduce friction as well but ultrasonic frequencies have shown to reduce the

yield strength of the material due to acousto-plastic effect, therefore less load is required during forming. Bunget and Ngaile also introduced vibration to the microforming process to enhance the material flow along die surface (Bunget & Ngaile 2011). The three different setups used in Bunget and Ngaile study are shown in Figure 2. 12. The three setups are ultrasonic forward-rod extrusion, ultrasonic double cup backward extrusion and a combination of ultrasonic forward-rod-backward-cup extrusion process and forward-rod and backward-cup processes. The author describes three zones in each of the setups. For ultrasonic forward-rod extrusion Zone I is described as guiding zone, Zone II the deformation zone, and Zone III the exit zone. For ultrasonic double cup backward extrusion zones I and III where the lower and upper cups are formed and Zone II where plastic deformation occurs. For the combination of the ultrasonic forward-rod-backward-cup extrusion process and forward-rod and backward-cup processes setup Zone I is where the cup is formed, Zone II is where the dimension of the rod is decreased and Zone III is the exit zone. The author reported that when ultrasonic vibrations were imposed, the results showed a significant drop on the forming load. They also reported a significant improvement in the surface of the micro-formed parts. They concluded that their study demonstrated high potential for using ultrasonic oscillations as a way to overcome the difficulties that are associated with miniaturisation.

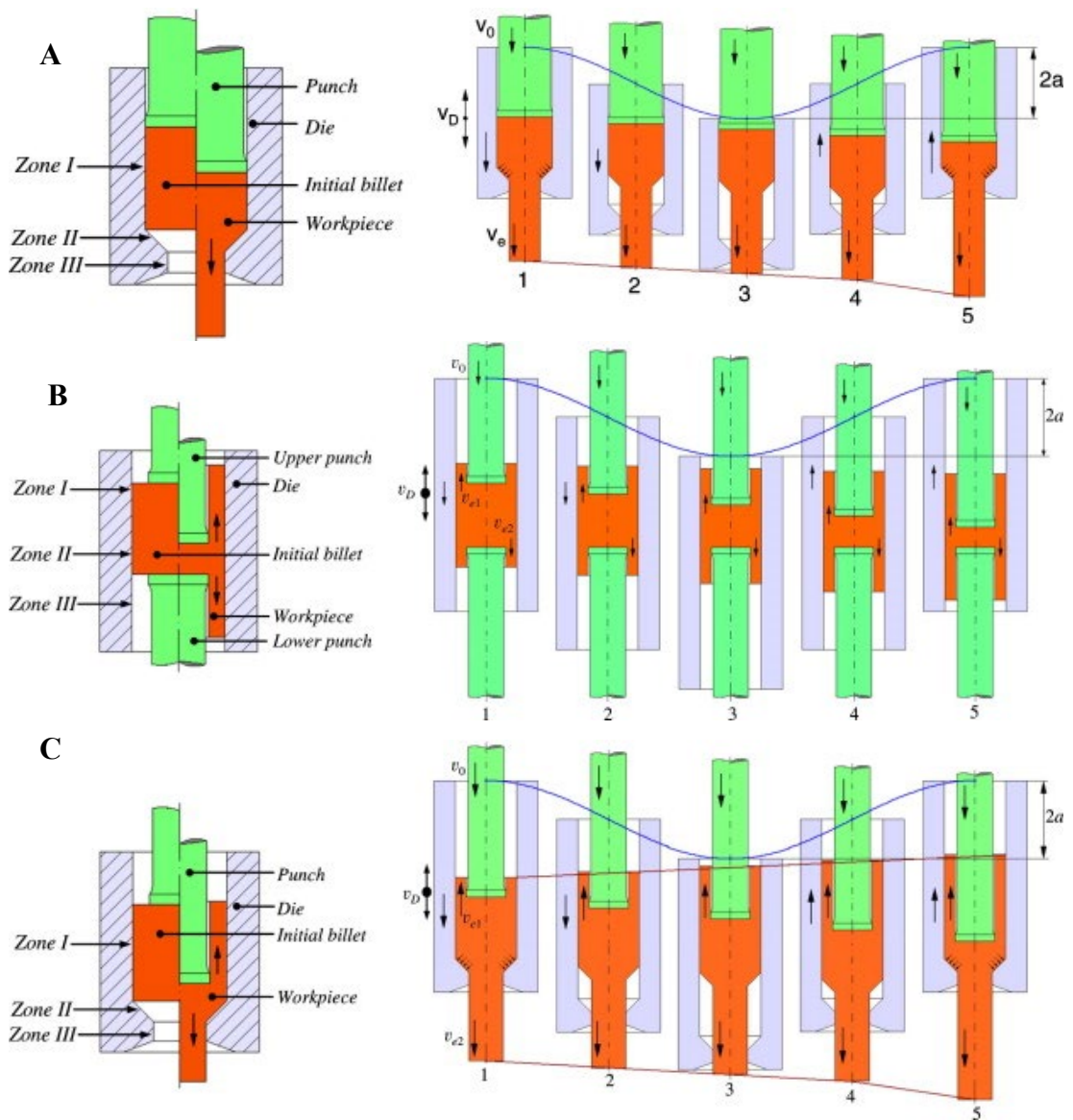


Figure 2.12: *Schematic diagram of A- ultrasonic forward-rod extrusion, B-ultrasonic double cup backward extrusion, C- combination of the ultrasonic forward-rod-backward-cup extrusion process and forward-rod and backward-cup processes (Bunget & Ngaile 2011).*

As the name suggests, in the vibration assisted microforming process, ultrasonic vibration is superimposed on the forming tools. Small gaps are created and closed between the component and the die with the oscillation movement. This will result in a change in the friction conditions and improve the component quality. Ultrasonic vibration assisted forming could resolve many of the problems associated with microforming, therefore, a more in-depth investigation is required.

2.6.8.1. Ultrasonic – Background

Ultrasonic is the branch of acoustics focused on the generation and use of sound waves propagating through fluids or solids at frequencies above human hearing range. The lowest ultrasonic frequency is normally taken as 20 kHz. The top end of the frequency is limited only by the ability to generate the signals. Frequencies in the gigahertz range have been used as well. Ultrasonic have a wide range of applications and *Figure 2.13* illustrates some of the *Common frequency ranges for various ultrasonic processes*

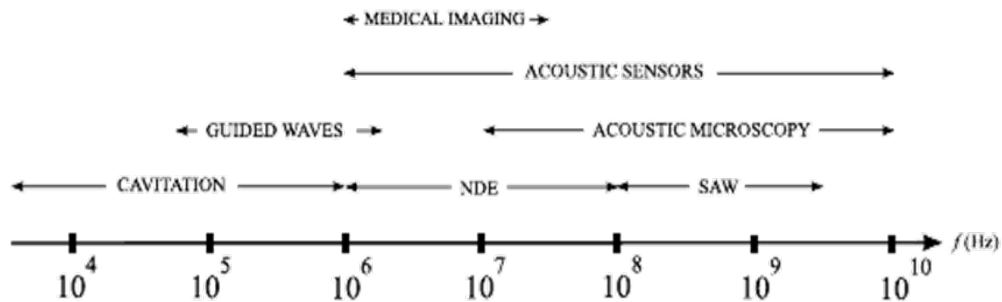


Figure 2.13: Common frequency ranges for various ultrasonic processes.

Historically ultrasonic vibrations have been used for a huge variety of applications. These can mostly be divided into two broad categories

- Low power ultrasound
- High power ultrasound

2.6.8.2. Methods of generating ultrasonic vibrations

To generate and maintain vibrations in an object, a transducer converts an electrical signal to mechanical motion. Depending upon the power, frequency and the media into which the ultrasonic waves are to be emitted, the proper transducer/emitter (radiator) is chosen for each case. There are different types of ultrasonic transducer; based upon the method they utilise to produce ultrasonic vibrations. These methods include mechanical, electromagnetic, laser generation, electrostriction, magnetostriction and piezoelectricity. To excite ultrasonic oscillations in liquids and solids, magnetostrictive and piezoelectric transducers are most frequently used (Severdenko et al. 1972).

2.6.8.3. Magnetostrictive Transducer

The magnetostrictive transducers are based on the magnetostrictive phenomenon. Magnetostriction is a change in dimensions (elongation or contraction) of a ferromagnetic material when it is subjected to an applied magnetic field.

A typical construction of magnetostrictive transducer consists of a coil of wire wrapped around a ferromagnetic metal core in the form of a winding. The wire in the transducer is powered with alternating current by a generator. An alternating magnetic field induced by the current in the core of the transducer, causes the core to stretch and contract at a rate determined by the frequency of the driving current. In doing so, it emits vibrational energy into another element (Ensminger & Stulen 2009). Typical magnetostrictive materials are nickel, nickel alloyed with iron, iron-aluminium alloys and permendur (an iron 49%, cobalt 49%, vanadium 2% alloy).

Magnetostrictive transducers are extremely robust and can work over a wide frequency band, therefore, tolerate frequency mismatching. They can be water cooled to maintain a high power throughput over a period of time, however, their main disadvantage is relatively low efficiency (60%). This is caused by non-linearity in the magnetostrictive effect, eddy currents in the core and resistance losses in the wire coils (Cheers 1995). The vibration amplitude generated by the transducer is thereby limited.

2.6.8.4. Piezoelectric Transducer

Pierre and Jacques Curie discovered the direct piezoelectric effect in single crystal quartz in 1880. Under pressure (tension or compression), quartz generated an electrical charge/voltage. Piezo comes from the Greek word 'piezein' which means 'to press'; hence the original meaning of the word piezoelectricity implied 'pressure electricity'. The term piezoelectric refers to producing electricity on specific faces of certain crystalline materials subjected to pressure.

Conversely, an electric field applied between the specific faces produces mechanical stresses (and consequently, strains) in the piezoelectric crystals. Applying alternating electric field to the crystals results in expansion and contraction at a rate determined

by the frequency of the applied field. This is the basis for the design of active piezoelectric transducers.

Piezoelectric elements are most widely used in today's commercially available ultrasonic transducers. Their physical characteristics make them readily adaptable to active devices (i.e. sources of ultrasonic energy) and passive devices (i.e. receivers) (Ensminger & Stulen 2009).

Using Quartz crystals, it is possible to generate ultrasonic waves of high power. Natural Quartz crystals are strong and have stable properties. Quartz also has good resistance to chemical action and its piezoelectric effects are almost independent to temperature (Bunget 2006). Other than quartz crystals, there are many materials that have piezoelectric properties. These are classified as single crystals and polycrystals. Generally, single crystals like SiO₂, LiNbO₃, LiTaO₃ and La₃Ga₅SiO₁₄, etc., have a steady construction of elements so their characteristics are stable. Polycrystals such as Pb(Zr.Ti)O₃, BaTiO₃, and PbTiO₃, etc. differ in that way (Uchino 2010).

A piezoelectric transducer comprises a number of piezoelectric discs that are clamped under compression between metal blocks by a high tensile screw. When alternating voltage is applied, the disks expands and contract - proportional to the applied voltage - transmitting vibrations to the blocks (Cheers 1995). The efficiency of a piezoelectric transducer is approximately 95%. However, the disadvantage is the narrow frequency bandwidth (Rosochowska 2003).

2.6.8.5. Transducer Selection

Most of the earlier works in the field of metal forming (during 1960's and 1970's) have used magnetostrictive transducers, mainly because piezoelectric transducer was not fully developed during that time. Recent publications (Cheers 1995), (Lucas 1996), (Siegert & Möck 1996), (Jimma et al. 1998), (Littmann et al. 2001), (Siegert & Ulmer 2001), (Lucas et al. 2009), have shifted from magnetostrictive to piezoelectric transducers. The reasons for this is that for the majority of uses, piezoelectric materials have been shown to be more efficient (i.e. maintain higher operating amplitude), less

expensive, fabricated easier, and require less complicated electronic circuitry for driving the transducers (Ensminger & Stulen 2009).

2.6.8.6. Ultrasonic Assisted Metal Forming

It has been observed experimentally that when ultrasonic vibrations are superimposed during static tension or compression loading, the metal specimen being tested would experience brief softening.

The application of ultrasonic vibration in metal forming has been discussed for many years. The very first use of ultrasonic or vibrational energy applied to metals was reported by Garskii and Efromov (Garskii & Efromov 1953). This was followed by Blaha and Langenecker (Blaha & Langenecker 1955). They conducted a compression test by using a zinc crystal. Initially a static tension load was applied to the metal. Then they applied ultrasonic vibrations to the metal at a frequency of 800 KHz. When the ultrasonic vibrations were activated during the plastic deformation, the reading of the static compression force was reduced by 40% (see curve A in Figure 2.14). It can be seen that during the time period when ultrasonic vibrations are superimposed on the static load, the flow stress is significantly reduced and when the ultrasonic vibration is removed, the flow stress increases to the normal value.

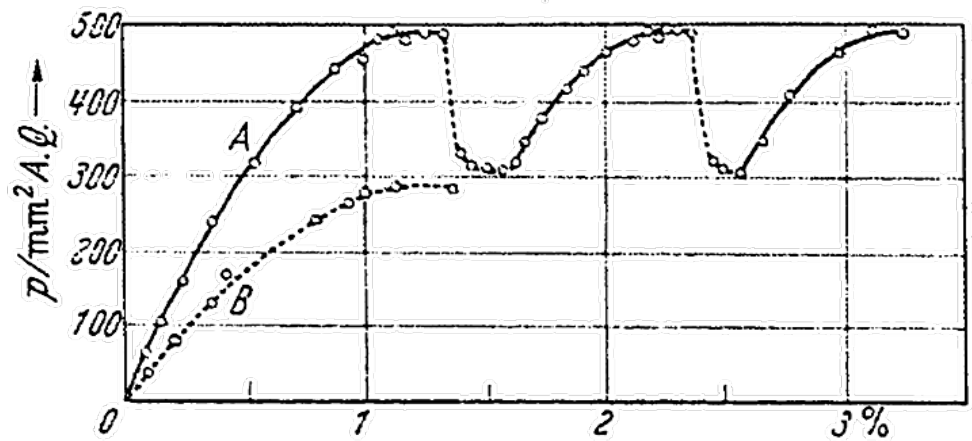


Figure 2.14: *Blaha and Langenecker observed the first Acousto-Plastic Effect. Blaha and Langenecker, 1955.*

In another test, (Blaha & Langenecker 1955) simultaneously applied ultrasonic vibrations with the static tension load from the start of the experiment (see curve B in

Figure 2.14). The stress-strain curve from this test followed curve B, instead of curve A, and the yielding stress of curve B is about 40% less than curve A. They concluded that the applied ultrasonic vibrations caused a much lower yield stress than the regular yield stress of zinc crystal. This phenomenon is, therefore, often referred to as Blaha effect and is also known as the acoustoplastic effect. They further observed that the magnitude of stress reduction was dependent on the amplitude of vibration but was independent of the excitation frequency for the ultrasonic range.

2.6.8.7. Acoustoplastic Effect

The acoustoplastic effect has been described as a decrease in the flow stress during the plastic deformation at a constant strain rate (Blaha & Langenecker 1955), (Izumi et al. 1966a), (Izumi et al. 1966b), (Baker & Carpenter 1967), (Kaiser & Pechhold 1969), (Endo et al. 1979), (Ohgaku & Takeuchi 1987), (Kirchner et al. 1984) or an increase in strain rate under a constant stress (Malygin 2000), which is observed when an oscillatory stress of a sonic or an ultrasonic frequency is superimposed to the deforming crystal.

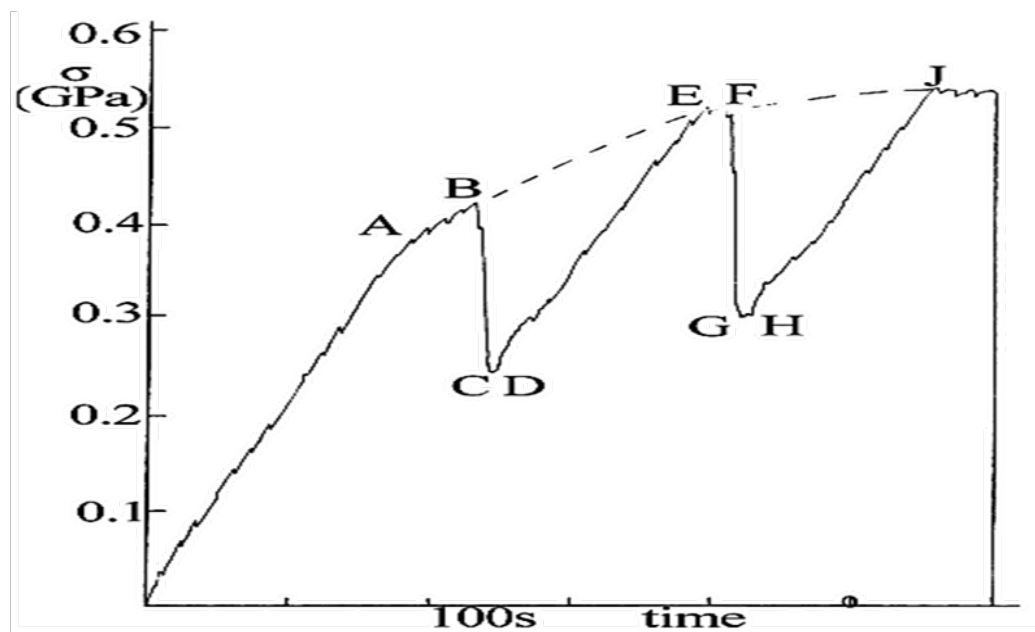


Figure 2.15: *The acoustoplastic effect reported by Kirchner et al, 1984. Adapted from Kirchner et al, 1984.*

Many researchers have conducted similar natured experiments to study the acoustoplastic effect, after the initial findings of Blaha and Langenecker. Figure 2.15 shows a typical effect test that was reported by Kirchner et al in 1984. Hourglass shaped Aluminium alloy 6061, were used as test specimens. A quasi-static compression load, increasing at a strain rate of 1×10^{-4} per second was applied on the specimens. This load was superimposed by a 20 KHz of cyclic loading through a double resonator. As can be seen in Figure 2.15, when the vibratory loading was activated at point B, the measured mean stress decreased considerably to a lower point C. After subsequent deactivation of vibrations at point D, the stress increased and returned to point E on the original static stress-strain curve. The process is repeated again and similar effect can be observed in the following points.

In several other publications reporting the results of tension test, for single crystal of aluminium, cadmium, beryllium and polycrystalline zinc, similar results were obtained when longitudinal mode ultrasonic vibrations was applied continuously or intermittently throughout the test (Winsper & Sansome 1967), (Tisza 1983a), (Tisza 1983b).

2.6.8.8. Ultrasonic Oscillations Force Reduction

Langenecker (Langenecker 1966) observed that applying ultrasonic excitation to the tool or the work piece during metal forming operations, resulted in useful effects such as reduction in process stress (lower static force required to deform material). As a result, higher deformations can be achieved in single stage and, therefore, less passes are required to obtain the finished product.

The beneficial reduction in stress can be attributed to the “volume effect” and the “surface effect”. The volume effect also known as ‘softening effect’, is related to a reduction in flow stress of the material being deformed. The surface effect is related to a change in frictional conditions at the interface between the vibrating tool and component.

2.6.8.8.1. Volume Effects

The volume effects are connected with the reduction in the flow stress which can be explained by localised heating as well as the stress superposition mechanism. The ultrasonic movements induced in the forming process propagates into the material and is scattered and absorbed. This causes energy loss and heat generation. The heat that is generated locally can be very high, therefore, resulting in the lowering of the flow reluctance of the material. The energy will also be absorbed in the dislocations causing them to move; resulting in the lowering of the flow stress (Blaha & Langenecker 1955).

2.6.8.8.2. Surface Effects

The surface effects are connected to the variation of the frictional conditions at the tool and component interface. Better lubrication can be achieved due to elastic strain relaxation. Lubrication can flow into the gap between the tool and component as the tool oscillates. The lubrication pocket and the separation of surfaces will reduce the frictional stress. After every cycle of oscillation, this gap will be closed. The roughness peaks at the contact surfaces will experience elastic and plastic deformation. This elastic and plastic deformation can result in further localised heating. The increased temperature at the tool and component interface can have an effect on the behaviour of the lubricant.

Forming techniques are often seen as a cheap method of producing large numbers of components. When microforming is utilised for micro components it could drastically reduce the cost of producing micro components while achieving greater productivity. Micro forming can suffer from several challenges such as high flow stresses, high surface roughness, poor lubrication and galling. Note that flow stress depends on the chemical composition (alloying elements), microstructural and deformation state (work hardened/ stress relieved) of the material. As discussed earlier the flow stress increases with reduced component (needle) size, but utilising ultrasonic vibrations could overcome those challenges, while improving lubrication and component surface quality as well as eliminating galling. Size of the component may affect the load

required for the forming. A combination of the two manufacturing techniques could allow metal microneedles to be formed at high volume and low cost.

The microstructure of the material is also a very important factor as illustrated in Figure 2.16. In conventional metal forming operations materials are normally considered as homogeneous. Due to their relatively large grains size to the billet volume they could be considered as heterogeneous in microforming processes. Using relatively large grains can result in void in the formed micro component.

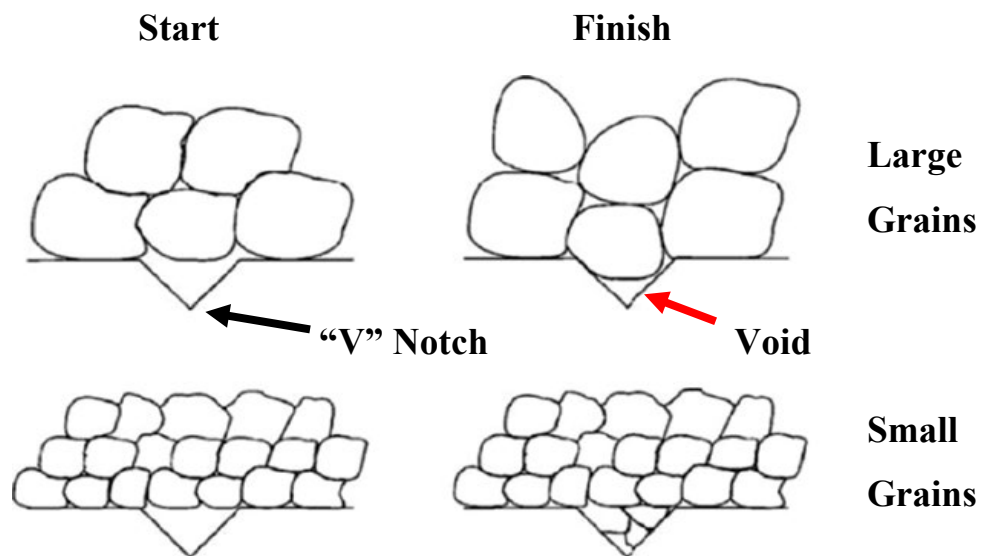


Figure 2.16: Illustration comparing large grain and small grain for filling a small “V” notch. Adapted from Saotome et al. 1998

2.7. GRAIN REFINEMENT

2.7.1. Severe Plastic Deformation Processes:

Plastic deformation techniques are most widely used in industries to shape materials to the desired geometry with the required mechanical properties. By controlling the amount of deformation that is induced in the material, superior mechanical properties can be achieved in the final product.

Conventional mass production forming processes such as rolling and near net shape processes such as forging and extrusion are the most widely used for manufacturing industrial components. Mode of deformation activated is combination of tension, compression (plain-strain) and shear.

In all these above mentioned processes, depending on the shape and size of the component, the amount of imposed strain and also the strain mode have limitations to reduce the grain size below few tens of micron. To produce bulk materials with ultra-fine grains (i.e. grain size below 1 micron), variety of severe plastic deformation techniques are developed and explored nowadays. Shear mode of deformation occurring in the materials subjected to severe plastic deformation technique lead to formation ultra-fine grains with large fraction of high-angle grain boundaries. Low angle grain boundaries created as result of recovery process during deformation will transform in to high angle grain boundaries as amount of strain imposed in the material increases. Advantage of these severe plastic deformation techniques is high level grain refinement has been made without much change in the external dimensions of the billets processed. Different mechanisms like dynamic recovery and dynamic recrystallization are believed to the main reason behind in formation of fine grains with high angle grain boundaries. Due to this bulk ultra-fine grained materials with exceptional combination of strength and ductility is developed.

UFG materials have several advantages when compared to coarse grained materials:

1. Increased strength – due to more grain boundary areas through the Hall-Petch relationship. Hall-Petch relation relates the grain size and tensile strength of the material. Grain refinement occurring in these process is due to formation of grain boundaries as a results of dynamic recovery process which leads to increase in the number fraction of grain boundaries within the pre-existing grains. This causes enhancement in the strength of material.
2. Exhibiting excellent superplastic ability at relatively lower temperatures

There are several different Severe Plastic Deformation processes available; which will be further explained in the following section. These are:

- Equal channel angular pressing (ECAP) or also previously called Equal channel angular extrusion (ECAE)
- Accumulative roll bonding (ARB)
- High pressure torsion (HPT)

- Constrained groove pressing (CGP)
- Cyclic extrusion and compression (CEC)
- Multi axis forging (MAF)
- Equal channel angular drawing (ECAD)
- Twist –Extrusion (Reshetov et al. 2017)
- Conshearing process

2.7.2. *Equal Channel Angular pressing (ECAP) or Extrusion (ECAE)*

The concept of ECAE was first introduced by Segal in a Russian patent (Segal 1977) and discussed in following papers (Segal et al. 1981); (Segal 1995). Equal channel angular extrusion is a severe plastic deformation technique, which is used to induce large amount of plastic strain into a material without much change in the cross-section of the work piece (Sklenicka et al. 2012). The schematic diagram of an ECAE die is shown in Figure 2.17.

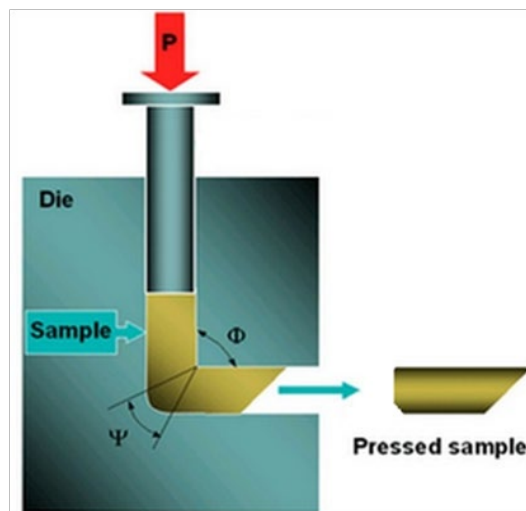


Figure 2.17: *Schematic diagram of an ECAE operation – die, tool, billet and workpiece. Adapter from Sklenicka et al. 2012.*

The tool consists of two intersecting channels of same cross section meeting at an angle of ϕ . The values of ϕ generally varies from 90° to 135° . The work piece is extruded from the top channel to the bottom channel with the help of hydraulic ram under well-lubricated conditions. The deformation of the material happens at the

intersecting channel and the material is deformed by simple shear at ideal, frictionless conditions. Since the cross-section of the specimen remains the same, before and after deformation, it is possible to subject the same specimen several times to ECAP so that highest degree of plastic deformation is attained.

The strain imposed on the sample in ECAE depends primarily on the angle ϕ between the intersecting channels, but also to a smaller extent the angle ψ represented by the outer arc of curvature (Bowen et al. 2000).

The total strain accumulated in the material after 'N' number of passes, ε_N , is given by (Iwahashi et al. 1996).

$$\varepsilon_N = \frac{N}{\sqrt{3}} \left[2 \cot \left(\frac{\phi}{2} + \frac{\psi}{2} \right) + \operatorname{cosec} \left(\frac{\phi}{2} + \frac{\psi}{2} \right) \right]$$

For a sharp corner die, $\psi = 0$, then

$$\varepsilon_N = \frac{N}{\sqrt{3}} [2 \cot \phi]$$

Similarly, the magnitude of the shear strain γ when the material passes through the shearing plane is given by

$$\gamma = 2 \cot \left(\frac{\Phi}{2} + \frac{\Psi}{2} \right) + \Psi \operatorname{cosec} \left(\frac{\Phi}{2} + \frac{\Psi}{2} \right)$$

When a material is subjected to more than one pass in ECAE, rotating the sample by certain angle between the following passes produces different shearing characteristics in the material. Iwahashi et al experimented on modifying the shear plane (by rotating the sample between consecutive passes) and reported that it was possible to develop different microstructures and textures in the material - (Iwahashi et al. 1998). In general, four different processing routes are commonly employed in ECAP/ECAE.

Route A – specimen is not rotated between consecutive passes

Route BA – specimen is rotated by 90° clockwise and anti-clockwise alternatively between consecutive passes

Route Bc – specimen is rotated by 90° clockwise between consecutive passes

Route C – specimen is rotated by 180° between consecutive passes

Figure 2.18 shows the deformation behaviour of a cubic element during one pass of ECAP and it is possible to see that the deformation is simple shear mode because it occurs on only one principal direction (Furukawa et al. 2001). Figure 2.18 also shows the shearing behaviour of a cubic element with the increase in the number of passes for the different processing routes of ECAP (Furukawa et al. 1998).

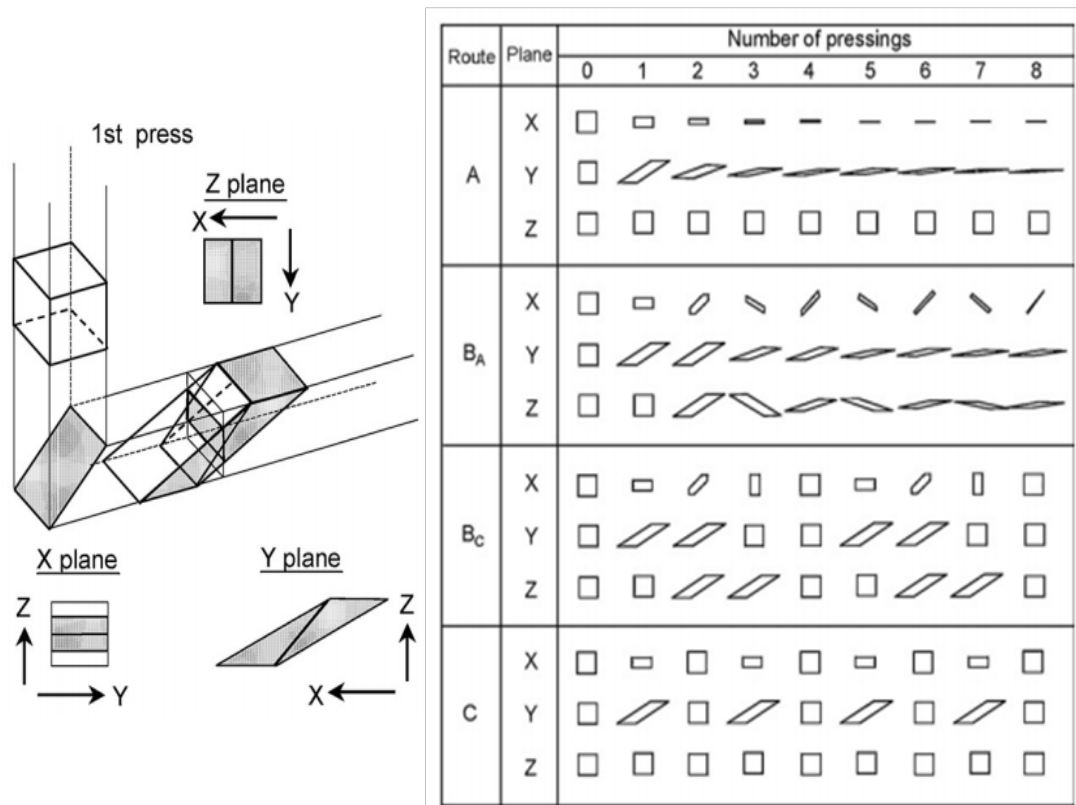


Figure 2.18: *Left: Deformation behaviour of a cubic element during a single pass in ECAP*
Right: Shearing behaviour of a cubic element with the increase in number of passes during different processing routes of ECAP.
Left: (Furukawa et al. 2001), Right: (Furukawa et al. 1998).

Although ECAP/ECAE are often used to produce UFG material this is a drawback to using the process. As the length of the channel and billet increase so does the frictional forces experienced by the billet during processing, but utilising short billet lengths results in poor utilisation of the material. Combining short billets and the accosted end effects can result in utilisation of less than 50 percent of the billet (Olejnik & Rosochowski 2008).

2.7.3. Incremental ECAP process

In response to some of the problems associated with conventional ECAP/ECAE, a new SPD process, called incremental ECAP (IECAP), was proposed by Rosochowski and Olejnik (Rosochowski & Olejnik 2007). The main difference between ECAP and IECAP is separating the feeding and deformation step. In a way this will reduce the friction between billet surface and the die walls during the process. Hence it leads to possibility of processing fairly long billets. Using the IECAP process it is possible to process bars (Rosochowski et al. 2008) and plates (Olejnik et al. 2008). A schematic showing the IECAP process is shown in Figure 2.19.

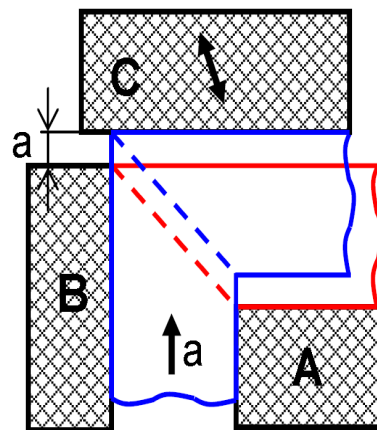


Figure 2.19: Schematic showing the Dies and punch in the Incremental ECAP process. A=Die, B=Pusher and C=Punch. Adopted from Rosochowski and Olejnik 2011.

In this simple representation of IECAP, dies A and B define the input channel. The output channel is defined by die A and punch C. The billet is fed from the bottom in a stepped manner. The size of the step is defined by “a”. The height movement of the punch C must exceed the step value of “a”. Punch C movement is reciprocal and at an angle to the billet. As punch C moves upwards, the billet is fed into the channel. Once

the feeding stops then punch C is moved downwards and into contact with the billet to cause plastic deformation in the zone represented by dashed lines in Figure 2.19. When the feed stroke “a” is not exceeded then the mode of deformation is that of simple shear. As this process is cyclic and the billet is fed into the channel the shear zones overlap and result in the uniform strain distribution along the length of the billet.

2.8. SUMMARY

In this chapter the various layers of the skin and the anatomy of the skin was thoroughly examined. The literature review suggests that the main barrier to transdermal drug delivery is the stratum corneum. The other routes of drug delivery were also examined as well as the methods for overcoming the skin barrier. After examining the various methods, microneedles were found to be a novel drug delivery method that could be used to overcome the skin barrier. It was found that there are four main types of microneedles and that they can be made from an assortment of materials based on the function of the needles. Microforming was identified as a method that could be used for mass production of solid microneedles, but microforming has challenges that need to be overcome like the size effect. Lubrication was identified as a key factor that could affect the correct forming of the parts. One method that could alleviate some of the problems associated with microforming was using ultrasonic oscillations during the forming process. Another key factor that could affect the small components is the size of the grains. Various methods of grain refinement have been examined.

Due to the multi-disciplinary scope of this research, several different fields have been examined. It has been identified that various methods will have to be examined and new rigs would have to be designed and adapted to produce microneedles using the backward extrusion process with the addition of ultrasonic oscillation during the forming process. Several lubricants need to be examined and fine grain material need to be produced as they cannot be purchased of the shelf.

The next chapter will examine the different materials and methods that need to be used to overcome the challenges of this research.

3. MATERIALS AND METHODS

3.1. ALUMINIUM

Aluminium is the second most common metallic element on planet's crust. It is widely used in engineering applications because of its low density, it has excellent physical, mechanical and corrosion resistant properties and it is highly manufacture-able and recyclable. Aluminium has a face centred cubic (fcc) structure and a density of 2.7 grams per cubic centimetre; which is approximately one-third of steel (7.83 grams per cubic centimetre), copper (8.93 grams per cubic centimetre), or brass (8.53 grams per cubic centimetre). It demonstrates corrosion resistance in most extreme environments such as atmosphere, salt water, petrochemicals, as well as other chemical environments. Aluminium is often selected for electrical applications due to its high conductivity, which is nearly twice as high as copper on an equivalent weight basis. Similarly, the thermal conductivity of aluminium alloys is about 50% to 60% of copper. This can be advantageous in applications such as heat exchangers, evaporators, electrically heated appliances and utensils, and automotive cylinder heads and radiators.

Aluminium is non-ferromagnetic in nature; therefore, it is widely used in the electrical and electronics industries. It is also non-pyrophoric, which means it will not easily ignite in air. Therefore, it can be used in applications involving flammable or explosive-materials handling or exposure. Aluminium is also non-toxic and is often used for food and drinks containers.

3.1.1. Classification of Aluminium Alloys

Aluminium alloys are classified into two major categories: cast alloys and wrought alloys. A further classification for each group is based on the major alloying element that is present in the alloy system. They are generally classified as 1xxx through 8xx.x for the cast alloys, and 1xxx through 8xxx for the wrought alloys. Many alloys series respond to thermal treatment based on the phase solubility. These treatments include solution heat treatment, quenching, and precipitation or age hardening. For both the casting and wrought alloys. These alloys are described as heat treatable alloy systems. The alloy systems that do not respond to the thermal treatment rely instead on

mechanical working or reduction, usually in combination with various annealing procedures for property development. These alloys are referred to as work hardenable alloy systems.

For wrought alloys a four-digit system is used to produce a list of wrought composition groups. These are:

- 1xxx - Pure Aluminium
- 2xxx - Copper is the predominant alloying element, but other elements such as magnesium may also be present
- 3xxx - Manganese is the predominant alloying element
- 4xxx - Silicon is the predominant alloying element
- 5xxx - Magnesium is the predominant alloying element
- 6xxx - Magnesium and silicon are predominant alloying elements
- 7xxx - Zinc is the predominant alloying element, but other elements such as copper, magnesium, chromium, and zirconium may also be present
- 8xxx - Lithium and some Tin are predominant alloying elements. Also characterising miscellaneous compositions
- 9xxx - Reserved for future use

In the 1xxx group, the series 10xx is used to designate unalloyed compositions that have natural impurity limits. The last two of the four digits in the designation indicate the minimum aluminium percentage. In the 2xxx through 8xxx alloy groups, the first digit indicates the group or major alloying present in the alloy system, and the second digit indicates the alloy modification. If the second digit is zero, it refers to the original alloy; and integers 1 through 9, assigned consecutively, indicate modifications of the original alloy. The last two digits of the four digits in the 2xxx through 8xxx groups have no real importance, but are used to identify the different aluminium alloys in the group.

3.2. ALUMINIUM 1050

Aluminium of 99.50% or higher purity is present in this alloy series and, iron and silicon are the major impurities. The chemical composition of the aluminium 1050 is shown in Table 3.1. The density of the alloy is about 2.71 grams per cubic centimetre at 20 °C, the liquidus temperature is 657 °C, and the solidus temperature is 646 °C. This grade of aluminium is characterized by excellent corrosion resistance, high

thermal and electrical conductivities, low mechanical properties, and excellent workability. The mechanical properties of the alloy are shown in Table 3.2.

Moderate increases in strength can be obtained by strain hardening. Typical uses include extruded coiled tube for equipment and containers for food, chemical, and drinks industries, pyrotechnic powder; chemical equipment, reflectors, heat exchangers, electrical conductors and capacitors, architectural applications, and decorative trim.

Table 3.1: *Chemical Composition of the 1050 Alloy BS EN 573-3: 2009.*

<i>Element</i>	Al	Si	Fe	Cu	Mn	Mg	Ti	Others
<i>%</i>	99.50	0 - 0.25	0 - 0.40	0 - 0.05	0 - 0.05	0 - 0.05	0 - 0.05	0.03

Table 3.2: *Typical Mechanical Properties of the 1050 Alloy.*

Temper	Tensile Strength (MPa)	Yield Strength (MPa)	Elongation (%)	Shear Strength (MPa)
Annealed - O	76	28	39	62
Strain Hardened - H14	110	103	10	69
Strain Hardened - H16	131	124	8	76

The alloying elements that are present in the alloy system completely go into the solid solution with aluminium during melting and the room temperature equilibrium microstructure after solidification consists of a single phase aluminium rich α -phase. However, the final microstructure may consist of little amounts of Al_3Fe (needle shaped) or $\alpha-Al(FeSi)$ precipitates distributed in the aluminium rich α -phase, depending upon the actual cooling rate of the alloy. Figure 3.1 shows the single phase equilibrium microstructure of a 1050 alloy.

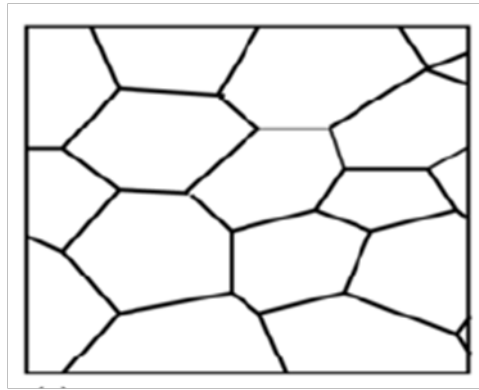


Figure 3.1: *Equilibrium Microstructure of the Aluminium 1050 Alloy.*

3.2.1. Aluminium biocompatibility

When the biocompatibility of aluminium is examined, the first items that always appeared in the literature are the links between aluminium and Alzheimer's disease. Aluminium is a strong neurotoxicant (World Health Organization 1997). The link between aluminium and its neurotoxicity was first reported over one hundred years ago by Siem and Dollken (Alfrey 1993). In the mid-1960s Terry and Pena (Terry & Pena 1965) reported that intracerebral inoculation of aluminium phosphate in rabbits resulted in neurofibrillary degeneration that were very similar to the neurofibrillary tangles of Alzheimer's disease. There have been many debates into the role of aluminium in Alzheimer's disease since that publication. Soon after that a link was also made between aluminium and kidney failure (Alfrey 1993). Many different toxic actions of aluminium have been identified at the molecular and cellular level (McLachlan 1995). There are also studies that suggest aluminium in high concentrations being a factor in Alzheimer's disease but ingesting or exposure to high enough concentrations being unlikely (Flaten 2001). Drinking water and antacids are common sources of aluminium but the concentration of aluminium in drinking water is very low, however, higher concentrations can be found in antacids (Berthon 2002).

3.2.2. Choice of Material

As described previously, many challenges will have to be overcome for metal microneedles to be created using backward extrusion. The best material for this may not be the material with the highest biocompatibility rating. Once the concept has been refined and shown to be possible to create metal microneedles using this method then

in the future it would be possible to create the microneedles from a more biocompatible metal. Due to its numerous, previously stated, advantages it was decided that aluminium 1050 would be selected for this study. It is understood that aluminium has many biocompatibility drawback and may not be the most ideal material for future micro needles, but for the scope of this study it will only be used for demonstrating the process.

3.3. SURFACE ROUGHNESS MEASUREMENT

One of the variables that can be measured and quantified is surface roughness. The surface profile of a part can be measured using a variety of methods. All methods try to measure the peaks and troughs at the surface. On a macro scale surfaces appear flat but when examined under a microscope it is possible to see the surface undulations. These can lead to increased friction between parts; resulting in greater wear and shorter part life. The surface roughness of a die can also impart its roughness onto parts created using that die. Surface roughness can also play an important part in material flow for forming processes.

There are a variety of contact and non-contact methods available for surface roughness measurement. A contact method device known as a stylus instrument and a non-contact method known as a focus variation instrument was available. Initially the stylus instrument was used but most of the surface roughness measurements were carried out on the focus variation instrument. Both instruments have been described in the following section.

3.3.1. Stylus Instrument

Over the last one hundred years a very simple method was used to determine surface roughness. A stylus was pulled along a surface and the trace was produced showing its vertical movement. This method was very successful and very little has changed. The stylus instrument available today still measure by a method that involved tracing a stylus that is in contact with the surface of a part and measuring the vertical motion of the stylus as it travelled across the surface features. The stylus is often tipped with a diamond to minimise wear and maintain accuracy. However, these hardened tipped styluses can also damage the surface being measured. A hard object coming in contact

with a softer object can damage the softer objects, therefore, contact methods are not best suited for soft materials.

Another limitation is the sharpness of the tip. The smallest feature that can be measured is determined by the point at the tip of the stylus. Large tips can only measure large troughs and valleys whereas small sharp tips can increase that resolution and detect smaller features. Stylus instruments can also be used to measure areal surface topography. This is done by sweeping the stylus across the surface in a predetermined pattern to build up a topography map.

3.3.2. *Focus Variation Instrument*

Compared to other surface roughness measurement methods focus variation instruments are relatively new. In short, they allow the measurement of surface roughness without contact by using optics that have limited depths of field and by utilising vertical scanning.

For this study an Alicona InfiniteFocus (Austria) was utilised to determine the surface roughness and form of many parts. This device utilises the focus variation method to determine the surface roughness of the parts as well as the form without making contact with the part. Being non-contact is the most important feature of this method as some of the parts are made from aluminium and could easily be scratched and damaged; if contact methods are used.

In simple terms the Alicona searches for the best focus position by changing its distance from the sample. By using very small vertical step sizes in a predetermined range, it captures pictures of a small area of the sample. Then by comparing contact levels, it can find the sharpest image (the most in focus). This is then designated as the height of that point. There are four main elements to focus variation instruments such as the Alicona InfiniteFocus:

Depth of field - Complex lenses have a limited depth of field. Depth is determined as a function of focus, therefore, good optics are required to allow distinguishing between sharp and blurred areas. High quality optics will maximise the optical transfer but minimise the less desirable stray light. This in turn minimises the errors in the reading

from the charge coupled device. It is also possible to collect colour information, therefore, for complex chromatically corrected optical elements are used. The optical system should minimise unwanted light, barrel distortion, axial and longitudinal chromatic aberration as well as other optical phenomena. A polariser might also be required for reflective components e.g. metal parts.

Light source – The light that is reflected from the component is captured on the charge coupled device, therefore, the parameters and characteristics of the light must be known.

The light is a critical element of the way a focus variation instrument works, and good variation in the contrast of the images is required. White Light Emitting Diodes are used in the Alicona system to allow colour information to be collected and to extend the life of the system.

Charge coupled device for contrast detection – high quality charge coupled device is critical to any focus variation instrument. The charge coupled device is the part of the instrument that digitises the image and allows for software interpretation. The charge coupled device has a high radiometric and spatial resolution. The radiometric resolution allows focus to be calculated in areas when the contrasts are low and spatial resolution is used to determine the size of the focus area. The Alicon system has a colour system, therefore it is able to show the real colour to ease the operator interpretation of the component in 3D visualisation.

Motor for driving the vertical movement of the lenses – either the component or the lenses can be moved. The movement must be precisely controlled, therefore, the motors are often calibrated to high precision. There are various different types of motors and drivers available for focus variation instrument. Each have their advantages and limitations. Piezo-electric motors are known for the high resolution they can achieve but their range of movement is limited. Once calibrated the working range of the instrument is fixed, therefore, the height of the sample must be altered to bring it into the working range of the instrument. A motorised XY stage is used to allow precise control of the movement of the scan area. Vibration and movement will have

a detrimental effect on the quality of the data collected, therefore, these instruments are often placed on passive vibration isolations units.

Advanced software – complex algorithms are used to interpret the images that are collected by the charge coupled device. These algorithms determine the optimum height of the component surface by comparing the stack of images collected during the vertical movement of the lenses.

Similar to a microscope, various objective magnification lenses are available. The magnification determines the minimum roughness that can be measured using the instrument. The 2.5x, 5x, 10x, 20x, 50x magnification lenses are available and the smallest roughness they can measure is 7, 1.2, 0.3, 0.15, 0.06 microns respectively. As the magnification increases the time taken to scan each component increases, therefore, it is important to select the correct lens for the measurement requirements. The Alicona Infinite Focus instrument and a schematic view are shown in Figure 3.2.

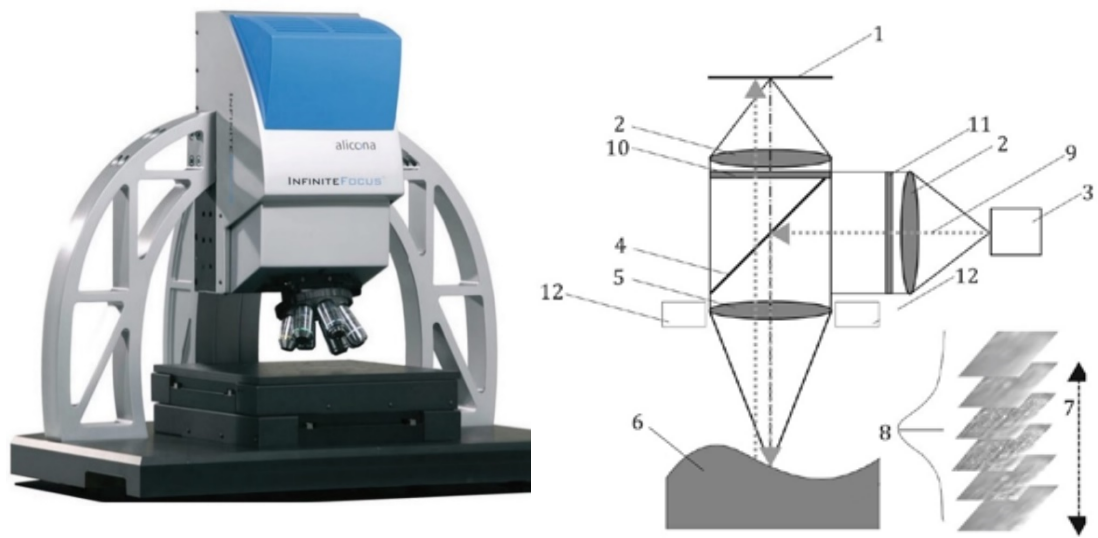


Figure 3.2: *Alicona Infinite Focus and the schematic diagram of a typical focus variation instrument: (1) CCD sensor, (2) lenses, (3) white light source, (4) semi-transparent mirror, (5) objective lens with limited depth of field, (6) sample, (7) vertical movement with driving unit, (8) contrast curve calculated from the local window, (9) light rays from the white light source, (10) optional analyser, (11) optional polariser and (12) optional ring light. Adapted from Leach 2011.*

3.4. HARDNESS TESTING

Hardness is an interesting material property concept. Unlike other material properties, it is not defined in the usual fundamental units of mass, length and time. There are publications linking the hardness to the yield and tensile strength of some materials (Pavlina & Van Tyne 2008). It is the measurement procedure that gives the material its hardness value; therefore, it is important to firstly describe the concept of hardness. In short, hardness is the property of a material that allows it to avoid plastic deformation. One of the first test scales that were produced to determine hardness was the Mohs scale.

In 1824 Friedrich Mohs (Tabor 1953) selected ten minerals that could be used to qualitatively assess a material's hardness. The minerals in the scale were arranged in increasing order of hardness so that each mineral could scratch the one on the scale below it, but will not scratch the one above it. The minerals were arranged in the following order: 1) talc, 2) gypsum, 3) calcite, 4) fluorite, 5) apatite, 6) orthoclase, 7) quartz, 8) topaz, 9) corundum and 10) diamond. It is important to note here that the scale is not linear, therefore, not best suited for engineering purposes.

Nowadays there are various testing procedures for determining materials' hardness that are more suitable for engineering purposes. Amongst many available test methods, Brinell, Rockwell, Knoop and Vickers are most often mentioned in the literature. The first two tests are more suited to macro hardness testing. The elongated diamond shape of the Knoop test is ideal for brittle and sheet material but the diamond shape of the Vickers test is ideal for micro hardness testing.

3.4.1. *Vickers Micro Hardness Testing*

The Vickers hardness test method uses a square based pyramid diamond with an angle of 136 degrees between opposite faces (22 degrees each side from the sample surface). Often the loads applied can range from 1 to 100 kgf. Once contact has been made the full load is applied for 10 seconds. The diamond indenter is then removed and the remaining diagonals on the sample surface are measured using a microscope. The average of the two diagonals is used to calculate the area of the sloping surface. The following equation is used to determine the Vickers hardness.

$$HV = \frac{2F \sin 136^\circ / 2}{d^2}$$

Where HV is the Vickers hardness, F is the applied Load in kgf, d is the average of the two diagonals in mm. The main advantage of the Vickers hardness test is the high accuracy that can be achieved. Under the correct load conditions, this method allows for the testing of the softest and hardest of materials.

The same concepts and equations can be used for micro hardness testing using the Vickers method. The load used for micro hardness testing is often less than 1 kgf and high magnification microscopes. A higher surface finish is also required during micro hardness testing; as the load decreases, the better surface finish is necessary. The higher magnifications used allow for greater accuracy to be achieved. Care and experience is required to obtain accurate results. The systems that are integrated into modern instruments allows for the capture and software processing of these images. This minimises the operator error and maintains repeatability and reproducibility of the results. Automatic test surface focusing, motorised XY tables and automatic effective case depth determination are common place in advanced laboratories around the world whom require the latest technology offering fast, reliable and traceable testing.

A Zwick ZHV μ micro hardness tester was used to determine the hardness of the various samples for this project. This system is capable of testing to ASTM E-384 standards. It has a test-load range of HV0.01 to HV2. It is equipped with a six position turret that can have four lenses and two indenters. Both Vickers and Knoop indenters are available with 2.5X, 5X, 10X and 20X objective lenses. This system also has a motorized xy table for accurate sample movement and automation. The Zwick ZHV μ micro hardness tester and a schematic of the Vickers hardness method is shown in Figure 3.3.

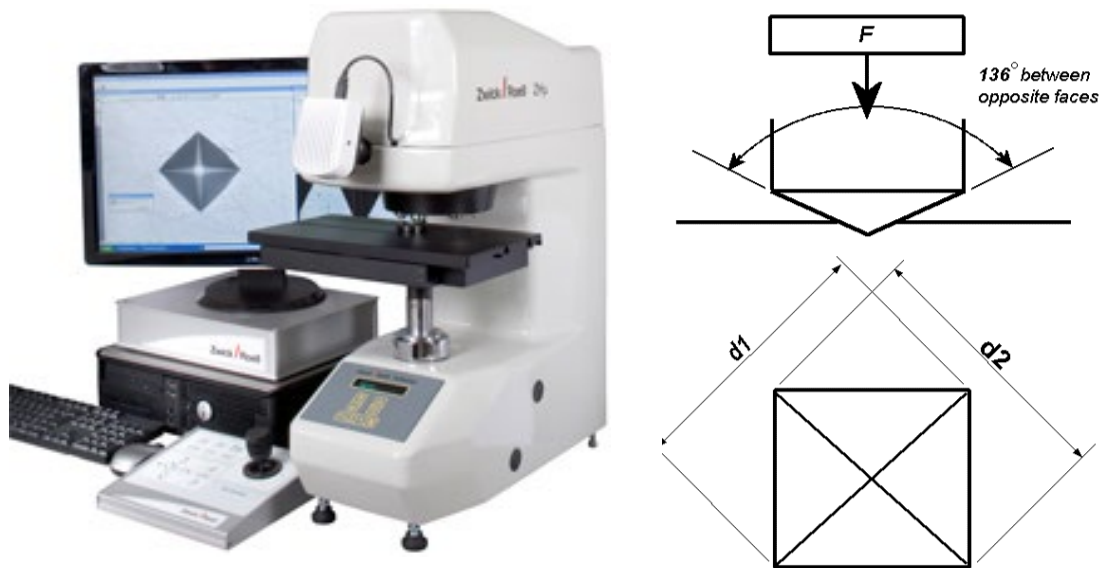


Figure 3.3: *The complete Zwick ZHV μ micro hardness tester shown on the right. On the left a schematic of the Vickers hardness testing method. Adapted from Zwick ZHV μ micro hardness tester user manual*

3.4.2. Sample Mounting

Mounting of the specimens is important because it simplifies the handling and allows the edges and small features to be preserved. There are two main mounting methods available; compression mounting and cast-able mounting. It is often recommended that prior to choosing the casting method three main parameters are considered:

- Size and geometry of the specimens,
- Specimens' vulnerability to pressure and temperature,
- Required throughput.

Compression mounting is used when optimal edge conservation and highest throughput are required. There are a wide variety of mounting compounds available, each with advantages and limitations. There are a range of conductive compounds also available for use with electron microscopes. The temperature and pressure and time required for mounting each specimen is dictated by the compound that is used. Some compounds may require temperatures of a few hundred degrees at relatively high pressures for over 10 minutes to achieve a good mount. The mounting presses use electro-hydraulic compression to achieve the required pressures and have an integrated cooling system to cool the samples once mounting has been completed. This mounting

system is the preferred system for many engineering metals but soft metals such as aluminium can be misshapen by the pressures and grain growth can occur due to high temperatures.

Castable mounting is used for specimens that are sensitive to heat and/or pressure. This mounting system requires no heat or pressure because acrylics and epoxies are used to surround the specimen. Since the epoxy mounting systems start in liquid form, they can flow into porous materials, cracks and capture small features without damaging them. To achieve the best results, it is necessary to use a vacuum system. By conducting the casting in negative pressure, the edge retention is enhanced and delicate specimens can be well supported during the preparation steps such as grinding and polishing.

Castable mounting was used for the specimens in this project because the material could be vulnerable to heat and pressure. The soft starting material would result in the small features that were produced to be easily damaged. The temperature could also have adverse effects on grain growth. The required throughput was also relatively low, therefore, casting was the ideal choice.

A Buehler Cast N' Vac 1000 Vacuum System was utilised with 20-3440-032 resin and 20-3432-016 hardener to produce the epoxy EpoThin 2 castable mount. The EpoThin 2 mount was chosen because it is clear and has a very low viscosity. The clearness would allow more precise grinding and polishing to be carried out without losing the required features. The low viscosity would ensure the best surrounding for the features without voids forming. Figure 3.4 illustrates the Castable mounting equipment used to mount the specimens.

The specimens were placed in the moulds with the surface of interest facing down. The moulds were placed into the vacuum chamber and a vacuum produced. The EpoThin 2 mix (resin to hardener ratio 2:1) was poured into the moulds, while under vacuum, and allowed to set for 12 hours. Pouring and casting in an uninterrupted vacuum allows for the best results to be obtained.



Figure 3.4: *Castable Mounting Equipment: (1) Vacuum pump, (2) air filtration chamber, (3) vacuum chamber, (4) vacuum pressure indicator, (5) motorised base for rotating specimens, (6) EpoThin 2 resin and hardener mixed and ready for pouring, (7) casting moulds.*

3.5. FRICTION

Friction between two surfaces can be attributed to several different processes. In most cases adhesion is the largest contributor to friction. When a surface is examined at high magnification, it is possible to observe the peaks and valleys. The applied loads are only supported at the points where the peaks come into contact with each other. Therefore, the pressures generated at these points are very high because the contact areas are so small. These high forces can be greater than the yield point of one or both materials; resulting in elastic and plastic deformation. By deforming, these peaks increase the contact area between the surfaces, which can also lead to adhesion.

Friction often follows the two laws known as Amontons' laws:

- Frictional force is independent of contact area,
- Frictional force is proportional to the concept load.

Examining the second law can lead to a concept known as the coefficient of friction.

$$\text{Coefficient of friction} = \frac{\text{Friction}}{\text{Load}}$$

One way to reduce the friction between surfaces is to use lubricants. The use of Lubricants leads to a reduction in the coefficient of friction, therefore, result in greater loads being able to be applied without adverse surface effects.

3.5.1. Grease and Oil

As discussed previously lubrication is a key factor in many forming processes. Surfaces contain peaks and valleys that can lead to friction when surfaces come into contact with one another. One way to manage the friction is to minimise these peaks by meticulously preparing all contact surfaces. This is a very time consuming and costly procedure. Another method is by lubricating the contact surfaces. The lubricant can flow into the valleys and the hydrostatic forces would allow for sliding of the contact surfaces to occur.

The two main types of lubricants that are available are oils and grease. These two lubricants work in identical ways but differ in their usage. Oil is the term used when referring to liquid lubricants and grease is the term used for semi solid lubricants that are often made from oils and have a thickening agent added to them. The thickening agent is used to hold the lubricant in place rather than adding additional lubricity.

The selection of the lubricant type depends of the application. The reduced viscosity of oil makes it an ideal candidate for applications that require flow. For forming processes lubrication viscosity plays a very important part. Since the viscosity of lubricants can change with pressure and temperature it is important to select the right lubricant to minimise friction and metal to metal contact. There is an equation that is often used for selecting bearing lubricants. The following equation could be used to aid the lubrication selection for forming processes.

$$K = \frac{V}{V^1}$$

In this equation K is the viscosity ratio, V is the actual operating viscosity of the lubricant (units millimeters² per second) and V¹ is the rated viscosity of the lubricant which depending on the bearing mean diameter and rotational speed (units millimeters² per second). It is recommended that a minimum viscosity ratio of K = 1 should be maintained for bearings. When K ≥ 4 then full hydrodynamic film is formed. When K

< 1 then metal to metal contact can occur because full hydrodynamic film cannot be formed. This is the situation in which most forming processes find themselves, therefore, the theoretical recommendations for improving bearing lubrication can be applied to some forming processes. There are two main recommendations for these situations to increase the load carrying capability of the lubricant. Using lubricants that have extreme pressure additives or / and anti-wear additives (SKF bearings website).

Extreme pressure additives – used to overcome metal-to-metal contact caused by the roughness of the contact surfaces. The contact between the rough surfaces causes the temperature to increase locally. This elevated temperature activates the additives and causes mild chemical wear to take place at the points of contact. This results in smoother surfaces and lower contact stresses. Solid lubricant additives such as graphite and molybdenum disulphide can be used to improve the extreme pressure additives effect at low speeds. The graphite and molybdenum disulphide additives used in the lubrication have a small particle size and a high purity level.

Anti-wear additives – used to overcome metal to metal contact but they work in a different way to extreme pressure additives. These additives build a defensive layer that clings to the metal surface. This allows the roughness peaks to slide over each other therefore, minimising contact. Unlike extreme pressure additives, the materials surface finish is not affected by mild wear.

3.5.2. Molybdenum Disulphide

Molybdenum disulphide (MoS_2) occurs naturally as the mineral Molybdenite. Lansdown published a book that looked extensively into the properties of MoS_2 (Lansdown 1999). Lansdown mentioned that initially, graphite and MoS_2 were thought to be the same, but in 1778 they were distinguished by Scheele. With the onset of the industrial revolution MoS_2 was more readily used in engineering and scientific applications.

Molybdenum is a grey metal with an element atomic number of 42. It is known to have a very high melting temperature of 2610 °C. It is often used as an alloying element and coatings. Various sulphides of Molybdenum exist but MoS_2 occurs most often. MoS_2 has a melting temperature of 1700 °C and a very low coefficient of friction. It has a

hexagonal and rhombohedral crystal form and has a hardness of 7 – 8 Moh's scale along the crystal edges and 1 – 1.5 Moh's scale in the basal planes. The crystal structure of MoS₂ is shown in Figure 3.5.

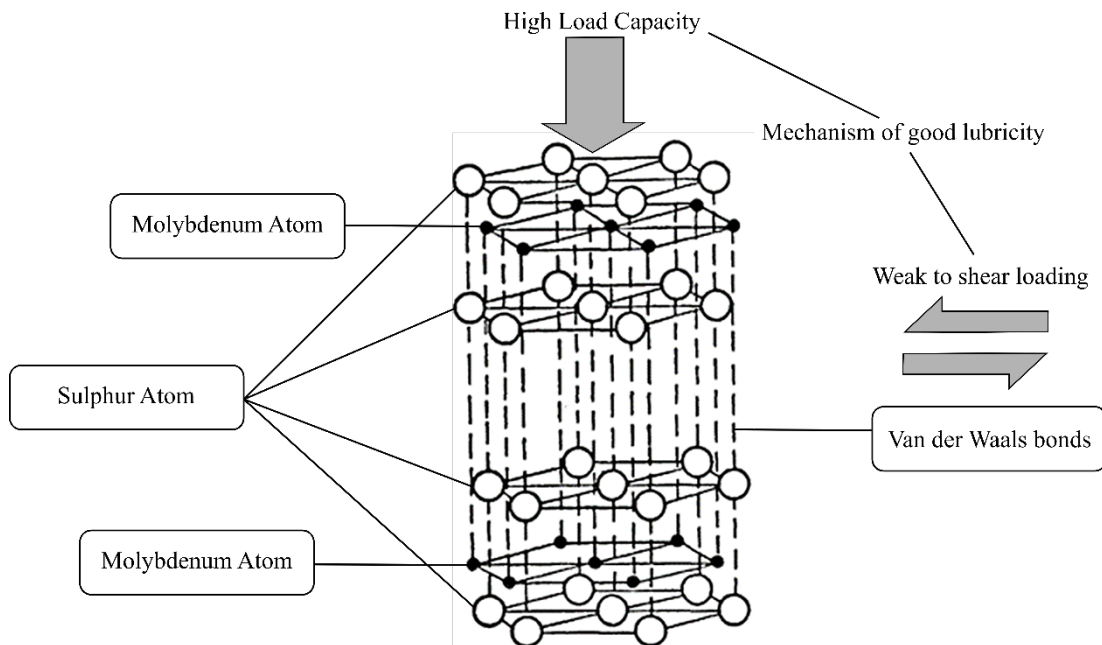


Figure 3.5: *Crystal structure of MoS₂. Each sulphur atom is equidistant from three molybdenum atoms. Each molybdenum atom is also equidistant from six sulphur atoms. Each molybdenum atom is at the centre of right angled prism that has sulphur atoms in each of its six corners. Adapted from Lansdown, 1999.*

Figure 3.5 illustrates the layered structure of MoS₂. MoS₂ adheres to most other substrates. As discussed previously, under loading conditions adhesion can take place, which results in generation of frictional forces. The adhesion forces between the surface and MoS₂ is often very high but the forces keeping the layered structure of the MoS₂ is low. Unlike ionic and covalent bonds, Van der Waals bonds are very weak. The layers of the MoS₂ will, therefore, split and allow the surfaces to slide. MoS₂ has a very high load carrying capacity and it can maintain its lubrication properties even at higher temperatures. In powder form it can be used as a dry metal to metal lubricant or it can also be added to oils, greases and silicones to improve their load carrying capabilities.

3.5.3. Graphite

Graphite is a crystalline form of carbon. It is soft enough to be used in pencils. It is dark grey in colour and can be found in metamorphic rocks such as marble etc. It has good thermal and electrical properties similar to metals. It is also non-reactive and has a high thermal resistance.

Carbon has an atomic number of 6 and can take many form such as diamonds and graphite due to its valency. Graphite has a hexagonal layered crystal structure as shown in Figure 3.6. The carbon atoms are held together by strong covalent bonds but the layers are only held together by weaker Van der Waals bonds. Each carbon atom is bonded to three other surrounding carbon atoms. The flat rings of carbon atoms are bonded into the hexagonal structures

From the diagram it is possible to observe that graphite has a layered structure. As discussed previously, under loading conditions adhesion can take place and generate frictional forces. The adhesion forces between the materials surface and graphite is often very high but the forces keeping the layered structure of the graphite is low. The layers of the graphite will, therefore, split and allow the surfaces to slide. Graphite can maintain its lubricity properties up to very high temperatures. Therefore, it is often used in many hot forming processes as well as cold forming ones. It can be used in powder form as a dry metal to metal lubricant but it can also or it can also be added to oils, greases and silicones to improve their load carrying capabilities. Compared to MoS₂, graphite has one drawback. It relies on the absorption of vapours to achieve its high lubricity, therefore, would not be suitable in high vacuum environments.

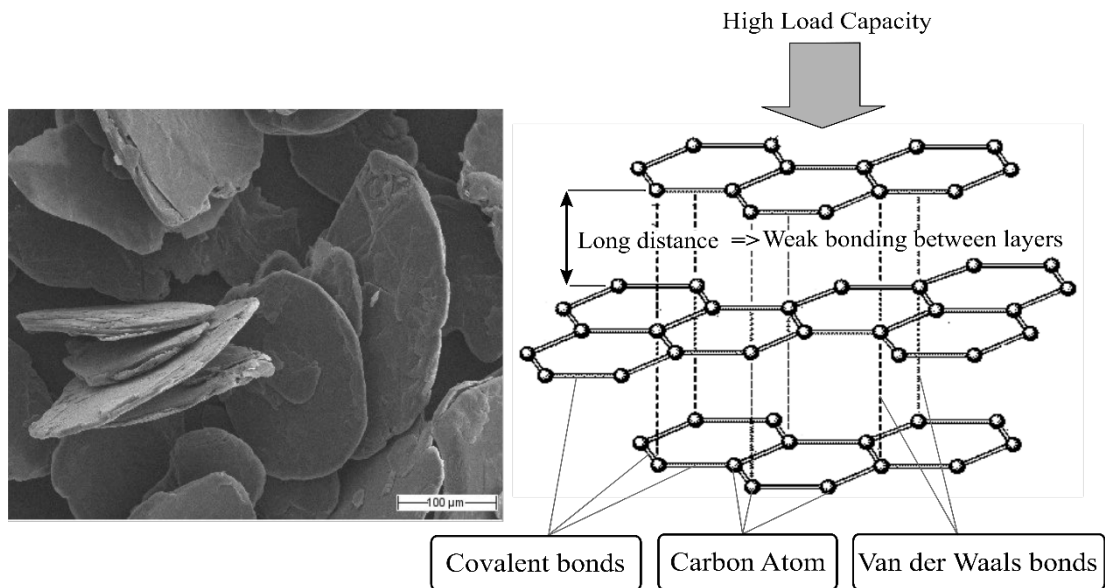


Figure 3.6: *The flat structure of graphite is clearly visible under a scanning electron microscope. Crystal structure of graphite. Each carbon atom is bonded to three other surrounding carbon atoms. The flat rings of carbon atoms are bonded into the hexagonal structures. The layers are then held together using weak Van der Waals bonds.*
Adopted from Eagle Graphite website (www.eaglegraphite.com/portfolio-posts/graphite-flakes-sem-showing-some-sideways)

Antony et al investigated the combination of using both MoS₂ and graphite as an additive in grease for anti-wear and extreme pressure purposes (Antony et al. 1994). The author found a synergistic effect in extreme pressure and anti-wear characteristics when both additives were added to the grease but the level of synergism depends on ratio of two components and type of grease. It has been found that it is possible to mix lubrication techniques in order to achieve improved lubricity.

3.6. CONVERSION COATING

Sort aluminium and its alloys often stick to metal forming tools. This can lead to the increased friction, poor surface finish and material pick up and fussing to the die. Lubricants such as grease, oils and additives like MoS₂ can be used to reduce this, however, in some cases this is not enough. One method for reducing the occurrence of pickup and friction is to use conversion coating. By changing the surface of the component it is possible to reduce the frictional forces and improving its formability performance. It is also possible to add other lubricants once conversion coating has been applied.

Applying a conversion coating of calcium aluminate to aluminium is a multi-step process, that required special chemicals such as the ones provided by Chemetall GmbH Germany (Part of BASF). The process of applying the conversion coating and soap lubricant as described by Bay (Bay 1994) is as follows:

Degreasing – Essentially the component surface must be clean and free from foreign materials and debris. Alkalines are used in a bath to remove some of the contaminants that may be present on the surface. As the pH increases so does the aggressiveness of the degreasing. To improve the degreasing capabilities of alkaline elevated temperatures are also used. This is followed by cold water rinsing, to remove the alkaline, and then component inspection before moving on to the next step.

Pickling – This is also part of the surface preparation step. The surface must be meticulously prepared to allow a good conversion coating to form. Hydrochloric acid is used to pickle the components. This is carefully timed to prevent / minimise over-pickling. This is followed by cold water rinsing to remove the hydrochloric acid. Hot rinsing is then performed to activate the component prior to the next step.

Conversion coating – Aluminate bath containing calcium hydroxide and other activating compounds is prepared. The pH value of the bath is above 11. In this strong alkaline environment, the aluminium dissolves from the surface; forming aluminium hydroxide. This in turn reacts with calcium hydroxide solution in the bath and forms calcium aluminate. This forms a thin layer all over the component. This step is carried out at elevated temperatures (60 to 80°C) for 5 to 15 minutes. The components are then rinsed in cold water. In some cases, soap is also required for lubrication, therefore, a further step is required. If this is required then hot rinsing will be carried out to prepare the component for the next step.

Lubrication – An alkaline soap bath is prepared. Due to chemical reactions that can occur the soap lubricant coating can adhere better to the component surface. This is also carried out at elevated temperatures (60 to 80°C). The layer of soap is physically bonded to the calcium aluminate conversion coating. The conversion coating process is shown in Figure 3.7 with a schematic of the coating build-up.

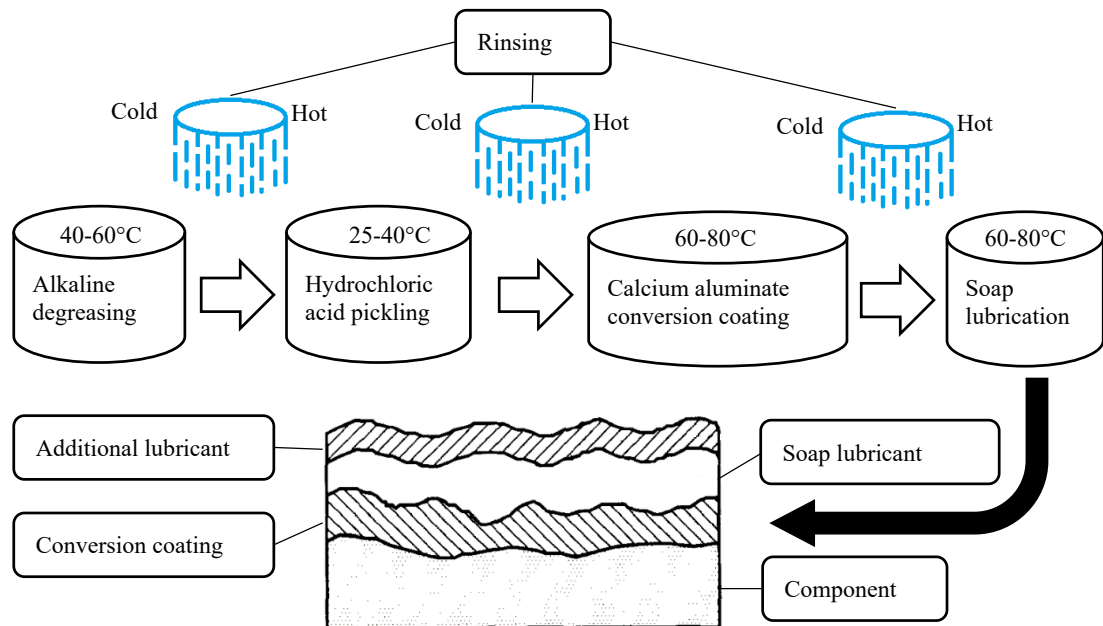


Figure 3.7: Steps required for calcium aluminate conversion coating. A schematic showing conversion coating layer and the lubrication layers.

3.7. GOLD SPUTTER DEPOSITION

Sputter coating method is predominantly used to coat nonconductive surfaces. It is used in industry for a variety of purposes such as producing thin films for the solar cell industry but in laboratory settings, it is used for preparing nonconductive material for scanning electron microscopy; SEM only works for conductive materials, therefore, ceramics, polymers and organic specimens require a conductive coating to be applied.

There are 5 main components to a sputter deposition system;

Chamber – designed to maintain and withstand the loads applied under a vacuum atmosphere.

Vacuum pump – required to remove the air in the chamber allowing a plasma to be formed.

Gas – high purity inert gas such as argon is used.

Sputter target – the material that will be used to coat the sample.

Thickness measurement system – various systems are available to measure the thickness of the deposition on the component.

Air is removed from the chamber by a vacuum pump and the chamber pressure is reduced. Once the pressure has dropped to 0.05mb then argon gas is leaked into the chamber. A magnetic field is generated and high voltage is applied to the target. A plasma is formed and concentrated around the magnetic field. The plasma contains argon, positively charged argon ions and free electrons. Once these free electrons coming into contact with the argon atoms they produce the positively charged argon ions.

The sputter target is negatively charged, therefore, the positively charged argon ions are drawn towards the target. Positive argon ions are accelerated in the electric field towards the negative sputter target. When they collide with the target the gas ions eject target atoms by momentum transfer. It is this process that is called 'sputtering'. The sputtered target atoms then diffuse away from the target and deposit onto the component's surface. This builds layers of the target material onto the component surface. The longer the sputtering continues the thicker the layer becomes therefore various measuring methods have been developed to measure the thickness of the layer and stop the process when the desired thickness is achieved.

The system used to monitor the thickness of the sputter layer is a quartz crystal microbalance. When the sputtered material is deposited on an oscillating quartz crystal, its frequency is decreased in relation to the mass of material that is deposited. It is this frequency change that is used to calculate the film thickness because the density of the target material is known. A picture of the Agar scientific MB7341 auto sputter coater is shown in Figure 3.8 along with a schematic of the sputter process.

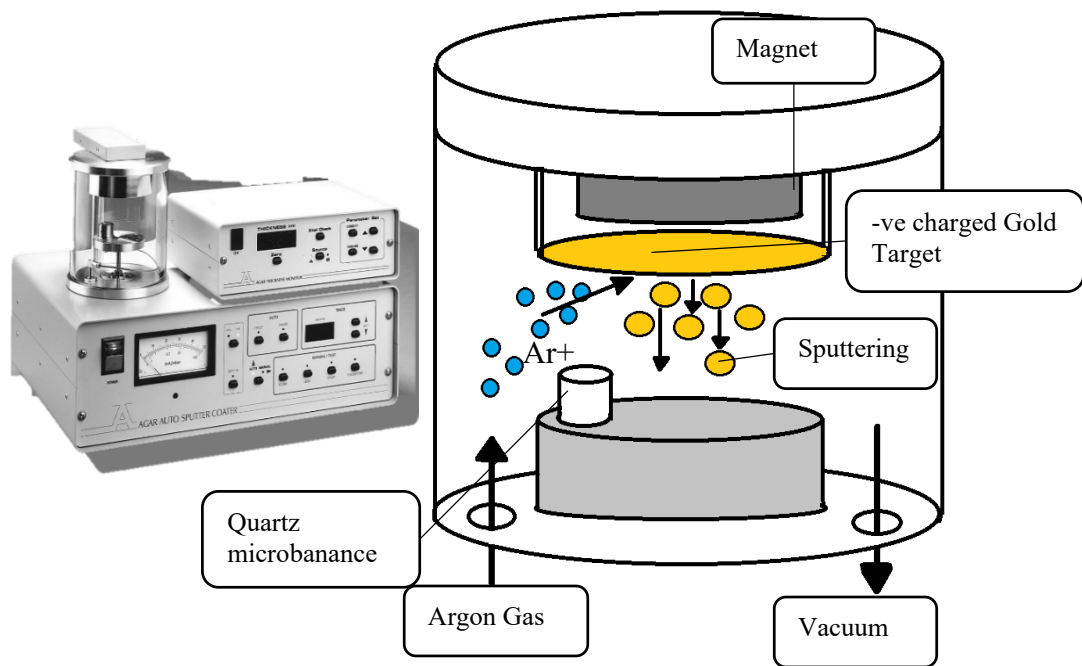


Figure 3.8: *Agar scientific MB7341 auto sputter coater and the sputtering process*

The sputtering process is mostly used for increasing the sample conductivity but for this project it was used to apply a 100nm coating onto the surface of the component. This layer could then act as a solid lubricant and reduce the frictional forces during the forming process.

3.8. TENSILE TESTING

A tensile test is the most important mechanical test that can be conducted on a material. Tensile tests are standardised tests (ISO 6892-1 and ASTM E8/E8M-13) that are inexpensive and simple to perform. These tests have been performed for over one hundred years but today's modern testing machines integrate sophisticated sensors and computer algorithms to maximise the amount of information that can be captured from each test.

In simple terms; tensile force is applied to a specimen and the reaction of that material is examined in a tensile test. As the tensile force is applied it is possible to determine the materials' strength and elongation. The load is increased until the material breaks. This allows for a load profile in the form of a curve to be determined. The point at which the material failure is known as the ultimate tensile strength. This is the highest

load the material can withstand during the test. The ultimate tensile strength might not be equal strength at the point of break. Different materials behave in different ways. Once this simple concept is understood then it is possible to look into the behaviour of the material in detail.

During the tensile testing of most materials it is possible to observe that in initial part of the test the relationship between load and the elongation of the specimen is linear. In the initial linear region, the line obeys the relationship known as Hooke's Law; the force required to extend or compress a spring by a distance is proportional to that distance. In other words, the ratio of stress to strain is a constant. As shown in the following equations:

$$\sigma = \frac{F}{A}$$

- Where σ is the stress, F is the forces and A is the area.

$$\epsilon = \frac{\Delta L}{L}$$

- Where ϵ is the strain, L is the final length and ΔL is the change in length.

$$E = \frac{\sigma}{\epsilon}$$

- Where E is the slope of the line in the linear section, σ is the stress and ϵ is the strain.

This is also called the Modulus of Elasticity or Young's Modulus. When a material is loaded within the linear region it will return to its exact same condition when the load is removed. In this region the material behaves elastically.

When the curve stops being linear, Hooke's Law can no longer be applied because the material has permanently deformed. This point is called the elastic limit of the material and beyond this point the material is said to have plastically deformed; when the load is removed the material will not return to its initial condition. An example of a typical stress versus strain curve for aluminium and copper, provided by Djavanroodi (Djavanroodi et al. 2012), is shown in Figure 3.9.

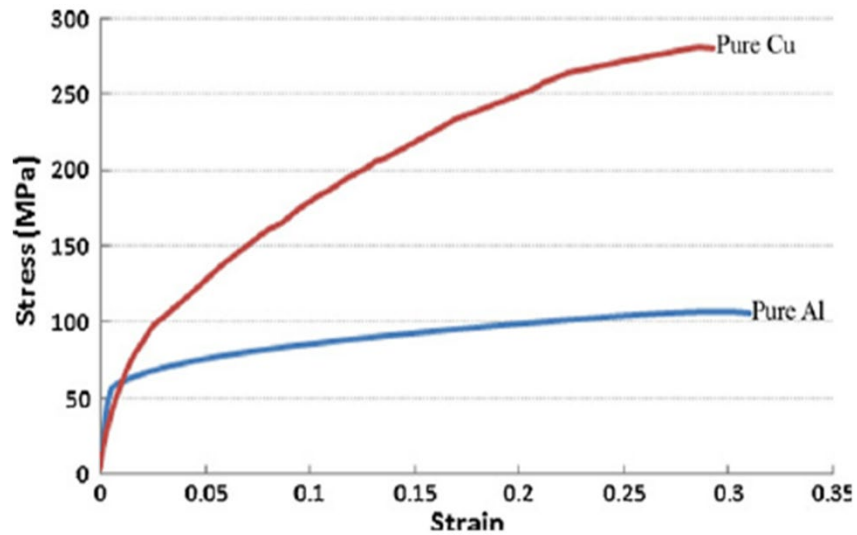


Figure 3.9: True stress Vs. true strain curve showing the difference between the behaviour of pure aluminium and pure copper. Djavanroodi et al, 2012.

To conduct tensile tests on the material a Zwick Roell Z150 was used. This machine is capable of both Tensile and compression testing. As the name suggests it can deliver a maximum load 150kN in both tension and compression. Since aluminium is a relatively soft material, this was deemed more than sufficient for testing purposes. A picture of the Zwick Roell Z150 and a drawing of the tensile test samples are shown in Figure 3.10.

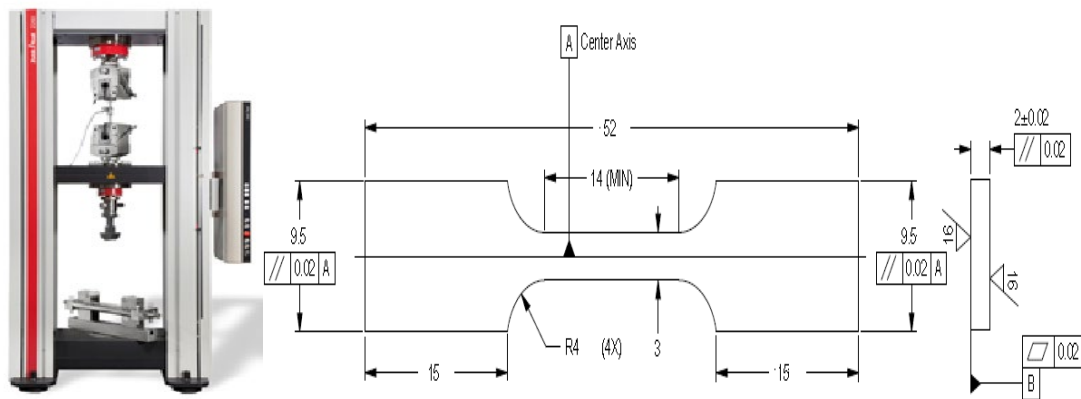


Figure 3.10: Zwick Roell Z150 and a drawing of the micro tensile test samples.

3.9. CONFIGURATIONS OF IECAP RIGS

The IECAP process has been described in Chapter Two. This section describes the equipment that was used to process two billets simultaneously.

Processing the billets in this configuration will avoid lateral forces. The punch setup shares some similarities to conventional ECAP process such as movement of the billet but in IECAP a pusher is used to feed the material into the channel and a punch is used to deform the billets. The punch moves in a sinusoidal reciprocating manner and the pusher only moves when the punch is on the retracting phase. A small sharp tapered point on the punch is used to direct the billets into the exit channels. The billets used for these experiments had a 10X10mm cross-section, therefore, the input and exit channels had to have a tight tolerance to avoid undesired material flow. Hence, the channels were machined to 20X10mm and the billets would be ground slightly smaller so a pair of billets would fit snugly into the channel after lubrication was applied.

To perform the required IECAP experiments and to produce ultra-fine grain material the research group produced an IECAP rig. A 1000kN press with a hydraulic servo actuator was used as the base for this IECAP rig. As well as the die and punch, various other elements were added to the rig to make it fit for controlled IECAP.

3.9.1. IECAP COMPONENTS

This IECAP rig was initially manually fed but data recording, position control, an electric motor, and safety features were added to automate some of the process. The 1000kN IECAP rig is shown in Figure 3.11. Figure 3.11 also illustrates a schematic diagram of the rig with the various elements that were integrated into the rig. The elements in this IECAP press are as follows:

Hydraulic actuator – was used to apply the required force onto the billets. Hydraulics is an integral part of this process as high forces are required to deform the billet.

Punch – transfers the load from the hydraulic actuator and onto the billets. The shape of the punch is very important. The punch must be made from a hard material and the surface must be polished to minimise the frictional forces that can be experienced at the punch-billet interface.

Servo valve – precision control over the movement of the hydraulic actuator is achieved by using a servo valve. This valve controls the flow of hydraulic fluid to and from the actuator.

Linear variable differential transformer – these devices are used to measure the movement of the actuator. The signal sent from the controller can be compared against the actual movement and modifications can be made accordingly.

National Instruments module – data acquisition devices are used to capture the data from the various sensors. The data that was captured can then be recorded for later analysis or can be used in the control system. Some modules were also used to control the press movement. Custom made virtual instruments were made to interact between the user and the rig.

Motor controller – this controls the speed, direction and duration of the motor movement. This was controlled by the modules.

Electric motor – move the screw jack. There is also code wheel attached to the motor to feed back the exact location of the motor during rotation.

Screw jack – converts the rotational movement of the motor into linear movement. The motor drives the screw jack, which in turn moves a pusher rod, which then moves the billets up towards the punch. Another important feature of the screw jack is its self-locking capability. This function allows it to supporting the load that was applied by the punch during the forming phase.

Load cell – to monitor the force that was being applied by the punch. TWO load cells were utilised. One at the top between the actuator and the punch and another at the bottom between the pusher rod and the screw jack.

Temperature controller – to heat up the punch and die, fire rods could be inserted. The temperature of the fire rods was controlled by the temperature controller that also had thermocouples inputs. For Al1050 the IECAP process was carried out at room temperature because this material is relatively formable at room temperature. This rig was designed to be flexible so other materials that have poor formability at low temperatures could also be IECAPed.

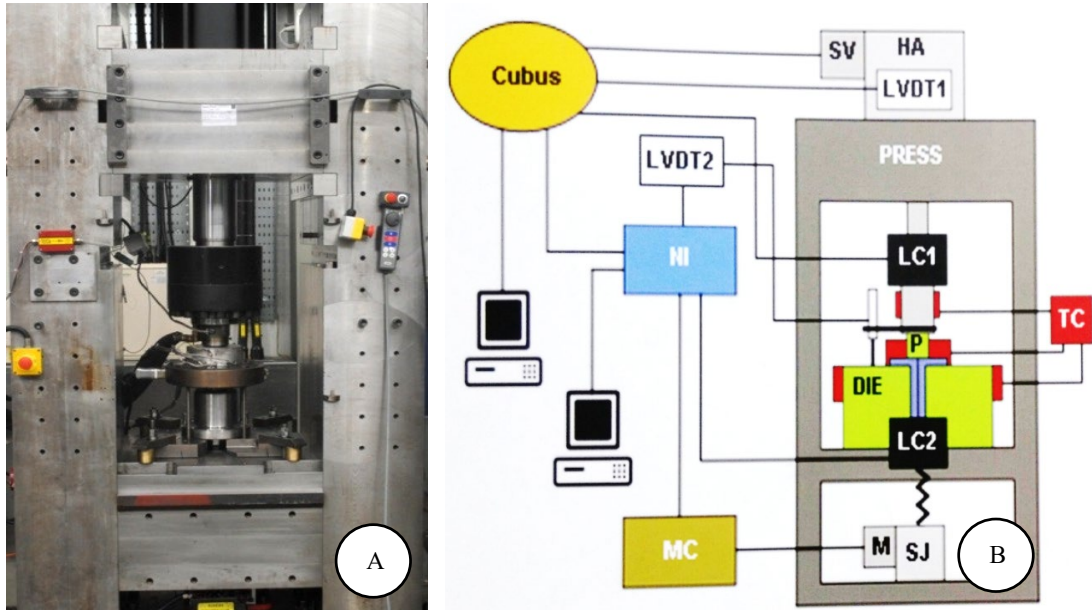


Figure 3.11: *The 1000kN hydraulic press setup used to IECAP process pairs of billets. A – shows the press setup in the laboratory. B – a schematic of the various elements of the IECAP press. HA= Hydraulic actuator, SV= Servo valve, LVDT= Linear variable differential transformer, NI= National Instruments module, MC= Motor controller, M= Electric motor, SJ= Screw jack, LC= Load cell, P= Punch, TC= Temperature controller, Die=Die setup, Cubus= Software*

In addition to these components other elements were also required to operate the IECAP press. A storage tank and motor that pressurised the hydraulic fluid was also used. As the pressure increases and hydraulics are pumped in and out of the system, heat builds up very quickly. In the interest of safety this equipment requires thermocouples inside the hydraulic storage tank. When the temperature rises above a set point the hydraulic system would automatically shut off. A chiller was used to maintain the temperature of the hydraulic fluid so it was possible to process several pairs of long billets. These components can be seen in Figure 3.12.

A multifunctional electrical controller box was also used in this setup to control the various electrical elements of this rig. The safety stop in the system were also integrated into this system to cut power and stop the press in the event of an emergency. The feed motor driver was also integrated into this box.



Figure 3.12: *Other hardware used for the IECAP rig. A- the black hydraulic storage tanks and pump, the blue chiller. B- rig's electrical components control and safety box. C- 4 National instruments modules used to control and record rig movement. D- manual control hand controller.*

A CompactDAQ 4-Slot USB chassis was also used to house the National Instruments modules. This chassis could power the modules and send the signals to and from the computer via a single USB cable. These modules could then interface with the LabVIEW software to allow controls and recordings using the virtual instruments.

To control the actuator, Zwick Roell Cube controller was used. This component was key to the precision control of the actuator and punch. The actuator LVDT was also

connected directly into the Cube so the control signals and the actual output could be monitored and matched. Cubus software with additional software modules allowed for the programming of the Cube. It was also necessary to have precision control when the actuator was being moved manually. This manual movement is necessary for alignment purposes before the controls could be turned to automatic. To minimise the chances of finger entrapment a two handed hand controller was utilised. An emergency stop was also integrated into the hand controller. The output from the Cube was also sent to the national instruments modules so the data could be recorded.

A custom LabVIEW vertical instrument was designed and built by Muhammad Jawad Qarni and can be seen in Figure 3.13. This instrument allowed for control of the motor and could record the output from both load cells. Both LVDTs could also be monitored so the movement of the feeder pusher could be synchronised with the punch movement. This precision control allowed for repeatable and reliable experiments to be conducted. The ability to record the data is also very important as this allowed the effect of changing parameters to be compared later when further data analysis was conducted.

Once the system was fully assembled, it was calibrated and certified. This system is very complex and has several systems communicating with each other, therefore, it is important that all parts are accurate and errors are minimised. The load cells and the LVDTs in the system showed correct and dependable values. This calibration step is critical as it increases reliability of the outcomes of the experiments. Once all the necessary safety check had been completed, trial experiments were conducted and the rig was fully commissioned for use.

Once aluminium grain become small it can be very difficult to observe them using a standard scanning electron microscope (SEM). Hence, Transmission Electron Microscopy (TEM) can be utilised to observe and verify the grain reduction achieved by further passes and processing of the billets.



Figure 3.13: IECAP custom virtual instrument front panel.

3.10. Backward Extrusion Rig

Following investigation of various manufacturing methods, it was decided that extrusion would be the best method for producing low cost microneedles. This method also had the added potential of being scalable at relatively small cost. The normal forward extrusion method would require very complicated handling and ejection methods as well as having greater contact pressures on the punch as described by (Rosochowska et al. 2010), therefore, the backward extrusion method was used in this study.

3.10.1. Backward Extrusion

In the backward extrusion process, the billet of material is placed inside a closed die. A punch with a cavity is pressed upon the billet. Since the material cannot follow downwards, it flows backwards into the punch. This is where the process gets its name. The punch is then retracted and the formed part is exposed. This process is illustrated in Figure 3.14.

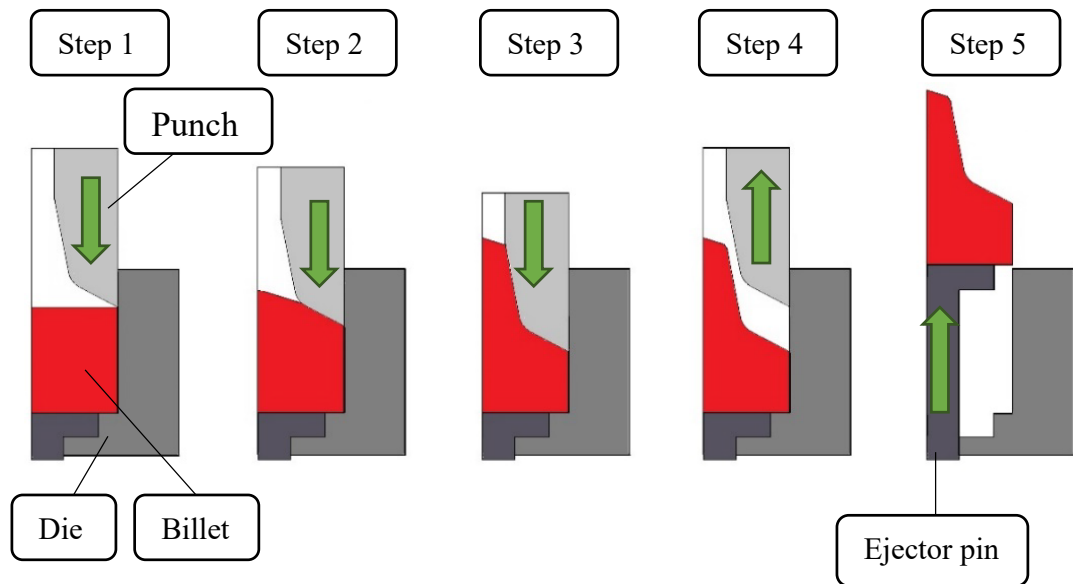


Figure 3.14: *An illustration of the five steps in the backward extrusion process and the four main elements: punch, die, billet, ejection pin.*

There are four main elements and five steps in this forming process. The four elements are: 1) the Punch; with the desired cavity, 2) die; closes the die so material cannot flow outwards, 3) billet; small cylinder of material with close tolerance to the die walls, and 4) ejector pin; for ejecting the formed component without making contact with the formed surface. The main steps of the forming process are as follows:

1 – Billet is inserted into the die and the die is closed when the punch is inserted into the die. The punch and die have very little clearance to the material flowing outside the punch.

2 – Punch comes into contact with the billet. The billet experiences some load but not enough to deform the billet. This step pushes the billet onto the bottom of the die before the forming displacement is initiated.

3 – Punch is then moved downwards and the material starts to flow into the punch cavity. The punch moves downwards until the pin is fully formed.

4 – Punch is then retracted and removed from the die.

5 – Once the punch is clear from the die the ejector pin ejects the formed part from the die.

To conduct the forming trials, an adaptable forming setup was required. Flexibility had to be designed into the setup to allow a variety of parameters to be examined. The setup also had to be controllable and able to record load and displacement values. Various parts of equipment were available from previous experiments, therefore, it was decided that they would be repurposed and adapted for use in a backward extrusion rig. Some of the original equipment can be seen in

Figure 3.15. A 250kN press with a hydraulic actuator was available and the rest of the setup was designed around this. An extrusion rig had previously been used for experimentation.

In

Figure 3.15 it is possible to see A: Four pillar 250 kN servo hydraulic press with upper drive utilised the same HSU as 1000 kN press. B: Dismounted commercial four-pin die set; lower part: lower shoe having two ball-bearing die-set guide pins in a diagonal configuration and mounted die elements for extrusion, upper part: upper shoe with two guide-bushings assembled. Two of the pins were later removed from the commercial four-pin die set to allow other elements to be added. C: the metal C section and extenders that could be used to transfer the hydraulic actuator displacement and force to the top shoe. The role of the C section was to transfer to load to the 2 extenders. The extenders would then transfer to load and displacement of the hydraulic actuator to the top shoe where the other elements of the rig are located.

The other function of the extenders is to provide sufficient space for the ultrasonic transducer and amplitude booster. The hydraulic actuator force will not be applying the load through the ultrasonic transducer and amplitude booster into the punch but the top shoe and other elements will instead be used for that function.

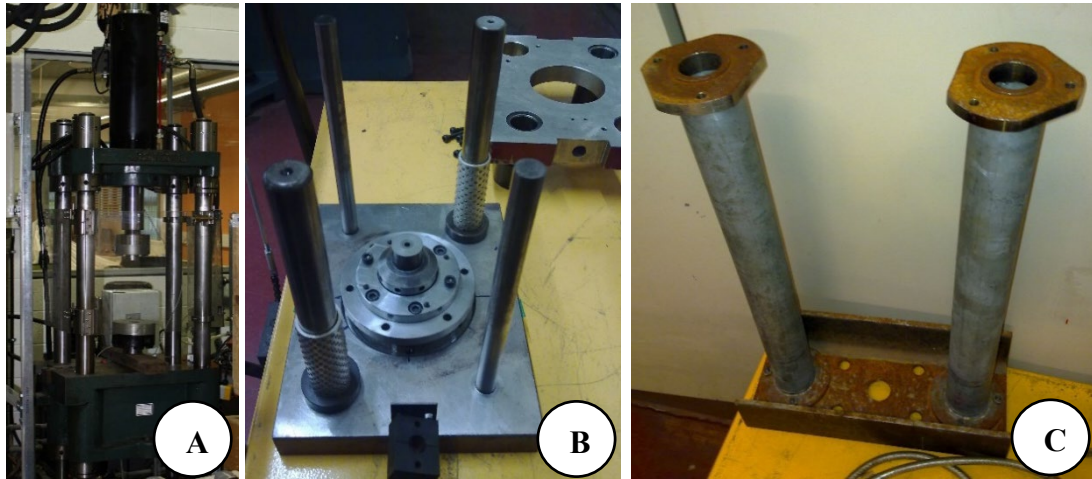


Figure 3.15: *Available equipment. A- 250kN hydraulic press, B- some components that were salvaged and reused from a previous setup upper and lower shoes are visible as well as the guide pins and the ball bearings, C- the metal C section and extenders that could be used to transfer the hydraulic actuator displacement and force into the top shoe.*

All available components were measured and a CAD model of the components was created. A backward extrusion rig was then designed in CAD (see Figure 3.16). With the aid of the CAD model it was possible to specify the alterations that were required for each component so a backward extrusion rig could be produced. Since the hydraulic actuator had a limited reach and more space was required to house the ultrasonic components of the rig, extender cylinders were utilised.

In Figure 3.16 A a CAD model of the fully assembled rig that would be placed inside the Four pillar 250 kN servo hydraulic press previously shown in

Figure 3.15A is shown. There are many key elements to this setup. At the top of the setup, it is possible to see the grey component that attaches to the load cell that in turn is attached to the press ram. This is then attached to the metal C section and the extenders. The extenders are attached to the top shoe that houses other smaller elements of the rig.

In a diagonal configuration front and back, it is possible to see the bushings. The bushing and the ball bearings allow the rig to remain centralised and minimise horizontal movement of the punch. This is very important as it will eliminate the chances of the punch colliding with the die during insertion. The die has an inner

diameter of 5mm and the punch has an outer diameter of 4.95mm therefore the tooling must remain in alignment after setup is completed for the experiments to be conducted correctly. Since backward extrusion will be used in the experiments, any misalignment will result in the material being extruded between the punch and die.

In the other diagonal front and back, it is possible to see stopping blocks and have been highlighted with red circles. These components served two purposes. The first purpose was to aid the raising and lowering of the rig during the initial centring of the punch and die. Once the tools were centred then the screws in the rig were tightened systematically to maintain the central location of the tools. In line with safety protocols and to minimise the chances of accidental finger entrapments it was necessary to disconnect the hydraulic actuator from the tools and to manually move the top section during the initial alignment step. A metric fine thread was applied to the bolts that come in contact with the block allowing fine movement control in during the moving the top half of the rig. The second function of these blocks was to lock the position of the rig while the hydraulic system was switched off. It is possible for hydraulic systems to develop leaks or for seals to perish which can lead to the actuator gradually lowering due to gravity and the weight of the tooling. This feature would prevent the hydraulic actuator from creeping down while the hydraulic system was switched off. Once the hydraulic system was switched on, the controller would return the hydraulic actuator to the correct location. Additional safety precautions were also included in the control system, in the event of a collision (large load registered when the bolts came in contact with the blocks), the control would alert the user. This protected the system from possible damage.

Between the extenders, it is possible to see the ultrasonic transducer and the amplitude booster shown in the yellow arrows of Figure 3.16B. This is then connected to the sonotrode and punch. The sonotrode is connected to the top shoe with couplings that are held into the top shoe with screws.

The load of the hydraulic actuator does not go directly through the piezoelectric stock of the ultrasonic transducer. Red arrow in Figure 3.16B have been used to illustrate how the hydraulic actuator force is transferred to the punch and eventually into the

billet to form the part. The hydraulic actuator provides the liner displacement of the rig and the ultrasonic transducer setup provides the vibration during the forming cycle.

The other components that can be seen in Figure 3.16A are the yellow component located in the centre of the rig, this is the target for the eddy current non-contact displacement sensor and the red component is the sensor holder. The blue arrows in Figure 3.16B show the extender section of the rig, the purple arrows show the top half of the rig and the green arrows show the bottom half of the rig.

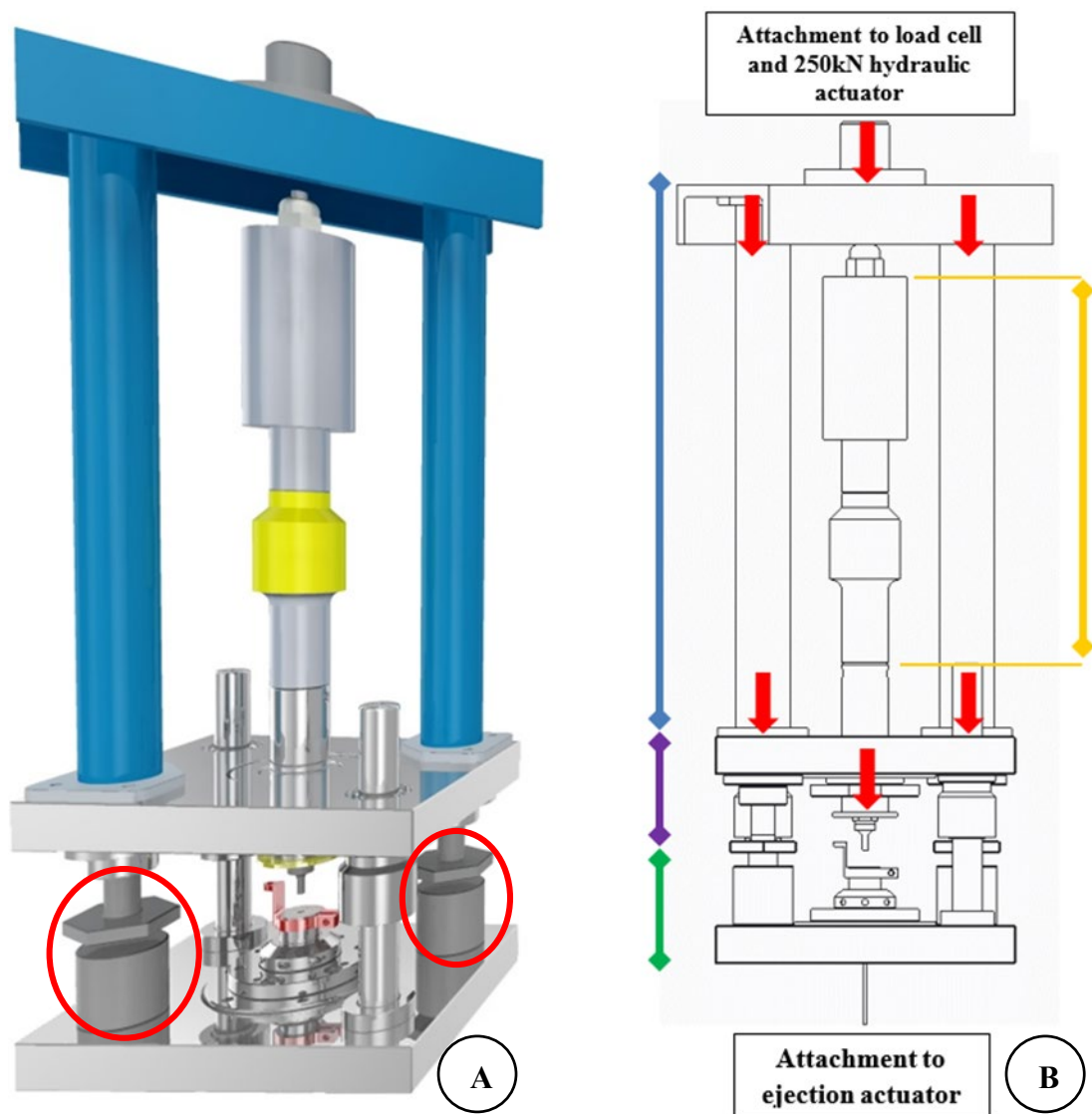


Figure 3.16: *A: CAD model of the microforming backward extrusion rig. The yellow component is the target for the eddy current non-contact displacement sensor and the red component is the sensor holder. The red circles indicating the bolt and block components used during the setup phase of the tooling. B: Some of the main sections of the rig. Blue arrows- extenders, Yellow arrows- ultrasonic*

transducer and amplitude booster, purple arrows top shoe and other top half of the rig components, green arrow- bottom shoe and rig bottom half components.

Using the CAD models, it was possible to reuse many of the existing equipment. New components were also designed and fabricated to allow for the accurate control and recording of the forces and movement of the rig. This rig was also designed to be used with ultrasonic vibration during forming, therefore, to isolate the vibrating components from the rest of the rig and to maximise the effects of the vibration on the forming material Nylon rings were used. The location of these four rings can clearly be seen in Figure 3.17. The vibration would have adverse effects on the rig if allowed to propagate freely. The vibrational behaviour of the punch would also change if the central components were not isolated from the rest of the rig.

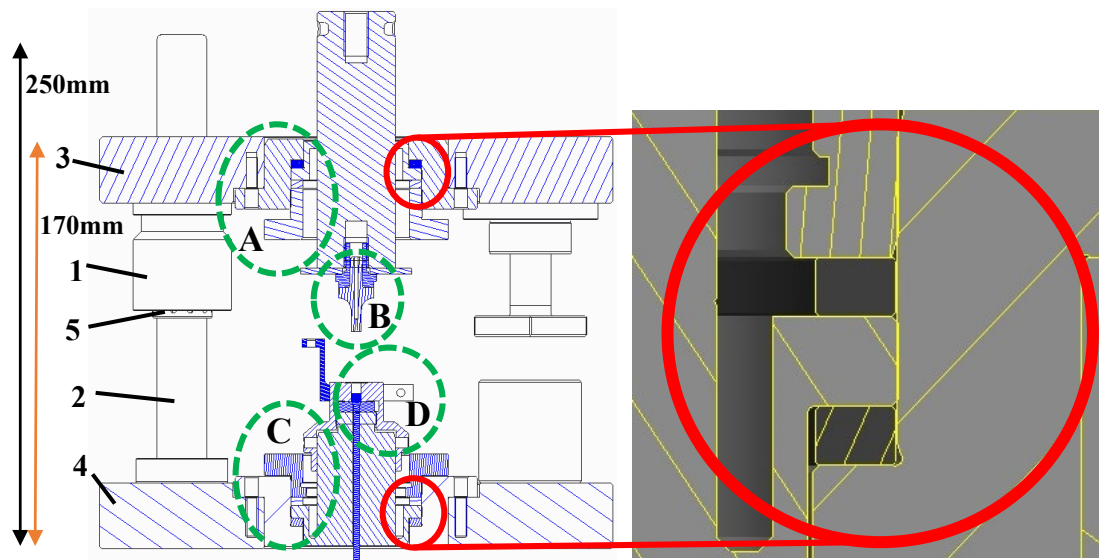


Figure 3.17: *Nylon rings used in the top and bottom of the rig to isolate the vibrating components of the rig from the rest of the rig. The ejector pin can also be seen in the centre of the bottom half of the rig.*

Both parts of the die set for micro extrusion should be guided properly; therefore, an accurate guide-pin system with close tolerances was used. Bushing (1) and guide-pins (2) are press-fitted into the Upper (3) and lower (4) shoes, respectively. Assembly with press fit of balls (5) between the pins and bushes was used on this high-precision tool.

Areas A,B,C and D have been highlighted with green circles. These areas are of interest and detailed look at the rig and the assembly of the components is shown in Figure 3. 18.

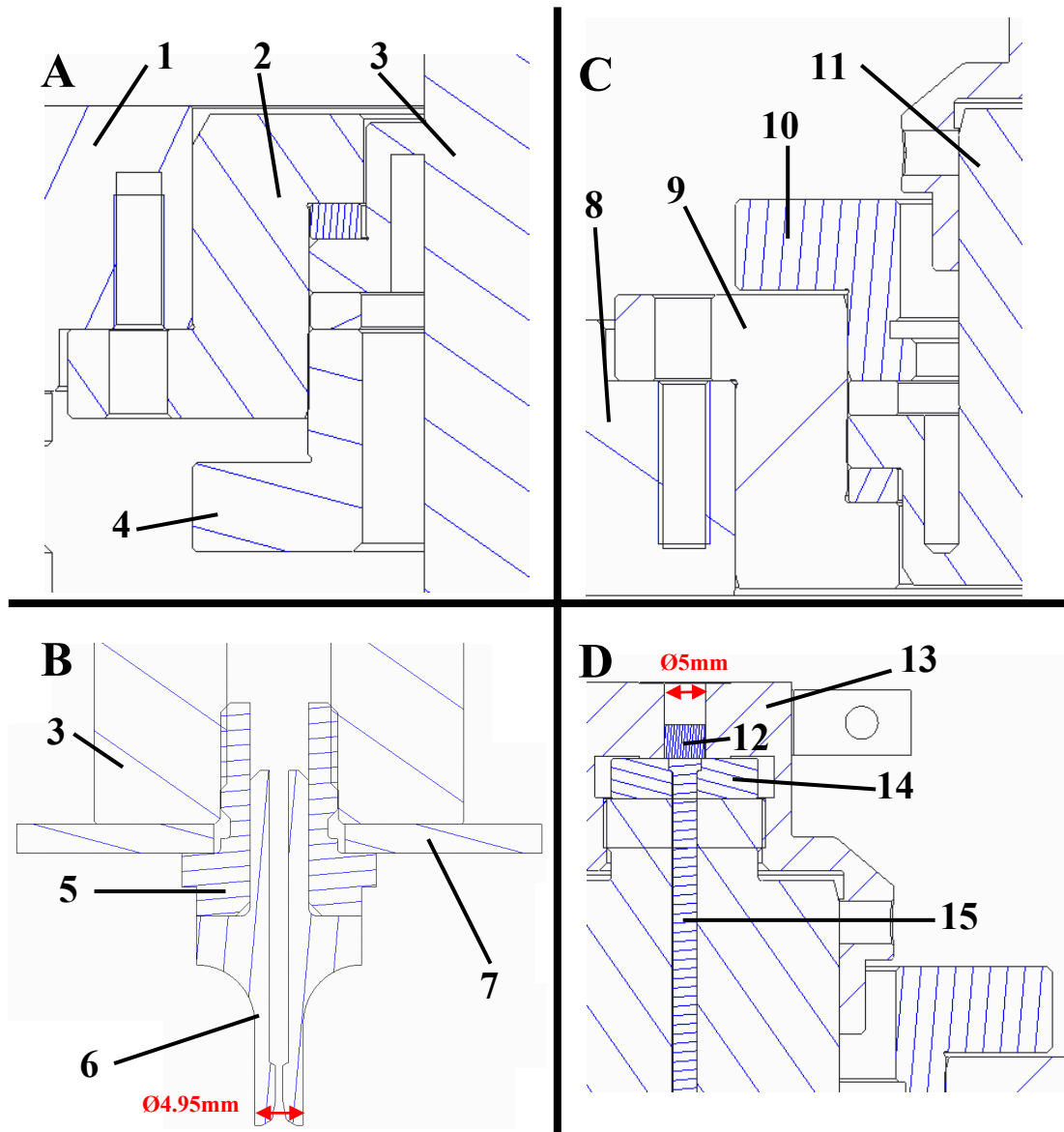


Figure 3.18: 1- Top shoe, 2- top shoe coupling, 3- Ultrasonic sonotrode, 4- Sonotrode to top shoe coupling coupling. (B) 5- Punch holder, 6- Punch, 7- Target disk. (C) 8- Bottom shoe, 9- Bottom shoe coupling, 10- Bottom die holder to bottom shoe coupling coupling, 11- Bottom die holder (D) 12- Billet, 13- Die, 14- Die Disk, 15- Ejector pin. Red arrows also showing the diameter of the punch 4.95mm and the diameter of the die 5mm

The forming force from the top shoe to the bottom shoe is transmitted as follows with reference to the component numbering convention used in Figure 3. 18. Component 1 transmits the force to horizontal contact surfaces between component 1 and 2. Component 2 is held in place with screws and is firmly attached to component 1. Component 2 transmits the force to horizontal contact surfaces between component 2

and 3. Component 4 is held in place with screws and is firmly attached to component 2 therefore hold component 3 in place. Component 6 was fitted into component 5 with an interference fit and adhesive. Component 5 is threaded and is used to tightly connect 6 and 7 to component 3. The forming force travels through component 7, 5 and into 6. During forming component 6 comes into contact with component 12. Some of the force is then transmitted to component 15 and 14. The shoulders on component 15 transmit the force to component 14. the force is then transmitted to component 11, then 9 and then to 8. The Nylon ring shown in Figure 3.17 also play an important role in the transmission forming force going from component 2 to 3 in the top rig components and also the forming force going between component 11 to 9 in the bottom rig components.

Screws are used to fasten the many of the components of the rig together securely. There is an element of flex in most forming processes. This is due to small movement of each component in tool and press assembly. As the number of components increases and the overall number of contact surfaces between the components increase, it is likely to introduce additional flex in the system due to the tolerance of each fabricated component. Best practice would be to increase the stiffness of the experimental rig by reducing the number of components but in this case, each component is required as elaborated above.

The press is stopped using the precision hydraulic controller and Cubus software. The most reliable method for achieving the desired results would be to load a billet into the die and then lower the punch into the die until it came in contact with the billet. This was done using the manual controls on the hydraulic controller in the slowest setting. once the punch was lowered and had come into contact with the billet a small load would be registered on controller. This would then be set as the zero and start position of that experiment. The velocity and displacement of the experiment would be then entered into the software and the experiment started. Once the experiment was completed then the hydraulic ram would be returned to the topmost position and allow for the part to be ejected.

All components of the previous rig were dismantled, inspected and where required re-machined, ready for the new backward extrusion rig. These components are illustrated in Figure 3.19.

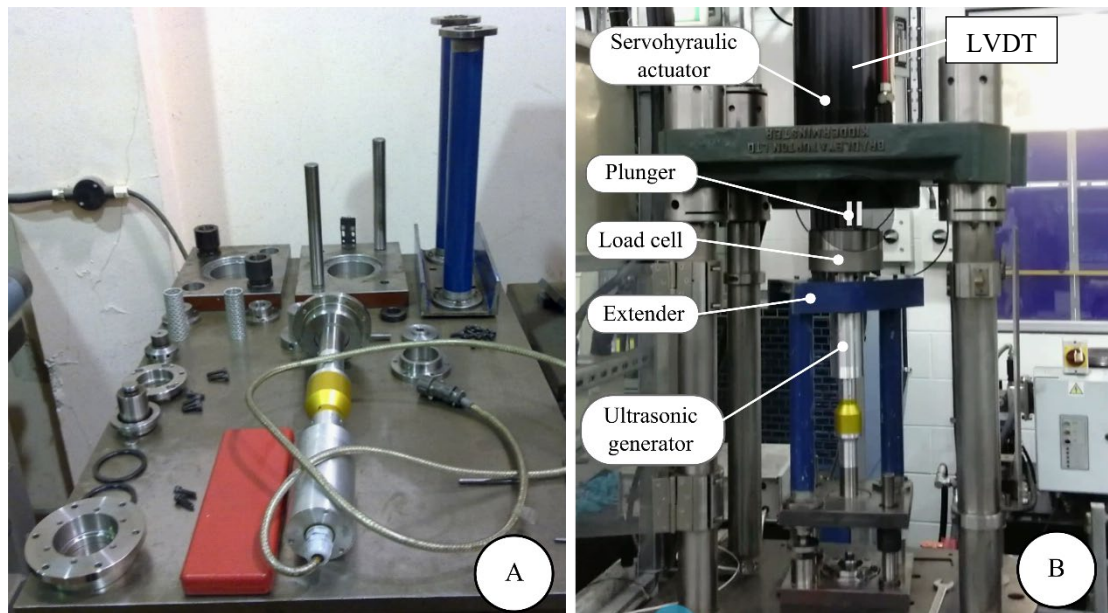


Figure 3.19: *A - The components of the rig before assembly and testing.
B - Fully assembled rig inside the 250kN hydraulic press.*

Many of the elements that were used on the 1000kN IECAP press that were shown in Figure 3.12, were also used for the 250kN press. To capture the load exerted by the actuator, a new load cell was connected between the 250kN actuator and the micro-forming rig extenders. This load cell was then tested and calibrated prior to the experimentation. To capture the forming stroke of the punch, an eddy current non-contact sensor (Micro Epsilon eddyNCDT 3010, Germany) was utilised. This sensor is capable of achieving a resolution of $0.05\mu\text{m}$ so should be able to capture the small amplitude variation of the oscillating ultrasonic punch. The eddy current non-contact sensor was mounted on the die (as shown by the red component in Figure 3.16). This type of sensor has specific read surface requirements, therefore, a steel target disk was produced (as shown in yellow in Figure 3.16) and attached to the punch. The technical specification of the eddy current non-contact sensor can be seen in Figure 3. 20.

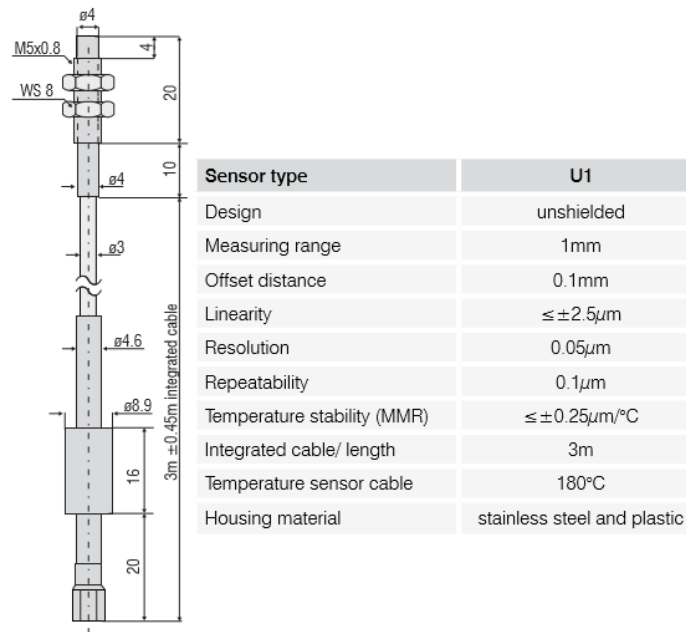


Figure 3.20: *Micro Epsilon U1 eddy current non-contact sensor specifications*

Similar to the configuration of the 1000kN IECAP press, Zwick Roell Cube controller and Cubus software with additional modules were used to control the actuator of the 250kN press. This allowed precise control of the displacement of the actuator, therefore, allowing the experiments to be repeatable to a high level of accuracy.

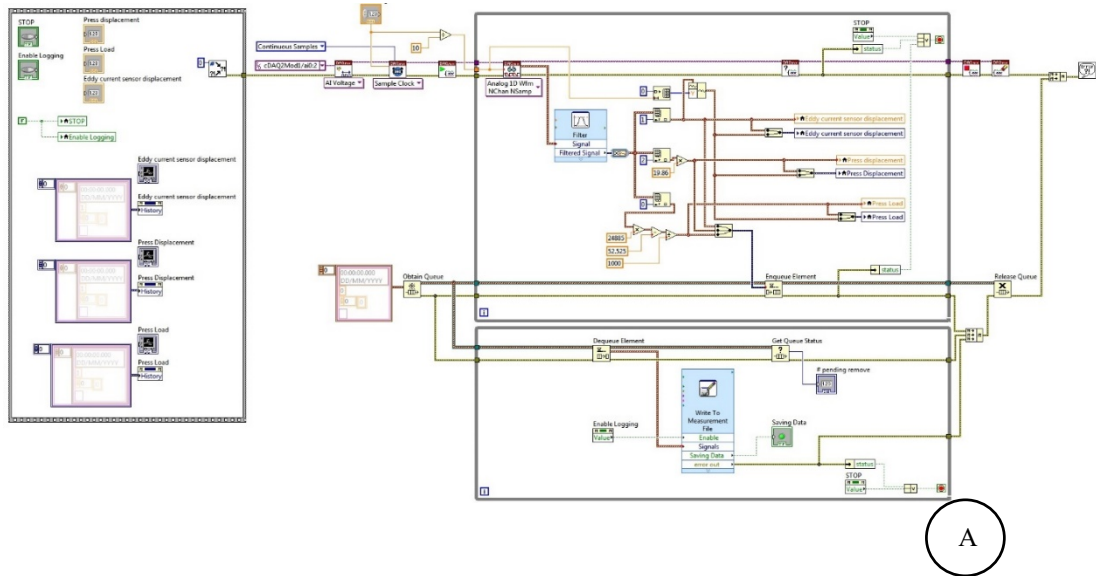
A new LabVIEW virtual instrument was designed and built to capture the information from the eddy current non-contact sensor, actuator LVDT and the load cell. The system diagram and front panel for this custom virtual instrument is shown in Figure 3.21. A large image of the full system diagram for this virtual instrument can be found in appendix A.

For a device to be referred to as ultrasonic, it has to oscillate at over 20kHz. To capture these signals a scan rate of at least 2 times this frequency is necessary, this is referred to as the nyquist frequency. The scan rate that was chosen for these experiments was 100kHz. This would allow more of the data to be captured per cycle, therefore, a smoother signal could be captured. A buffer was designed into the virtual instrument during the read cycle to capture the data without losing the sensor data during writing cycle. In addition to the National Instruments modules that were used in the IECAP

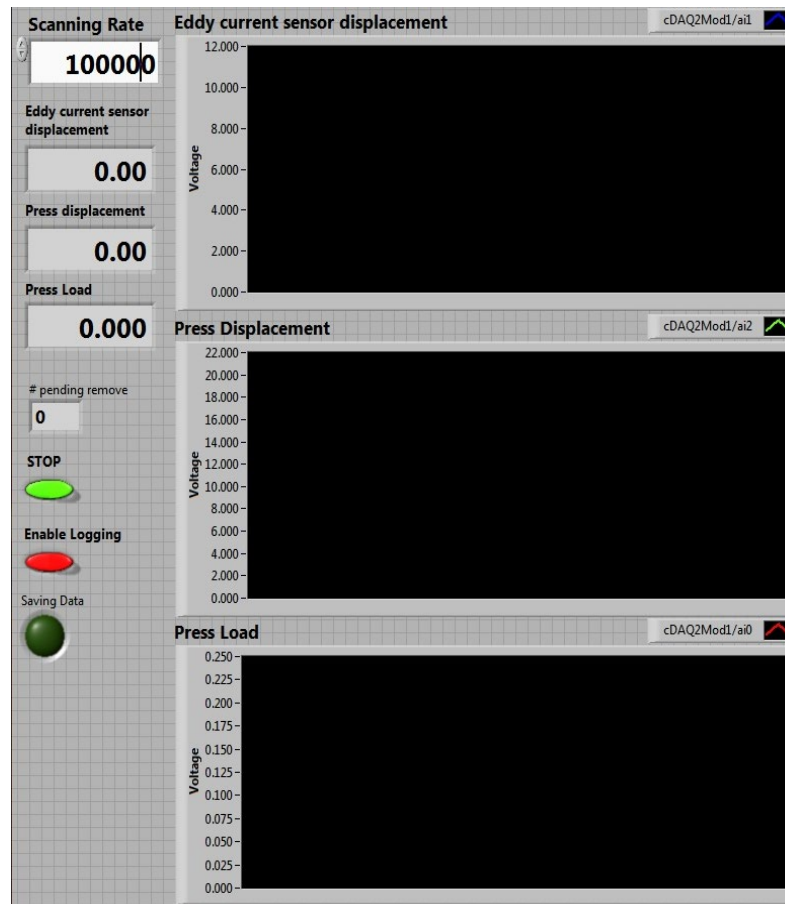
press a NI9222 module was also used. This module allowed for very high signal capture rates to be achieved.

A simple hydraulic actuator was installed at the bottom of the 250kN press and used for ejection of the formed components. An ejection pin was designed and placed at the bottom of the central component of the bottom half of the rig. The ejection pin can be seen in Figure 3. 18.

Once the rig was fully assembled, it was tested for function and safety. This rig is complex and has several different systems and sensors from different manufacturers and suppliers, therefore, it was necessary to fully test the system assess its controllability and data collection ability. Once the die and punch had been aligned, small adjustments were made to the sensor locations to achieve the best results during experimentation. All sensors were used within their calibration range. The calibration step is critical as it gives confidence to the results from the experiments. Once all the necessary safety checks had been completed, then trial experiments were conducted and the rig was fully commissioned for use.



A



B

Figure 3.21: The custom made virtual instrument used to capture the data from the eddy current sensor, actuator LVDT, and load cell. A- the LabVIEW system diagram for the virtual instrument. B- the front panel of the custom virtual instrument.

3.11. ULTRASONIC EQUIPMENT

The advantages of ultrasonic forming have been discussed previously in chapter two (literature review). To induce the ultrasonic oscillations required for ultrasonic forming various components are required. Ultrasonic experiments had previously been conducted within this research institution, therefore, some equipment were available. The four main components for ultrasonic forming are, the generator, transducer, booster and the sonotrode. The following section will describe the components used in the ultrasonic setup.

3.11.1. Ultrasonic Generator and Control Circuit

A custom made controller box was designed and built, by Dr Kris Chodnikiewicz and Dr Paul Fabijanski. It was used to generate the signals required to excite the piezoelectric transducer at the required resonance frequency. The ultrasonic generator converts 50/60 Hz AC power into high frequency ultrasonic power. The high frequency power is used to drive the transducer. Sophisticated control circuits in the generator are used to control the amplitude and the frequency of the oscillations. The maximum output power of the generator was 1.5kW. The amplitude at the transducer face is 0.006mm and it operates at frequency of about 20.1kHz. A 2:1 amplitude booster was also utilised during forming therefore, an amplitude of about 0.01mm could be achieved at the punch contact surface. The custom control box and the internal electronics can be seen in Figure 3.22.

After initial testing it was found the box had developed a fault. The box was repaired and fully tested prior to the ultrasonic experiments being carried out.

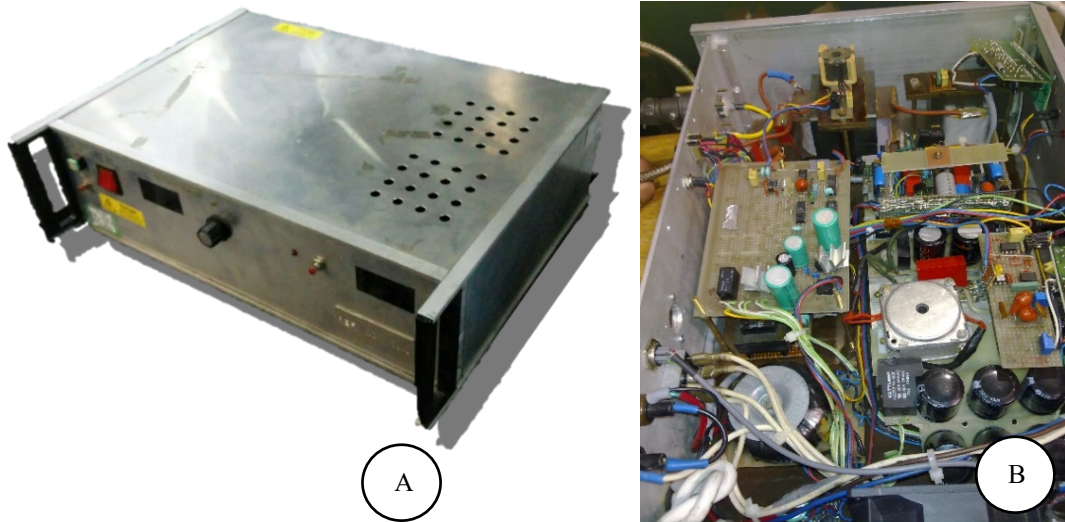


Figure 3.22: *A) the custom made ultrasonic control is shown. A dial for controlling the amplitude is located in the middle of the control facing. Seven segment displays are used to display the frequency of the oscillation. B) the internal electronics of the control box after repairs had been carried out.*

3.11.2. Ultrasonic Transducer

The ultrasonic transducer is a stack of piezoelectric plates that are used to convert the electrical energy from the generator into movement. This special properties of piezoelectric material causes them to produce a potential when their shape is altered. This also works the other way around and it is this property that is exploited in the process. The high frequency energy pulses from the generator causes small changes in the shape of the piezoelectric plate. These changes in dimensions are very small, therefore, a series of plates are connected together to increases this movement. The transducer used for the experiments can be seen in Figure 3.23.

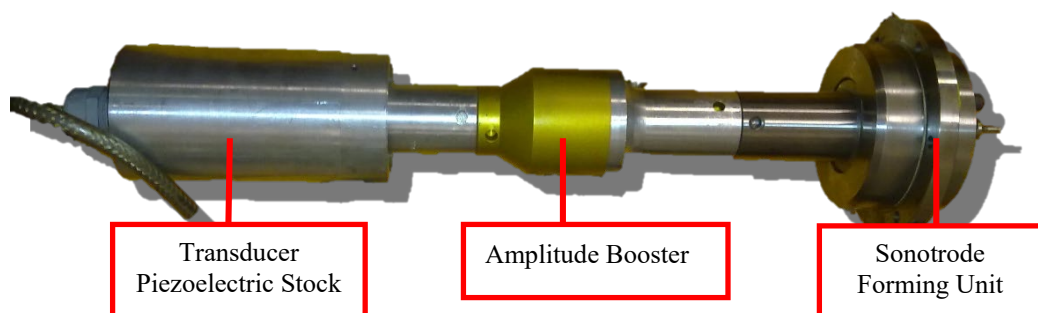


Figure 3.23: *The fully assembled ultrasonic generator consisting of transducer, booster, and sonotrode that was used for the ultrasonic experiments.*

3.11.3. Ultrasonic Booster

The amplitude of the oscillations produced by an ultrasonic transducer is not sufficient for practical applications, therefore, a booster is required. The booster increases the amplitude of oscillation of the sonotrode while resonating at the same frequency as the transducer. The booster used can be seen in Figure 3.23. Boosters are usually made from metals that have high fatigue strengths and low acoustic losses such as titanium, stainless steel and aluminium. This allows the vibrational energy from the transducer to be sent to the work piece.

The frequency used should be similar to the natural frequency of the system, otherwise the effect of the vibrations will be limited and the energy will be lost from the ultrasonic system. Other adverse effects can be the transmission of the vibration to the rest of the structure, which can lead to loosening of screws in other parts of the rig.

3.11.4. Sonotrode

Sonotrode are also known as the tool in the ultrasonic forming system. As can be seen in Figure 3.23, in our configuration, this was the punch. This was attached to the booster of the ultrasonic system and was used for the purpose of delivering the oscillating action and effects to the material. Since the tool is the actual component that comes into contact with the work piece, it is often made from very strong material such as tool steel. More details of the punches used for this study are discussed in the following section.

3.12. PUNCH AND DIE FABRICATION

Punches and a die were required for the backward extrusion process. The design of the punch cavity was based on the findings of FE analysis that will be described on the results and discussion chapter. Producing punches that could be used for micro backward extrusion was challenging but several technologies and manufacturing techniques were examined. The following section will describe the manufacturing techniques used to produce the single pin and the multi micro needle punches.

3.12.1. Punch Material

The material that the punch was fabricated from was critical as it would be subjected to large loads, but would have a small cross sectional area as shown in the CAD model in Figure 3.16 and Figure 3.18. The chosen material would also have to be very machine-able so the small features and the smooth surface finish could be achieved. From previous experience it was recommended that the punch to be produced in two parts. A harder material should be used for the working area and a softer material for the threaded section that attached to the rest of the upper rig. Using a softer material for the threaded section would minimise the chances for fracture when ultrasonic vibration was applied.

Vanadis 23 was chosen as the punch material and standard tool steel was used for the threaded section. Vanadis 23 is a high alloyed powder metallurgical high speed steel. It has good abrasive wear resistance and has high compressive strength. It is often used in industry for cold work applications. It has high machinability and grind-ability when compared to high speed steel. It is also dimensional stable after additional hardening heat treatment. Several blanks were produced at Pascoe Engineering Ltd and sent for hardening. The cylindrical part of the punch was ground to the final dimensions to achieve the required tolerances.

3.12.2. Single Pin Punch Fabrication

The shape and dimensions of the single pin was determined by FE analysis. The single pin was scaled larger than the final needles so it would be manufacture-able and could be used for initial testing and verification. Pascoe Engineering were commissioned to produce the conical cavity of the single pin punch using sink EDM. They produced a copper tungsten electrode of the required shape, which can be seen in Figure 3.24.

This electrode material is known for its low wear and high definition feature creation abilities. It is also possible to achieve good surface finishes with this material. Prior to using the electrode to produce the required cavity, a spark drill was used to produce a through hole in the centre of the punch. This centre hole would minimise the wear on the tip of the electrode and would allow lubricants to pass through the punch when it was being used in the backward extrusion process. Once the fabrication process was

completed, the two parts of the punch were connected with an interference fit and chemical adhesive. The completed punch can be seen in Figure 3.24B. To verify the shape of the punch one of the punches was cut in half and inspected. The half punch can be seen in Figure 3.24C.



Figure 3.24: *A- the copper electrode used for the sink EDM manufacture of the single pin punch. B- the fully fabricated single pin punch. C- single pin punch sectioned in half so the profile of the cavity can be verified.*

3.12.3. Microneedle cavity punch fabrication

Due to the small size of the features required for the microneedles, it was not possible to use sink EDM as used for the single pin punch. As well as the size of the cavities there was also a further challenge of producing an array of identical cavities. Hence, an alternative manufacturing technique was required.

Cardiff University was contacted due to their specialist knowledge and capability in the field of micro and Nano machining. They have research groups and machinery dedicated to laser machining. They had recently acquired a DMG Mori Lasertech 40 and were eager to test its capability. Dr Samuel Bigot agreed to produce the micro cavities on the Vanadis 23 blanks. The Lasertech 40 used the laser ablation technique to remove material from the punch. It has a complex assembly of lenses that can be moved to direct the laser to the required section, so complex shapes can be produced. This system is capable of Pico second pulses, therefore, cavities can be produced with

very little alterations to the surrounding material. Laser power calibration trials were conducted on the Vanadis 23 material and can be seen in

Figure 3.25 A. A small square was removed from the centre of the sacrificial blank. A series of cavity shapes were removed from the perimeter of the blank to fine-tune the laser parameters before a new blank was used for the required conical holes.

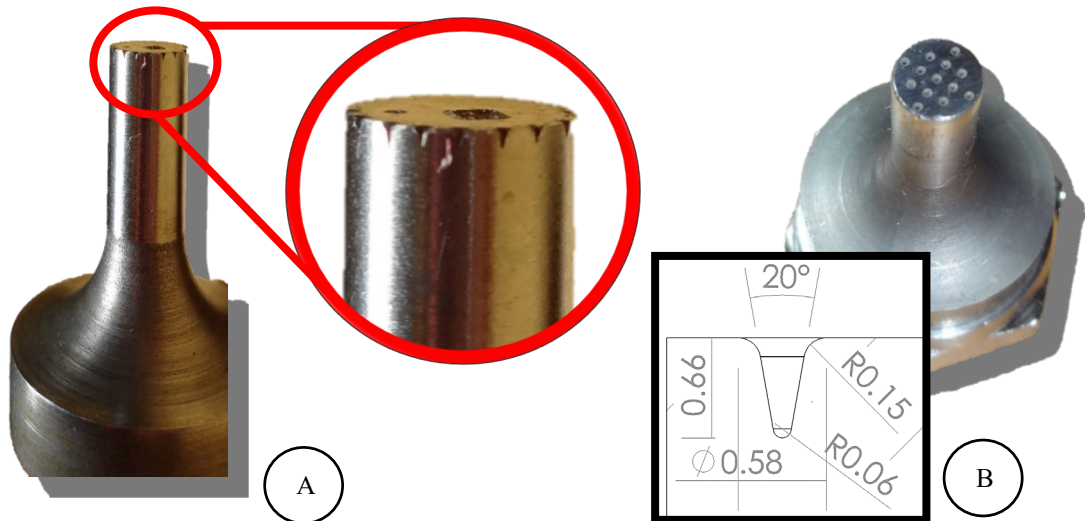


Figure 3.25: *A- the sacrificial blank that was used for calibrating the laser in the DMG Mori Lasertech 40. A series of conical holes can be seen on the perimeter of the blank. B- the microneedle punch with an array of micro conical cavities. The cavity dimensions are shown. Cavities are 1mm apart*

Once the laser equipment had been calibrated to the Vanadis 23 material, an array of micro cavities was produced in a new blank, as shown in Figure 3.25 B the cavities were 1mm apart. The two parts of the punch were connected together with an interference fit and chemical adhesive. This maximised the connection between the 2 components so they would not come apart when vibration was applied.

3.12.4. Die Fabrication

Compared to the punches, the die for backward extrusion process is very simple. A cylindrical hole was created the same size as the punch. Then it was precision ground to slightly larger than the punch diameter. The diameter of the punch was 4.95mm and the inner diameter of the die was 5mm as can be seen in Figure 3.18. This small difference was designed to allow the punch to go into the die but be too small for the material to extrude out from the sides during the backwards extrusion process. The bottom of the die was closed with a polished disk of hardened steel.

As can be seen in Figure 3.18, a stepped hole was made in the bottom of the disk to allow an ejection pin to be inserted into the die. The hydraulically driven ejection pin would remove the formed billets after the backward extrusion cycle was completed. The ejection mechanism was at the bottom of the die so damage by contact to the pins was avoided.

The two halves of the rig had to be aligned carefully to allow for the punch to be inserted into the die and for a uniform clearance along the parameter to be maintained. The adjustable elements that were designed into the rig allowed for some movement for alignment during setup these can be seen in Figure 3.18. The two couplings in the top and the two couplings in the bottom of the tool set allowed for small adjustments to be made. Once the die and punch had been aligned correctly, all the screws that held the couplings in place were cross tightened to maintain alignment of the punch and die. This allowed for a uniform clearance along the parameter

3.13. SUMMARY

In summary this chapter looked into the materials and methods that are required to perform the experiments for this project. Aluminium was chosen as the material that would be used for these experiments due to its low young's modules. Although it is not known for its bio-compatibility properties, it will be a good indicator of the processes that would be required to produce metal microneedles. One of the key factors affecting formability in the micro scale was identified - in the literature - as surface roughness. Methods for measuring the surface roughness of the parts and tools was explored and identified. The surface roughness will have an effect on lubrication usage, therefore, a variety of lubricants have been identified and the methods by which they achieve their lubricity explored. Liquid and solid lubricants are available as well as conversion coating. Gold sputter coating was also examined as a method for producing a coating layer on the surface of the part to increase the formability of the micro components.

To quantify the change in the physical properties of the material during the IECAP processing steps, hardness testing methods and equipment have been examined. An IECAP rig with several sensors and virtual instruments have been created to produce

ultra-fine grained materials. Tensile testing equipment will also allow for the properties of the material to be examined, so a direct relationship can be created between the IECAP process and the materials ultimate tensile strength.

In the literature review chapter, ultrasonic oscillations were identified as a method that could be used to further improve the formability of the components. A backward extrusion micro-forming rig that was designed and fabricated was also equipped with ultrasonic oscillation equipment to allow for this factor to be examined.

A punch with a larger conical hole was produced using sink EDM but for the small array of microneedles this method would not be suitable, therefore, laser machining was identified and used to produce the backward extrusion punch what would be used to produce an array of microneedles.

The following chapter will examine the IECAP process for refining the grain size of the aluminium. The change in the mechanical properties of the material will be explored. The micro forming rig will be used to form components from the coarse grain and ultra-fine grain material. FE analysis will be used to refine the processes and the effect of ultrasonic oscillations will be explored in depth to find the best process parameters for producing metal microneedles.

4. RESULTS AND DISCUSSION

4.1. INTRODUCTION

This chapter is arranged in four parts as follows:

In part 'A': Effect of channel angle on the material flow, hardness distribution and process forces during incremental ECAP of A11050 billets have been studied. Incremental Equal Channel Angular Pressing (IECAP) is an evolution of the classical Equal Channel Angular Pressing (ECAP) method used to produce Ultra-Fine Grained (UFG). These metals have increased mechanical properties compared to their coarse grained counterpart. Initially this section looked at the effects of using 90° and 120° die channels for the processing of 10X10X60mm A11050 billets. Factor that can affect the induced strain and the resulting grain refinement is the channel intersection angle (ϕ). Where Typically, $\phi=90^\circ$, which produces equivalent plastic strain of approximately 1.15 and $\phi=120^\circ$ produces equivalent plastic strain of approximately 0.67 based on the equation mentioned shown in chapter 2.

Larger value of this angle reduces the amount of strain generated in each pass but can potentially reduce the chance of material fracture. The forces required to process the billets for the first pass was examined and compared. Hardness maps were created to examine the change in materials mechanical properties. It was found that using the 90° configuration results in higher press forces and greater uniformity of hardness distribution when compared to 120°. The results correlated to the findings of the simulations that were carried out prior to the experimental investigation. The 90° configuration was chosen for further billet processing since it resulted in greater shear and better grain refinement. The results of further processing passes are discussed in part B.

In part 'B': Seven more passes were conducted using root B_C for a total of eight IECAP passes. Following the multi-pass experiments for the 90° die configuration, the effects of punch load during further IECAP steps, hardness evolution of the billets and the tensile strength of the material is studied and reported. TEM was used to verify the refinement of the grains after further processing passes.

In part 'C': In this section a variety of surfaces and lubrication conditions have been examined experimentally for the production of a single pin using backward extrusion. The effects of lubrication, billet grain size and surface condition have been compared against surface roughness, press forming force and pin height. Following on from the single pin experiments, multiple smaller metal microneedles were produced using backward extrusion. Ultrasonic oscillations were also superimposed on the forming process and the effects of this have been examined, analysed and discussed.

In part 'D': Extrusion of micro components poses several challenges, which need to be overcome before becoming a commercially viable production method. Firstly, there are technological and practical issues such as the requirement for very small tools, lack of suitable handling devices for both the micro billet and the formed component and suitable quality control methods. As well as the challenges mentioned previously there are other fundamental differences that make the micro-extrusion process different from macro-scale metal forming (Engel et al. 2007). Micro-billets have lower yield strength for surface grains, different metallurgical orientation of the grains results in less uniform material flow and large surface grains increase friction due to open lubricant pockets at the billet end surfaces.

To overcome some of these problems it is possible to use ultrafine grained (UFG) metals (average grain size less than 1 μm) in preference to coarse grained (CG) metals (grain sizes 10-300 μm) (Olejnik et al. 2009). One of the main advantages of using UFG metals for micro forming is that the material acts as a polycrystalline solid rather than the one made of only few large grains per billet. Other advantages of using UFG metals over CG metals are the improvement in uniformity of material flow, better surface finish and increased hardness and strength. UFG metals require higher forming forces, which is the result of having higher yield strength compared to their CG counterparts. UFG metals can be produced by severe plastic deformation of CG metals but large commercial quantities of UFG metals are not available yet. On the other hand, small billets required for micro forming can be produced using a small amount of UFG material.

FE analysis is used in assessing backward extrusion of multiple micro-pins. The effects of pin geometry, layout and spacing have been examined in this study. The effect of

friction on material flow and accuracy of pin geometry has been investigated. FE analysis was performed for a commercial grade A11050 as well as its ultrafine grained version, allowing a comparison to be made. Pin layout plays a significant role in achieving uniformity of pin height. Material starvation resulted in the central pins being shorter than the surrounding pins. Simulations without the centre pin were conducted, which resulted in increased pin height uniformity. Simulations with friction resulted in a greater uniformity of pin height, but required a greater load. Using stronger ultrafine grained material has resulted in an increase in the required load and pin height uniformity.

4.2. PART A: EFFECT OF CHANNEL ANGLE ON THE MATERIAL FLOW, HARDNESS DISTRIBUTION AND PROCESS FORCES DURING INCREMENTAL ECAP OF AL-1050 BILLETS

Severe Plastic Deformation (SPD) is gaining significant attention by researchers as a method for refining the average grain size of material and to obtain ultrafine grain (UFG) material where grain size is below 1 micron (Valiev et al. 1991), (Akhmadeev et al. 1992), (J. Wang et al. 1993).

This section systematically examines the first pass of Al1050 during IECAP, with the channel intersection angle $\phi=90^\circ$ and $\phi=120^\circ$, via experiments and FE simulation, to compare both processes.

Continuing to simulate the process can often be difficult and cumulatively introduce errors into the FE analysis resulting in large errors in further passes, therefore, the effect of further passes will be examined experimentally once the suitable die has been chosen. The mechanical properties of the material produced can also be examined using a tensile testing machine. If the material has been processed correctly, then a marked improvement in the Young's modulus of the material should be observed. This can also influence the hardness of the billets. Therefore, the hardness of the billets will also be examined to observe the hardness distribution throughout the billet.

4.2.1. IECAP Process

In IECAP, the material feeding stage and the deformation stage are separated as opposed to classical ECAP (Rosochowski & Olejnik 2011). The IECAP process is described in detail in 'Chapter Three', but to increase productivity, a dual processing method was used in this study. The illustration of IECAP process shown in Figure 4.1 illustrates the two billet simultaneous processing version that was used in this study. A punch, which follows a sine wave form (oscillates at a certain frequency and amplitude), comes cyclically in contact with the billets. The billet material is pushed into the deformation zone in increments of distance 'a' – feeding stroke by the pusher tool.

Material feeding is timed to occur when the punch is retracting. The punch and pusher movement is shown in Figure 4.1. The punch moves down and deforms the billets

during the deformation stage. To help separate the two billets the punch has a spike in the middle to facilitate material flow into the output channels this is not shown in the schematic. The mode of deformation is similar to that in classical ECAP i.e. simple shear, provided the feeding stroke is not large. Separating the feeding and deformation stages, it is possible to reduce or eliminate friction during feeding. Resulting in a large reduction in the feeding force and enabling the processing of longer billets.

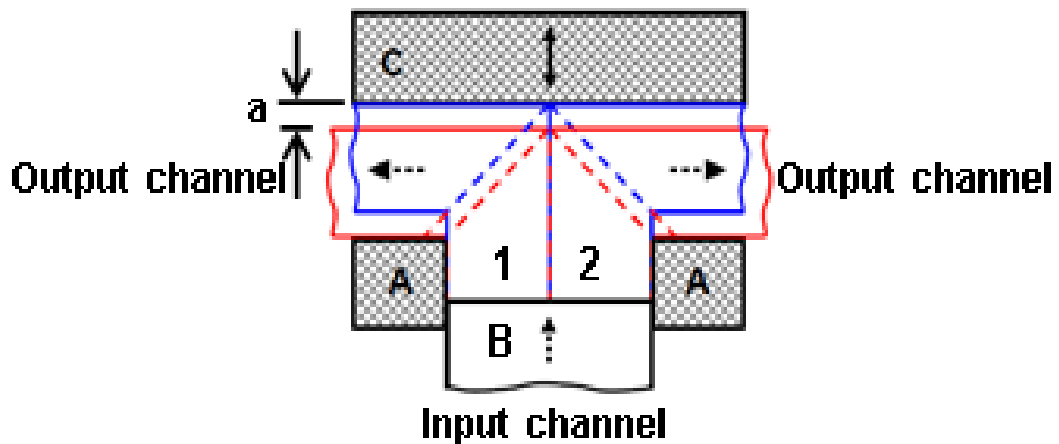


Figure 4.1: *Schematic of IECAP process (A=Die, B=Pusher and C=Punch)*
Rosochowski and Olejnik 2011.

The Figure 4.2 shows the relative motion of tools (punch and pusher) in a typical IECAP process. Here the punch is oscillating with an amplitude of 1.6mm at 1 Hz and feeding stroke is 0.5mm/cycle. Timing the pusher movement is critical as mistiming would result in the pushing the billet up and the punch moving down at the same time, resulting in large forces being exerted on the screw jack and causing its breakage. As well as damaging the pusher the billet microstructure distribution would not be uniform. Therefore, it is critical that pusher moves up only during stage one – feed stage, and remains stationary during stage 2 – deformation stage.

The IECAP press was described in detail in ‘Chapter Three’, but an overview is described in the following section. The IECAP process is carried on the customised 1000KN servo-hydraulic press. To achieve the coordinated movement that was described in Figure 4.1, the punch and pusher were controlled by the Zwick Control Cube via the Cubus software. The required movement of the punch and pusher was

programed using the graphical user interface provided by the Cubus software and translated into the required movements.

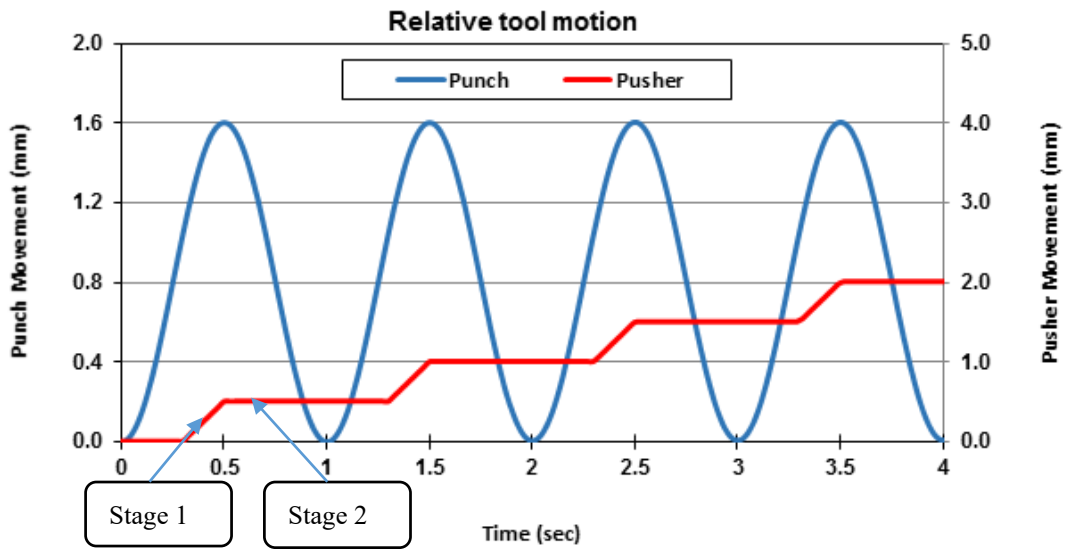


Figure 4.2: Relative movement of punch and pusher tools during the IECAP process. Stage 1 – feed stage. Stage 2 – deformation stage.

4.2.2. Experimental Setup

Two different punches and dies suitable for them were investigated and can be seen in Figure 4.3. This will allow for the investigation of the effects of punch and output channel angle. The difference between the 90 degree and the 120 degree punch angles can clearly be seen in

Figure 4.3. Since the punch angles are different matching output channel dies also had to be fabricated. The punch is attached to the press actuator and follows a sinusoidal cyclic command during processing.

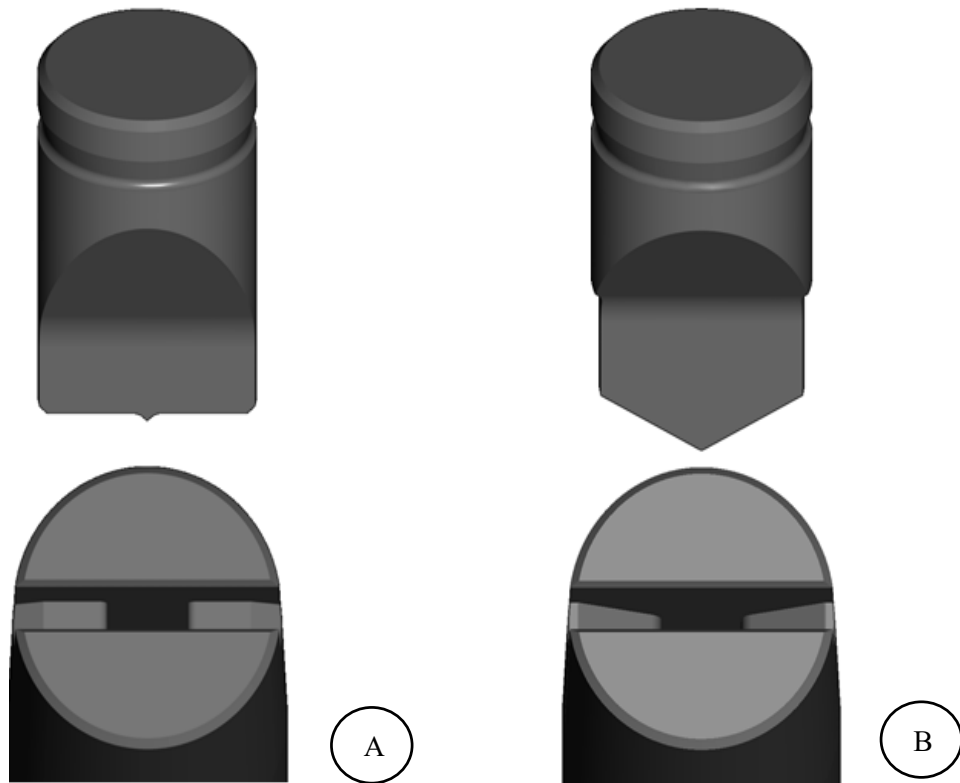


Figure 4.3: The punch and split die design for A $\phi=90^\circ$ IECAP die and B $\phi=120^\circ$ IECAP die.

The billet feeding is performed by a servo-motor driven screw jack. A dedicated LabVIEW application controls and synchronises the material feeding by monitoring the punch oscillation. The application also records and captures deformation and feeding force during processing.

4.2.3. First Pass Experiments

Prior to starting the experiments, the chemical composition and microstructure of the starting Al1050 billets were examined. Al1050 is 99.5% Aluminium with traces of the following elements Cu, Mg, Si, Fe, Mn, Zn, Ti. A sample of the material was polished and prepared for Scanning Electron Microscope (SEM) examination. The image obtained can be seen in Figure 4.4A. Image analysis was used to map the grains (as shown in Figure 4.4B), allowing for the determination the mean grain size of material to be calculated as 140 μm .

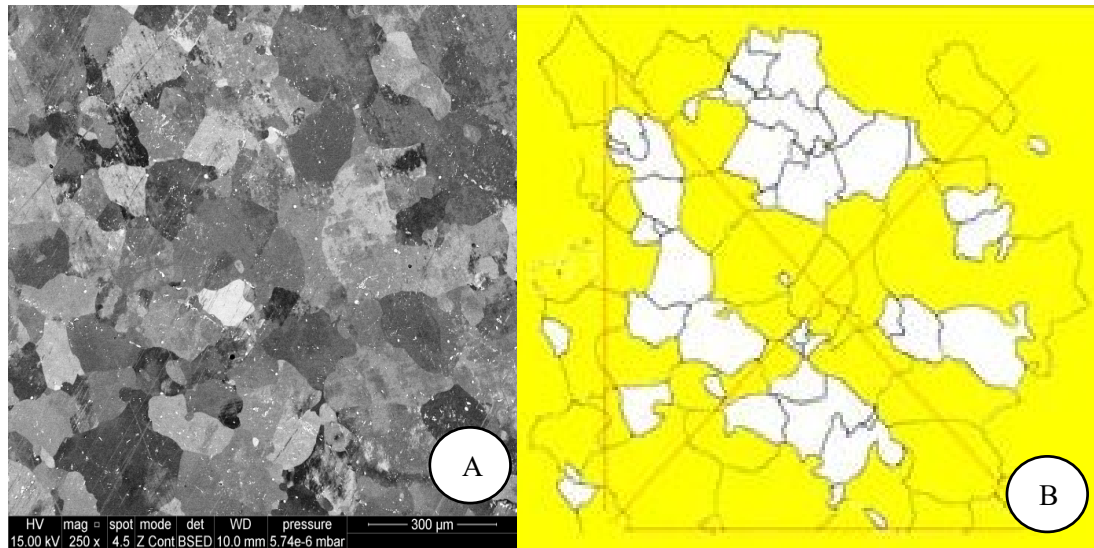


Figure 4.4: *A – the initial microstructure of the Al1050 material using SEM.
B – The grain boundaries determined by software to calculate grain size.*

Experiments were performed using Al1050 billets measuring 10x10x60mm, the billets were machined slightly larger than required from round bars in the extrusion direction. Prior to starting the processing of the billets, it was necessary to perform some preparation steps to minimise the chances of billets sticking to the input and output channels. These preparation steps taken for the first pass included final pair grinding because billets were cut slightly larger than the channel. A tight fit is required, therefore, the final size grinding was performing in pair will allow the best fit to be achieved the billets where then conversion coated with Calcium Aluminate as described in chapter three and a final thin layer of Loctite 8009 (a graphite based anti-seize lubricant) from Henkel technologies was applied. The multi layered billet lubrication steps should minimise friction during the processing and avoid sticking of material to the die walls.

IECAP process was carried out at room temperature with a cycle frequency of 30 strokes per minute (0.5 Hz), peak to peak punch amplitude of 1.6 mm and a feeding stroke of approximately 0.2 mm. The process was stopped once half the billet was processed to allow for a study of billet to be undertaken. By stopping the billet once it is half processed it is possible to get further insight into how the material is changing during IECAP processing. The two pair of half processed billets from the 2 different processing angels are shown in Figure 4.5.

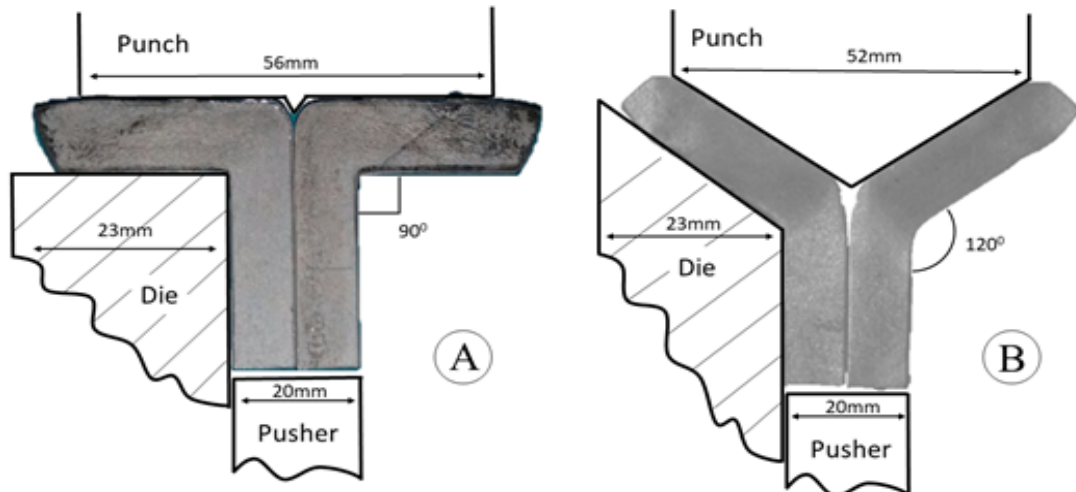


Figure 4.5: *Pair of billets after cleaning. Represents the shape of the billets after 50% processing with A – $\phi=90^\circ$ and B – $\phi=120^\circ$.*

The billets were washed with cold water and soap to remove some of the black graphite based lubricant to allow a closer examination to be made. The channels and punches were also closely inspected to see whether material from the billet had adhered to the walls of the channel or the surface of the punch.

It was observed that no material had adhered to the surface of the 120° punch and no material was remaining in the corresponding channels. It was also observed that the conversion coating had remained on the 120° billets. The conversion coating on the top surface of the 90° billets (the surface that was in contact with the punch) appeared to have been removed and that surface appeared very smooth and reflective. There was a sign that greater wear and rubbing had taken place on that surface. A small amount of material could be seen to have adhered to the channels and there were small sharp burrs visible on the billet.

The LabVIEW virtual instrument that was designed for this experiment was capable of recording the forces exerted by the punch at the top and the pusher at the bottom. The results of the forces from the punch and pusher are shown in Figure 4.6.

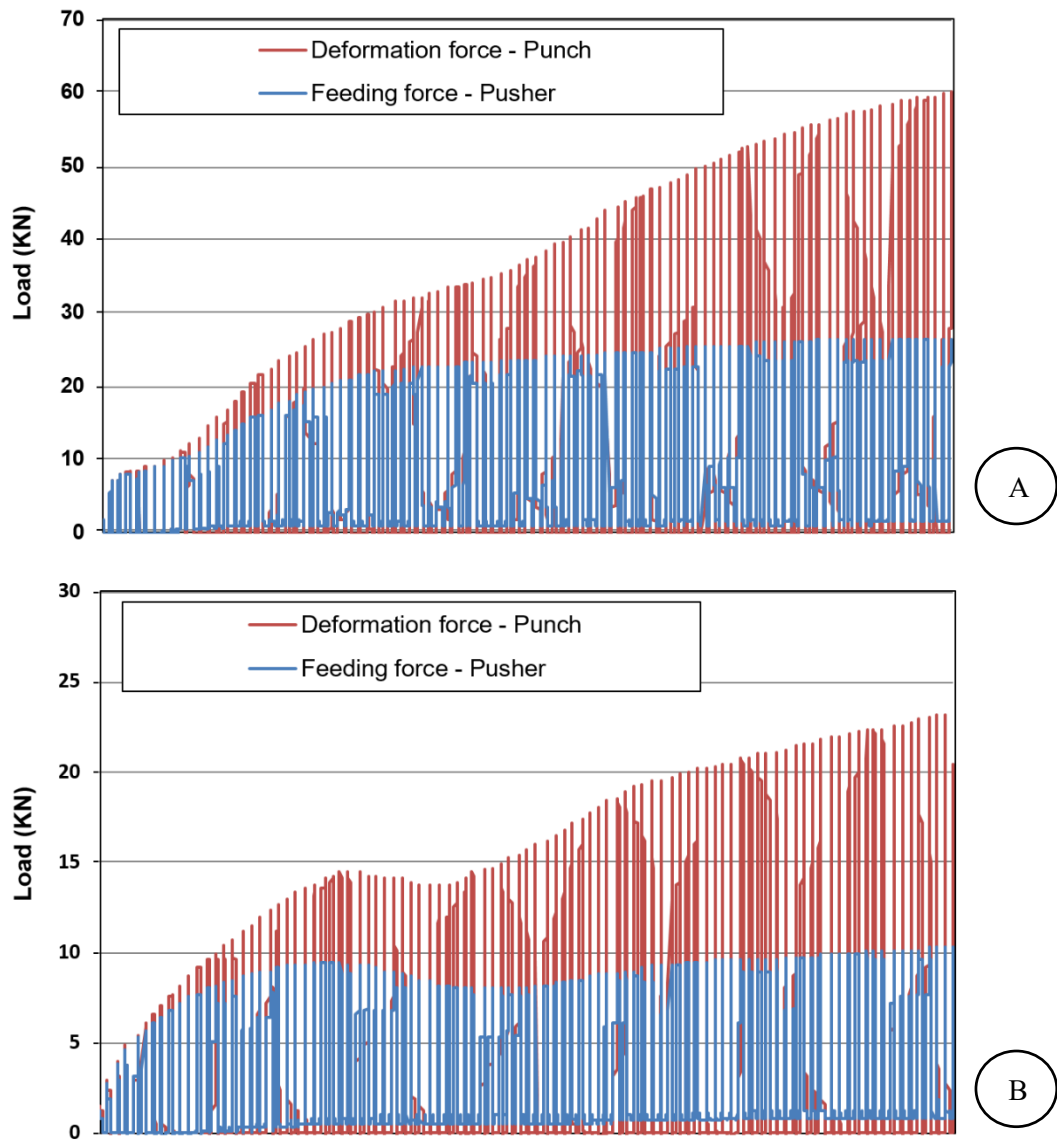


Figure 4.6: *Deformation and feeding force recordings for A – $\phi=90^\circ$ and B – $\phi=120^\circ$. The punch force is shown in red and the pusher force is shown in blue.*

The cyclic loading and unloading is shown in the graphs in Figure 4.6. It is also possible to see the load increasing once contact was made with the billet. Since only a small amount of material is available for deformation at the beginning of the process only a small load is recorded but as more material comes into contact with the punch the load increases.

From the recordings it is possible to observe that the force exerted by the punch for the 90° configuration is more than twice that of the 120° configuration. This can be expected as more shear is being exerted onto the material. The load on the pusher for

the 90° configuration is also more than twice that observed on the 120° configuration. This could be caused by a small amounts of material adhering to the corners of the channels. As the material builds up in the corners of the channel it will also cause greater resistance for the pusher's movement which could result in the billet permanently sticking inside the channel.

From these measurements it is possible to note that the pusher force and the punch force are very similar at the beginning stages of the process. After the initial stages the punch force seems to level of but the punch force continues to increase. As the billet processing continues, the pusher force is almost half that of the punch force. This observation seems to be true for both configurations.

Simulations were conducted to predict the plastic strain in each configuration.

4.2.4. Finite Element Simulation

In order to analyses the behaviour of the billets in the channel die, the total equivalent plastic strain, material flow and temperature rise in the billets and tools during IECAP processing, FEM simulations were carried out. A 3D model of IECAP process for two channel intersection angles (ϕ) of 90° and 120° has been developed using commercial FE analysis software QForm. Previous experience had shown the QForm software was capable of complete simulations quickly and accurately. The material model used for these simulations can be found in the standard QForm material library therefore they did not have to be found experimentally prior to setup.

The two models that were created to simulate the IECAP process for the different channel and pusher configurations are shown in Figure 4.7 (A and B). All tools (punch, die channel and pusher) were modelled with H13 tool steel and are considered as rigid bodies; however, the heat transfer capabilities are included in the model. The two die channel elements were constrained in all degrees of freedom, however the punch and pusher were allowed to translate only along the Z-direction. The two Al1050 billets were modelled with the built-in elastic-plastic material model in the QForm material library. The materials property library included the strain hardening behaviour and strain rate effects. The billets were divided into four node tetrahedral elements.

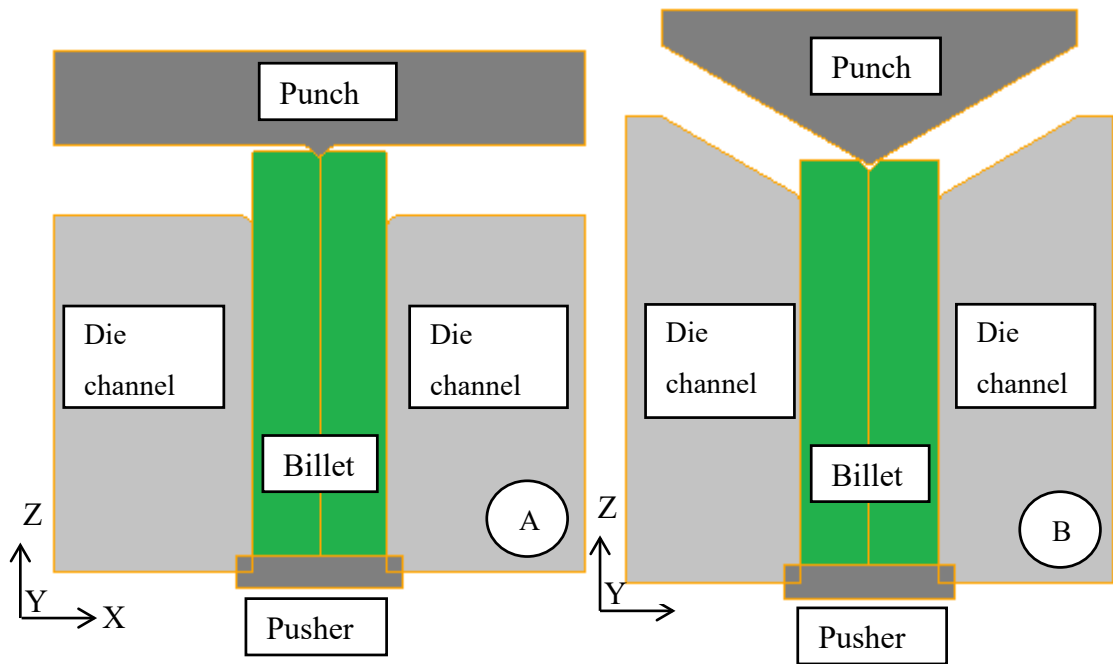


Figure 4.7: *FE analysis model for channel intersection angles of A – $\phi=90^\circ$ and B – $\phi=120^\circ$ IECAP process. The billets are shown in green, the channel in light grey and the pusher and punch are shown in dark grey.*

Billet Heating due to plastic deformation and friction during IECAP process was considered. The friction between the inner surfaces of the tools and the outside surface of the billet was modelled using Levanov law with friction factor taken as 0.3 under the graphite based lubricating conditions. However frictionless conditions were assumed between billet-billet interfaces, as the two billets are moving relative to each other. Also, no interactions were considered between the tools. All simulations used automatic re-meshing in billets to replace excessively distorted elements due to large strain and the occurrence of flow localisations. Volume constancy was also selected to ensure that overall billets volume remains same after each re-meshing step. Explicit method of integration was selected for solution.

4.2.5. First Pass Channel and Pusher Configuration Results

Simulation was used to determine the material flow, strain distribution and temperature behaviour of the billets during the IECAP process. This was followed by micro hardness measurement and microstructure analysis of the processed billets to further the understanding of the process and the effect of the two channel and punch configurations.

4.2.6. Material Flow

The material flow pattern and the ability of the billets to fill the die is examined by dividing the billets in a grid format using 30 lines along the billet axis and 7 lines along the transverse axis. Figure 4.8 (A and B) shows the influence of ϕ on the material flow at 50% processed state for $\phi=90^\circ$ and $\phi=120^\circ$. The Figure 4.8 also shows an enlarged single element passing through the shear zone.

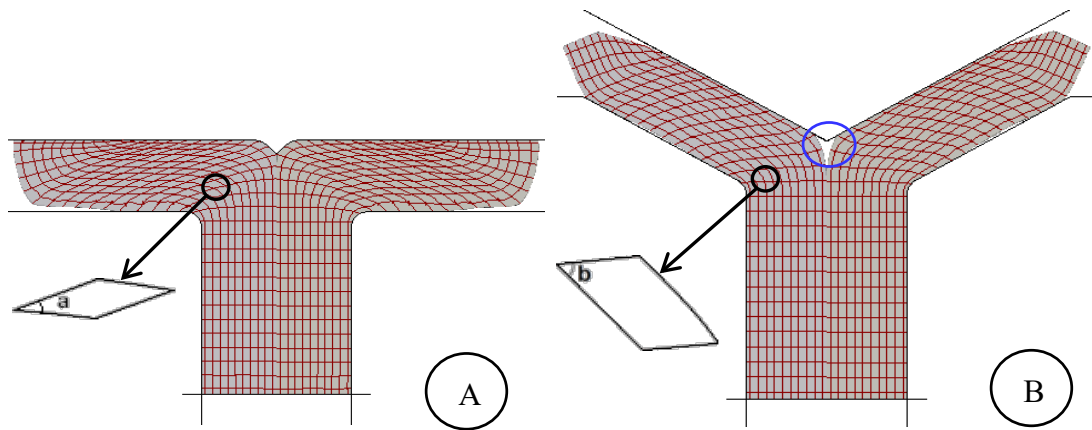


Figure 4.8: Influence of channel intersection angle ϕ on the material flow A – $\phi=90^\circ$ and B – $\phi=120^\circ$.

Shear angle 'a' in the case of $\phi=90^\circ$ is smaller as compared to shear angle 'b' in the case of $\phi=120^\circ$. It is also clear to see that no distortion accrues prior to the billets reaching the shear zone, therefore, not forming occurs in the input channel of both configurations. The shear angle distribution in the leading sections of the billets also appears to be non-uniform, which will result in larger grains when compared to the bulk of the billets, therefore, it will have to be cut and discarded. Compared to the $\phi=120^\circ$, the $\phi=90^\circ$ angle exhibits better die filling and has almost no corner gap. Formation of end gap between these billets at the intersection (marked by blue circle) at the intersection of inlet channel and exit channel of 120° die as shown in Figure 4.8(B) may lead to initiation of cracks from minor surface defects from the billet surface.

4.2.7. *Strain Distribution*

The strain evolution and distribution of the billets were calculated using FE analysis. Figure 4.9 (A and B) show the evolution of equivalent plastic strain at various stages of processing for $\phi = 90^\circ$ and $\phi = 120^\circ$ channel intersections respectively. As predicted the overall plastic strain is higher for the $\phi = 90^\circ$ as compared to $\phi = 120^\circ$. For both cases, along the billet axis from left to right, there are three distinct deformation regions: tail, steady state and head.

The steady state region of $\phi = 90^\circ$ seems to show little strain in-homogeneity along both the billet axis and also along the transverse axis from top to bottom. However, $\phi = 120^\circ$ shows strain in-homogeneity along both axes, it is also showing some bowing which was observed during actual experiments as well. This means the billets require straightening before they can undergo other passes. The front surfaces of the two billets in the head region are quite different from each other because of the different ϕ .

From the strain distribution simulations, it is clear to see that the head region of the billets experiences less strain than the steady state region of the billets. The strain observed in billet head region of $\phi = 120^\circ$ was almost zero whereas in billets for $\phi = 90^\circ$ it was almost 0.3; which, was half the amount of strain calculated in the steady state region for the $\phi = 120^\circ$ configuration. In general, the plastic strain seems to be double in the $\phi = 90^\circ$ configuration when compared to $\phi = 120^\circ$. Upon close inspection it is also possible to notice some strain evolution taking place in the bottom outer section of the tail region. This only occurs at the end of the billet and is greater in the $\phi = 90^\circ$ configuration.

With these simulations it is possible to get greater insight into the IECAP process and the effect it has on the plastic strain distribution in the billets. It is clear to see that the simulations predict the head and tail section of the billet will not have the same strain distribution than the rest of the billet, therefore, these regions would have to be discarded. This is important to note, as this amount will have to be taken into consideration when deciding on the starting length of the billets.

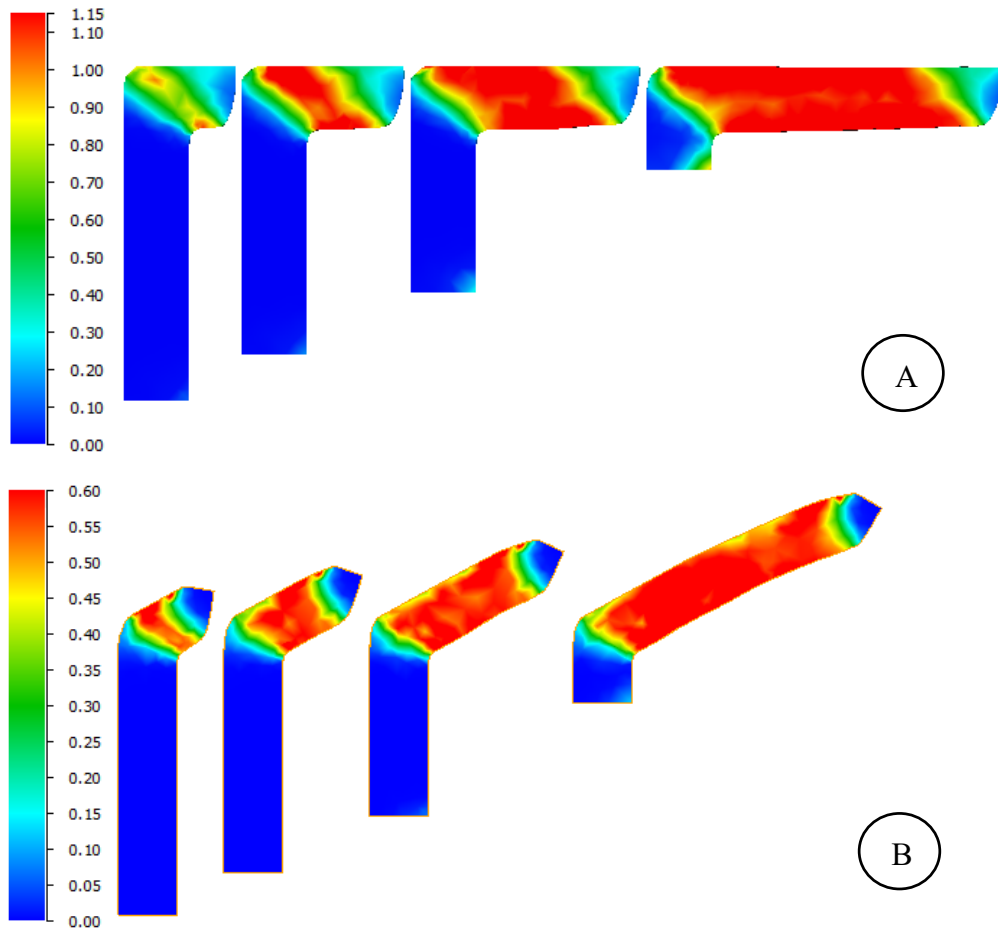


Figure 4.9: Evolution of equivalent plastic strain distribution at 15%, 30%, 50% and 90% processed state for (a) $\phi=90^\circ$ and (b) $\phi=120^\circ$.

4.2.8. Thermal Effects

It is well known that metals can generate heat during forming processed. There can be a variety of reasons for the heating of the material during deformation mostly related to strain introduction and changes in the micro structure. Thermal properties are included in the QForm material library and it was possible to analyse the effect of the IECAP process on the heating of the billets and the tooling. Since this process was carried out at room temperature, all temperatures were initially set to 20°C. Figure 4.10 shows the contour plots of transient temperature distribution after 25%, 50% and 90% processed state for the two configurations. It was observed that there was an abrupt temperature rise within the shear zone and the distribution of temperature rise in the billet during the different extrusion stages was in-homogeneous.

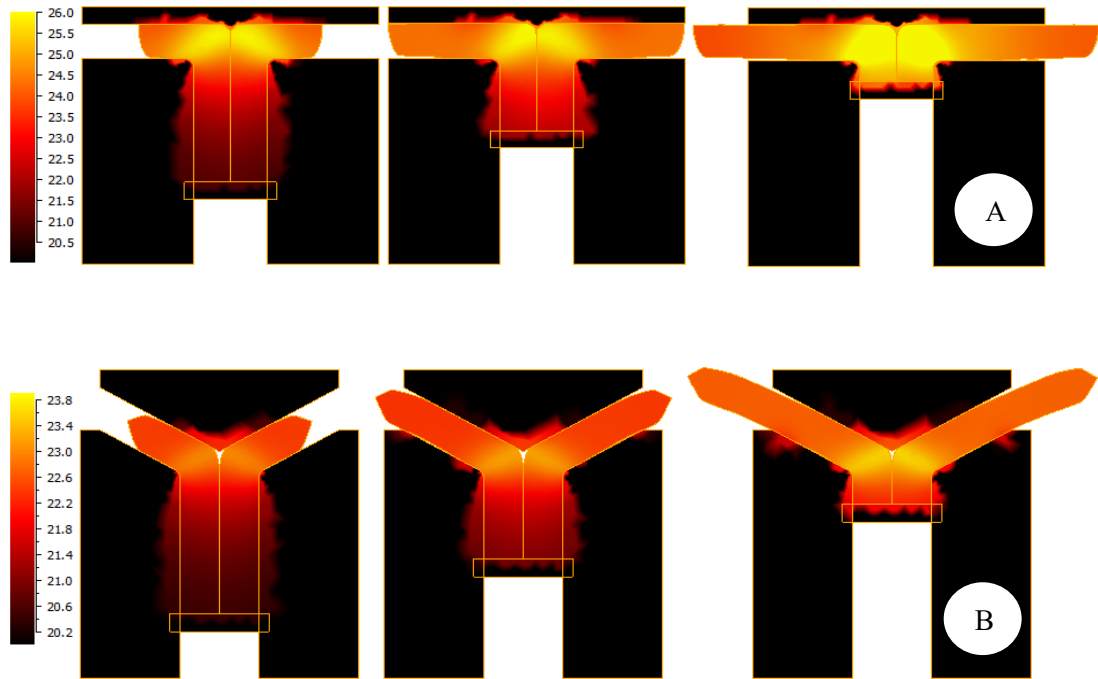


Figure 4.10: *Temperature distribution in tools and billet at 25%, 50% and 90% IECAP processed billets A – 90° and B – 120° configuration*

The maximum increase in temperature due to friction and plastic deformation for $\phi=90^\circ$ is 6.0°C compared to 3.8°C for $\phi=120^\circ$. The surfaces of the tooling that come into contact with the billets also experience a temperature increase. Since aluminium is a better thermal conductor than H13 steel, it is possible to observe that the temperature increase in the tooling is relatively localised whereas the temperature increase in the billet is more uniform. Even the tail region of the billet appears to have increase in temperature without going through the shear region.

Although the temperature of the billets was not measured after processing in the physical experiments it was possible to notice an increase in temperature after removing the billets from the tools. This increase in temperature was small but noticeable and only lasted a short period of time because aluminium is a good thermal conductor and would quickly adapt to temperature of the touch.

4.2.9. Hardness Measurement

A detailed hardness measurement study was undertaken to further the understanding of material change behaviour during the IECAP process and comparisons could be

drawn between the $\phi=90^\circ$ and $\phi=120^\circ$ configuration. A Zwick ZHV μ micro hardness tester was used to produce the hardness maps (presented in Figure 4.11). The ZHV μ Micro Vickers hardness tester covers Vickers and Knoop hardness tests to ISO 6507, ISO 4545 and ASTM E 384 with a test load range of 0.01 to 2Kg.

The specimens were cut in half along the flow plain. The cut surface was ground and polished. A large array was configured to measure the hardness of the specimen with 1 mm intervals. The hardness of the outer 1mm of the specimens was not measured. Performing hardness measurements close to the edge of a sample will result in incorrect low readings being achieved. About 500 hardness measurements were performed for each configuration and the results are illustrated in Figure 4.11.

After the first IECAP pass, the specimens show significant hardening both for $\phi=90^\circ$ and $\phi=120^\circ$. The $\phi=90^\circ$ first pass showed both the highest hardness and the greatest uniformity. There is a distinct region separating the softer unprocessed material and the post processed material in the $\phi=90^\circ$ configuration but for the $\phi=120^\circ$ configuration there is a widening “V” shape transitional area separating the processed and unprocessed material. It is also noticeable that a larger section of the starting billet has remained softer in the $\phi=120^\circ$ configuration and the following material exhibits less uniformity in its hardness as well as a lower peak hardness value. For both configurations, it is possible to see the hardest measurements were achieved in the centre section of the billets with the outer 1mm of the material remaining 5HV softer.

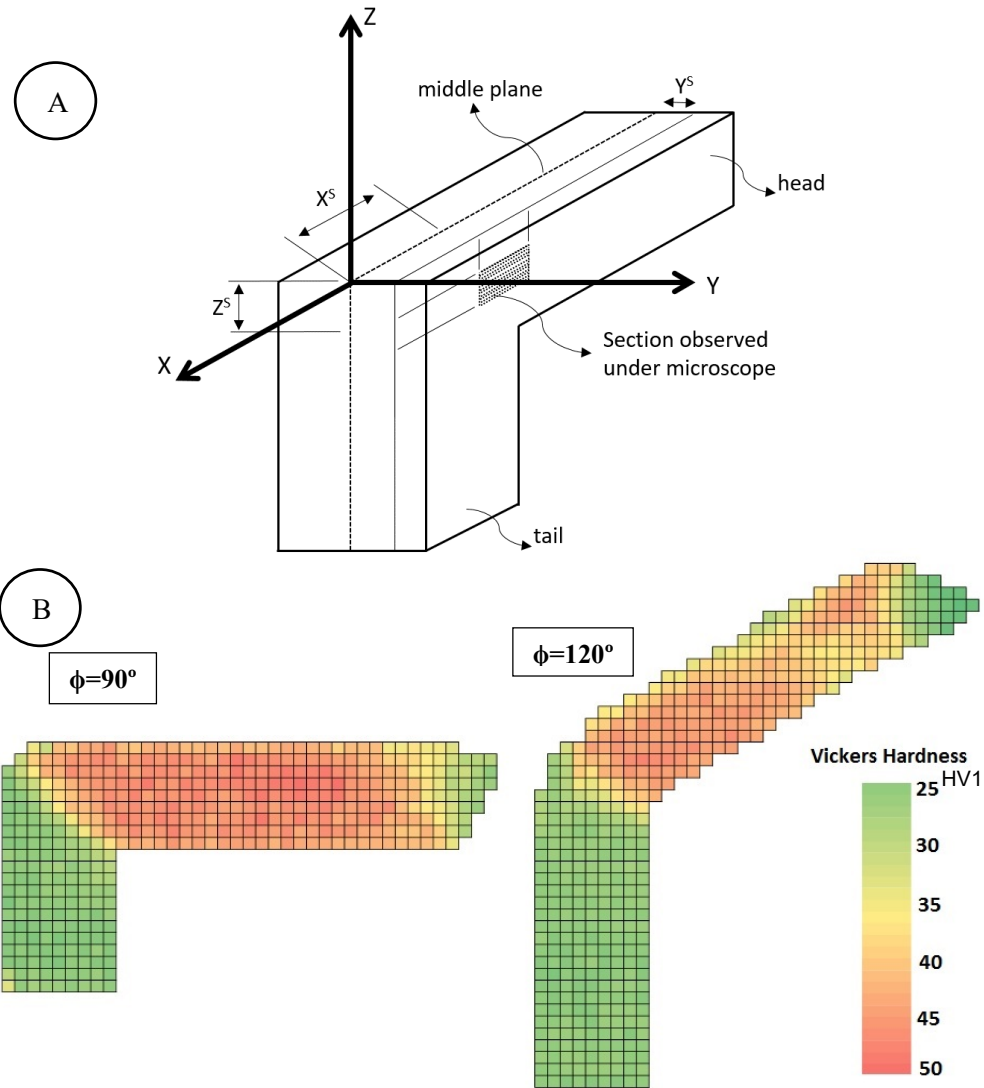


Figure 4.11: (a) Schematic showing the plane where hardness measurements were made. (b) Hardness maps from regions of the processed billets in inlet and exit channel of incremental ECAP dies having two different die corner angles.

4.2.10. Microstructure

Samples were cut along the flow plain and prepared for microscopy imaging. The preparation of the samples required a multi-step process to achieve the required surface finish. The final step of the polishing step required a vibration polish in a silica solution. The samples were then placed in an ultrasonic bath to remove most of the remaining silica from the surface. Most of the residue was removed but some silica remained on the surface. These small particles appeared to have embedded themselves into the aluminium surface. Aluminium is relatively soft, therefore, some particles can

be expected when this polishing method is used. The images that were captured under the SEM are shown in Figure 4.12 and some of the silica particles can be seen as small white speckles on the surface of the samples.

ASTM E112 standard test methods for determining average grain size was used. The mean grain size in the first pass of IECAP of $\phi=90^\circ$ and $\phi=120^\circ$ are 14 and 17 microns respectively. This illustrates that smaller shear angles lead to smaller grains, even after the first pass. The Figure 4.8 indicates that the shear deformation and consequently equivalent strain in $\phi=90^\circ$ is higher than $\phi=120^\circ$, which results in the grain refining at different rates. At the initial stages of IECAP, as a general accepted mechanism, new dislocations generated via shear deformation resulting in the sub-grains structure. In this first IECAP pass, disorientation of the sub-grains increase and may become grain boundaries. This could explain the increase in the mean hardness in $\phi=90^\circ$ as compared to that of $\phi=120^\circ$ configuration.

This attributed to the grain size as well as dislocation density. The differences between the microstructure in Figure 4.12A, and smaller mean grain size of $\phi=90^\circ$ compared to the $\phi=120^\circ$ is due to the number of dislocations produced in each process. The $\phi=90^\circ$ IECAP process appears to have resulted in a smaller and more uniform grain size as well as a higher and more uniform hardness in the billets.

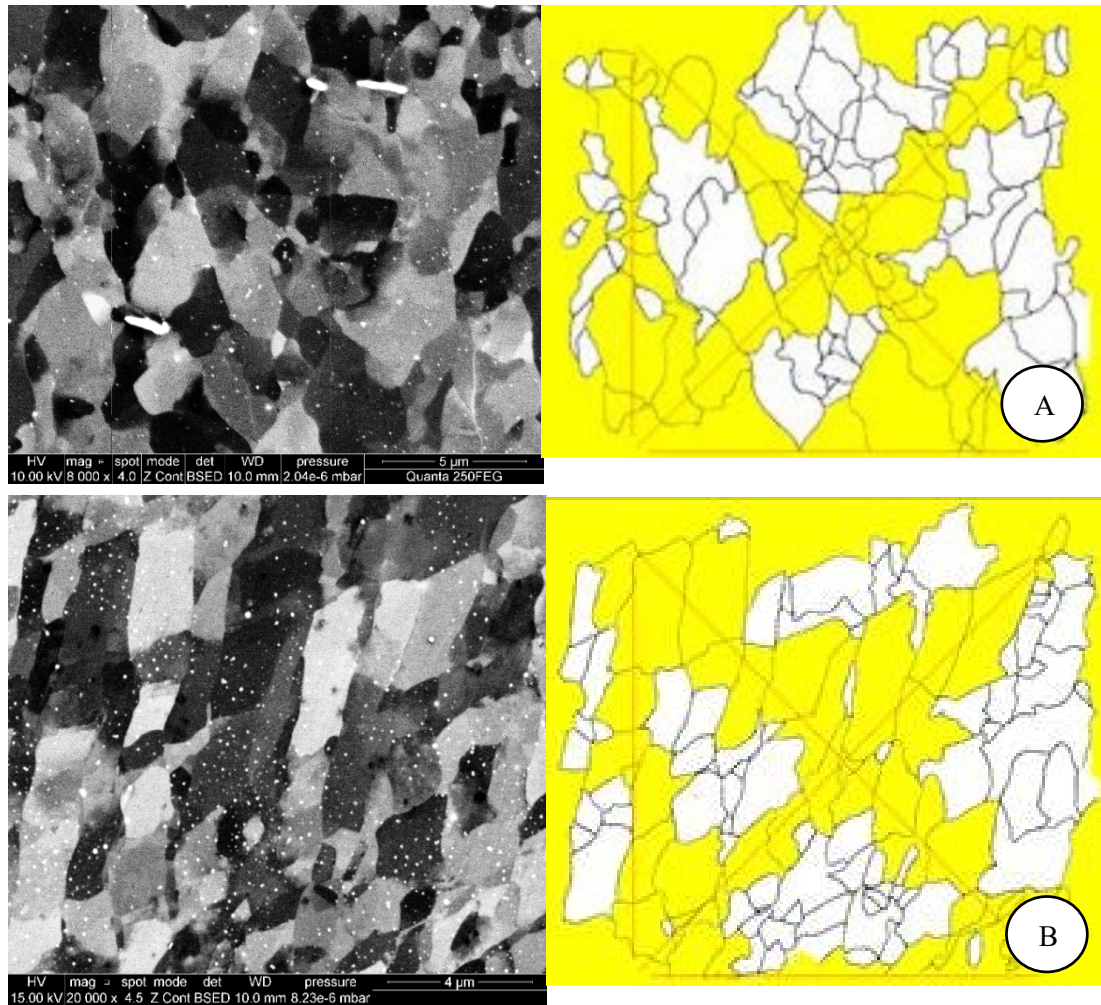


Figure 4.12: SEM examination of the microstructure of billets during first pass A – $\phi=90^\circ$ and B – $\phi=120^\circ$ IECAP with the corresponding grain boundary that were determined by software to calculate grain size.

4.2.11. Conclusion for the First Pass Various Geometry

- 1) First pass of the IECAP process was performed on Al1050 billets using the channel intersection angles of $\phi=90^\circ$ and $\phi=120^\circ$. Experimentally recorded process forces were approximately twice as high using $\phi=90^\circ$, compared to $\phi=120^\circ$.
- 2) Hardness distribution maps indicated doubling hardness in the processed part of the billets compared to the unprocessed parts. Higher and more uniform hardness was observed when using $\phi=90^\circ$.

- 3) FE simulation was performed using QForm for the first pass of IECAP process to predict billet geometry and strain distribution. The accumulated shear strain in $\phi=90$ was higher than $\phi=120$.
- 4) The FE simulation results predicted that the strain distribution in the $\phi=90^\circ$ case was higher and more uniform throughout the billet compared to the $\phi=120^\circ$ case. The 120° configuration lead to some bending of the billet
- 5) After the first pass the billets that were processed using $\phi=90^\circ$ IECAP configuration showed smaller and more uniform grains as compared to $\phi=120^\circ$ IECAP. There was significant grain size reduction in both $\phi=90^\circ$ and $\phi=120^\circ$ IECAP.
- 6) The FE simulation results would also suggest the $\phi=90^\circ$ configuration experience greater and more uniform shear strain throughout the billet.
- 7) Strain distribution established by FE simulation and hardness measurement results show qualitative agreement, which confirmed their suitability for estimating billet properties.

Since we only have a finite amount of material and time, it would not be possible to continue processing both configurations and carrying out a detailed study of both. Although it has been proven that both configurations can refine grains, the $\phi=90^\circ$ configuration showed the smallest and most uniform grain, highest and most homogenise hardness for A11050, therefore, this configuration will be used to carry out further passes of the IECAP process to refine the grain.

4.3. PART B: MULTI PASS EXPERIMENTS

Analysing the first pass of IECAP it became clear that it would be possible to improve material properties using this process. It became clear that using the $\phi=90^\circ$ configuration would possibly produce the best results, therefore, this configuration was chosen for further processing passes. When deciding on the number of further passes and the route the billets should take, several other published studies were examined. It became clear that for A11050 the optimum route was route BC and eight passes. There are studies that have taken more passes than eight but the material properties do not see significant improvements.

The conversion coating showed to be very effective in the $\phi=120^\circ$ configuration. From the contact surface of the punch and billet in the $\phi=90^\circ$ configuration the effectiveness of the conversion coating was less. For that configuration the billet experiences more shear and greater forces, therefore, a lubricant with a greater load carrying capability would be required. From previous experience and from a study of the other available lubricants it was concluded that combining lubricants could result in the lowest friction conditions during processing.

A combination of graphite and MoS₂ could be used to maintain low friction conditions during the IECAP process. Graphite and MoS₂ achieve their low friction behaviour due to their layered structure. Each layer contained strong bonds that make it resistant to breaking up under load. There are also weak bonds between the layers which enables them to slide over one another.

Firstly, a coating of Graphite would have to be applied and then the MoS₂. Once the billets had been ground to the correct dimensions then the surfaces were roughened using sand blasting. The increased and relatively uniform roughness that was achieved by sand blasting allowed for the graphite coating to adhere to the billet surface. The valleys that were created by the sandblasting process allowed the graphite to pool inside and not be easily removed. A thin layer of graphite and water mix was applied using a spray and allowed to dry in room conditions. The graphite coating was only applied twenty minutes prior to billet processing. The drying process took five to ten

minutes and was then inspected. Handling the graphite coated billets is relatively straight forward.

Just before insertion of the billets into the input channel the billets received a coating of MoS₂. The MoS₂ coating can also be used in high temperature applications but this process was carried out at room temperature for Al1050. MoS₂ is a relatively dirty lubricant because it can adhere to all surfaces, therefore, it was only applied prior to billet insertion and gloves were used when handling the MoS₂ coated billets.

To minimise the effect of grain growth due to heating the billets were placed in a freezer after processing. They were kept in the freezer at -20 °C conditions until they were prepared for further processing. Temperature fluctuations in the laboratory can have an effect on grain growth after a period of time, therefore, it was decided that low temperature environment would be the best place to keep the billets until they were further processed.

Between each pass the billets had to be ground and the corner flashing removed. From the initial study that was carried out it was possible to see that a small chamfer in the edges of the billet allowed for better adhesion of the lubricant coating and should result in less material sticking in the channels. After each processing pass the billets were prepared and the chamfer ground into them. As previously stated route BC would be used for the multiple passes, therefore, an indicator was made to show the direction of flow after each pass. Since the billets were kept in a freezer after each pass they were allowed to reach room temperature before the next processing pass was undertaken.

The results of the multiple passes are presented in the following section.

4.3.1. Effects of Load during Multi Step IECAP

Each pair of billets was IECAP processed eight times using the B_C route. The punch load and the pusher load was recorded using a custom made virtual instrument that is shown in figure 3.13. The results of the pusher and punch recordings are shown in Figure 4.13. The incremental loading and unloading cannot be seen due to the line thickness and scale of the graphs. The incremental behaviour can be seen in more detail

in Figure 4.6. In Figure 4.6 the billets were half processed but in these experiments the billets were fully processed, therefore, the forces for the first pass are higher.

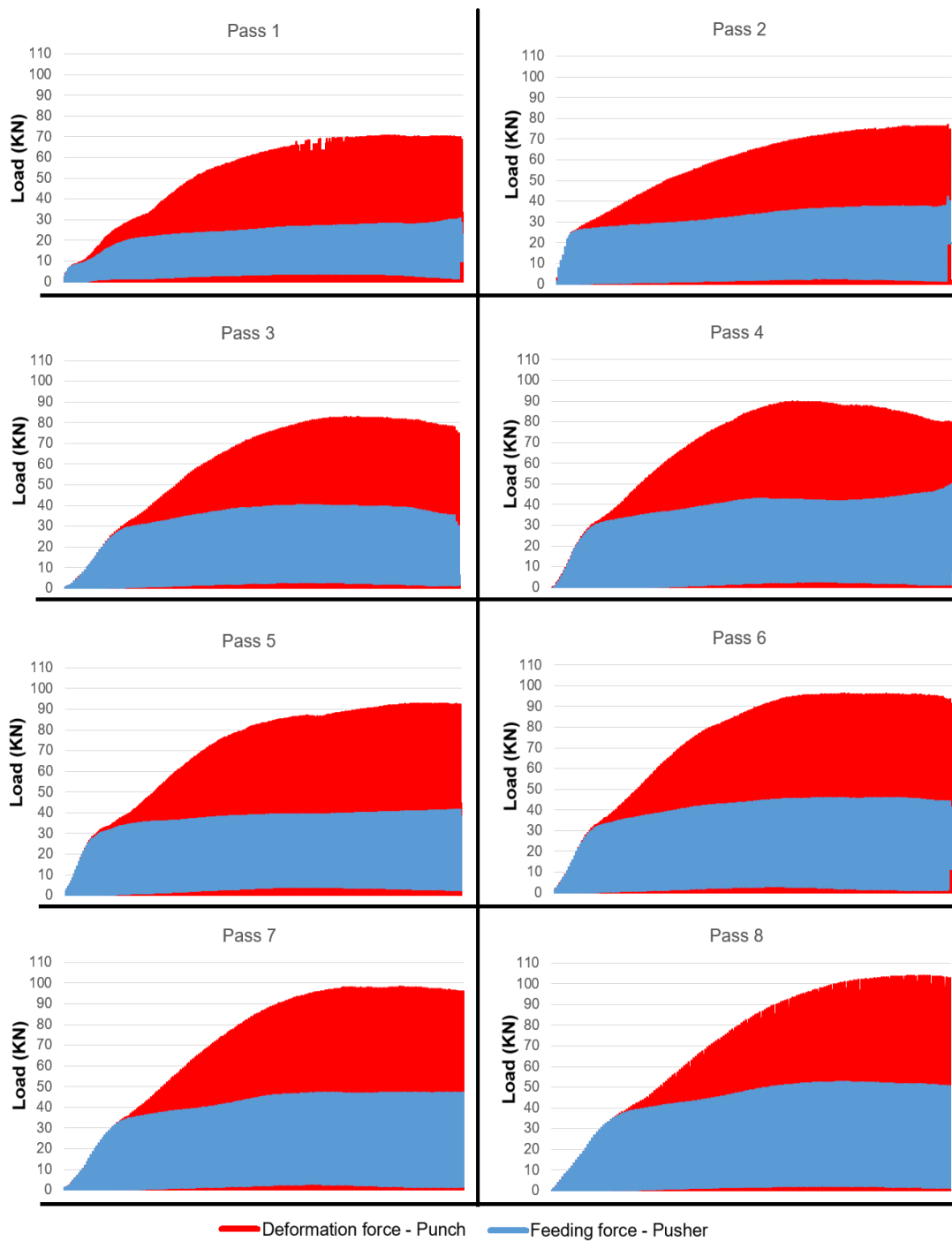


Figure 4.13: The feeding force and deformation force recordings for IECAP passes 1 to 8.

The general trend from all the passes is that at the initial stages the pusher force and the punch force are equal. Before the billets come into contact with the punch very

little load is recorded. Once the billet comes into contact with the punch, the pusher load and the punch load are equal until the material starts to flow into the output channel. It is possible to see that once the material starts flowing into the output channel the load reading from the punch starts to level out and remains relatively constant until the end of the process. The load recording from the punch continues to increase and at a later stage starts to level out. Continuation of load increase could be due to the increased contact area between the billet and punch. Once the head of the billet exits the output channel and is no longer in contact with the punch surface then the true processing load can be seen.

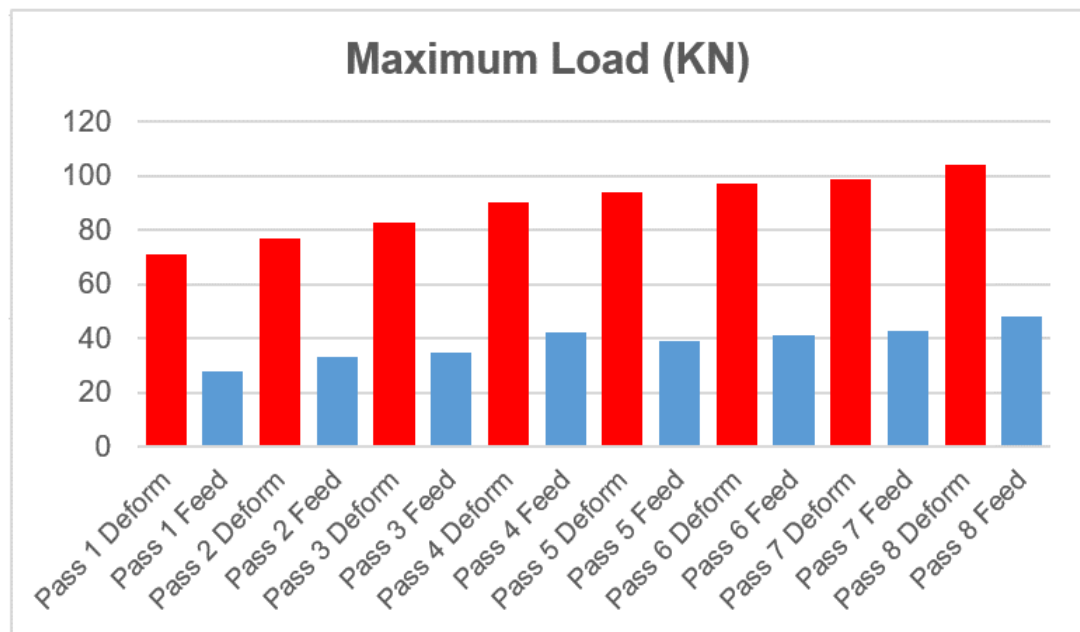


Figure 4.14: Graph showing the peak loads recorded for the punch and pusher during the IECAP of Al1050 from pass 1 to pass 8.

The maximum load recording during each pass is shown in Figure 4.14. It is clear to see the load increasing with each pass as the material properties are changing. Both the punch force and the pusher load increase but the pusher load remains around 40KN. The punch load increases from below 70KN in the first pass to about 105KN in the 8th pass. The first four passes showed the greatest punch load increases from about 70KN to about 90KN. Passes 5 to 8 only showed a punch load increase of 10KN. This was similar to the behaviour pusher as the first four passes seen the greatest load recordings for the pusher.

4.3.2. *Hardness Evolution during Multi Pass IECAP*

To further the understanding of the processes that are taking place during the IECAP process, five billets were partially processed at the required passes. The billets were fully processed until the pass of interest then they were half processed. These billets were then cut in half along the flow plain and prepared for micro hardness measurement. The results of the micro hardness measurements are shown in Figure 4.15.

For each billet about 500 micro hardness measurements were taken. A grid pattern identical to the pattern used in the initial study micro hardness shown in Figure 4.11. The indentation process was automated but the measurement process could not be automated due to automatic image analysis, issues, therefore each indentation image was analysed manually. An unprocessed billet was also prepared and analysed to show the evolution of the micro hardness. The hardness measurements carried out for the first pass for $\phi=120^\circ$ has also been included as a comparison. The IECAP process passes 1, 2, 3, 4, 6 and 8 for $\phi=90^\circ$ are shown in Figure 4.15.

It is clear to see that after the first pass the billet has the largest increase in hardness. The hardness appears to increase from about 22HV to 45HV. The following passes do not see a dramatic increase in hardness but see the hardness increasing to 59HV after 8 passes. The subsequent passes also show a more uniform hardness being achieved within the billets. It is also possible to see that the head section of the billet still remains non uniform in hardness from the rest of the billet. The first 10 to 15mm of the billet remains different from the rest of the billet even after 8 passes. It is also interesting to note that the hardness in the subsequent passes at the bottom of the tail section changes compared to the rest of the billet. The side towards the output channels appear to be hardening, whereas the side away from the output channel appears to be softening. The simulations predicted that this effect could take place and can be seen in Figure 4.9.

It is also possible to see that there is a clear change in hardness measurement in all passes of the billets as they pass through the plastic shear zone. An area 10mm either side of the centre line of the shear zone was examined closer and the results can be seen in Figure 4.16.

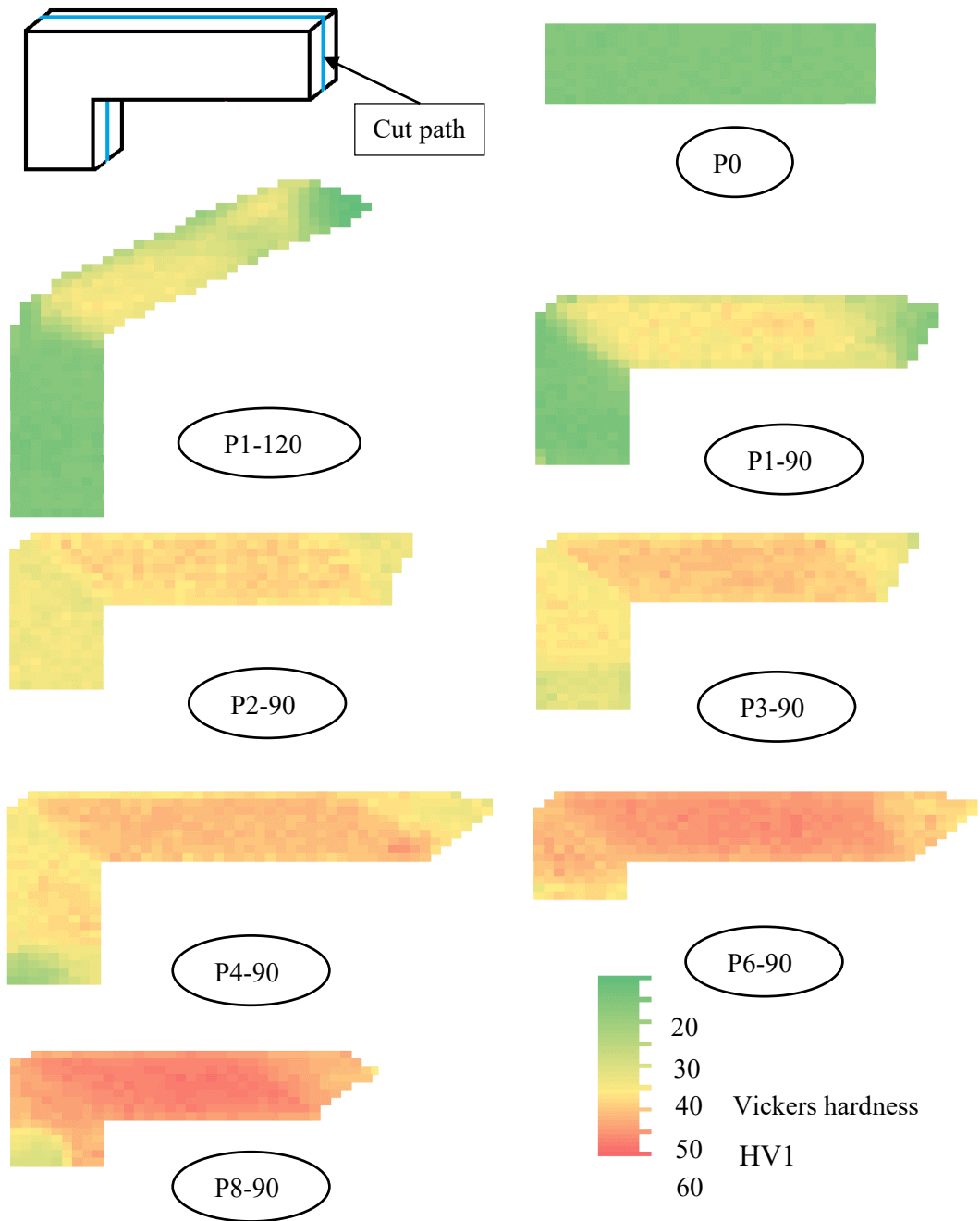


Figure 4.15: *Micro hardness measurement along the flow plain for partially processed billets after IECAP passes of $\phi=90^\circ$ at 1, 2, 3, 4, 6, 8 and $\phi=120^\circ$ first pass.*

Hardness Evolution

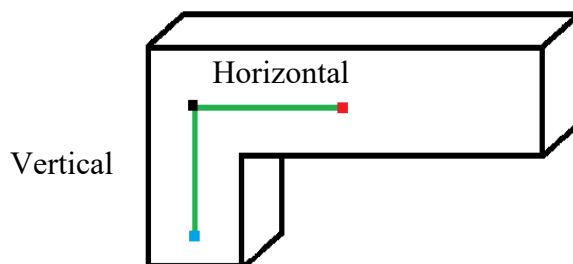
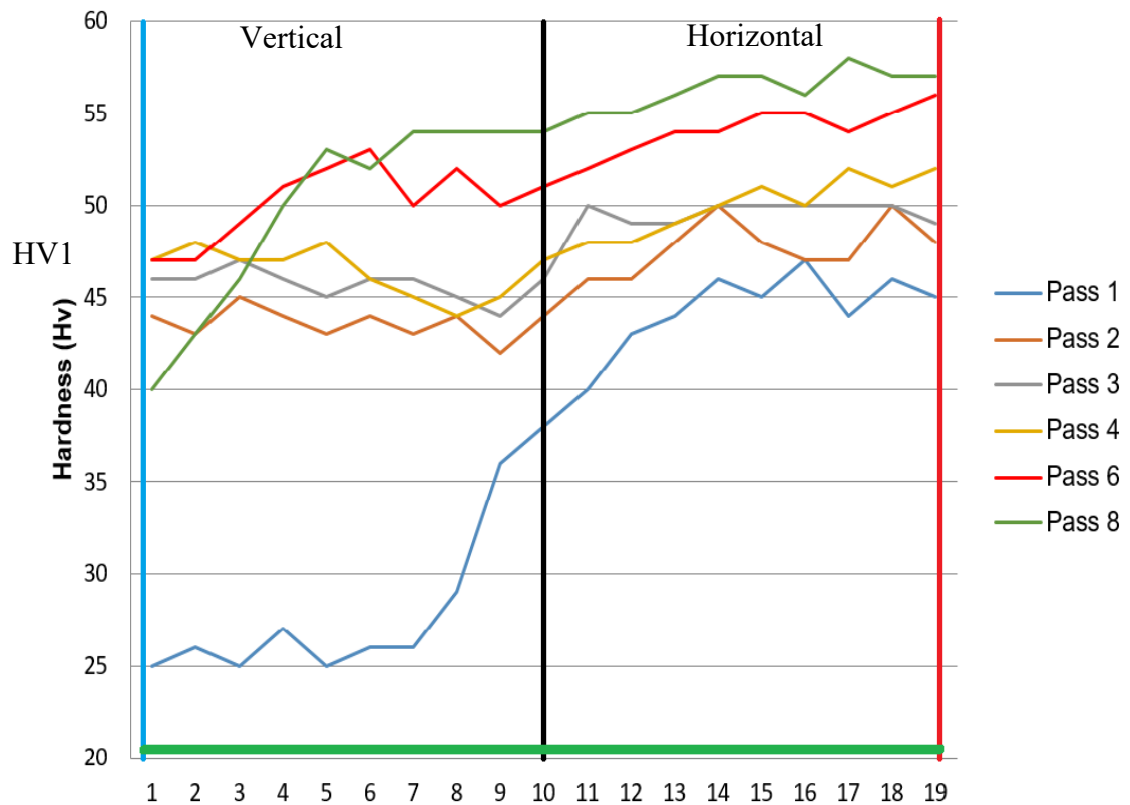


Figure 4.16: *Hardening results of billets after passing through the plastic shear zone for passes 1, 2, 3, 4, 6, 8. The green line represents the centre of the billet and the location of the hardness measurements. The blue dot (starting point of hardness results shown in graph), is located 10mm from the centre of the shear zone in the vertical axis and the red dot (ending point of hardness results shown in graph), is located 10mm from the centre of the shear zone in the horizontal axis.*

From this graph it is possible to see that most of the hardness changes seem to occur 5mm before and after the centre of the plastic shear point shown in by the black dot in the schematic and the black line in the centre of the graph. Before and after this 5mm zone the hardness of the billet appears to be relatively consistent. This is true for all cases apart from the 8th pass where the partial processed billet was processed further

than intended. Partially processing billets can be challenging as it is very difficult to see the billet during processing and determining the processing progress. The transverses to flow micro hardness of the billets was also investigated and can be seen in Figure 4.17.

Since the billets were processed in pairs it was possible to carry out further investigation into the hardness evolution behaviour of the partially processed billets. The remaining billet was cut into 3 sections as shown in the schematic in Figure 4.17. Two cuts were made 10mm from the centre of the shear zone (one horizontal and one vertical). The third cut was done directly in the centre of the shear zone. Three cuts were also made in an unprocessed billet and the hardness analysed. As expected, the unprocessed billet showed almost homogenise hardness measurements.

It is clear to see from Figure 4.17 that even in the transverses to flow direction that all billets get harder as they are getting processed. The input channel of pass one shows the same material hardness as the unprocessed material but as it goes through the shear zone the hardness goes from 23HV to about 45HV. This is almost exactly the same as what was observed in the flow direction hardness measurements. All consequent passes increase the hardness of the billet. Hardness as high as 59 was recorded in the 8th pass. The centre section of pass 8 shows the highest hardness recording but the hardness distribution also appears to be relatively uniform.

This is true for most cases apart from the input channel hardness measurement for pass 6 and 8. There is a big hardness fluctuation in these 2 samples as they were processed farther than intended. These findings are in line with the findings of Figure 4.15 and the predictions of the simulation shown in Figure 4.9.

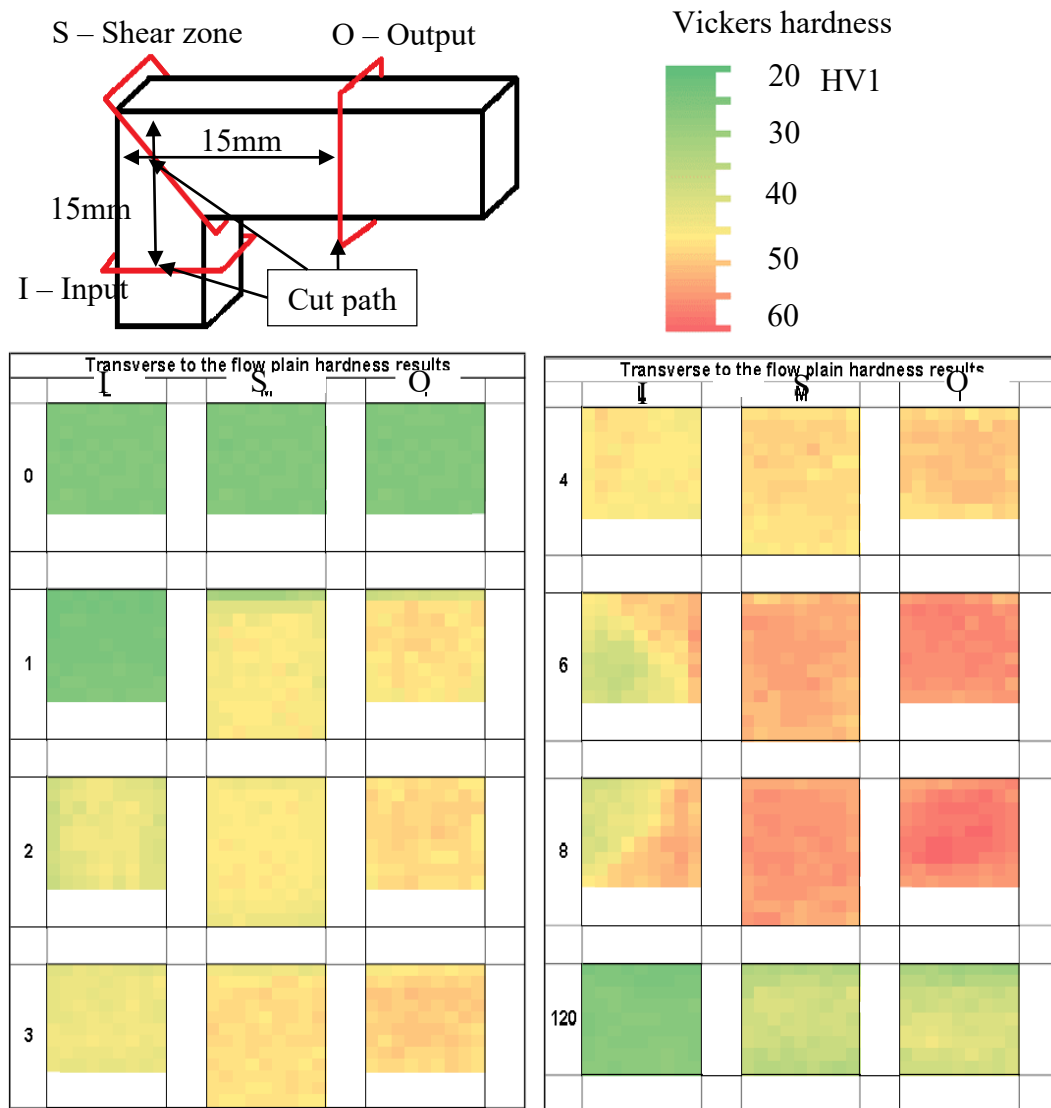


Figure 4.17: *The partial billets were cut into 3 cross sections and hardness of the sections were investigated. The regions of interest from the billets were the input channel, shear zone and the output channel. The cut path of the three sections for the billets are shown in the top schematic.*

This transverse to flow hardness study was also carried out for the single pass $\phi=120^\circ$ billet. The findings are interesting and in line with the initial predictions that in the $\phi=90^\circ$ configuration the billet would experience greater plastic shear. When comparing the first passes configurations that in $\phi=120^\circ$ the hardness is as much as 8HV less than in the shear zone of the $\phi=90^\circ$ configuration.

To further the understanding, the effect of increased IECAP passes have on the material properties tensile testing was also carried out.

4.3.3. Tensile Testing

The material hardness changes seen in the above section is a clear indication that the material properties have changed permanently. To investigate the effects of these changes, tensile testing was conducted. Before tensile tests could be conducted several billets were fully processed to produce the required material for tensile testing. Figure 4.18 shows a pair of billets being processed using the IECAP rig. The tensile testing machine described in chapter 3 was used to further quantify these changes in the Al1050.

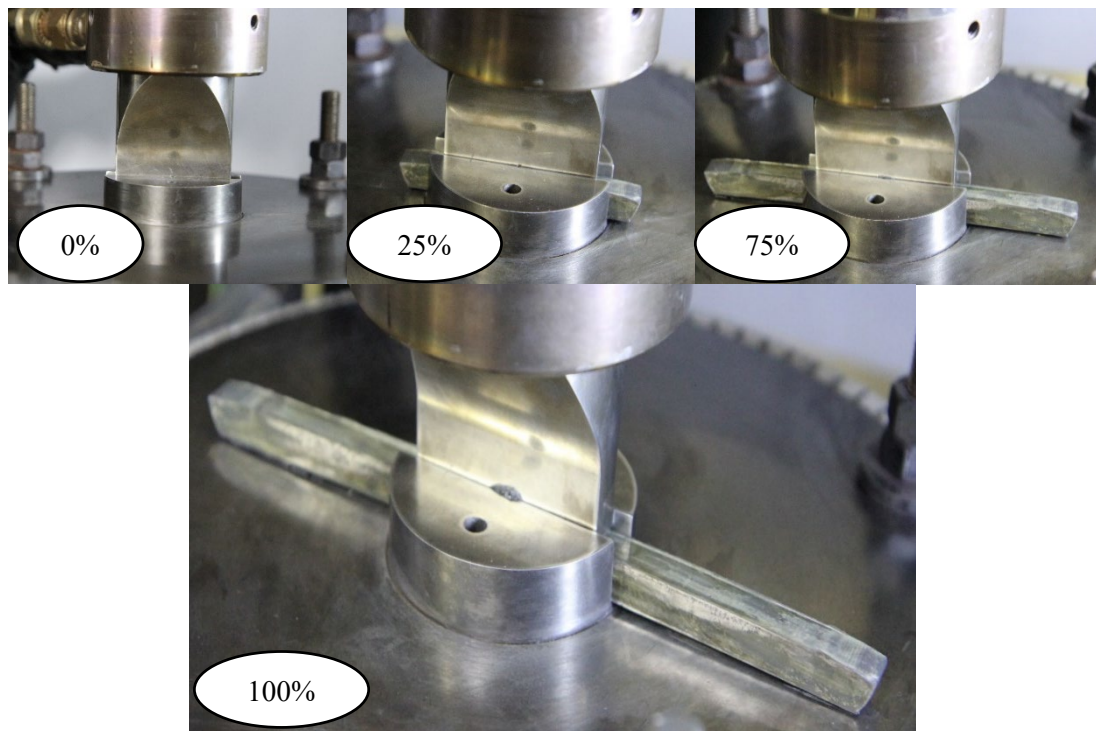


Figure 4.18: Various stages of IECAPing a pair of Al1050 billets.

Small tensile specimens that were described in figure 3.10 were produced using wire EDM cutting. It is important to note that once the billets were produced the material was kept in the freezer to minimise the chances of grain growth due to temperature fluctuations and time. The tensile specimens were also kept in the freezer until they were used for testing. Before testing began the specimens were brought into the lab and allowed to reach room temperature. The results from the tensile testing are shown in Figure 4.19.

Due to the relative small size of billets produced in this IECAP process only miniature tensile specimens could be produced. Even with these small specimens it is clear that the tensile strength of the Al1050 significantly increases with the number of IECAP processing passes. The ultimate tensile strength was about 80MPa in the 'as received' condition, but was higher than 200MPa after 8 IECAP passes. The elongation before fracture is significantly higher in the 'as received' condition but more than halves after the first pass of IECAP. After the first pass, the ultimate tensile strength increases by about 75%. This trend continues with subsequent passes until the 6th pass but after that, the ultimate tensile strength only increase slightly. This pattern of stepped increase in mechanical properties with the initial passes was also seen in hardness measurements. It was also observed in hardness measurement that after a certain point the increases in mechanical properties levels out; in this case it seems to occur after 6 passes of IECAP.

Once the mechanical properties of the material were measured, then the grain size reduction was measured.

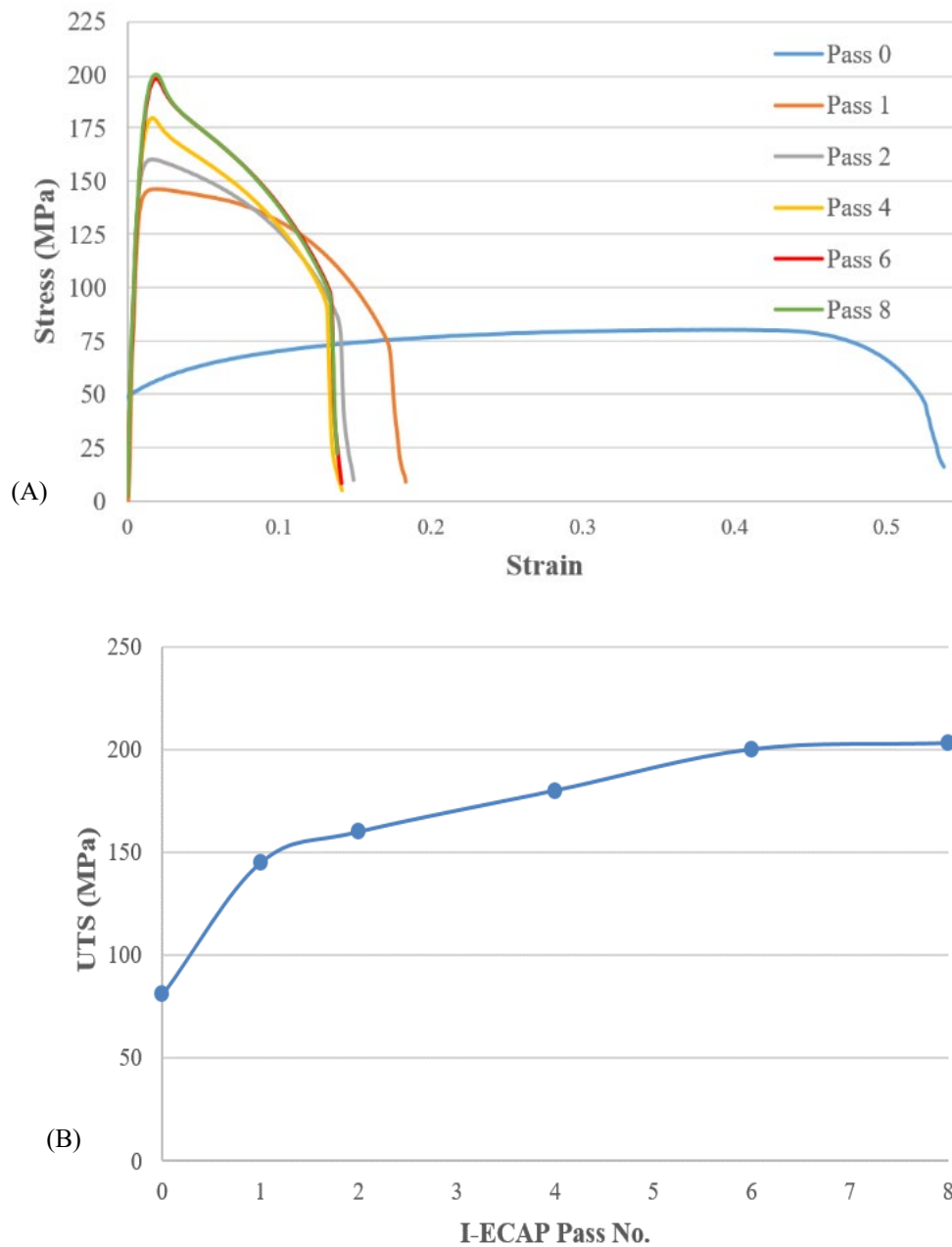


Figure 4.19: True stress-true strain curves of samples from billets before and after IECAP process. Specimens were created from pass 0, 1, 2, 3, 4, 6 and 8 billets.

Flow curves derived from load –displacement values of samples subjected to tensile testing at strain rate of 10^{-2} s^{-2} is given in Figure 4.19. For this samples from as-received billet and billets after each pass of IECAP process are tested to see the influence of grain refinement on important tensile properties namely yield strength, ultimate tensile strength and tensile ductility (% elongation). Note that samples were

taken up to fracture in all the cases. It is observed that values of tensile strength increased drastically after very first pass as compared to the starting billet. But the tensile elongation (ductility) has dropped noticeably after first pass. This is primarily due to increase in the dislocation density with in the coarse grains as a result of activation many dislocation sources. As amount of strain imposed in the billet increases with number of passes, the amount of dislocations getting stored with in the pre-existing grains keep increasing. This is also reflected in the tensile behaviour of the samples from each passes. Apart from the samples from first pass billet, the flow curves from billets of subsequent passes has not shown a decrease in the ductility. This could be due to the dynamic recovery occurring in the billet beyond certain amount of strain levels imposed during IECAP process. But they do exhibit increasing trend in the ultimate strength values, which is also clearly shown in the Figure 4.19.

4.3.4. *Microstructure analysis*

In order to explain mechanical properties variation of the I-ECAP samples, the microstructure analysis of the samples after each pass was examined. The scanning electron microscope Quanta FEG 650, equipped with a field emission gun (FE-SEM) and with a NordlysF EBSD detector, was used. The AZtec acquisition software was utilized for data acquisition and Channel 5 software to analyse the data. All EBSD measurements were performed with a step size of 2 μ m, using the beam-scanning mode under dynamic focus conditions and with a SEM magnification of 200X. For EBSD analysis, samples were grinded and finally electro polished using Struers lectroPol 5 and electrolyte A2. Figure 4 20, shows the microstructure of the as-received and different stages of I-ECAP samples. The observed microstructures at different stages of the I-ECAP clearly indicates the shear deformation of grains. The density of the high angle grain boundaries (greater than 15°) and refinement of grain structure in I-ECAP samples increases significantly in comparison to the as-received sample. The average grain size of the material decreased significantly with increasing ECAP pass. The rate of grain refinement through the initial passes of I-ECAP is higher than the rate of grain refinement through the higher passes.

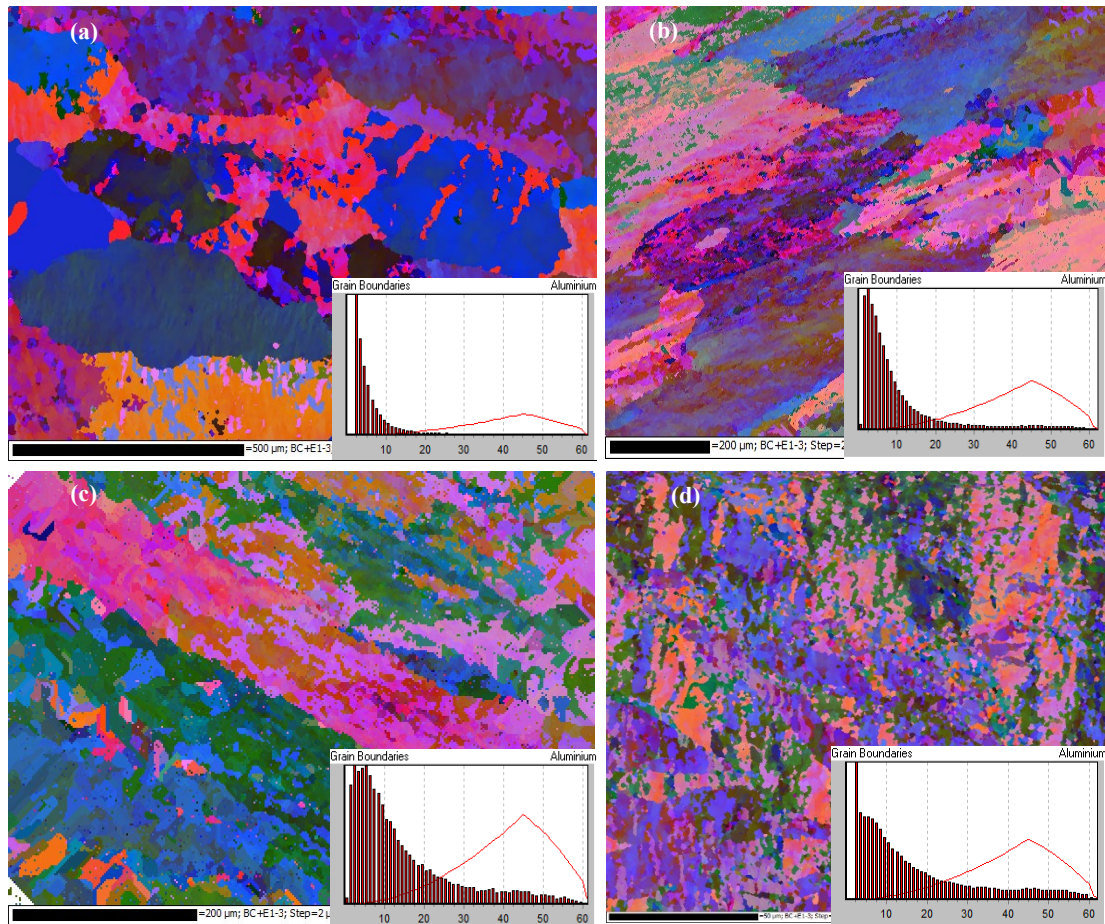


Figure 4.20: *Inverse pole figure maps showing the deformation characteristics of aluminium matrix of Al1050 billets before and after I-ECAP process (a) as received sample, (b) after 1st pass, (c) after 2nd pass and (d) after 4th pass.*

4.3.5. Microstructure Grain Size Refinement

To confirm that the grain refinement was being achieved by processing the Al1050 billets, it was necessary to observe the size of the grains. After the first pass it becomes very difficult to prepare samples and to visualise grain using the SEM method therefore transmission electron microscopy (TEM) was employed.

For TEM observations, the samples were sectioned to produce longitudinal sections (flow plane) using a slow speed abrasive saw to obtain slices of thickness less than 300μm. The slices were mechanically polished to reduce the thickness. Discs of 3mm diameter were spark eroded. The twin-jet electro-polishing with 25% HNO₃ and 75% CH₃OH (by volume) mixture as electrolyte was done as a final polishing. Bright field micrographs recorded from the flow plane of the I-ECAP process samples using TEM are presented and discussed in this section Figure 4 21. Evidence for the formation of banded structure in the flow plane of billet after first is shown in Figure 4 21(a). This

is primarily due to the intense shear experienced by the billet when it passes through the shear deformation existing between input and output channel. The orientation of these bands are at angle 25° . The dislocations got accumulated within those deformation bands are clearly shown by the regions having better contrast in micrograph Figure 4 21(a). Dislocations stored in the banded structure started to undergo recovery process called dynamic recovery, when the billet subjected to second pass. Micrograph of second pass samples given in Figure 4 21(b) revealed the formation of dislocations sub-grain structure developed as a result of dynamic recovery process. Dislocations annihilating the sub-grain boundaries are noticed.

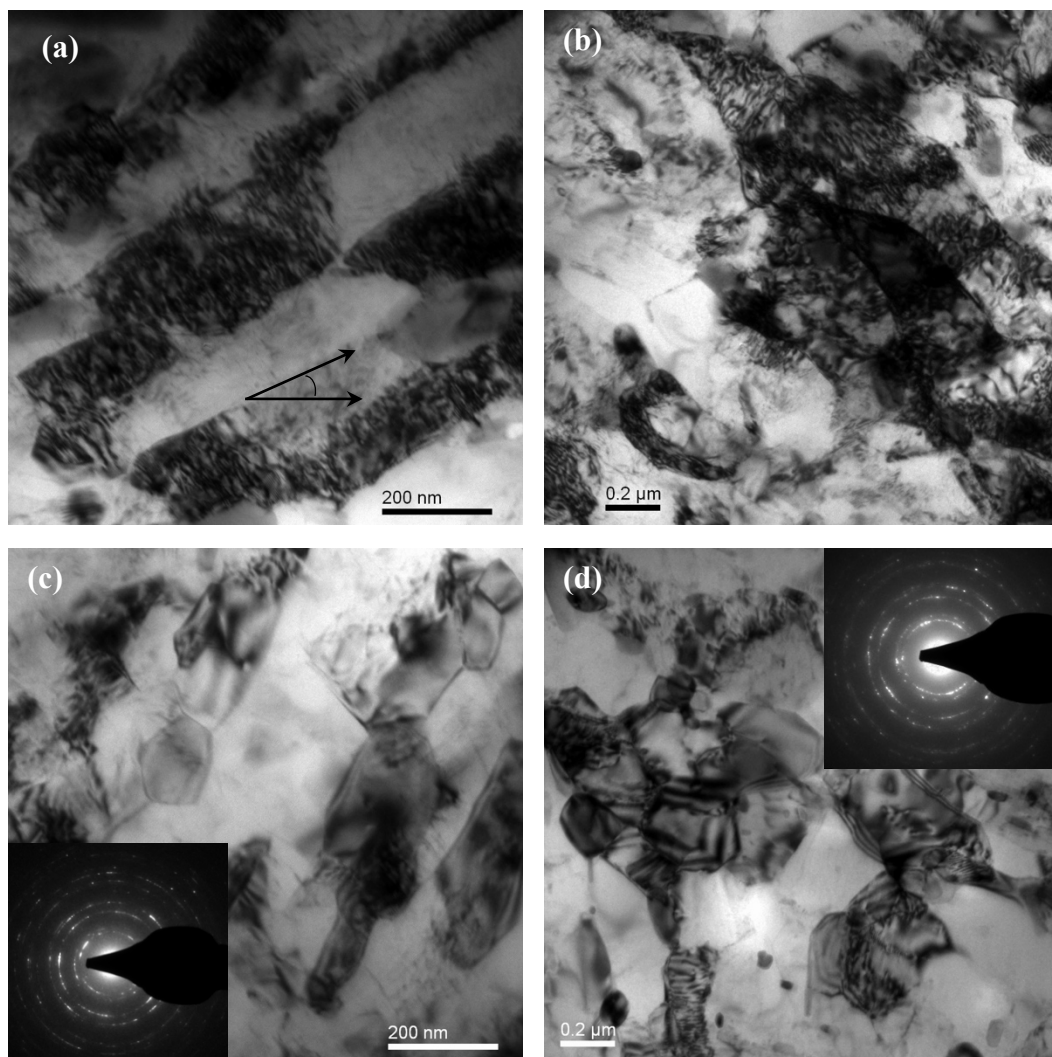


Figure 4.21: *Bright field TEM micrographs showing the deformation characteristics of aluminium matrix in AA1050 alloy billet subjected I-ECAP process after (a) one pass, (b) two passes, (c) six passes and (d) eight passes. Corresponding Selected area diffraction patterns (SADP) are given as inserts.*

As amount of strain imposed on the billets during subsequent passes increases dynamic recovery assisted recrystallization started to dominate in the matrix leads to the

formation of fine grains in the matrix Figure 4 21(c)-(d). Temperature rise in the billet while crossing the shear deformation zone also influences the process of dynamic recrystallization to some extent. Dynamically recrystallized grains in the size range 150-200 nm formed in the matrix after 6th and 8th passes are shown in Figure 4 21(c) and (d), respectively. Dynamic recovery and dynamic recrystallisation at the 6-8 passes of I-ECAP can explain why the rate of increasing hardness and tensile strength of the samples at the final passes of I-ECAP reduces in compared to the initial stage of the process Figure 4 21.

Continuous ring patterns shown by the selected area diffraction pattern (SADP) confirming the formations of fine grains in the regions he shown in bright field micrographs of 6th and 8th passes are provided as inserts.

4.3.6. Conclusions

In the literature several processes have been investigated for increasing the mechanical properties of engineering materials. One of the most common methods is the conventional ECAP process. An evolution of the conventional ECAP process has been described in the literature that has many of the benefits of the process but also removes several of the limitations. The Incremental ECAP process can achieve similar results in the mechanical properties of soft materials but is not limited to short billets. Two different configurations of IECAP were initially investigated, $\phi=90^\circ$ and $\phi=120^\circ$. Once one was chosen subsequent passes were performed. The findings of this study were as follows.

- 1) Tests were initially performed only on the first pass of the two configurations of IECAP. The process forces were approximately twice as high using $\phi=90^\circ$ when compared to $\phi=120^\circ$.
- 2) The hardness distribution of the processed billets via the 2 configurations were examined. This showed the hardness in the processed part of the billets compared to the unprocessed parts was significantly higher. The highest and more homogenised hardness results were observed when using the $\phi=90^\circ$ configuration.

- 3) The FE simulations suggested that the $\phi=90^\circ$ configuration experience greater and more uniform shear strain throughout the billet. FE simulations were also used to determine the heating effect on the billets during IECAP processing using the 2 different configurations. It was found that $\phi=90^\circ$ resulted in the greatest billet heat up but this heating was below 40°C which means it would not experience grain growth during processing and the billets could be handled safely post processing.
- 4) The grains from billets processed via the 2 configurations were analysed and compared to the 'as received' grain size. There is significant grain size reduction in both $\phi=90^\circ$ and $\phi=120^\circ$ IECAP. After the first pass the billets that were processed using $\phi=90^\circ$ IECAP configuration showed smaller and more uniform grains when compared to $\phi=120^\circ$ IECAP.
- 5) Strain distribution established by FE simulation and hardness measurement results show qualitative agreement, which confirms their suitability for estimating billet properties.
- 6) Once it had been established that the $\phi=90^\circ$ configuration resulted in the greatest mechanical properties in the A11050 billets, then the billets were subjected to further passes. Route BC was selected as this is the route suggested in the literature for A11050.
- 7) With each subsequent pass the pusher force as well as the punch force increase. The initial passes recorded the greatest step increase in maximum force for both the Punch and the pusher. After four passes the rate of increased force gradually declined and eventually evened out.
- 8) Half processed billets were then prepared and examined through the flow plain. The flow plain micro hardness analysis clearly showed the difference between the processed section and the unprocessed section. The shear zone was also clear to see. The hardness study showed that the first pass resulted in the greatest increase in hardness and the following passes had a more gradual increase effect on the hardness.
- 9) It is also clear that the head and tail section of the billets have an in-homogenise material properties and will have to be removed before using the billets in engineering applications.

- 10) The centre of the shear zone was analysed and it was found that the material experiences the greatest shear in a 5mm before and after this centre point.
- 11) The transverses to flow plain hardness was also examined in three locations for each billet; the input channel, the output channel and the shear zone. These hardness increases were very similar to the hardness readings seen in the flow direction study, therefore demonstrating isotropic behaviour.
- 12) Tensile tests were also carried out on micro specimens to further investigate the mechanical properties of the material. The findings of the tensile testing is in line with all the other findings and shows the increased ultimate tensile strength of the material even just after the first pass. The subsequent passes increase the ultimate tensile strength of the material, but the increase is rather gradual. Pass 6 and 8 saw very little differences.
- 13) Samples were then produced in the flow direction to analyse the effect of the multiple passes on the grain size of the billets. TEM was used to and it was observed that each pass has a grain refinement effect on the billet material. The microstructure results from EBSD and TEM indicate that grain size in the billet decreases with the increase in the number of passes of I-ECAP. In addition, dynamic recovery and recrystallization take place which influence the mechanical properties of the material at the later passes of I-ECAP.
- 14) In this study we examined the next natural evolution of the classical ECAP method for grain refinement and improved mechanical properties in billets. I-ECAP improves some of the limitations that are often associated with ECAP. The results of this study showed that the first pass leads to the greatest increase in mechanical properties and the following passes had a more gradual increase in these effects.

It has been shown that the mechanical properties of Al10 50 can be greatly improved by processing them using the IECAP process. The hardness of the material increases in both the flow direction and the transverse to flow direction therefore the produced material will have isotropic mechanical properties. This improvement in mechanical properties can be attributed to the grain refinement effects that are achieved in the IECAP process. This grain size reduction was using TEM. This study proves that it is possible to produce ultra-fine grain Al1050 using 8 passes of route BC IECAP. These

small grains have also shown their increased mechanical properties. Although the amount of material produced is relatively small, only small quantities are required to produce small components such as the microneedles.

The next step would be producing billets of ultra-fine grain Al1050 to assess their suitability for producing the microneedles. Their increase in mechanical strength is very important when considering them for micro components. This is due to the fact that there is less mass in these products therefore, it is critical that the material is strong enough to withstand the forces applied without deforming and breaking prematurely.

4.4. PART C: METAL FORMING EXPERIMENTS

In Part C a variety of surface preparation and lubrication conditions have been examined for single pin backward extrusion. Experimentally, the effects of lubrication, billet grain size and surface condition have been compared against surface roughness, press forming force and pin height. Punch speed and displacement on the pin forming stroke have also been investigated during both ultrasonic and non-ultrasonic assisted forming trials. A punch with a conical cavity created by EDM and a punch with an array of micro conical cavities created by laser ablation were used. The surface roughness of both punches has been analysed and presented. The inner surface roughness of the EDM cavity has been reported. The result of the laser ablation for the micro cavities is also presented. Experimental parameters were used for metal microneedle backward extrusion. The findings of these experiments are examined, analysed and discussed.

4.4.1. Billet Surface Conditions

Billets were cut from the centre of the billets of Al1050. To ensure that every billet had an identical size, they were cut using wire EDM. Each cylindrical billet was cut to a diameter of 4.95mm and a height of 4mm. The die used for this forming study had a diameter of 5mm, therefore, the diameter of the billets was chosen to be slightly smaller to allow for snug insertion. The surface of the billets underwent a variety of treatments so the effects of surface finish could be compared against a variety of lubrication conditions. The surfaces were examined with the Alicona surface roughness analysis machine and the results can be seen in Figure 4.22.

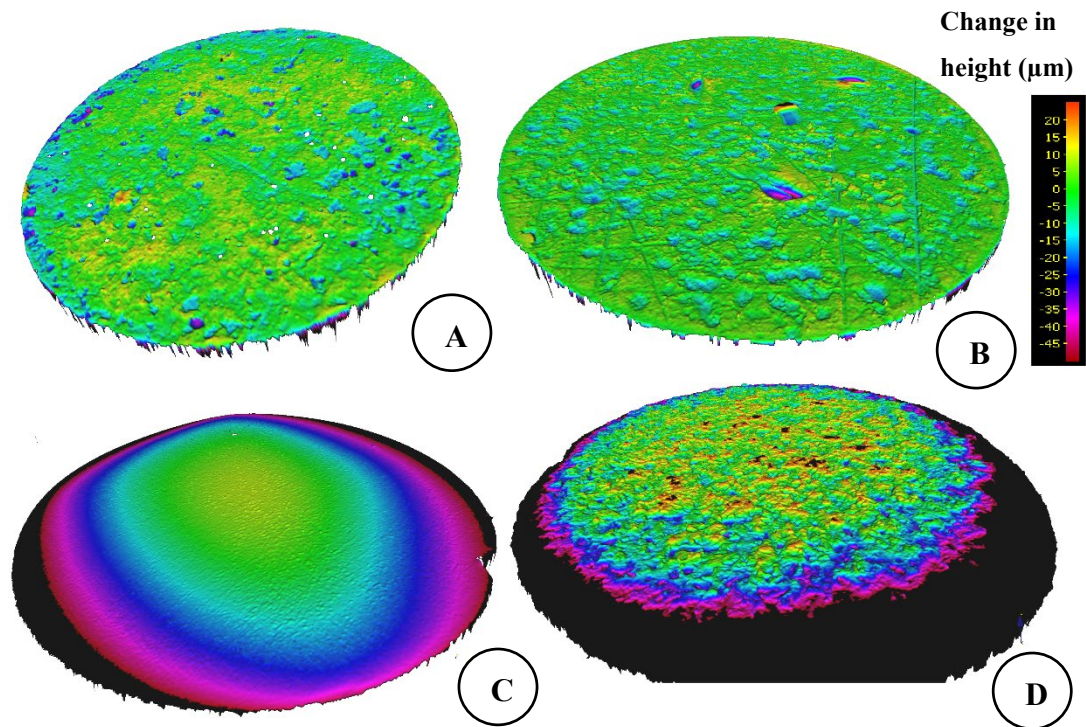


Figure 4.22: *Billet surface roughness analysis for a variety of condition. A- Surface after wire EDM cutting. B- Surface conversion coating. C- Surface after grinding with P2500 emery paper. D- Surface after sandblasting.*

As illustrated in Figure 4.22 the outcome of wire EDM cutting and conversion coating on the surface are very similar. Grinding with P2500 emery paper (average grit diameter $10.3\mu\text{m}$), however, results in the smoothest surface but uneven pressure can result in the surface becoming rounded. As expected, sandblasting gives the roughest surface but this process can remove more material from the perimeter of the surface causing it to become rounded. Increasing the roughness of the surface may result in a greater number of lubrication pockets, which could result in improved forming. The surface roughness was quantified to ISO 4287 standard and can be seen in Table 4.1.

Table 4.1 demonstrates that the sandblasting produces a surface significantly rougher than wire EDM and conversion coating. The surface of the billet was ten times smoother after P2500 emery paper than sandblasting.

Table 4.1: Surface roughness after a variety of conditions.

	Experiments	Ra (μm)
A	After wire EDM	3.67
B	After wire EDM and conversion coating	3.31
C	After wire EDM and grinding with P2500 emery paper	0.54
D	After wire EDM and sandblasting	5.21

4.4.2. Single Pin Punch

As discussed in chapter three, the single pin punch was created using sink EDM. This process required the production of a copper electrode before the punch cavity could be made. Examining the electrode surface after the conical hole had been produced it should be possible to predict the roughness of the inside surface of the punch. The surface of the copper electrode that was used to produce the punch was examined and can be seen in Figure 4.23.

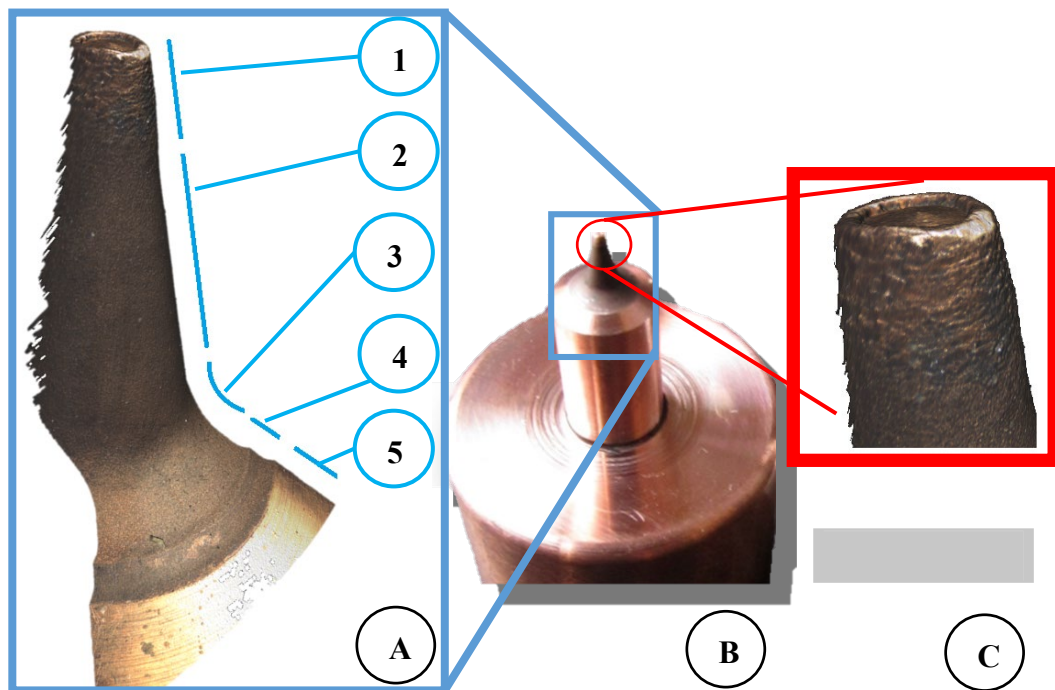


Figure 4.23: Copper electrode used to produce the single pin punch.
A- Electrode surface used for surface roughness quantification.
1 to 5 represent the areas of interest for roughness analysis.
B- The copper electrode. **C-** Close look at the tip of the electrode.

The electrode was studied and the surface roughness quantified. It was noticed that the tip of the electrode had the greatest deterioration (see Figure 4.23 C). This could be due to being the first point of contact with the punch material, therefore, being in contact with the material the longest and the spark removal. The sink EDM process uses a sacrificial electrode, therefore, the electrode is damaged as the part is created. Several locations (refer to Figure 4.23 A) of the electrode surface were measured and the surface roughness values are shown in table 4.3.

Table 4.2: Roughness measurement along the copper electrode surface.

Measurement Location	1	2	3	4	5
Surface Roughness Ra (nm)	910	196	204	186	303

The roughness measurements statistically confirm the initial observations of tip roughness.

Once the fabrication of the punch had been completed, the inner surface of the punch was examined. The punch was sectioned in half using wire EDM and counted in polymer simplify handling and allowing surface measurements to be made. This can be seen in Figure 4.24.

As illustrated in Figure 4.24 B, the tip of the conical hole appears rougher than the rest of the cavity. Surface roughness measurements were carried out to quantify these observations. Several locations (refer to Figure 4.24 B) of the punch inner surface were measured and the surface roughness values are presented in Table 4.3.

Table 4.3: Roughness measurement along the inner surface of the punch.

Measurement Location	1	2	3	4	5	6
Surface Roughness Ra (nm)	728	513	257	230	200	203

The roughness measurements statistically confirm the initial observations of tip cavity roughness.

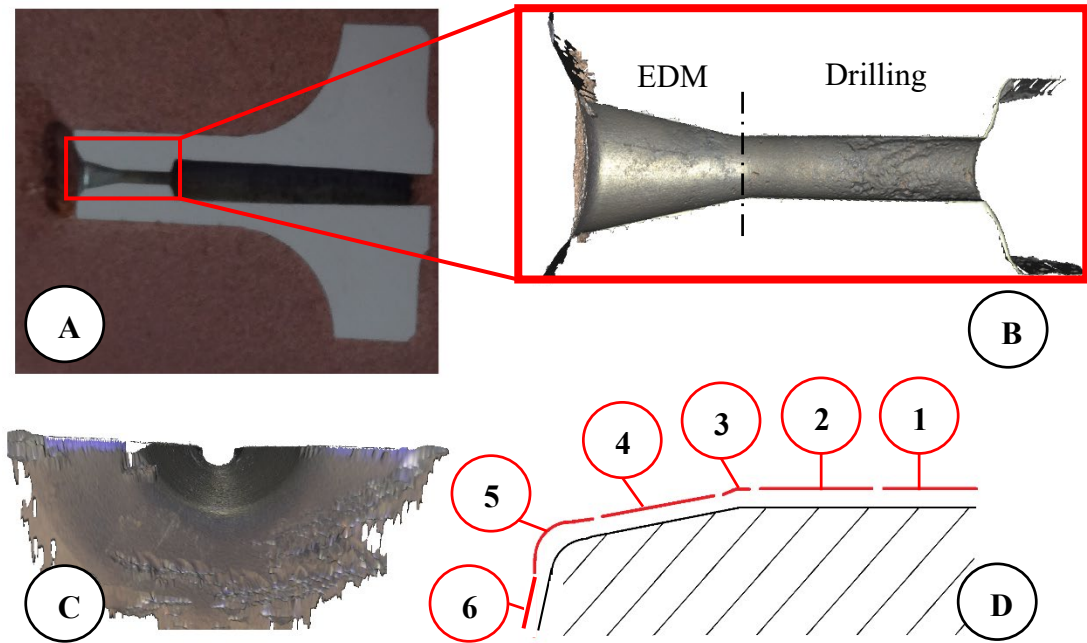


Figure 4.24: *Examination of the inner surface of the punch after sink EDM and spark drill production. A) Sectioned single pin punch counted in polymer. B) Side view of the inner cavity of the punch. C) Bottom view of the conical cavity of the punch. D) Locations of interest for surface roughness measurements.*

The findings confirm that it is possible to predict the surface roughness of the punch cavity by examining the electrode after usage. The inner surface of the punch is rougher than the surface of the electrode. The tip of the cavity is significantly rougher than the rest of the cavity but this is not an issue as this part was designed for the trapped air and lubricants to escape from the punch. The increase in the value of roughness can be explained due to the combination of manufacturing techniques used. Section 1 and 2 from Figure 4.24D were produced using the spark drill and not by using EDM method. A new punch was created and used for the single pin experiments for this study.

4.4.3. Single Pin Experimental Results

As discussed in Chapter three, a custom LabVIEW virtual instrument was created for these experiments. The virtual instrument was capable of recording load value from the load cell and voltage values from the eddy current sensor. The information from the virtual instrument is illustrated in Figure 4.25.

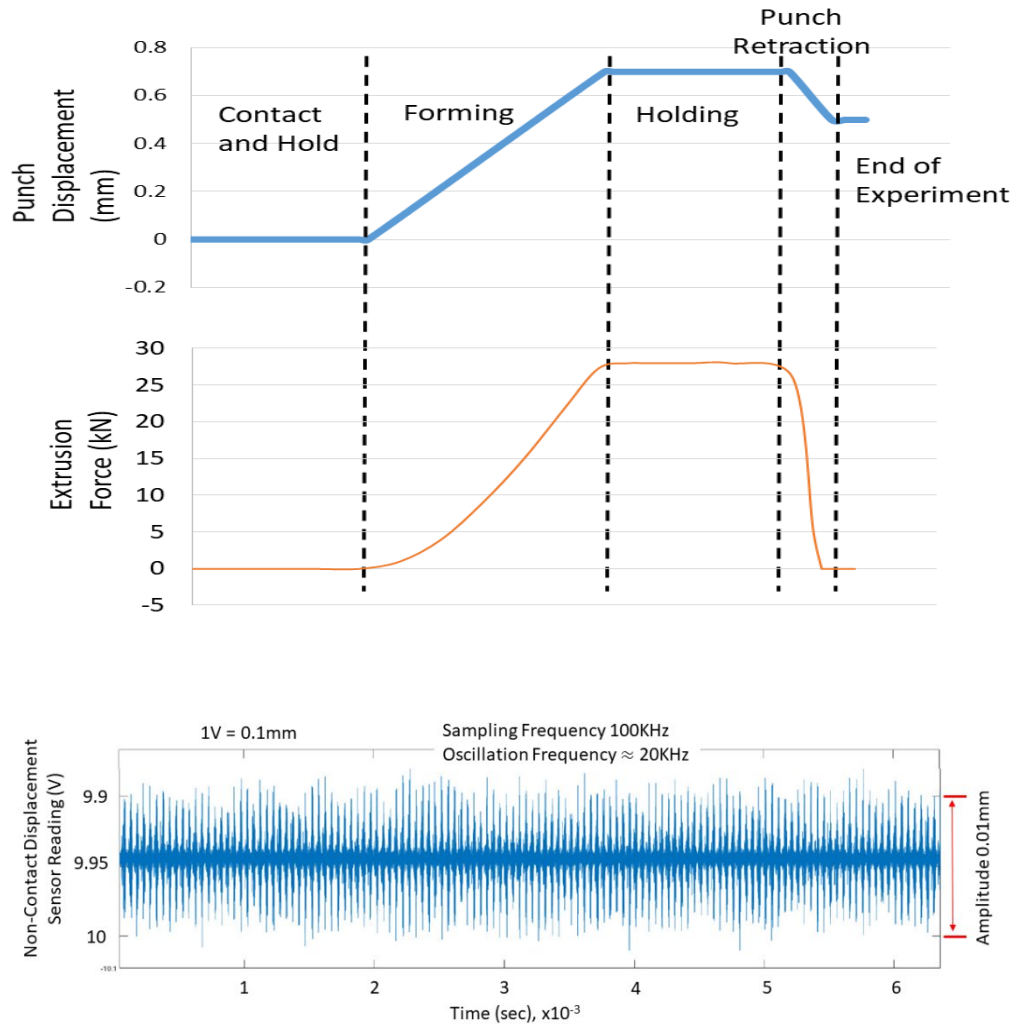


Figure 4.25: Graph showing the reading from (top) the eddy current non-contact sensor, (middle) force recorded by the load cell, (bottom) voltage signal captured from the non-contact sensor during an ultrasonic assessed forming trial. Voltage signal shows a 0.1 fluctuation, which represents the 0.01mm amplitude of the punch under excitation.

In Figure 4.25 the extrusion force detected by the load cell can be seen. The eddy current non-contact sensor shows the distance the punch has moved from the zero position. The zero position was set once the punch was slowly lowered and met the billet and a small force was registered by the load cell. Then the eddy current sensor is placed in position by using shims and locked into position. There was manual setup steps between each experiment. Although every precaution was taken to minimise these variations, small inconsistent can remain and be a source of variations in the results.

The experiments were carried out as follows, once the punch was in contact with the billet the punch was held in place for a few seconds (contact and hold). This allowed time to check everything was working correctly and run the data-capturing instrument. Then the forming was carried out. This was followed by another hold for a few more seconds before the punch was retracted and the experiment completed.

Examining the signal revived from the non-contact sensor, it showed a reading of 10v when the target is out of range. As the target gets near the sensor the reading reduces. The sensor has a 1mm range; therefore, each volt represents 0.1mm of travel by the punch. This sensor has a very high resolution and oscillations made by the ultrasonic equipment can be captured. Once the data is examined closely, it is possible to see the oscillation during the ultrasonic assisted forming test. This showed that the amplitude of the punch was about 10 micrometres and the punch was oscillating at about 20kHz.

4.4.4. Single Pin Coarse Grain Experiments

As the tensile testing and hardness studies had shown the coarse grain material was softer and should require less force to shape. Therefore, this was the initial billet condition used for testing. A variety of combinations of surface conditions and lubrication were tested. The surface of the formed pins was also measured and are presented in Table 4.4 shows an array of information for each test, therefore, Figure 4.26 was created as a key to interpreting the results in Table 4.4.

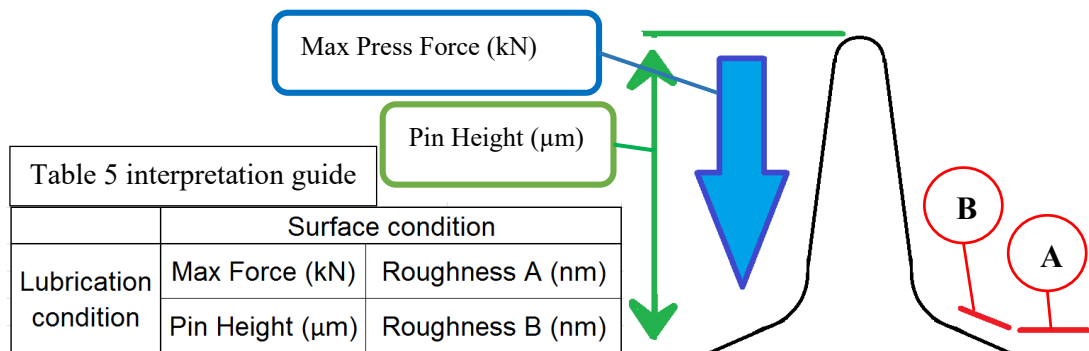


Figure 4.26: The press force and the pin height were recorded for each pin. A and B show the location of surface roughness measurements for each pin.

Table 4.4: *A combination of billet surfaces and lubrications tested. The load, pin height and surface roughness in two locations is presented in this table.*

Condition	EDM		Conversion coating		P2500		Sand Blast	
	Load	Pin Height	Load	Pin Height	Load	Pin Height	Load	Pin Height
Unlubricated	21.5	108	23.4	152	24.7	187	24.1	106
	2523	180	2920	118	2833	180	3431	213
Grease	23.1	102	19.8	205	26.2	83	24.3	400
	3208	190	3684	170	2981	180	3946	189
MoS2	22.6	93	24.8	350	25.1	188	25	240
	2940	167	3440	190	2964	170	4406	160

As expected the sandblasted surface resulted in rough pin surfaces. These surfaces allowed more lubricants to be trapped in the pockets, which resulted in the tallest pins. The smoother surface created by grinding with P2500 resulted in short pins and it is clear to see from the table that lubrication has very little effect on this surface condition. It is also possible to see that in some conditions the MoS2 resulted in the highest surface roughness readings.

To develop a better understanding of these results the pin heights and lubrication conditions were examined. This is presented in Figure 4.27.

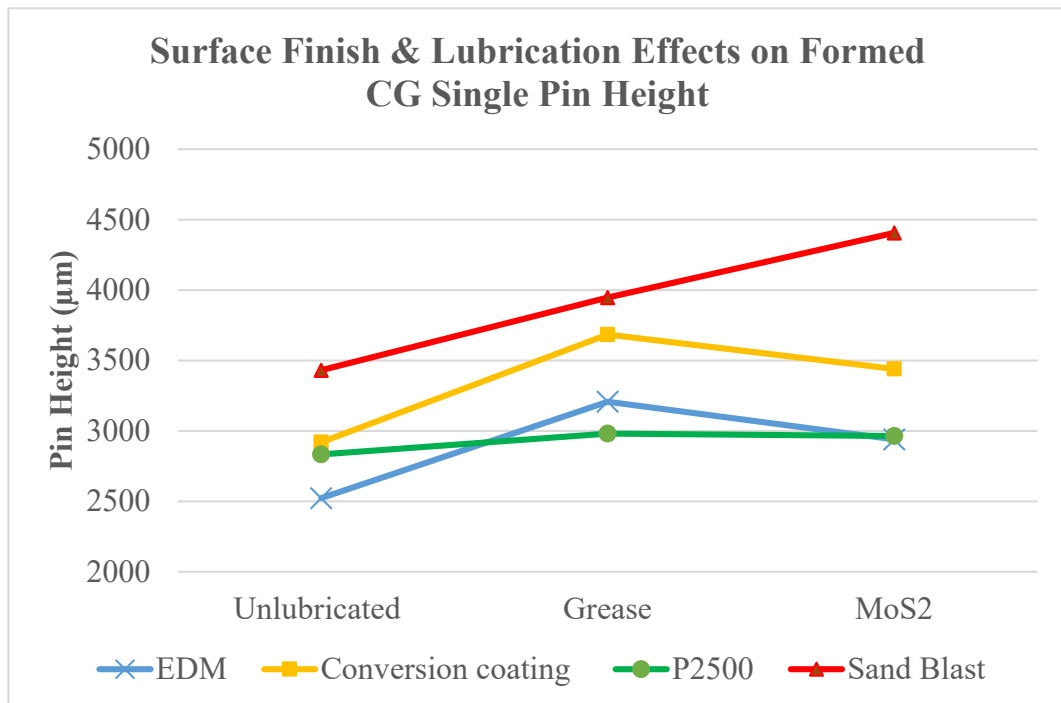


Figure 4.27: *Effect of the combination of surface conditions and lubrications is examined against the formed pin heights.*

From Figure 4.27 it possible to confirm the initial interpretation from the data. Pin heights can be improved with lubrication under all surface conditions apart from very smooth surfaces. Lubrication has no effect on pin height on P2500 surface condition. Sandblasted surfaces experience the greatest improvement with lubrication. Conversion coating follows the same trend as an EDM surface but with almost 500 μ m under all lubrication condition. The shortest pin has the EDM and unlubricated condition.

To develop a better understanding of the test results, the press force and lubrication conditions were examined. This is presented in Figure 4.28.

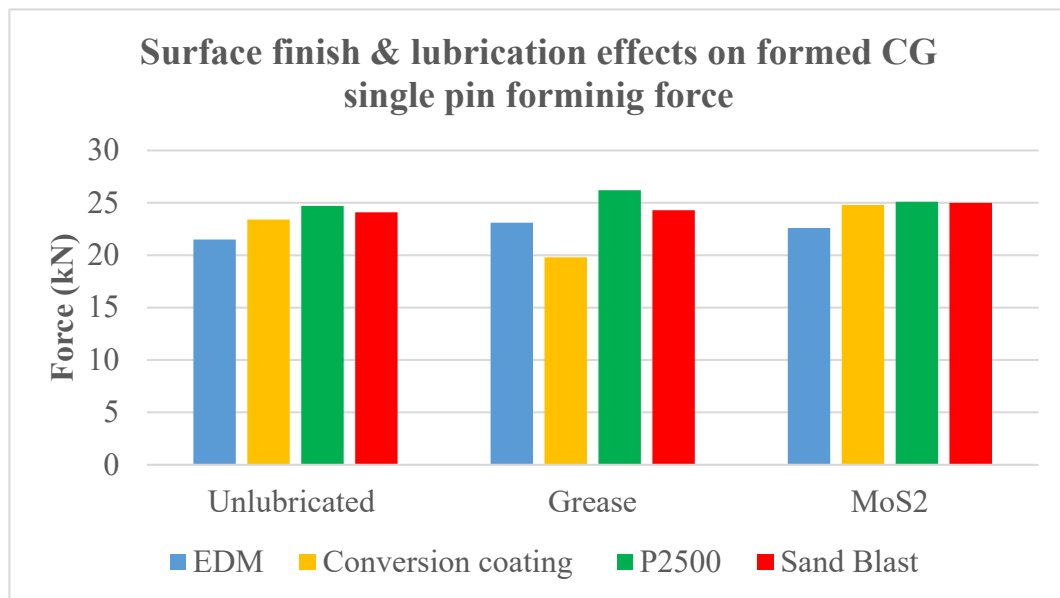


Figure 4.28: *Effect of the combination of surface conditions and lubrications is examined against the required forming force.*

From Figure 4.28 it is possible to see that the load required to form a pin is almost constant no matter which lubrication condition is used after sandblasting the surface. The forming load is the highest in all lubrication conditions when the surface is ground with P2500 emery paper. Combining grease lubricant and conversion coating achieves the lowest forming force but in general the standard wire EDM cut surface achieves the lowest forming forces in most lubrication conditions.

4.4.5. Single Pin Ultra Fine Grain (UFG) Experiments

The same experiments were then conducted for billets produced from UFG A11050. It was not possible to conversion coat the UFG billets; therefore, a fourth condition was required. Gold was used as the fourth condition and was applied using sputter coater. From the experimental results it was possible to see that EDM gave the most consistent results, therefore, this condition was taken forward for the UFG tests. The results of the UFG single pin forming trials are shown in Figure 4.29.

From the graph, it is possible to note that unlubricated billet required the least press load but also resulted in the shortest pin. The new gold coating resulted in the tallest pin and the force was not significantly higher than unlubricated condition. Grease and MoS2 resulted in very similar pins. The results of the two grain size were then examined and can be seen in Figure 4.30.

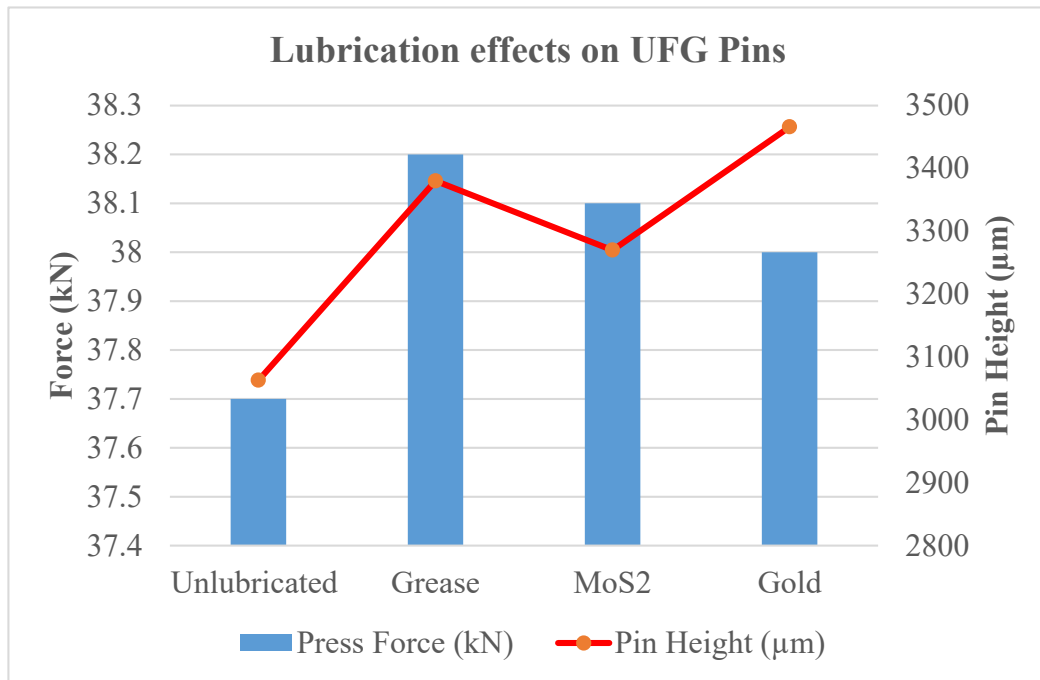


Figure 4.29: Using UFG to form single pin under a variety of lubrication conditions.

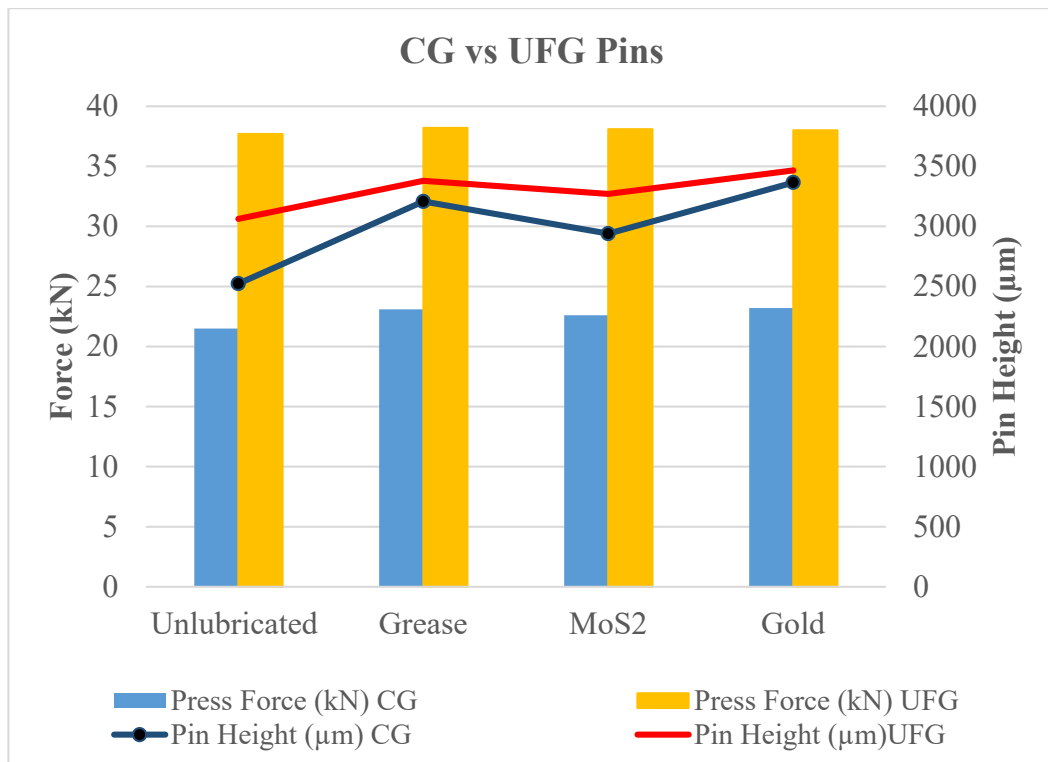


Figure 4.30: Comparison drawn between the effects of the two grain sizes on pin height and press force.

UFG billets require significantly higher loads to form the pins when compared to CG A11050. The forming force is not significantly higher between the different lubrication conditions within the same grain size conditions. All lubrication conditions improve on heights. The pin heights achieved by using UFG is very similar to CG but up to 60 percent greater force is required.

The effect of the punch displacement speed was then examined. Three different speeds were chosen 0.1, 0.5, 1.0mm/s. The press was capable of achieving these speeds, but with the added weight of the rig it was possible that the actuator would over shoot the set distance. The findings of the punch speed tests are shown in Figure 4.31.

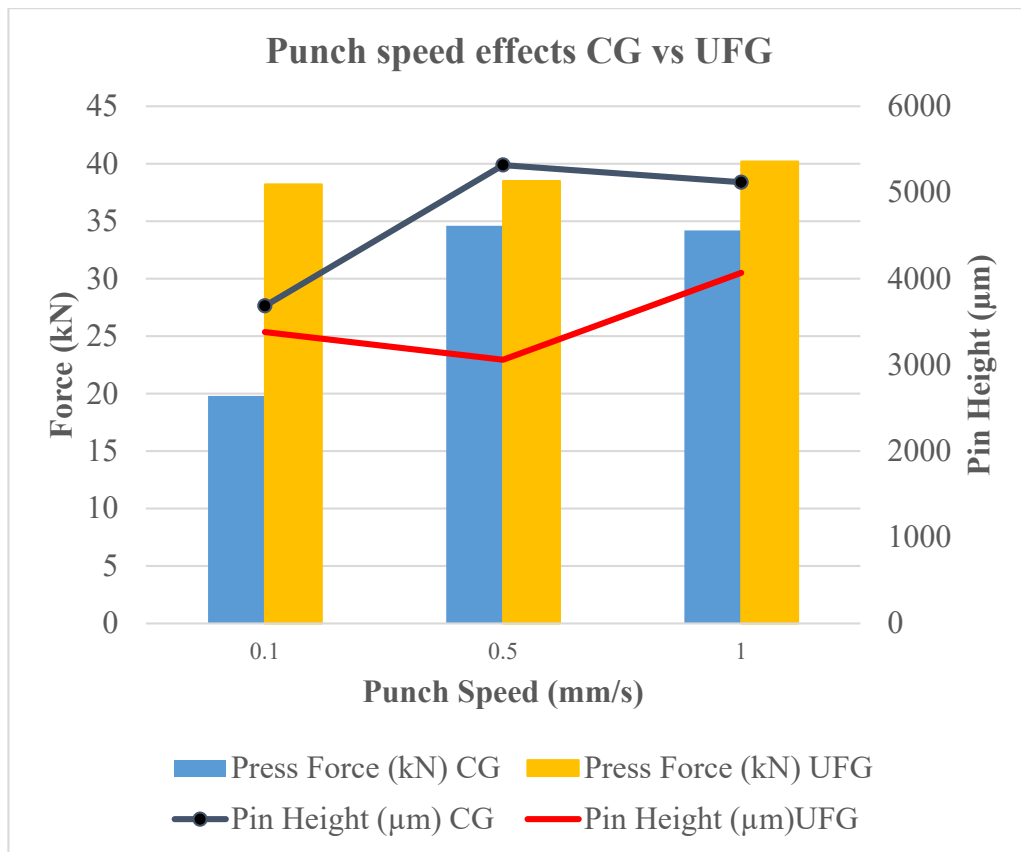


Figure 4.31: *The effects of punch displacement speed on the press force and pin height under 2 different billet grain sizes.*

The force did not significantly increase when UFG material was used and the pin height did not see significant changes until 1mm/s punch speed was used. As the speed of the punch increased, so did the force recorded during the CG tests. As the force increased so did the height of the pins when CG was used.

4.4.6. Ultrasonic Assisted Single Pin Forming

Similar experiments as above were conducted with the addition of ultrasonic oscillation. The ultrasonic equipment was described in Chapter three. 20kHz oscillation with an amplitude of 100µm was used. The effects of ultrasonic oscillation were investigated on CG and UFG Al1050 and can be seen in Figure 4.32 and Figure 4.33 respectively.

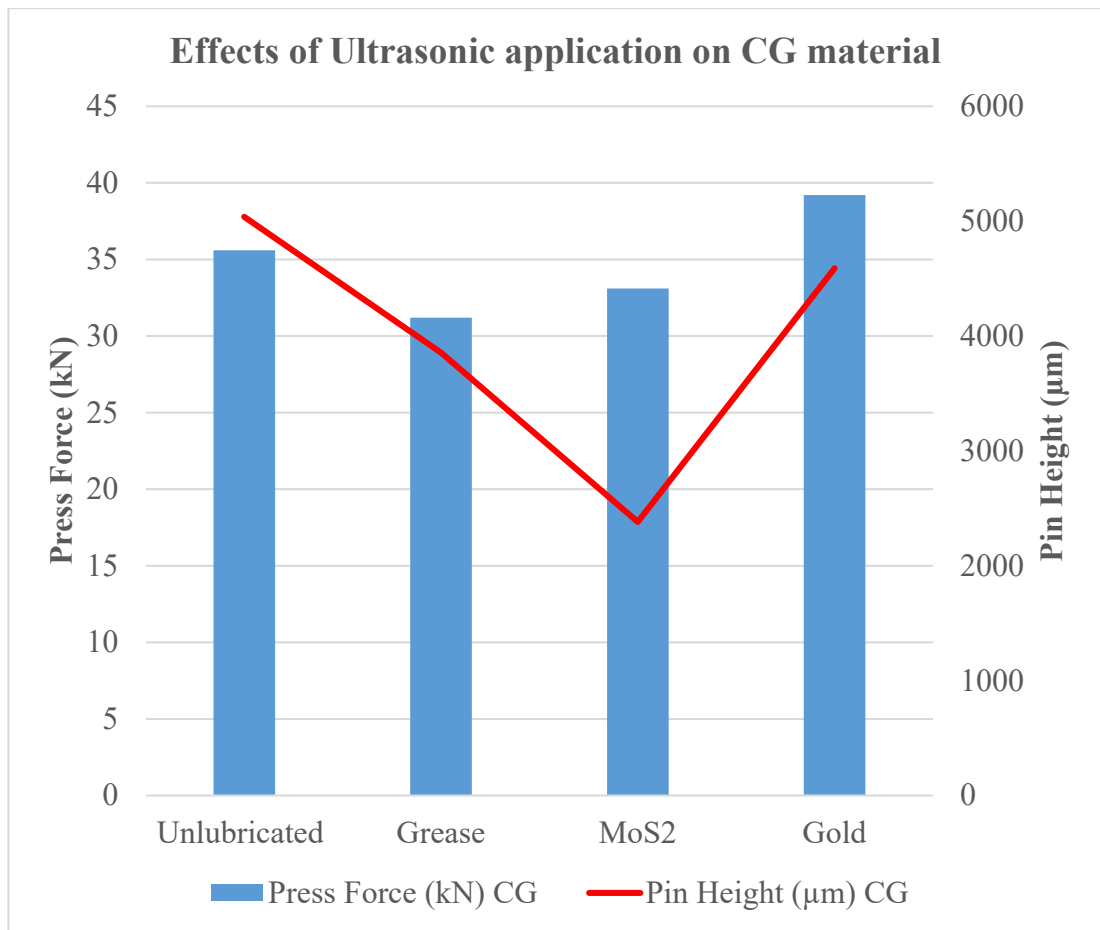


Figure 4.32: *Effects of ultrasonic assisted backwards extrusion on CG Al1050. Press force and pin height are investigated with respect to lubrication condition.*

The force required to form the pins is highest for unlubricated and gold coating conditions but also resulted in the tallest pins. Lubrication of the CG billets resulted in lower forming forces but also shorter pins. MoS2 application significantly adversely effected the height of the pin. The height of the MoS2 lubricated was about half that as the gold coated condition. This was an unexpected result. There might have been an experimental error. Other users have access to the MoS2 and the brush that is used to apply it. There could have been other particulates or dirt mixed with that particular some of MoS2 used for this test. MoS2 is a very dark coloured lubricant and it would be difficult to distinguish foreign particulates in the lubricant.

Using ultrasonic assistance in forming UFG material was also investigated and can be seen in Figure 4.33.

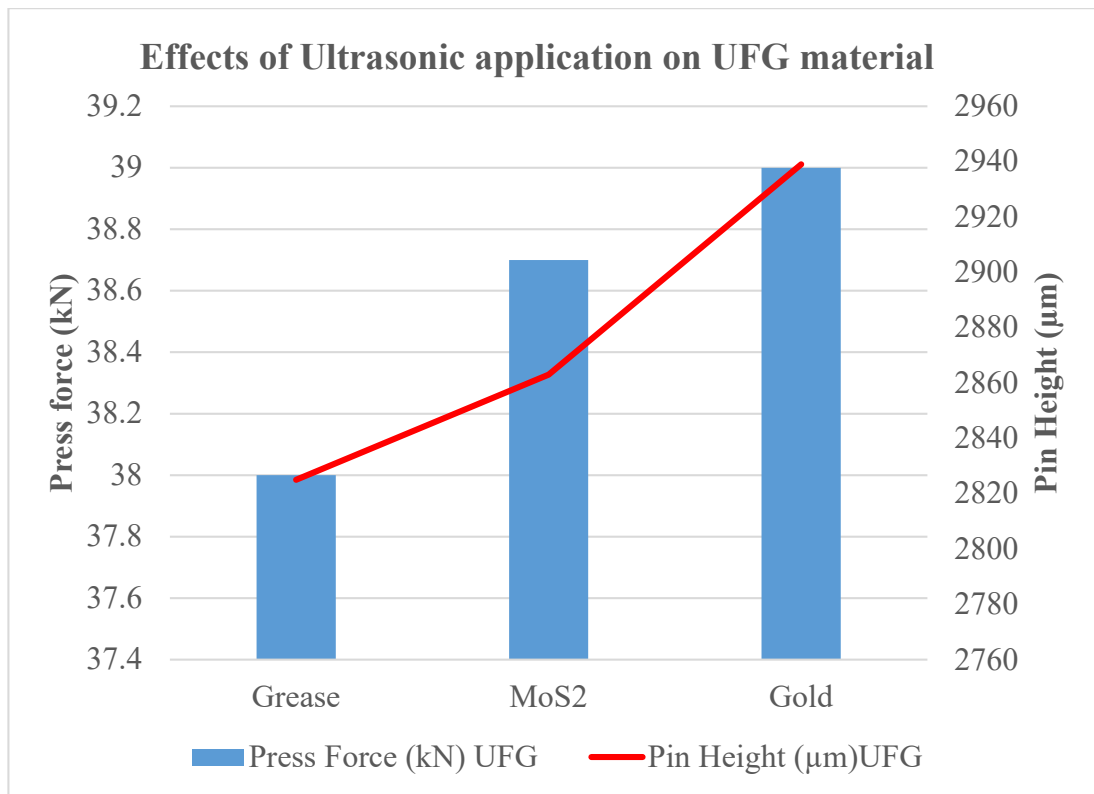


Figure 4.33: *Effects of ultrasonic assisted backwards extrusion on CG Al1050. Press force and pin height are investigated with respect to lubrication condition*

The application of gold also saw the tallest pins in the UFG billet condition. Application of grease resulted in the lowest forming forces but also the shortest pins. MoS2 application resulted in medium pin height and force. Overall the forming forces and pin heights are very similar in all three conditions. It was expected that there would be a more significant reduction in the forming force when ultrasonic oscillation were applied but the results for these tests did not show that. This again could be partly due to the dirty MoS2 that was used for the previous experiments or slight misalignment between the tools. The cylindrical tools could have started to rub against each other and cause bigger loads to be captured and the misalignment could cause the material not to flow uniformly. It was initially thought that the tool pressure was becoming too high and was causing the punch to slightly bulge. The tools were also inspected for cracks as well but no fractures were detected.

The effects of punch displacement and ultrasonic assistance were investigated and can be seen in Figure 4.34. As described in Figure 4.25 the punch was first lowered and put in contact with the billet inside the die the experiment was started. The ram was then set to the required displacement. As the punch was oscillating by an amplitude of 10 μ m, an attempt was made to consider this while programing the movement of the ram. For the CG conditions, as the punch displacement increased, so did the press force and height of the pin but for UFG conditions, the height of the pin remained constant and the force increased by 15 percent between 1.5mm and 1.7mm. For CG conditions the force doubles between 1.5mm and 1.6mm but sees a marginal increase between 1.6mm and 1.7mm. As the UFG material has a higher Young's modulus it could causing the rig to slightly flex. As shown in the schematic diagram, there are many elements to the rig. As expected, the force required to form UFG material is greater than CG material but the difference is about 20 percent after introduction of ultrasonic oscillation.

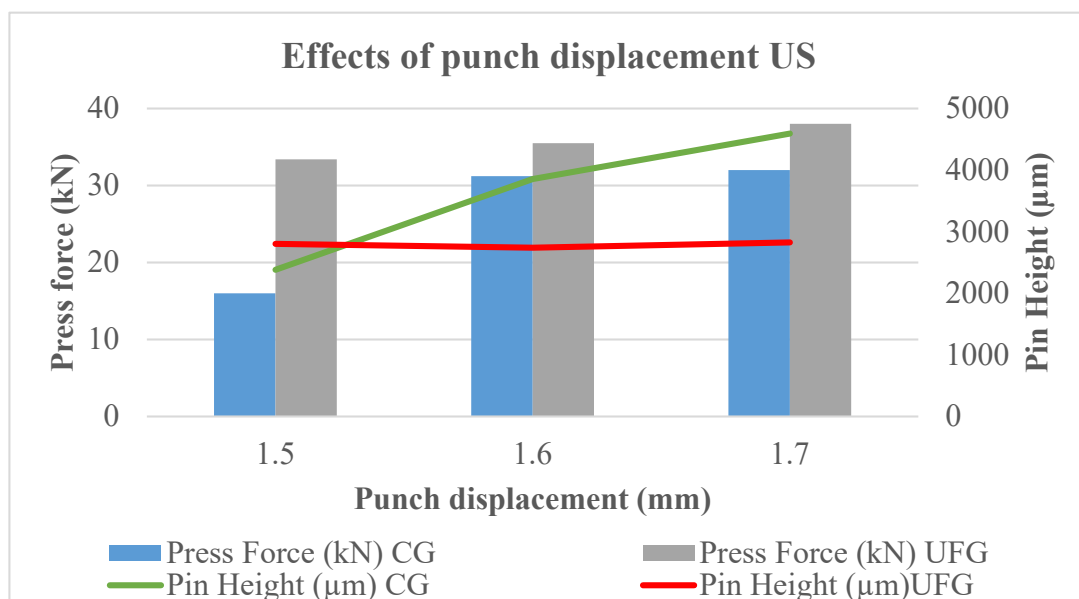


Figure 4.34: *The effects of punch displacement length while ultrasonic oscillations were induced on the press force and pin height under two different billet grain sizes.*

The effects of punch displacement speed and ultrasonic assistance was investigated and can be seen in Figure 4.35. It was found that no significant difference can be clearly seen between the three punch speeds.

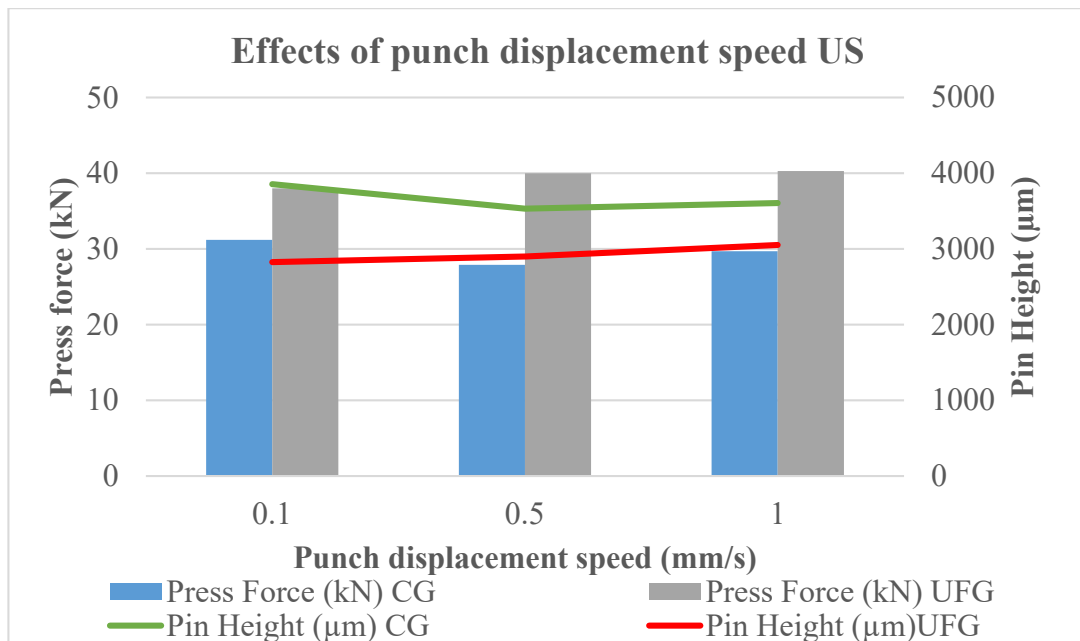


Figure 4.35: *The effects of punch displacement speed while ultrasonic oscillations were induced on the press force and pin height under two different billet grain sizes.*

To develop a full understanding of the effects of ultrasonic oscillation in backward extrusion a comparison was made between lubrication conditions grain size and the press forming force. The results can be seen in Figure 4.36.

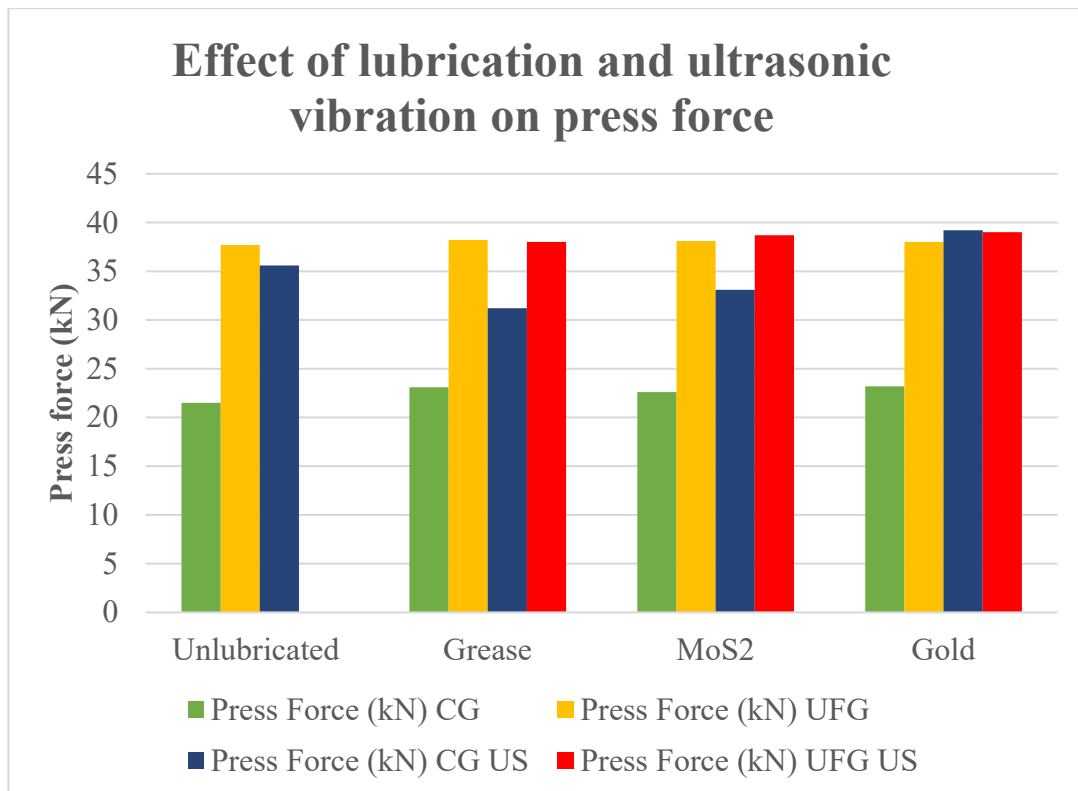


Figure 4.36: Comparing press force for pins that were created with different grain sizes and with/without ultrasonic assistance during various lubrication conditions.

In all cases the CG material with no ultrasonic assistance resulted in the lowest forces. Gold coating resulted in pins that required the same forming force in all grain and oscillation conditions apart from condition stated previously. UFG material behaves very similar in all lubrication and oscillation conditions.

To get a full understanding of the effects of ultrasonic oscillation in backward extrusion a comparison was made between lubrication conditions grain size and the pin heights. The results can be seen in Figure 4.37.

In most cases the gold coating results in the tallest pins. Applying MoS2 to most surfaces will result in heights similar but not as tall to grease application but the application of MoS2 CG billet when ultrasonic vibration is added will significantly reduce the height of the pin. MoS2 does not appear to be a good lubricant when ultrasonic oscillations are introduced. These fast movements may cause the MoS2 plates to break prematurely and reduce the formability of the material.

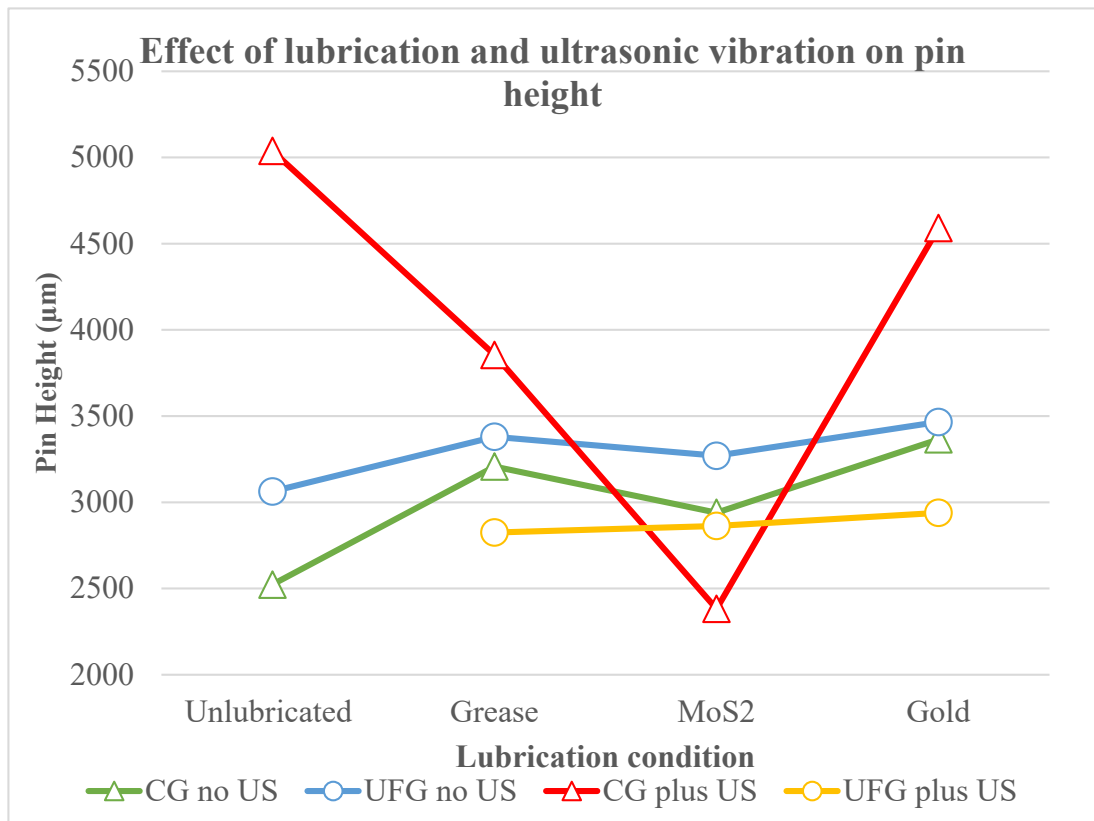


Figure 4.37: Comparing pin heights for pins that were created with different grain sizes and with/without ultrasonic assistance during various lubrication conditions.

A formed pin was sectioned in half and an electron backscatter diffraction (EBSD) made. This can be seen in Figure 4.38. It is possible to see the grains have all directed themselves in the direction of flow. The grains in the middle of the pin are large and elongated but the grains near the perimeter of the pin are small and round. This could be due to the high shear stress caused as the material flows backwards into the punch. The amount of strain imposed due to applied force of punch causes the grains to undergo fragmentation process as a result of dynamic recrystallization. EBSD analysis has been made on a pin and the results are given in Figure 4.38. Red rectangular box from the pin shows the area used for EBSD scan. Inverse pole figure map given demonstrated the flow of grains from the base of the pin to forwarding end. Evidence for formation of shear/ deformation bands at angle of 45° to direction of tip. The crystallographic orientation of constituting grains can be identified with the aid the colour coded inverse pole figure provided as an insert Figure 4.38.

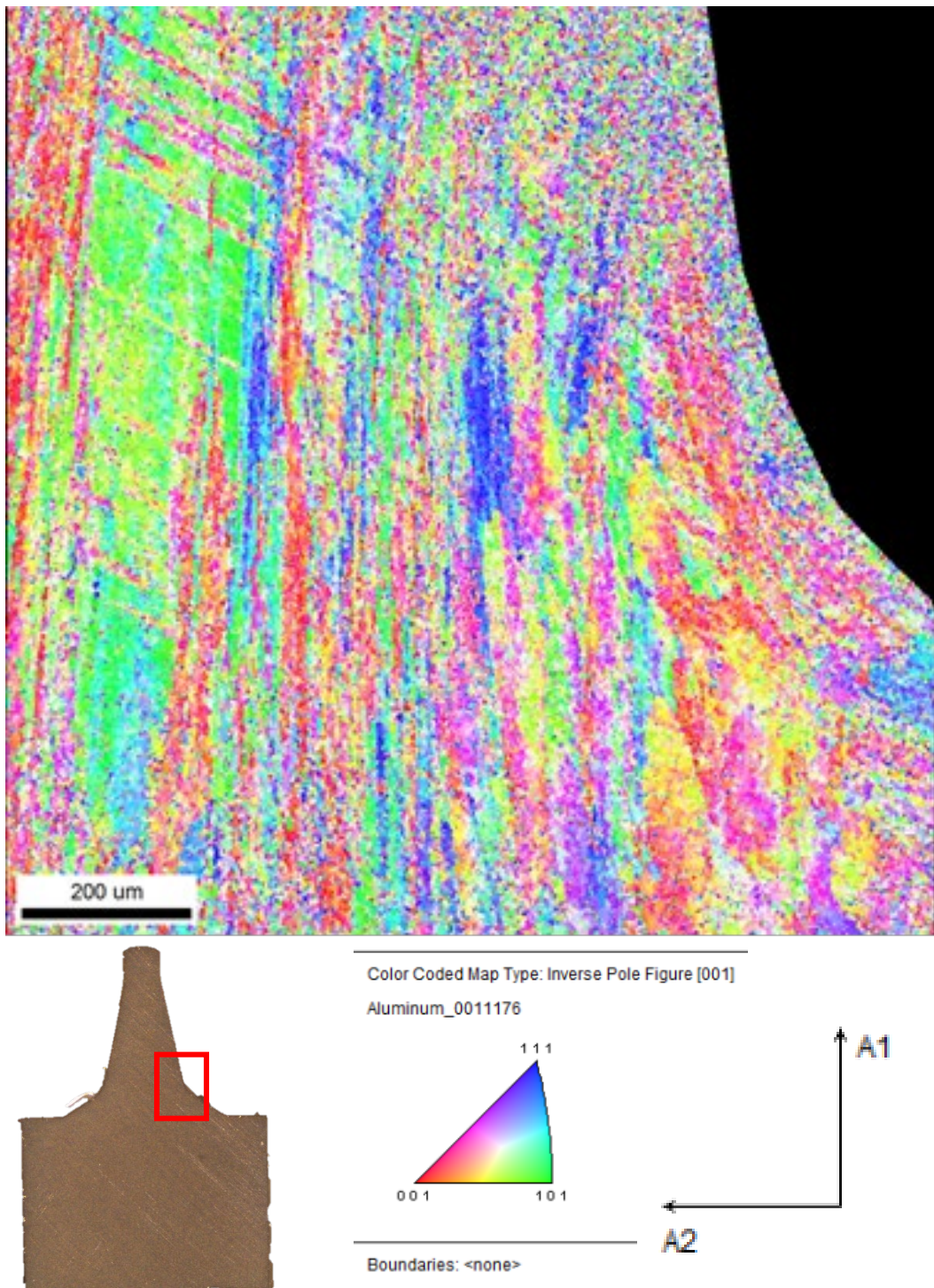


Figure 4.38: *EBSD of a single pin. Pin conditions – CG billet, no ultrasonic oscillations, grease lubrication.*

4.4.7. *Micro punch*

To investigate the effects of backward extruded micro forming a punch with an array of conical holes was created. As discussed in Chapter three, laser ablation was used to create these micro conical holes. The punch with the array of conical holes can be seen in Figure 4.39.

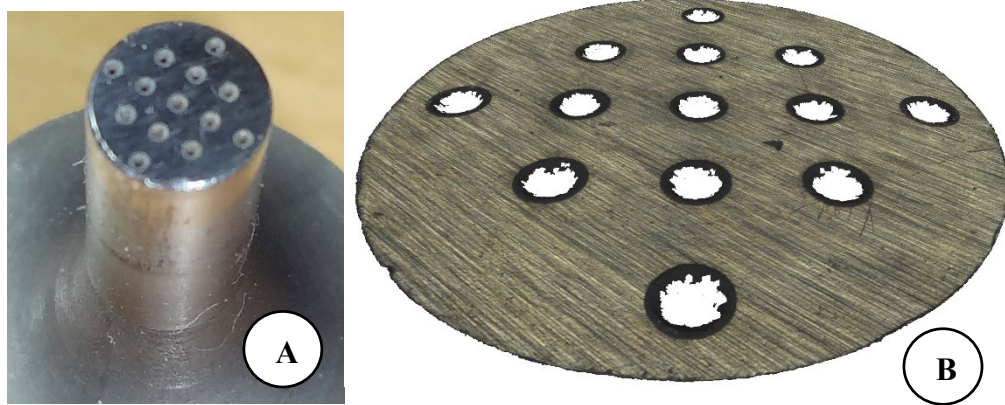


Figure 4.39: *Punch with micro conical cavities created by laser ablation. A- the completely fabricated punch. B the surface of the punch.*

The surface of the punch was ground prior to laser ablation. The surface roughness was measured and was found to be $R_a = 210$ nm. On inspection the 13 conical holes had the required 1mm spacing. No conical holes were made close to the edge of the punch, to reduce the possibility of the punch fracturing.

The surface of the punch was scanned under high magnification and can be seen in Figure 4.40. From the scan it was evident that the process of laser ablation had created a perimeter around each conical hole. These protrusions around the holes measured $10\mu\text{m}$. Ideally this surface would be flat but re-grinding of this surface could result in the punch material being lodged in the micro cavity, therefore, no further regrinding steps were undertaken. In this design the conical cavities do not have a through hole therefore it would not be possible to remove fragments that would inevitably fall into the conical cavities grinding post laser ablation. It could be possible that if this design is used in a later study some modifications could be made to the laser settings to minimise this perimeter feature.

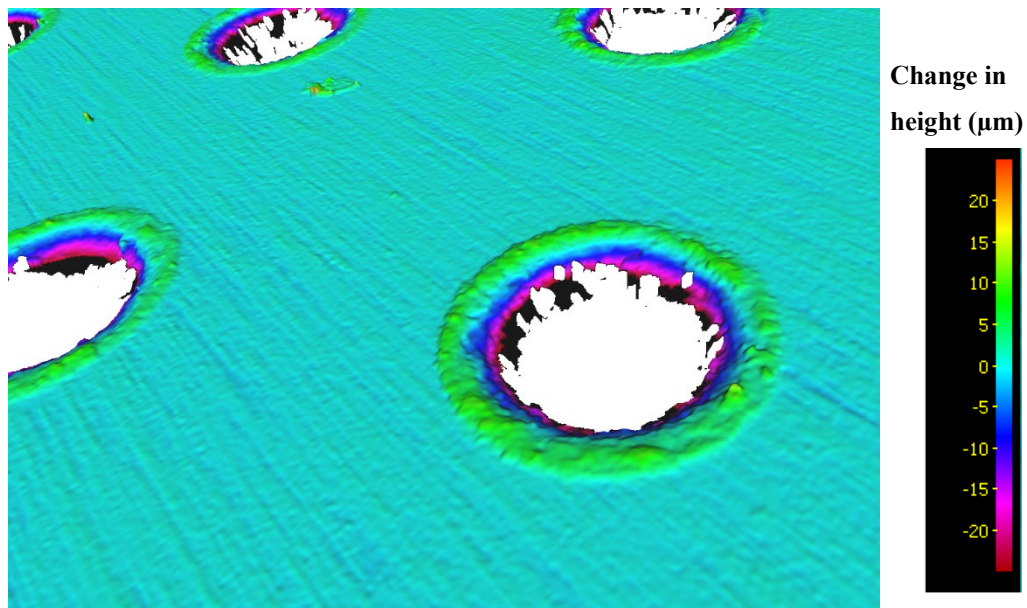


Figure 4.40: Surface height fluctuation for the micro needle punch.

4.4.8. Micro forming experiments

The punch with the single pin cavity shown in Figure 4.24 was replaced with the punch with the micro needle array cavities shown in Figure 4.39. The results of the testing are presented in the following sections. Conditions such as surface condition of the billet, excitement state of the ultrasonic tool and height of the needles have been recorded and presented in the following section.

Prior to the starting the experiments, a few initial trials with the microneedle array cavity punch were conducted. Due to the limitations of cylindrical micro billets it was important to have an experimental plan. An experimental plan was created and can be seen in Table 4.5 Experiments for each condition was repeated several times. In order to minimise the repeat of information in the following section the extrusion force for each condition has also been added to table Table 4.5. Initially the ram stroke was set to 2mm for all experiments but the recording of high tool pressures resulted in a decision being made to reduce the ram stroke to 1.8mm. The microneedle array cavity punch was unique and damage or breaking of the punch could result in not completing the remaining experiments. All experiments were conducted with a ram speed of 0.1mm/s

Table 4.5: *Experimental plan for microneedle array cavity punch. Also includes the extrusion force recorded from the experiments.*

Condition	Grain size	Lubrication and Surface Condition	Ultrasonic oscillation yes/no	Ram Stroke (mm)	Extrusion Force (kN)
1	CG	Grease	N	2.0	54.5
2	UFG	Grease	N	2.0	56.8
3	CG	CC	N	2.0	55.5
4	CG	CC + Gold	N	2.0	56.6
5	CG	Gold	N	2.0	57.9
6	UFG	P2500	N	2.0	57.7
7	UFG	Gold	N	2.0	57.9
8	CG	P2500	Y	1.8	48.4
9	CG	CC	Y	1.8	46.8
10	CG	CC + Gold	Y	1.8	46.6
11	CG	Gold	Y	1.8	47.7
12	UFG	P2500	Y	1.8	51.4
13	UFG	Gold	Y	1.8	50.0

4.4.8.1. Grease lubricant

The results from the single pin study suggested that grease would be a good lubricant for forming. This was applied to the surface of the billet and tested. The results are shown in Figure 4.41. Firstly, CG was used (Figure 4.41 A) then the same test conditions were used and UFG material was used (Figure 4.41 B). For both grain size conditions, the press experienced high forces, but very short pins were produced. The distribution of the needle heights was uneven and did not follow the finding of the simulation results. After further investigation it was noted that the grease lubrication had been trapped in the micro cavities and stopped the Al1050 from flowing into the cavities. This lubricant was not used further in this investigation. MoS2 was also not used for this investigation due to the findings of the initial experiments. The MoS2 could also clog up the micro cavity and stop the material from flowing into the punch. The lubrications used from this point forward were only gold and conversion coating

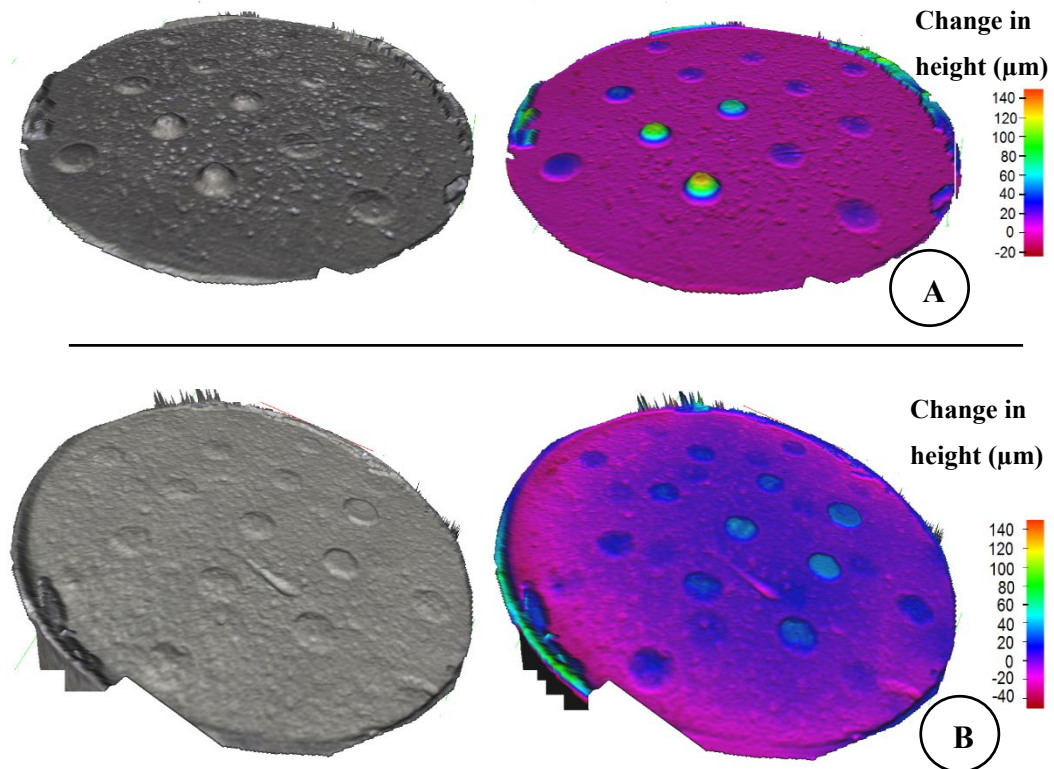


Figure 4.41: *Effect of grain size on surface topography when grease was used as a lubricant to coat the billet subjected to micro-forming: (A) GC and (B) UFG. Note that there is no ultrasonic excitation added to the punch,*

4.4.8.2. Coarse Grain Billet Surface Coating Conditions

Three different coatings were investigated for CG billets. These were, conversion coating, gold coating and a combination of conversion coating and gold coating. The results of the needle heights are shown in Figure 4.42.

Conversion coating resulted in the tallest needles and gold coating (about 20nm) resulted in the shortest needle. The conversion coating also saw the greatest fluctuation in needle height but the gold coating resulted in the most consistent needle height distribution. There were great differences between the height of the outer needles and the centre needle since the conversion coated billet. The conversion coating and gold coating combination billet result was half way between the two independent coating results.

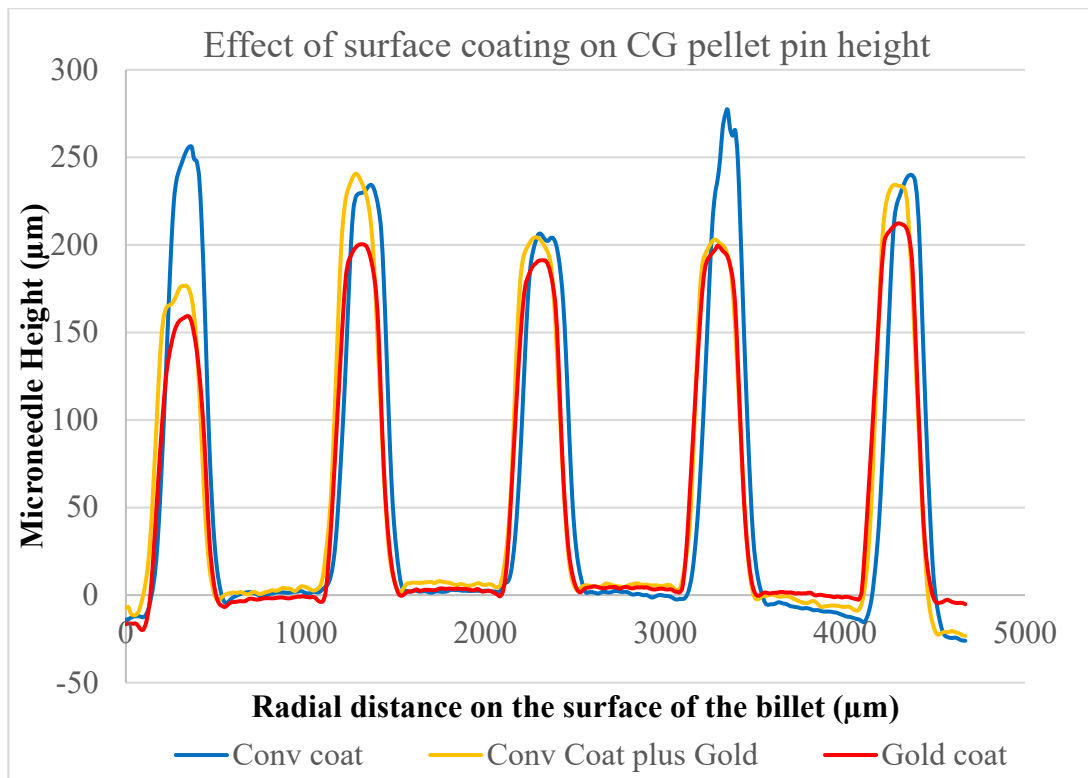


Figure 4.42: *Effect of using CG billets. Coating conditions compared against the needle height distribution.*

4.4.8.3. Ultra-Fine Grain Billet Surface Coating Conditions

Two different surfaces were investigated for UFG billets. These were, P2500 emery paper grinding and gold coating. The results of the needle heights are shown in Figure 4.43.

Using the P2500 surface UFG billet resulted in short needles but they were almost all identical heights. The gold coated UFG billet resulted in needles that were on average 100µm taller than the grinded surface.

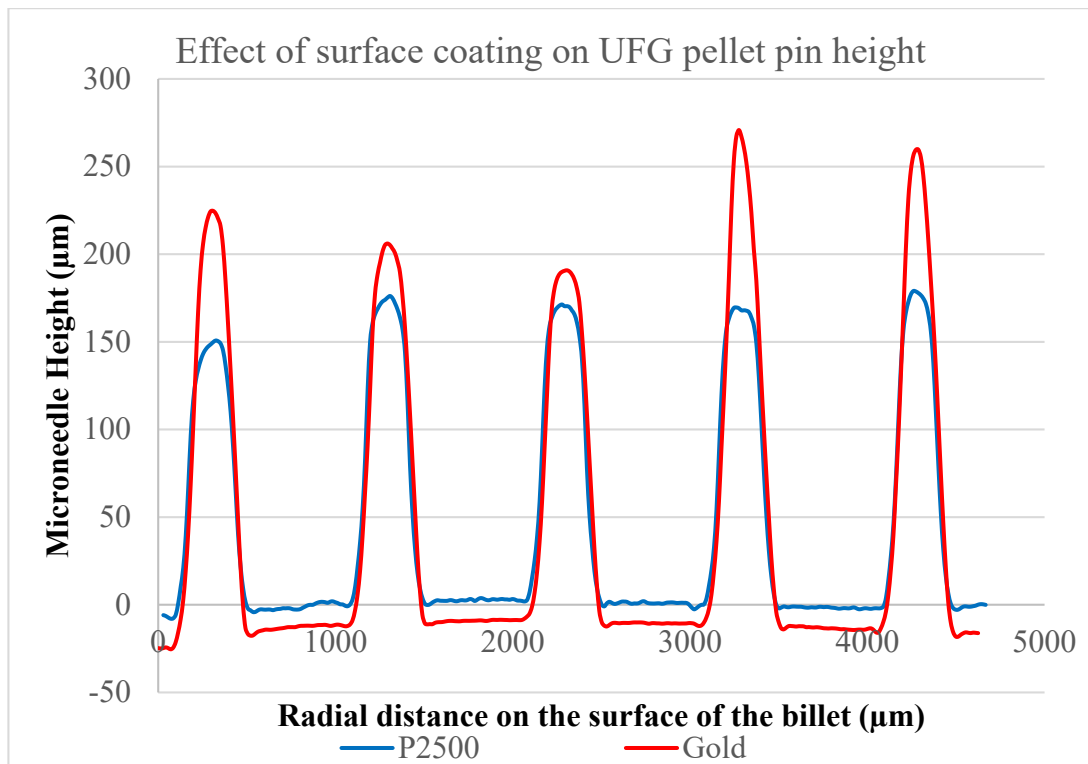


Figure 4.43: *Effect of using UFG billets. Surface conditions compared against the needle height distribution.*

4.4.9. Comparing the Gold Coating Surfaces against the Different Grain Size Billets

The effects of gold coating the billets was investigated. The gold coating layer was about 20 nano meters and was applied by the gold sputter technique described previously in material and methods section. A thick layer of gold could completely change the flow behaviour of the material.

Both grain sizes were used in the experiments and the results are shown in Figure 4.44. Using this coating resulted in the needle structures forming on the surface of the billets, as seen in Figure 4.45.

A section line was made along the middle of the billet and the surface shapes of the needles are presented in Figure 4.44. From Figure 4.45 it is evident that the needles are significantly taller than when grease was used. The needles also appear to be relatively uniform in height, with the inner needle being slightly shorter. One of the outer needles in both experiments appears to be shorter than the rest, suggesting there may have been debris lodged inside the cavity.

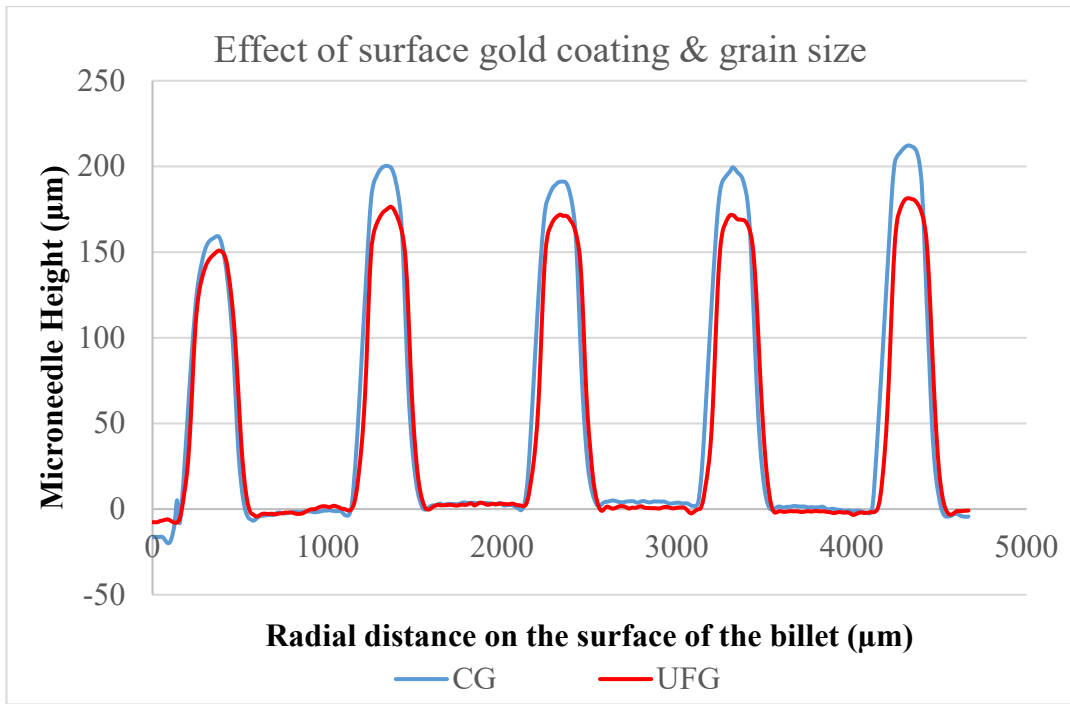


Figure 4.44: *Microneedle heights achieved when billets were coated in gold. Two grain sizes were investigated and compared.*

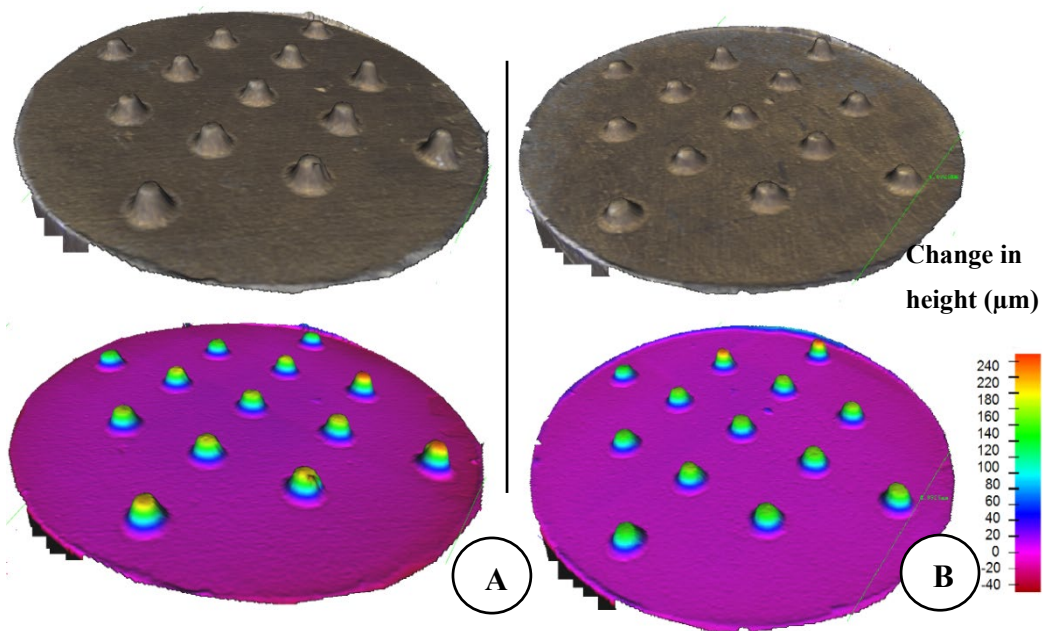


Figure 4.45: *The surface profile of gold coated microneedles on the billet. Two grain sizes compared. A- CG, B-UFG*

4.4.9.1. Application of Ultrasonic Oscillation on CG Billets

Ultrasonic oscillation was introduced to the backward extrusion forming process. For the ultrasonic experiments the ram displacement was reduced from 2mm to 1.8mm. The application of ultrasonic oscillations increased the height of all surface and lubrication conditions for CG billets. The results of the experiments are shown in Figure 4.46. The oscillation applied to the punch was about 10 microns therefore the total movement of the punch was 1.81mm, which is almost 10 percent less than the 2mm previously used.

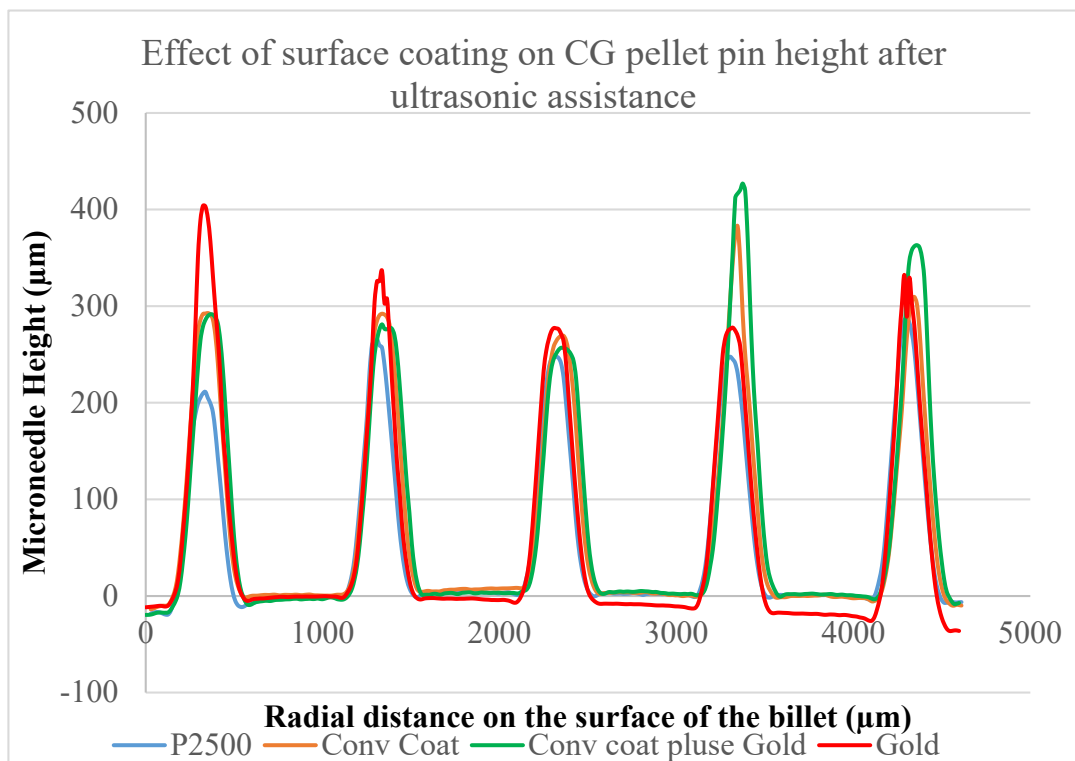


Figure 4.46: *Ultrasonic assisted backward extrusion of microneedles using CG billets with different surface conditions and lubricants.*

The billets with conversion coating plus gold and the billet with gold coating resulted in the tallest needles. The gold coating combined with ultrasonic oscillations produces tall needles but the oscillations seem to have resulted in tall outer needles and a shorter centre needle. The oscillations appear to have improved the flow-ability of gold coated billets. The needle with the P2500 grinding surface saw improvements when compared to when no ultrasonic oscillations were applied, but the needles were still shorter than the other billet surface conditions.

4.4.9.2. Application of Ultrasonic Oscillation on UFG Billets

Ultrasonic oscillation with the same characteristic as previously described were introduced to the backward extrusion forming process. The application of ultrasonic oscillations increased the height of all surface conditions for UFG billets. The results of the experiments are shown in Figure 4.47.

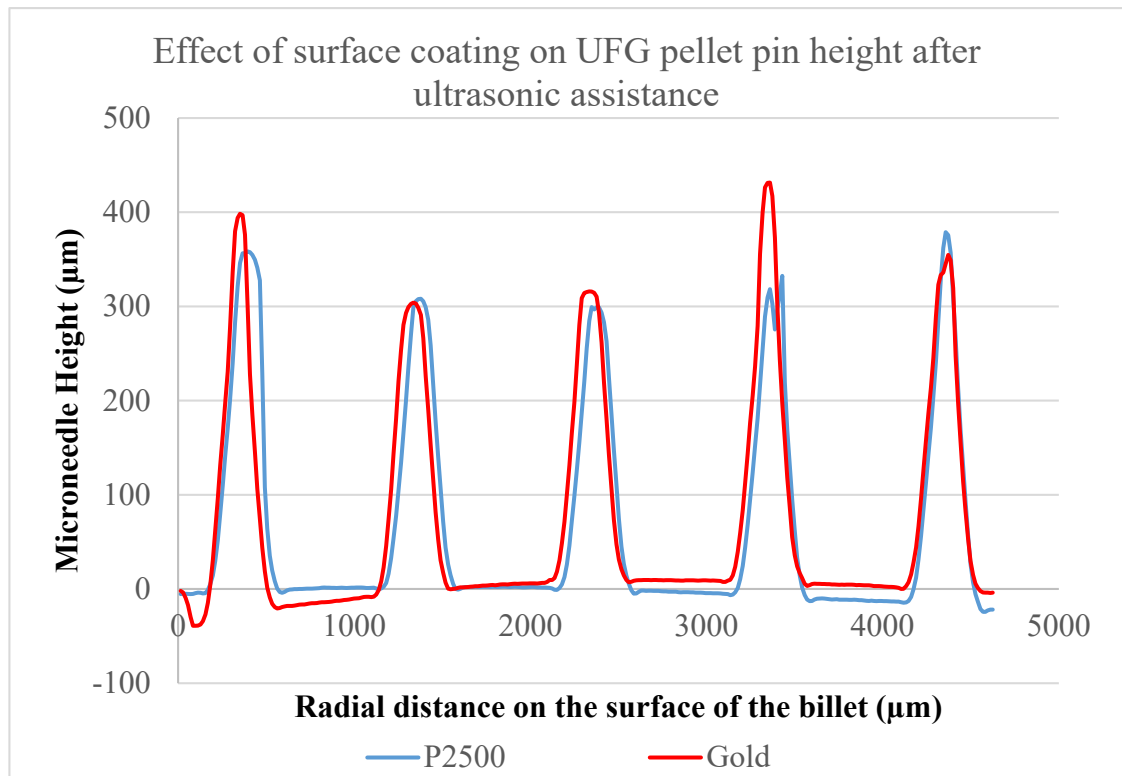


Figure 4.47: Ultrasonic assisted backward extrusion of microneedles using UFG billets with different surface conditions.

Once ultrasonic oscillations were introduced, the P2500 and the gold coated billet achieve very similar needle heights. The distribution of the heights also appears to be very similar.

4.4.10. Role of Ultrasonic assisted forming on needle height when billets with grain sizes are used

In the following subsections the needle height and the forming force will be examined.

4.4.10.1. Needle Height

The needle height for the microneedle experiments was recorded. A bar chart showing the average height of the needle of the different conditions used for these experiments has been presented in Figure 4.48. These conditions refer to Table 4.5. There are significant differences in the height of the needles when ultrasonic oscillation is added to the punch; all conditions experience an improvement in their average needle height. The surface of each billet was 3D scanned and the topography captured. The needle heights were measured from the base to the tip of the needle. For each condition five of the needles in a line through the centre of the billet were measured and an average was taken of those five measurements.

The factor that has the most significant effect on needle height improvement is the introduction of ultrasonic oscillations. Needle height increases by over 30 percent when oscillations are introduced in the backward extrusion microforming process.

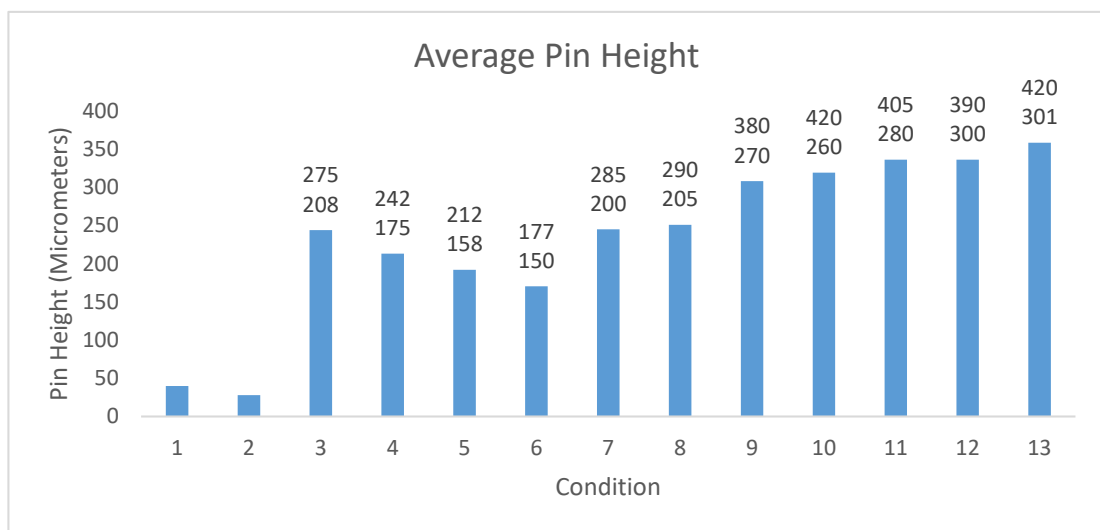


Figure 4.48: *Effect of ultrasonic oscillation assisted forming on needle height of CG and UFG billets. Bar chart showing average height. Top value showing tallest needle height, bottom value showing shortest needle.*

The effects of ultrasonic oscillation could be even more significant as all ultrasonic experiments were conducted with a ram displacement of 1.8mm whereas the non-oscillation tests were conducted with a ram displacement of 2mm. As previously explained the displacement of the ram was reduced to decrease the chances of tool breaking prior to experimentation completion.

Although not uniform, some of the needles that had been formed on the billet, that was used for ultrasonic assistance, gold coated UFG A11050 appeared very well formed and are presented in *Figure 4.49*. There is a significant difference in the forming force when ultrasonic oscillation is introduced in the backward extrusion micro forming process.

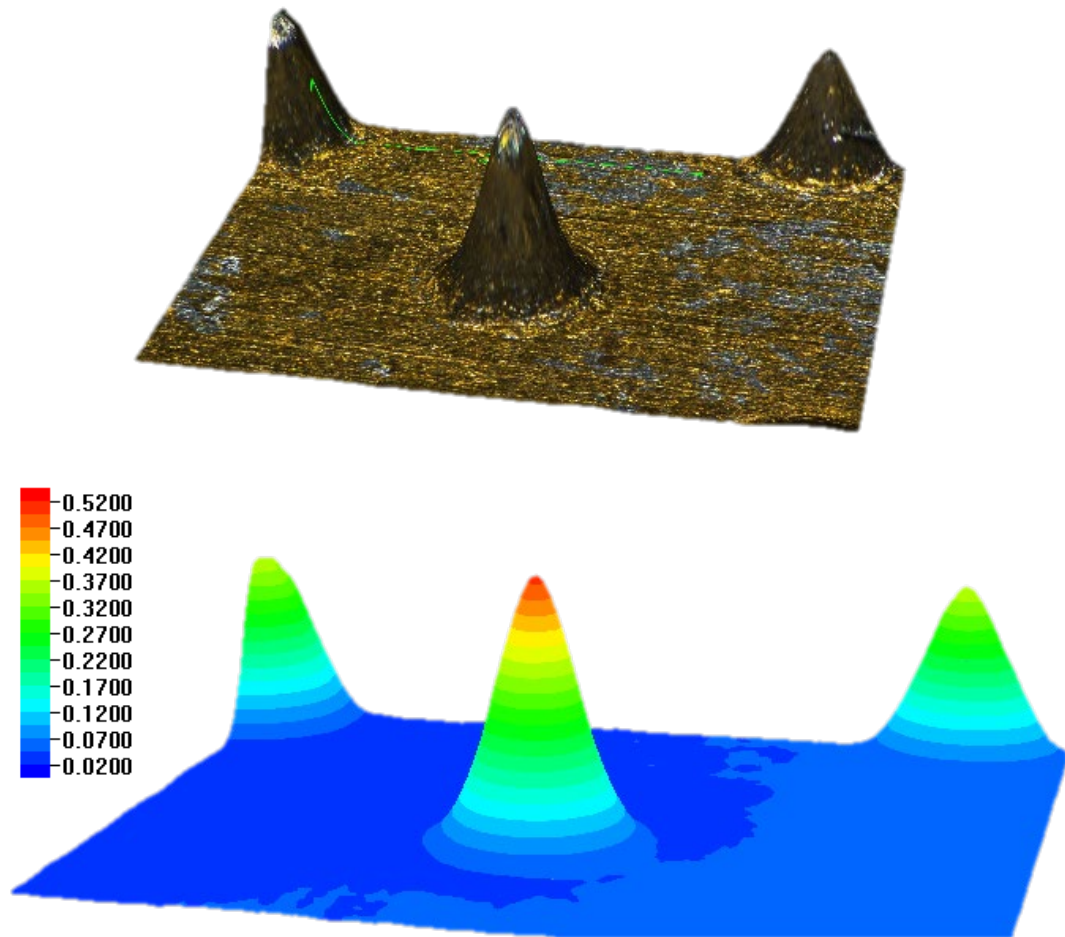


Figure 4.49: Formed microneedle.

4.4.10.2. Forming Force

The forming force for the microneedle experiments was recorded. There are three main factors that effect the force measured by the load cell.

First is the strength of the material, but in these experiments it appears this factor plays no significant role. Both CG and UFG A11050 register very similar forming force values during experimentation. This is predominantly because the features on the backward extrusion punch are very small and a good tolerance was achieved between the die orifice and the punch circumference. Once the die and punch close, the billet material has very little place to flow other than into the micro cavity. Therefore, what is being reported could possibly be the flex in the rig. There could also be some variation while conducting the experiments.

Secondly, it could be the application of ultrasonic oscillation. Examining the data it appears that the application of oscillations also plays little role in the forming force reported in this rig design. The material is surrounded by all sides and can only flow into the small cavity or into the small clearance space between the die and punch.

Thirdly, the displacement of the hydraulic ram. The biggest factor that affects this rig design and experiments was the reduction for the ram displacement. Reducing the ram displacement from 2mm to 1.8mm had a very significant reduction of force measured. A ten percent (10%) reduction in the travel of the ram resulted in a fifteen percent (15%) reduction in forming force.

4.4.11. Conclusion

A verity of surface and lubrication conditions have been examined for single pin backward extrusion in this section. Experimentally, the effects of lubrication, billet grain size and surface conditions have been compared against surface roughness, press forming force and pin height. Overall lubricants have been shown to improve the height of the pins but very smooth surfaces combined with lubricant see no improvement. As expected the forming forces for UFG material is significantly higher than CG billets.

The introduction of ultrasonic can have a big effect on the heights achieved. Ultrasonic assistance causes the lubrication to behave worse and in the MoS₂ condition the effect is very extreme and detrimental. As there is no through hole in the micro cavity punch design, grease and MoS₂ are not suitable for the microforming as they can easily get trapped in the microcavity which will stop material from flowing into the punch. Various surface conditions were examined in microforming and it was found that gold coated billets performed well. Using ultrasonic it is possible to vastly improve the needle height. Reducing the hydraulic ram displacement reduce the forming force required to produce an array of microneedles in one step backward extrusion. These conditions have resulted in the tallest, most even height distribution needles to be formed. A gold coated UFG billet with fully formed microneedles is presented in Figure 4.50.

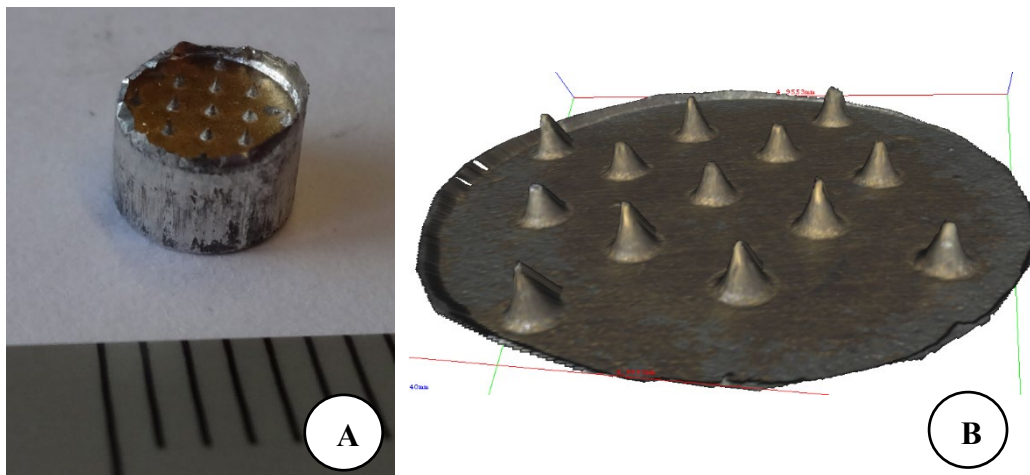


Figure 4.50: *Gold coated billet with fully formed microneedles.*
A- image with mm scale bar. B- scanned surface of the billet.

4.5. PART D: USING FEA IN ASSESSING BACKWARD EXTRUSION OF MULTIPLE MICRO-PINS

Using finite element (FE) analysis to simulate the micro-extrusion process of CG and UFG aluminium pins will allow several pin geometries, layouts, pin densities and lubrication conditions to be examined before a micro tool is produced. The findings of the simulations can be used to significantly reduce the numbers of iterations required to successfully produce micro pins in large numbers while improving pin height uniformity.

4.5.1. FE Model

QForm7.2 (QuantorForm Ltd) was used to carry out FE simulations described in this section. The extrusion process and the pin geometry examined are based on the findings of Rosochowska et al (Rosochowska et al. 2010). However, the single pin 2D model that Rosochowska et al. (2010) used in their investigation has been replaced by a multiple pin 3D model as shown in Figure 4.51. The billet Y, with 5mm diameter and 4mm height, is inserted in the bottom die Z. As the top punch X moves down, the billet's material flows backwards and fills the cavities in the top die. The geometry of individual cavities is also presented in Figure 4.51. Only one parameter was tested; the angle A could be either 90-5°, 90-10° or 90-15°. For the purpose of FE simulation all tools were assumed to be rigid. They were modelled in the Pro Engineer CAD software and imported into QForm.

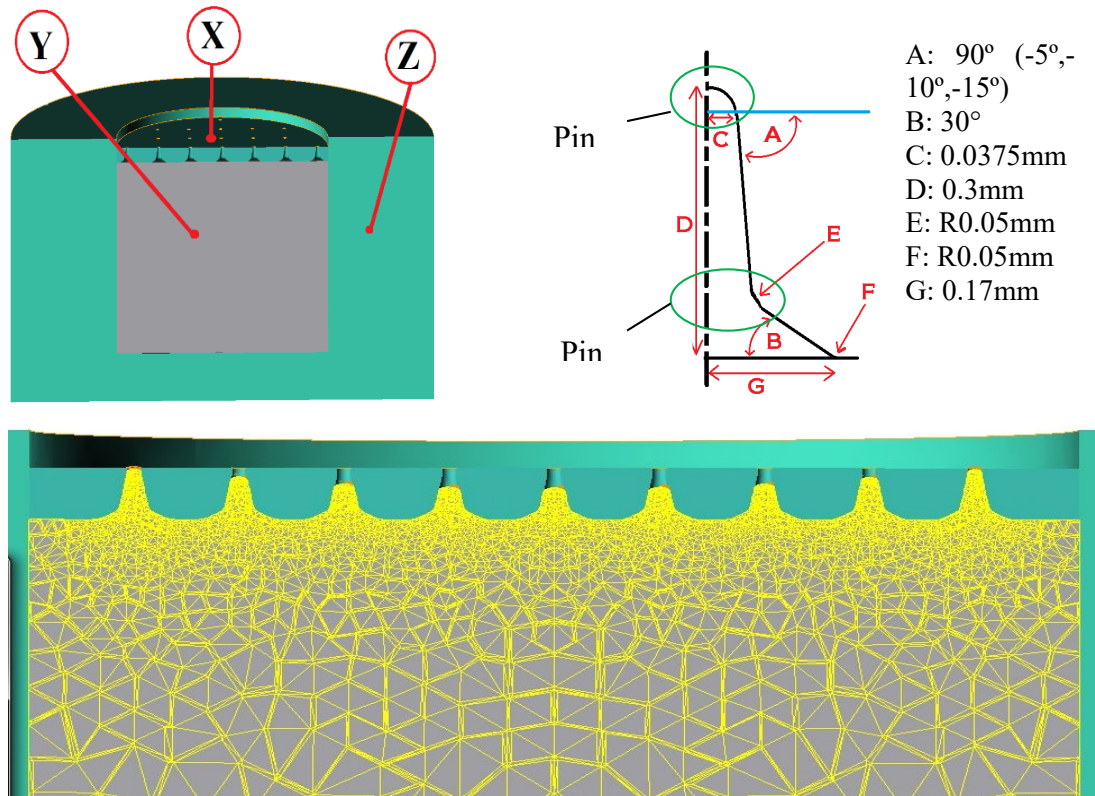


Figure 4.51: Top (Left): Process/tool configuration, Top (right) pin geometry and (Bottom) forming and adaptive meshing

One of the main advantages of using purpose built metal forming software is the built-in adaptive meshing. This type of meshing allows the number of elements to change with loading and forming conditions. This allows a coarse grain to be set initially and as the simulations progress and algorithm self-determines locations that require a finer mesh. In the bottom of Figure 4.51 it is possible to see that the region with micro pins has a finer mesh and the lower section has a larger mesh. This allow for faster and lower computational cost of the simulations.

One of the objectives of the FE simulation was to investigate the effects of pin layout and spacing on the material flow. The two layouts examined were based on a square array and a hexagonal array of pins; as illustrated in Figure 4.52. The difference between these two layouts is that each inner pin in the square array has 8 neighbouring pins at two different distances while in the hexagonal array one pin has 6 equidistant neighbours. The spacing of pins were 0.5mm, 0.75mm, 1mm and 1.5mm. The details of layouts and spacing are shown in Table 4.6. As can be seen from this table, the

hexagonal arrangement results in a greater concentration of pins on a round surface of the billet. However, this is only the case for the distance of 0.5mm and 0.75mm. For larger distances, this effect is reversed.

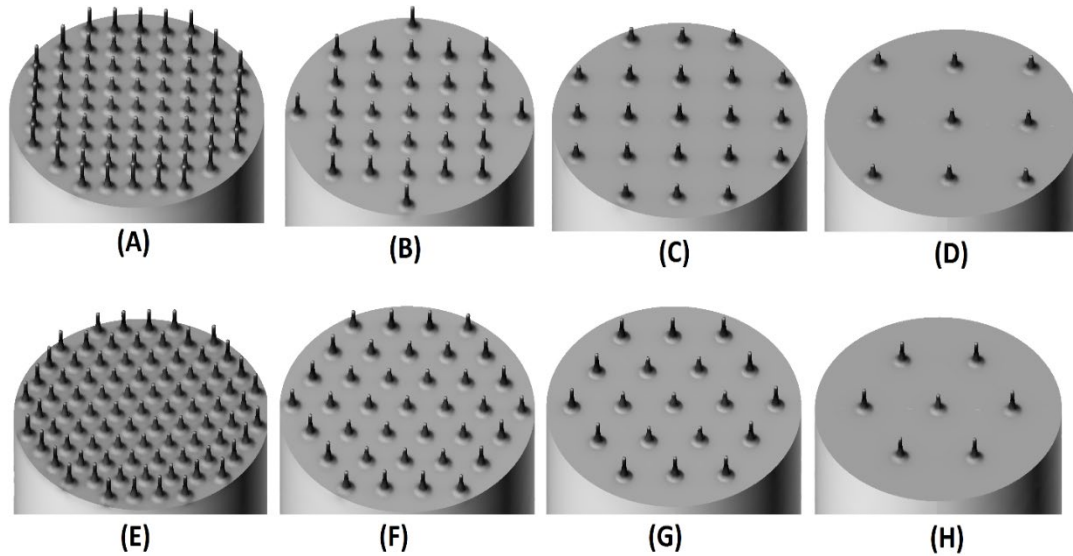


Figure 4.52: *A-D pins arranged in a square array. E-H pins arranged in a hexagonal array.*

The material used for the simulation was A11050. The simulation did not attempt to take into account deformation of individual grains but used the classical FE approach based on a phenomenological constitutive model describing a homogeneous polycrystalline material. The flow stress data for the CG material were already available in the QForm material library while the flow stress data for the UFG material were taken from Rosochowski et al (Rosochowski et al. 2006). Adaptive meshing with an adaptation factor of 1.5 was used to capture the required detail for the simulations. Most other settings were left as the default values.

Table 4.6: *Details of the micro pin layouts shown in Figure 4.52.*

Image	Layout	Spacing [mm]	Number of pins
A	Square Array	0.5	69
B	Square Array	0.75	29
C	Square Array	1	21
D	Square Array	1.5	9
E	Hexagonal Array	0.5	85
F	Hexagonal Array	0.75	37
G	Hexagonal Array	1	19
H	Hexagonal Array	1.5	7

Friction plays a significant role in micro forming. As well as having an effect on the forming force it also has an effect on the surface finish that can be achieved on the component and the ease of part removal once the forming process has been completed. The three friction conditions that were examined assumed friction factor equal to 0 (frictionless condition), 0.15 (lubrication using mineral oil) and 0.8 (dry condition).

4.5.2. Results

4.5.2.1. PIN Geometry

The forces required for micro forming are usually small and pose no challenge for conventional forming equipment. The knowledge of the forming force can show other issues that could arise. To show the effects of changing the pin angle $90^\circ - A$, the pin cavity was increased by a factor of ten to accentuate the differences in loading requirements (Figure 4.53); the same simulations were also conducted for a micro pin resulting in similar results. As expected, before the material reaches the waist of the cavity (Figure 4.51), the force for the three pin geometries is identical.

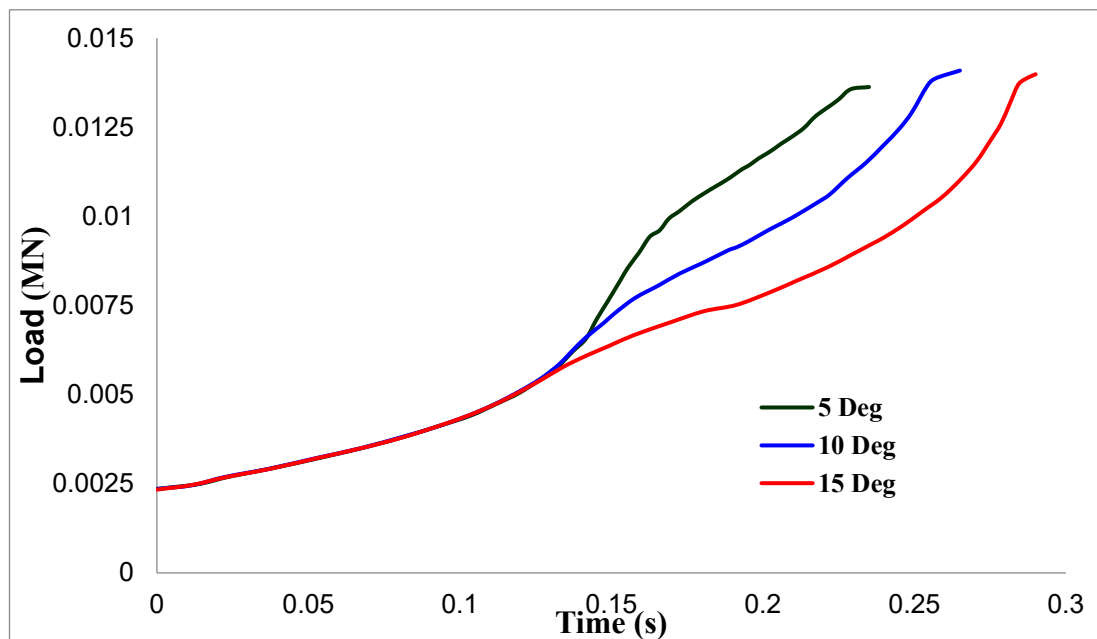


Figure 4.53: Effect of the pin angle $90^\circ - A$ on the extrusion load required to form a scaled-up single CG Al1050 pin friction condition used for simulations friction factor 0.15.

As soon as the material starts flowing into the cavity above the waist, the force becomes different, with the highest force observed for the pin angle of 5° . The

geometry that was chosen to be taken forward for the following simulations was the conical pin with an angle of 10°.

4.5.2.2. Friction

Friction plays a critical role in terms of the forming force as well as the formability of the pins. To analyse these effects, extrusion of a square array of micro pins with 0.5mm pin spacing was simulated. The material used was UFG Al1050. It is seen in Figure 4.54 that for friction factor of 0.8 (no lubrication), the load required to form the pins is 100% higher than when no friction exists. It is possible to simulate conditions without friction but these are unrealistic and cannot be applied to the real world conditions. Thus a friction factor of 0.15 (lubrication with oil) was also tested showing that the load can be substantially reduced compared to the case without lubrication.

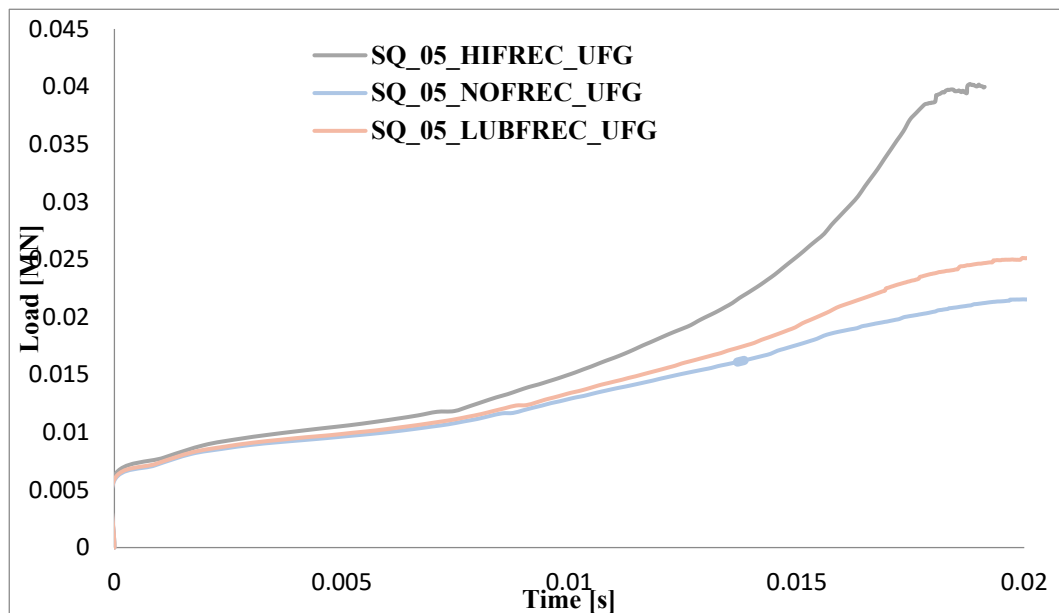


Figure 4.54: The effect of friction conditions on the load required to extrude a square (SQ) array of UFG Al1050 pins with spacing of 0.5mm.

4.5.2.3. PIN Density and Central PIN Removal

From early investigative simulations it became apparent that increasing the number of pins resulted in a reduction in the uniformity of the pin heights. To achieve a more uniform height throughout the pins, the centre pin was removed and the simulations carried out again. In both layouts the removal of the central pin resulted in a more uniform height being achieved throughout all the pins. This is shown in Figure 4.55 where the more uniform height distribution in cases B and D can be seen as uniform

distribution of the green colour in the pin array indicating the same strain. In the cases A and C, the outer pins are yellow in colour, which means that they have been deformed more than the inner pins.

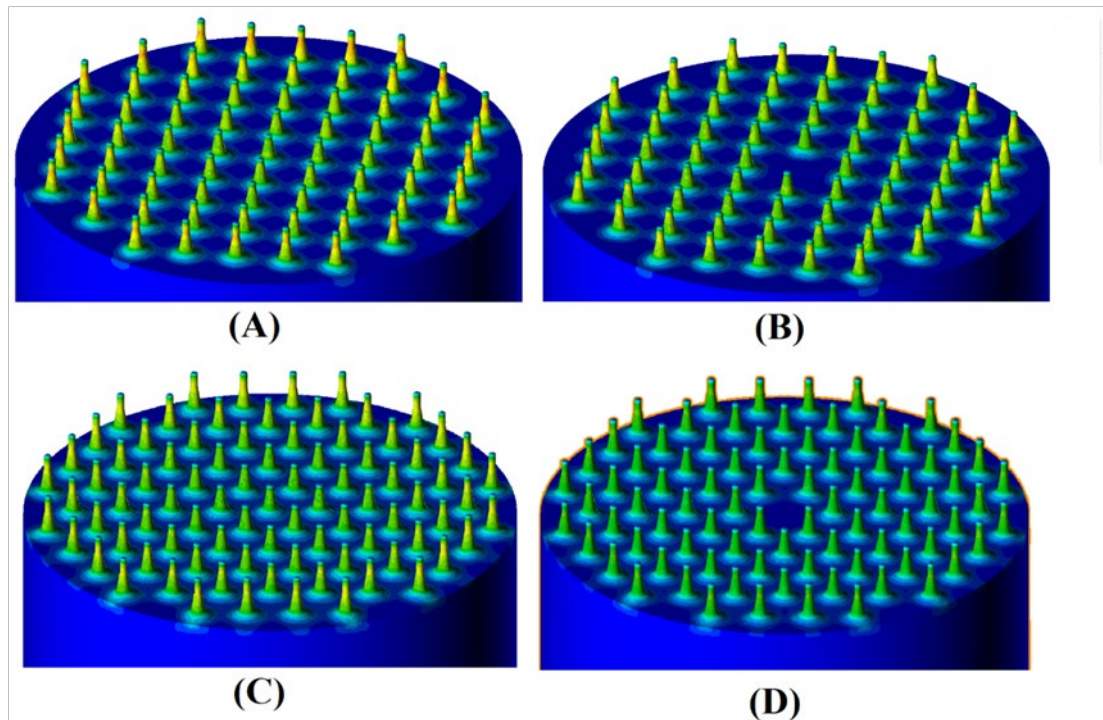


Figure 4.55: Removing the central pin in a 0.5mm spaced square array (case A-B) and 0.5mm spaced hexagonal array (C-D). Backward extruded micro pins on Al1050 billet.

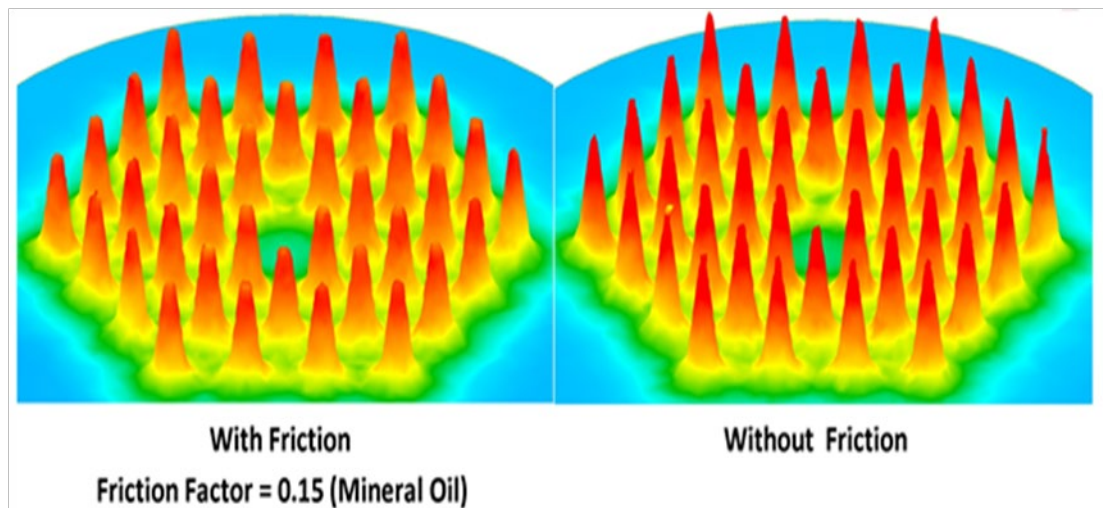


Figure 4.56: The effect of friction conditions on formability of CG Al1050 pins laid out in a hexagonal array without a central pin with a spacing of 0.75mm.

To examine the effect of lubrication on the pin height, extrusion of a hexagonal array of micro pins with 0.75mm pin spacing and a missing central pin was simulated. The

material used was CG Al1050. To compare the pin heights, the simulations were stopped when the forming force reached 20kN (Figure 4.56). Without friction the pins are taller but less uniform in height.

The issue of pin height uniformity will be discussed later in this section. The effect of pin density and central pin removal on the extrusion load was also examined and the findings are presented in Figure 4.57. The simulations were stopped when the centrally located pins achieved the height of 0.3mm. This obviously occurs earlier for less dense arrays as less material needs to be extruded from the billet into a smaller number of pins. The difference between cases with and without a central pin is minimal. The number of pins does not have a significant effect on the final load required to form the pins; in Figure 4.57 all the pins are fully formed between loads of 22kN and 24.5kN. However, there is a slight tendency for higher density of pins to require a lower final extrusion load.

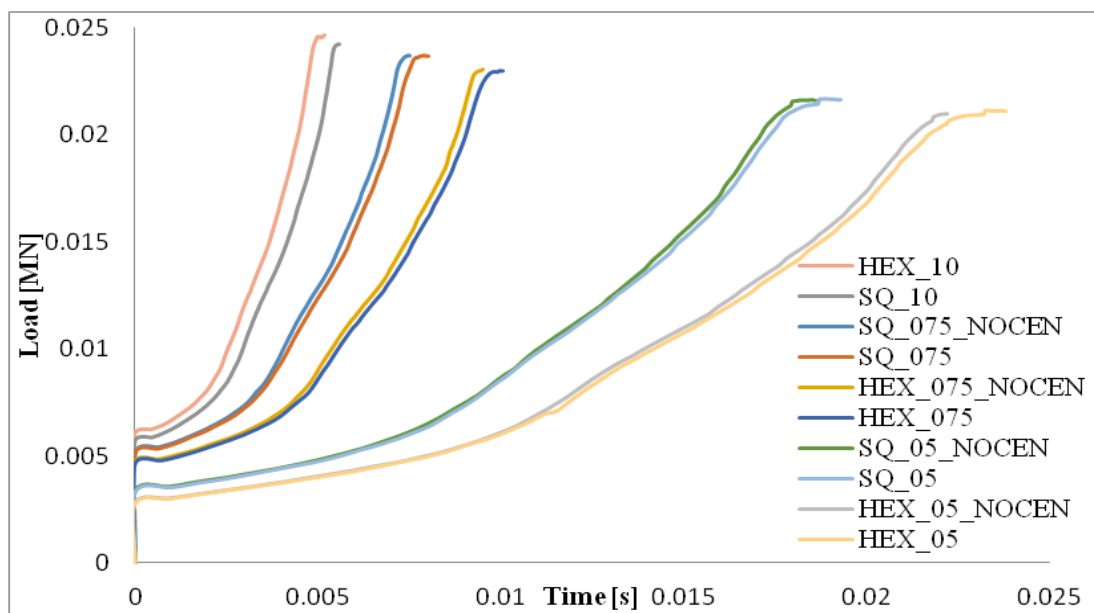


Figure 4.57: *Effect of pin density and central pin removal in square (SQ) and hexagonal (HEX) pin arrays on the extrusion load for CG Al1050*

4.5.2.4. Grain Size

It is known that UFG metals have higher yield strength compared to their CG counterparts so they require a larger forming load to produce the same component. This is also shown in the results of the simulations presented in Figure 4.58, where different grain sizes were accounted for by using different flow curves. The

comparison is possible because all simulations were stopped when the centre pins achieved a height of 0.3mm.

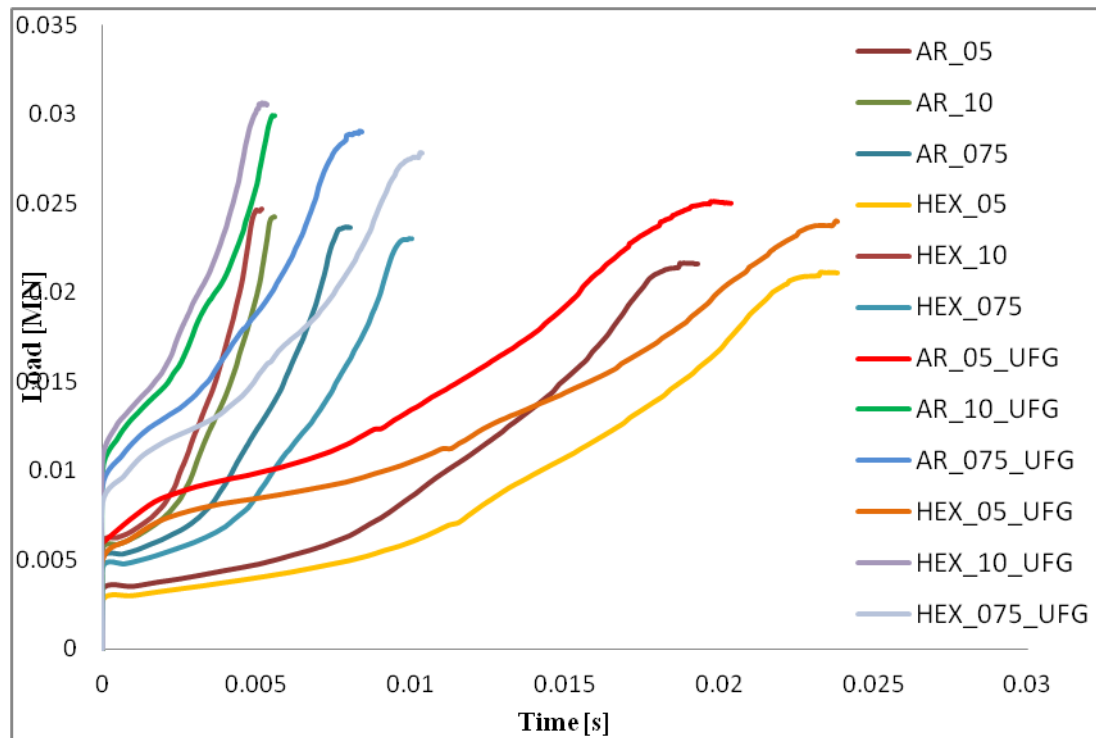


Figure 4.58: Comparing the effects of grain size on the forming load for different pin density and layout on Al1050 billet friction condition used for simulations friction factor 0.15.

When performing these simulations, the effects of physical size of the grain was not entered into the simulation parameters; the material behavioural data was used. This is a very important point to note, as size effects can play a significant role in the shaping of these small pins. As discussed previously the larger grains require a smaller force to deform on the macro scale. These larger grains may undergo fragmentation or refinement to form smaller grains as the forming continues. This behaviour was not taken into account for the simulations.

4.5.2.5. Pin Height Uniformity

Pin height uniformity is critical and can tell us a lot about the material flow characteristics into the pin cavities. The cross-sectional view of the billet centre allows measuring height of the pins and comparing forming of the central pin to that of the outer pins.

In Figure 4.59, it is possible to visually compare the effects of changing friction conditions, grain size and central pin removal on the height uniformity of the pins at the end of the extrusion process marked by the central pin achieving a height of 0.3mm.

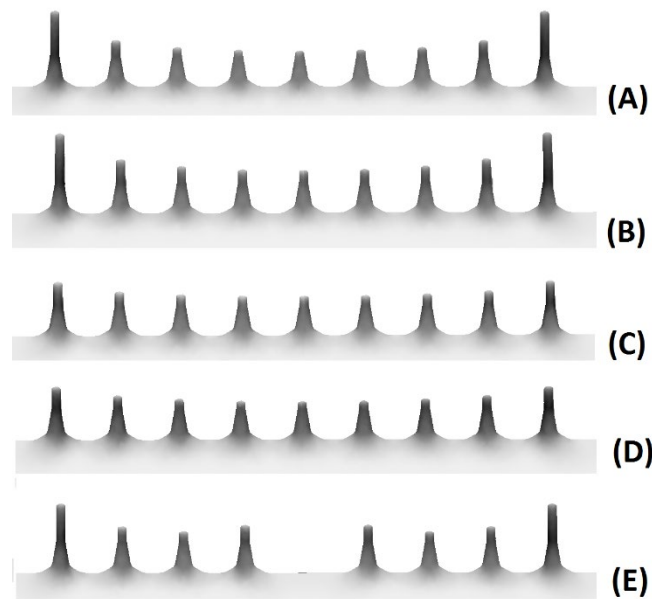


Figure 4.59: *Cross-sections through the centre of a billet extruded into a square array of 0.5mm spaced micro pins. A) UFG in frictionless conditions, B) UFG with friction factor = 0.15, C) CG with friction factor = 0.15, D) UFG with friction factor = 0.8, E) UFG with friction factor = 0.15 and central pin removed.*

When comparing cases, A, B and D (UFG material with different friction conditions), it is possible to see that friction plays a significant role in achieving uniform pin height. The outer pin in condition A has reached a height of 0.55mm while the centre pin is 0.3mm. Increased friction is not letting the material to slip outwards and start filling the outmost pin cavities before starting to fill the central pin cavity. When comparing cases B and C (UFG vs. CG material) it is also possible to see that using CG material will result in a more uniform pin height. This is assuming that CG material behaves as a polycrystalline material and not as an agglomeration of few grains. In real life, this may not be the case. Conditions for case B and E are identical but the central pin cavity in case E has been removed from the simulation. This has a significant effect on the surrounding pins. The central pins are now slightly taller than the surrounding pins and the outer pins are shorter which results in a more uniform overall pin height.

Case B was examined more closely to determine the reason for taller outer pins. The process was examined when the central outer pins had reached a height of 0.3mm. This is shown in Figure 4.60.

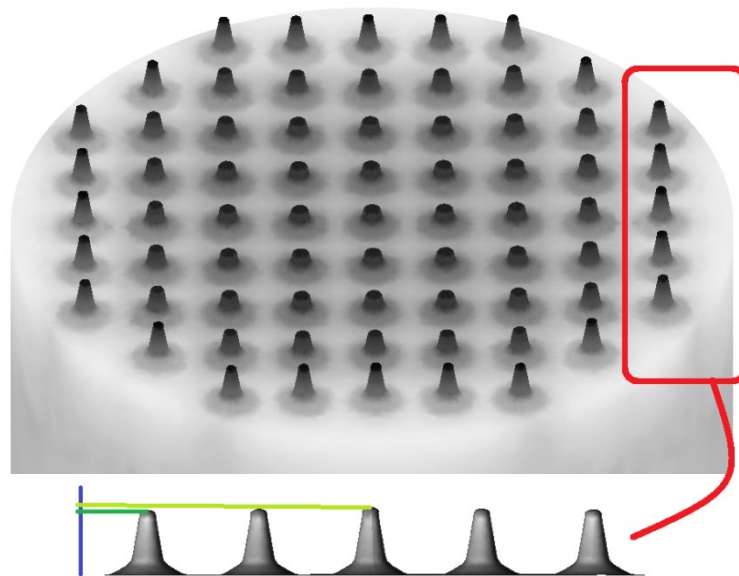


Figure 4.60: *UFG material formed into an array of micro pins using lubrication (friction factor = 0.15); process was stopped when the central outer pin reached a height of 0.3mm.*

While the outer pins have almost reached a height of 0.3mm the central pins can be seen to be significantly shorter and under-formed. Looking collectively at Figures 4.28, 4.29, 4.30 and 4.31 it is possible to determine that shortage of central pins can be a result of competing neighbouring pins. Material starvation in the central pin results in height differences that can be seen while moving towards the perimeter of the billet. Due to the array layout it is possible to see in Figure 4.60 that the central outer pins will have the largest amount of material and will not have competing neighbours on one side, therefore, it could be expected that they would be taller. This theory seems to be backed by the findings at the bottom of Figure 4.60, the central outer pin is slightly taller than the other outer pins.

4.5.3. Conclusions

When considering backward extrusion as the forming method for micro pins, it is important to understand the effects of pin geometry, friction, layout and grain structure

and size effects on the final product. From the FE simulations it is possible to arrive at several conclusions. These are:

- 1) Larger pin angles result in reduced forming forces, therefore, 10° or 15° pin angle should be used rather than 5°. Larger pin angles will also facilitate pin removal from the top die.
- 2) Reducing friction results in reduced forming forces. But the FEM analysis confirmed that the increase in friction lead to achieve uniform pin heights. This could be due to reaction forces offered die walls to the deformation mater and that makes the material to pass quickly through the holes in the punch. As the punch moves downwards the billet of material tried to flow in the direction of least resistance, therefore, it moves outwards. If the clearance between the die and billet is not minimized, then the billet material will flatten rather than undergoing the backward extrusion. Therefore, the billet and die must have a tight fit.
- 3) It is also critical that the billets are of identical uniform heights and diameters. Since the punch displacement, required to produce the pins, is less than a few millimetres then any shape distortions or irregularities will have significant adverse effects on the height and uniformity of the pins.
- 4) For smaller pin distances, arranging pin cavities in an equidistant hexagonal array will result in a greater number of pins being fitted onto the cylindrical billet compared to arranging them in a square array.
- 5) Larger pin angels increase the volume of material required to produce each pin, therefore, a greater punch displacement would be required.
- 6) The increasing number of pins increases the time required to fill the pin cavities through the increasing total volume of pins. Higher number of pins slightly decreases the final force required to produce the pins.

- 7) Competing neighboring pins can starve central pins and reduce material flow into the centrally located pins. Therefore, removing the center pin in a dense layout results in improved uniformity of pin heights throughout the billet.
- 8) Based on the lower flow stress for CG material compared to UFG material, it is possible to achieve more uniform pin heights for CG material. Although these simulations showed CG to be a better candidate for the backward extrusion of micro pins, it is important to note that actual grain size behavioral information was not taken into consideration, therefore, the model was simplified. Actual real forming behavior may be different. Note that grain size was not considered as parameter while doing FEM analysis.

Using FE analysis, it was possible to investigate and analyse a wide variety of variables at very little cost. The findings from the FE analysis will be invaluable to furthering the understanding of the backwards extrusion process and material flow behaviour in micro components. These findings will be used to further refine the layout and size of the micro pins prior to punch fabrication.

The fabrication of the shapes and densities explored in this study may poses their own challenges, therefore, manufacturing processes need to be examined for their suitability in producing the required backwards extrusion punch.

5. FINAL CONCLUSIONS AND RECOMMENDATIONS FOR FUTURE WORKS

5.1. CONCLUSIONS

After a literature review was conducted it was identified that metal microneedles could be the ideal candidate for transdermal drug delivery. An investigation was conducted examining the various components and techniques required to produce a rig that was capable of producing metal micro needles. New rig, virtual instruments and punches were designed and created. Ultra fine grain material was identified as a material that could be used in this process but not supply of this material was available therefore UFG Al1050 was created using the Incremental ECAP process. IECAP was used to process billets to produce UFG aluminium billets for future experiments. Two different channel and punch configurations were used. It was found that $\phi=90^\circ$ resulted in more shear and greater hardness so this was taken forward for more passes. Compared to $\phi=120^\circ$. Although it has been proven that both configurations can refine grains, the $\phi=90^\circ$ configuration showed the smallest and most uniform grain, highest and most homogenise hardness for Al1050, therefore, this configuration will be used to carry out further passes of the IECAP process to refine the grain.

Part processed billets were then prepared and examined through the flow plain. The flow plain micro hardness analysis clearly showed the difference between the processed section and the unprocessed section. The shear zone was also clear to see. The hardness study showed that the first pass resulted in the greatest increase in hardness and the following passes had a more gradual increase effect on the hardness.

Tensile tests were also carried out on micro specimens to further investigate the mechanical properties of the material. The findings of the tensile testing is in line with all the other findings and shows the increased ultimate tensile strength of the material even just after the first pass. The subsequent passes increase the ultimate tensile strength of the material but the increase are more gradual. Pass 6 and 8 saw very little differences.

FE simulation was conducted to investigate the shape and distribution of the needles. It was found that having the needles too close resulted in short central needles and

longer outer needles in the backward extrusion process. Competing neighbouring pins can starve central pins and reduce material flow into the centrally located pins. Therefore, removing the centre pin in a dense layout results in improved uniformity of pin heights throughout the billet.

Friction also seemed to play an important role in the height distribution of the needles. Reducing friction results in reduced forming forces while increasing friction results in more uniform pin heights. This is possibly due to the surface material not being allowed to slip to the outer perimeter of the billet and accelerate the outer pin forming. As the punch moves downwards the billet of material tried to flow in the direction of least resistance therefore it moves outwards. Due to the use of backward extrusion a tight tolerance between the punch perimeter and die orifice is crucial. If the tight tolerance is not maintained, then the billet material starts flowing in the space between the die and punch rather than through cavities in the punch.

Experiments were then conducted to examine the findings of the FE simulations. A variety of surface and lubrication conditions were examined for single pin and multi microneedle backward extrusion. Experimentally, the effects of lubrication, billet grain size and surface condition have been compared against surface roughness, press forming force and pin height. Overall lubricants have been shown to improve the height of the pins but very smooth surfaces combined with lubricant see no improvement. As expected the forming forces for UFG material is significantly higher than CG billets. But one good advantage is the tips of the needles formed from UFG material will be strong enough to retain its sharpness without breaking during incision and removal.

The introduction of ultrasonic can have a big effect on the heights achieved. Ultrasonic assistance causes the lubrication to behave worse and in the MoS₂ condition the effect is very extreme and detrimental. It was found that gold coated billets performed well. Using ultrasonic it is possible to vastly improve the needle height and to reduce the forming force required to produce an array of microneedles in one step backward extrusion.

5.2. RECOMMENDATIONS FOR FUTURE WORKS

The test condition that resulted in the best microneedles was when gold was used as a lubricant, UFG Al1050 was used, with a punch speed of 0.1mm/s for a displacement of 1.8mm with the punch oscillating at 20kHz with an amplitude of 10µm. For this specific rig and this shape of conical micro cavity array, these parameters performed well. I would recommend starting with a new rig design with stiffer elements. A new set of experiments would have to be conducted following on from the learning outcomes of this study.

To further improve on this body of work it is necessary to investigate the microstructure of the formed pins and needles. By analysing these microstructures, it will be possible to fully understand the effects of grain size and ultrasonic oscillation.

This investigation started as a medical device for increasing transdermal drug delivery, therefore, it would be necessary to examine the effectiveness of these needles for drug delivery. The needles that have been produced in this study could be used solid microneedles or coated microneedles as shown in Figure 2.3, therefore no through hole required.

Aluminium is not known for its biocompatibility properties, therefore, materials such as stainless steel or titanium should be investigated for real world applications. These materials are significantly stronger than Al1050 that was used for this study. Hence, a total new rig and punch would have to be designed that is capable of withstanding the additional forming load exertion. A larger working area and more needles would also have to be produced to make this a viable drug delivery product. Additional studies can be made to examine the influence of die wall as the surface of the work piece after micro extrusion starts to become convex.

APPENDIX A:

REFERENCES

- Akhmadeev, N. et al., 1992. Formation of submicro grain-structure in copper and nickel by extensive shear deformation. *Russian Metallurgy*, 5, pp.86–91.
- Alfrey, A.C., 1993. Aluminum and Renal Disease. In E. Bourke, N. . Mallick, & V. . Pollak, eds. *Moving points in nephrology*. pp. 110–124. Available at: <https://www.karger.com/Article/FullText/421918>.
- Ali, W.G. & Nagib, G., 2011. Embedded Control Design for Insulin Pump. *Advanced Materials Research*, 201–203, pp.2399–2404. Available at: <http://www.scientific.net/AMR.201-203.2399>.
- Amsden, B.G. & Goosen, M.F.A., 1995. Transdermal delivery of peptide and protein drugs: An overview. *AIChE Journal*, 41(8), pp.1972–1997. Available at: <http://doi.wiley.com/10.1002/aic.690410814>.
- Anderson, R.L. & Cassidy, J.M., 1973. Variation in physical dimensions and chemical composition of human stratum corneum. *The Journal of investigative dermatology*, 61(1), pp.30–2. Available at: <http://www.ncbi.nlm.nih.gov/pubmed/4718753>.
- Antony, J.P. et al., 1994. Antiwear/extreme pressure performance of graphite and molybdenum disulphide combinations in lubricating greases. *Wear*, 174(1–2), pp.33–37. Available at: [https://doi.org/10.1016/0043-1648\(94\)90083-3](https://doi.org/10.1016/0043-1648(94)90083-3).
- Arnou, R. et al., 2011. Willingness to vaccinate or get vaccinated with an intradermal seasonal influenza vaccine: a survey of general practitioners and the general public in France and Germany. *Advances in Therapy*, 28(7), pp.555–565. Available at: <http://link.springer.com/10.1007/s12325-011-0035-z>.
- Arora, A. et al., 2007. Needle-free delivery of macromolecules across the skin by nanoliter-volume pulsed microjets. *Proceedings of the National Academy of Sciences of the United States of America*, 104(11), pp.4255–60. Available at: <http://www.pnas.org/cgi/doi/10.1073/pnas.0700182104>.
- Arora, A., Prausnitz, M.R. & Mitragotri, S., 2008. Micro-scale devices for transdermal drug delivery. *International Journal of Pharmaceutics*, 364(2), pp.227–236.
- Ashraf, M.W. et al., 2010. Structural and microfluidic analysis of MEMS based out-of-plane hollow silicon microneedle array for drug delivery. *2010 IEEE International Conference on Automation Science and Engineering, CASE 2010*, pp.258–262.
- Baker, G.S. & Carpenter, S.H., 1967. Dislocation mobility and motion under combined stresses. *Journal of Applied Physics*, 38(4), pp.1586–1591.

- Bal, S.M. et al., 2008. In vivo assessment of safety of microneedle arrays in human skin. *European Journal of Pharmaceutical Sciences*, 35(3), pp.193–202. Available at: <http://linkinghub.elsevier.com/retrieve/pii/S0928098708003035>.
- Banga, A.K., Bose, S. & Ghosh, T.K., 1999. Iontophoresis and electroporation: comparisons and contrasts. *International Journal of Pharmaceutics*, 179(1), pp.1–19. Available at: <http://linkinghub.elsevier.com/retrieve/pii/S0378517398003603>.
- Banga, A.K. & Prausnitz, M.R., 1998. Assessing the potential of skin electroporation for the delivery of protein- and gene-based drugs. *Trends in Biotechnology*, 16(10), pp.408–412.
- Banks, S. et al., 2011. Diclofenac Enables Prolonged Delivery of Naltrexone Through Microneedle-Treated Skin. *Pharmaceutical Research*, 28(5), pp.1211–1219. Available at: <http://link.springer.com/10.1007/s11095-011-0372-2>.
- Banks, S.L., Stinchcomb, A.L. & Paudel, K.S., 2011. Microneedle-Assisted Transdermal Delivery of Opioid Antagonists for the Treatment of Alcoholism. In Dr. Chris Rundfeldt, ed. *Drug Development - A Case Study Based Insight into Modern Strategies*. Intech, pp. 525–543. Available at: <http://www.intechopen.com/books/drug-development-a-case-study-based-insight-into-modern-strategies/microneedle-assisted-transdermal-delivery-of-opioid-antagonists-for-the-treatment-of-alcoholism>.
- Barry, B.W., 1983. Dermatological formulations: Percutaneous absorption. *New York: Marcel Dekker*, p.480.
- Barry, B.W., 2001. Novel mechanisms and devices to enable successful transdermal drug delivery. *European Journal of Pharmaceutical Sciences*, 14(2), pp.101–114.
- Bay, N., 1994. The state of the art in cold forging lubrication. *Journal of Materials Processing Technology*, 46(1–2), pp.19–40. Available at: <https://www.sciencedirect.com/science/article/pii/0924013694901007>.
- Benet, L.Z. et al., 1996. Intestinal drug metabolism and antitransport processes: A potential paradigm shift in oral drug delivery. *Journal of Controlled Release*, 39(2–3), pp.139–143. Available at: <http://linkinghub.elsevier.com/retrieve/pii/0168365995001476>.
- Berthon, G., 2002. Aluminium speciation in relation to aluminium bioavailability, metabolism and toxicity. *Coordination Chemistry Reviews*, 228(2), pp.319–341. Available at: <http://linkinghub.elsevier.com/retrieve/pii/S0010854502000218>.
- Birchall, J. et al., 2006. Cutaneous gene expression of plasmid DNA in excised human skin following delivery via microchannels created by radio frequency ablation. *International Journal of Pharmaceutics*, 312(1–2), pp.15–23. Available at: <http://linkinghub.elsevier.com/retrieve/pii/S0378517305008513>.
- Birchall, J.C. et al., 2011. Microneedles in Clinical Practice—An Exploratory Study

Into the Opinions of Healthcare Professionals and the Public. *Pharmaceutical Research*, 28(1), pp.95–106. Available at: <http://link.springer.com/10.1007/s11095-010-0101-2>.

- Blaha, F. & Langenecker, B., 1955. Tensile deformation of zinc crystal under ultrasonic vibration. *Naturwissenschaften*, 42(556), p.0.
- Bommaman, D. et al., 1992. Sonophoresis. I. The Use of High-Frequency Ultrasound to Enhance Transdermal Drug Delivery. *Pharmaceutical Research*, 09(4), pp.559–564. Available at: <http://link.springer.com/10.1023/A:1015808917491>.
- Bos, J.D. & Meinardi, M.M.H.M., 2000. The 500 Dalton rule for the skin penetration of chemical compounds and drugs. *Experimental Dermatology*, 9(3), pp.165–169. Available at: <http://doi.wiley.com/10.1034/j.1600-0625.2000.009003165.x>.
- Bowen, J.R. et al., 2000. Analysis of the billet deformation behaviour in equal channel angular extrusion. *Materials Science and Engineering: A*, 287(1), pp.87–99. Available at: <http://linkinghub.elsevier.com/retrieve/pii/S0921509300008340>.
- Bramson, J. et al., 2003. Enabling topical immunization via microporation: a novel method for pain-free and needle-free delivery of adenovirus-based vaccines. *Gene therapy*, 10(3), pp.251–60. Available at: <http://www.ncbi.nlm.nih.gov/pubmed/12571633>.
- Brown, M.B. et al., 2006. Dermal and Transdermal Drug Delivery Systems: Current and Future Prospects. *Drug Delivery*, 13(3), pp.175–187. Available at: <http://www.tandfonline.com/doi/full/10.1080/10717540500455975>.
- Bundgaard, H., 1992. The utility of the prodrug approach to improve peptide absorption. *Journal of Controlled Release*, 21(1–3), pp.63–72. Available at: <http://linkinghub.elsevier.com/retrieve/pii/016836599290008F>.
- Bunget, C. & Ngaile, G., 2011. Influence of ultrasonic vibration on micro-extrusion. *Ultrasonics*, 51(5), pp.606–616.
- Bunget, C.J., 2006. *Microforming and Ultrasonic Forming*. North Carolina State University. Available at: <http://repository.lib.ncsu.edu/ir/handle/1840.16/966>.
- Burnette, R.R. & Ongpipattanakul, B., 1988. Characterization of the Pore Transport Properties and Tissue Alteration of Excised Human Skin during Iontophoresis. *Journal of Pharmaceutical Sciences*, 77(2), pp.132–137. Available at: <http://linkinghub.elsevier.com/retrieve/pii/S0022354915476294>.
- Burton, S.A. et al., 2011. Rapid Intradermal Delivery of Liquid Formulations Using a Hollow Microstructured Array. *Pharmaceutical Research*, 28(1), pp.31–40. Available at: <http://link.springer.com/10.1007/s11095-010-0177-8>.
- Bystrova, S. & Luttge, R., 2011. Micromolding for ceramic microneedle arrays. In *Microelectronic Engineering*. pp. 1681–1684.

- Chan, W.L., Fu, M.W. & Yang, B., 2012. Experimental studies of the size effect affected microscale plastic deformation in micro upsetting process. *Materials Science and Engineering: A*, 534, pp.374–383. Available at: <http://linkinghub.elsevier.com/retrieve/pii/S0921509311013220>.
- Chan, W.L., Fu, M.W. & Yang, B., 2011. Study of size effect in micro-extrusion process of pure copper. *Materials and Design*, 32(7), pp.3772–3782.
- Cheers, C.F., 1995. *Design and optimisation of an ultrasonic die system for forming metal cans*. Loughborough University. Available at: <https://dspace.lboro.ac.uk/2134/7231>.
- Chen, B., Wei, J. & Iliescu, C., 2010. Sonophoretic enhanced microneedles array (SEMA)-Improving the efficiency of transdermal drug delivery. *Sensors and Actuators, B: Chemical*, 145(1), pp.54–60.
- Choi, S.-O. et al., 2010. An electrically active microneedle array for electroporation. *Biomedical Microdevices*, 12(2), pp.263–273. Available at: <http://link.springer.com/10.1007/s10544-009-9381-x>.
- Cinti, S., 2005. The adipose organ. *Prostaglandins, Leukotrienes and Essential Fatty Acids*, 73(1), pp.9–15. Available at: <http://linkinghub.elsevier.com/retrieve/pii/S0952327805000542>.
- Comer, J. & Tam, K., 2001. Lipophilicity Profiles: Theory and Measurement. In B. Testa et al., eds. *Pharmacokinetic Optimization in Drug Research: Biological, Physicochemical, and Computational Strategies*. Zürich: Verlag Helvetica Chimica Acta, pp. 275–304. Available at: <http://doi.wiley.com/10.1002/9783906390437.ch17>.
- Davis, S.P. et al., 2004. Insertion of microneedles into skin: measurement and prediction of insertion force and needle fracture force. *Journal of Biomechanics*, 37(8), pp.1155–1163. Available at: <http://linkinghub.elsevier.com/retrieve/pii/S0021929003004731>.
- Davis, S.P., Prausnitz, M.R. & Allen, M.G., 2003. Fabrication and characterization of laser micromachined hollow microneedles. In *TRANSDUCERS '03. 12th International Conference on Solid-State Sensors, Actuators and Microsystems. Digest of Technical Papers (Cat. No.03TH8664)*. IEEE, pp. 1435–1438. Available at: <http://ieeexplore.ieee.org/document/1217045/>.
- Dean, C.H. et al., 2005. Cutaneous Delivery of a Live, Attenuated Chimeric Flavivirus Vaccines against Japanese Encephalitis (ChimeriVax™-JE) in Non-Human Primates. *Human Vaccines*, 1(3), pp.106–111. Available at: <http://www.tandfonline.com/doi/abs/10.4161/hv.1.3.1797>.
- Deng, J. et al., 2011. Friction and wear behaviors of the carbide tools embedded with solid lubricants in sliding wear tests and in dry cutting processes. *Wear*, 270(9–10), pp.666–674. Available at:

<http://linkinghub.elsevier.com/retrieve/pii/S0043164811000408>.

- Diehl, A., Engel, U. & Geiger, M., 2010. Influence of microstructure on the mechanical properties and the forming behaviour of very thin metal foils. *The International Journal of Advanced Manufacturing Technology*, 47(1–4), pp.53–61. Available at: <http://link.springer.com/10.1007/s00170-008-1851-4>.
- Djavanroodi, F., Daneshtalab, M. & Ebrahimi, M., 2012. A novel technique to increase strain distribution homogeneity for ECAPed materials. *Materials Science and Engineering: A*, 535, pp.115–121. Available at: <http://linkinghub.elsevier.com/retrieve/pii/S0921509311014316>.
- Donnelly, R.F. et al., 2012. *Microneedle-mediated and Intradermal Drug Delivery* First Edit., Oxford: Wiley-Blackwell.
- Donnelly, R.F. et al., 2009. Processing difficulties and instability of carbohydrate microneedle arrays. *Drug Development and Industrial Pharmacy*, 35(10), pp.1242–1254. Available at: <http://www.tandfonline.com/doi/full/10.1080/03639040902882280>.
- Doomernik, D.E. et al., 2011. Advancements in Catheter-Directed Ultrasound-Accelerated Thrombolysis. *Journal of Endovascular Therapy*, 18(3), pp.418–434. Available at: <http://jet.sagepub.com/lookup/doi/10.1583/10-3362.1>.
- Eckert, R.L., 1989. Structure, function, and differentiation of the keratinocyte. *Physiological Reviews*, 69(4), pp.1316–1346. Available at: <http://www.physiology.org/doi/10.1152/physrev.1989.69.4.1316>.
- Eichenhueller, B., Egerer, E. & Engel, U., 2007. Microforming at elevated temperature - forming and material behaviour. *The International Journal of Advanced Manufacturing Technology*, 33(1–2), pp.119–124. Available at: <http://link.springer.com/10.1007/s00170-006-0731-z>.
- Elias, P.M., 1981. Lipids and the epidermal permeability barrier. *Archives of Dermatological Research*, 270(1), pp.95–117. Available at: <http://link.springer.com/10.1007/BF00417155>.
- Endo, T., Suzuki, K. & Ishikawa, M., 1979. Effects of Superimposed Ultrasonic Oscillatory Stress on the Deformation of Fe and Fe-3%Si Alloy. *Transactions of the Japan Institute of Metals*, 20(12), pp.706–712. Available at: https://www.jstage.jst.go.jp/article/matertrans1960/20/12/20_12_706/_article.
- Engel, U. et al., 2007. Microforming and Nanomaterials. In F. Chinesta & E. Cueto, eds. *Advances in Material Forming: ESAFORM 10 years on*. Paris: Springer-Verlag, pp. 99–124. Available at: http://link.springer.com/10.1007/978-2-287-72143-4_7.
- Engel, U., 2006. Tribology in microforming. *Wear*, 260(3), pp.265–273. Available at: <http://linkinghub.elsevier.com/retrieve/pii/S0043164805003662>.

- Engel, U. & Eckstein, R., 2002. Microforming—from basic research to its realization. *Journal of Materials Processing Technology*, 125–126(January), pp.35–44. Available at: <http://linkinghub.elsevier.com/retrieve/pii/S0924013602004156>.
- Ensminger, D. & Stulen, F.B., 2009. *Ultrasonics: Data, Equations and Their Practical Uses*, CRC Press, Taylor & Francis Group. Available at: <https://books.google.com/books?id=u2XIPFCbVPgC&pgis=1>.
- Escobar-Chávez, J.J. et al., 2009. Electroporation as an Efficient Physical Enhancer for Skin Drug Delivery. *The Journal of Clinical Pharmacology*, 49(11), pp.1262–1283. Available at: <http://doi.wiley.com/10.1177/0091270009344984>.
- Farinas, K.C., Chad M. Miller & Soni, P.L., 1999. Supersaturated transdermal drug delivery systems, and methods for manufacturing the same - US 5906830 A. , pp.1–14. Available at: <https://patents.google.com/patent/US5906830A/en?q=5%2C906%2C830>.
- Flaten, T.P., 2001. Aluminium as a risk factor in Alzheimer's disease, with emphasis on drinking water. *Brain Research Bulletin*, 55(2), pp.187–196. Available at: <http://linkinghub.elsevier.com/retrieve/pii/S0361923001004592>.
- Fu, M.W. & Chan, W.L., 2013. A review on the state-of-the-art microforming technologies. *The International Journal of Advanced Manufacturing Technology*, 67(9–12), pp.2411–2437. Available at: <http://link.springer.com/10.1007/s00170-012-4661-7>.
- Furukawa, M. et al., 2001. Review: Processing of metals by equal-channel angular pressing. *Journal of Materials Science*, 36(12), pp.2835–2843. Available at: <http://link.springer.com/10.1023/A:1017932417043>.
- Furukawa, M. et al., 1998. The shearing characteristics associated with equal-channel angular pressing. *Materials Science and Engineering: A*, 257(2), pp.328–332. Available at: <http://linkinghub.elsevier.com/retrieve/pii/S0921509398007503>.
- Gardeniers, J.G.E. et al., 2002. Guidelines for etching silicon MEMS structures using fluorine high-density plasmas at cryogenic temperatures. *Journal of Microelectromechanical Systems*, 11(4), pp.385–401. Available at: <http://ieeexplore.ieee.org/document/1022850/>.
- Garskii, F.K. & Efromov, V.I., 1953. Effect of ultrasound on the decomposition of solid solutions. *Izvestiya Akademii Nauk, Beloroussk SSR*, 3.
- Gattiker, G.E., Kaler, K.V.I.S. & Mintchev, M.P., 2005. Electronic Mosquito: designing a semi-invasive Microsystem for blood sampling, analysis and drug delivery applications. *Microsystem Technologies*, 12(1–2), pp.44–51. Available at: <http://link.springer.com/10.1007/s00542-005-0015-9>.
- Gawkrodger, D.J., 2008. *Dermatology: An Illustrated Colour Text* 4th Ed., Edinburgh, London, New York, Sydney, Toronto: Churchill Livingstone Elsevier.

- Geiger, M., Messner, A. & Engel, U., 1997. Production of microparts - size effects in bulk metal forming, similarity theory. *Production Engineering*, 4(1), pp.55–58.
- Gerstel, M.S. & Place, V.A., 1976. Drug delivery device - US 3964482 A. Available at: <https://patents.google.com/patent/US3964482A/en>.
- Gill, H.S. & Prausnitz, M.R., 2008. Pocketed microneedles for drug delivery to the skin. *Journal of Physics and Chemistry of Solids*, 69(5–6), pp.1537–1541.
- Gillner, A. et al., 2000. Miniaturisierung von Bauteilen und Komponenten. *Umformtechnisches Kolloquium Darmstadt*, 7, pp.107–116.
- Griss, P. & Stemme, G., 2002. Novel, side opened out-of-plane microneedles for microfluidic transdermal interfacing. In *Technical Digest. MEMS 2002 IEEE International Conference. Fifteenth IEEE International Conference on Micro Electro Mechanical Systems (Cat. No.02CH37266)*. Las Vegas, NV, USA: IEEE, Published in Micro Electro Mechanical Systems, 2002. The Fifteenth IEEE International Conference on, pp. 467–470. Available at: <http://ieeexplore.ieee.org/document/984303/>.
- Gupta, J. et al., 2011. Kinetics of skin resealing after insertion of microneedles in human subjects. *Journal of Controlled Release*, 154(2), pp.148–155.
- Guy, R.H. et al., 2000. Iontophoresis: electrorepulsion and electroosmosis. *Journal of controlled release : official journal of the Controlled Release Society*, 64(1–3), pp.129–32. Available at: <http://www.ncbi.nlm.nih.gov/pubmed/10640651>.
- Guy, R.H., Hadgraft, J. & Bucks, D.A.W., 1987. Transdermal drug delivery and cutaneous metabolism. *Xenobiotica*, 17(3), pp.325–343. Available at: <http://www.tandfonline.com/doi/full/10.3109/00498258709043943>.
- Hadgraft, J. & Lane, M.E., 2006. Passive Transdermal Drug Delivery Systems. *American Journal of Drug Delivery*, 4(3), pp.153–160. Available at: <http://link.springer.com/10.2165/00137696-200604030-00003>.
- Hamilton, J.G., 1995. Needle Phobia: A Neglected Diagnosis. *Journal of Family Practice*, 41(2), pp.169–182.
- Han, M. et al., 2007. A novel fabrication process for out-of-plane microneedle sheets of biocompatible polymer. *Journal of Micromechanics and Microengineering*, 17(6), pp.1184–1191. Available at: <http://stacks.iop.org/0960-1317/17/i=6/a=012?key=crossref.6e86b15f8a16c6369e4d40ded584f51d>.
- Hanada, K. et al., 2003. Fabrication of diamond dies for microforming. *Diamond and Related Materials*, 12(3–7), pp.757–761. Available at: <http://linkinghub.elsevier.com/retrieve/pii/S0925963502002303>.
- Haq, M.I. et al., 2009. Clinical administration of microneedles: skin puncture, pain and sensation. *Biomedical Microdevices*, 11(1), pp.35–47. Available at: <http://link.springer.com/10.1007/s10544-008-9208-1>.

- Hauri, A.M., Armstrong, G.L. & Hutin, Y.J.F., 2004. The global burden of disease attributable to contaminated injections given in health care settings. *International Journal of STD & AIDS*, 15(1), pp.7–16. Available at: <http://journals.sagepub.com/doi/10.1258/095646204322637182>.
- Heller, L.C., Ugen, K. & Heller, R., 2005. Electroporation for targeted gene transfer. *Expert Opinion on Drug Delivery*, 2(2), pp.255–268. Available at: <http://www.tandfonline.com/doi/full/10.1517/17425247.2.2.255>.
- Henry, S. et al., 1998. Microfabricated Microneedles: A Novel Approach to Transdermal Drug Delivery. *Journal of Pharmaceutical Sciences*, 87(8), pp.922–925. Available at: <http://dx.doi.org/10.1021/js980042+>.
- Hingson, R.A. & Hughes, J.G., 1947. Clinical Studies with Jet Injection: A New Method of Drug Administration. *Current Researches in Anesthesia and Analgesia*, 26(6), pp.221–230.
- Hung, J.C., Tsai, Y.C. & Hung, C., 2007. Frictional effect of ultrasonic-vibration on upsetting. *Ultrasonics*, 46(3), pp.277–284.
- Hutin, Y. et al., 2003. Best infection control practices for intradermal, subcutaneous, and intramuscular needle injections. *Bulletin of the World Health Organization*, 81, pp.491–500.
- Iwahashi, Y. et al., 1996. Principle of equal-channel angular pressing for the processing of ultra-fine grained materials. *Scripta Materialia*, 35(2), pp.143–146. Available at: <http://linkinghub.elsevier.com/retrieve/pii/S1359646296001078>.
- Iwahashi, Y. et al., 1998. The process of grain refinement in equal-channel angular pressing. *Acta Materialia*, 46(9), pp.3317–3331. Available at: <http://linkinghub.elsevier.com/retrieve/pii/S1359645497004941>.
- Izumi, O., Oyama, K. & Suzuki, Y., 1966a. Effects of Superimposed Ultrasonic Vibration on Compressive Deformation of Metals. *Transactions of the Japan Institute of Metals*, 7(3), pp.162–167. Available at: https://www.jstage.jst.go.jp/article/matertrans1960/7/3/7_3_162/_article.
- Izumi, O., Oyama, K. & Suzuki, Y., 1966b. On the Superimposing of Ultrasonic Vibration during Compressive Deformation of Metals. *Transactions of the Japan Institute of Metals*, 7(3), pp.158–161. Available at: https://www.jstage.jst.go.jp/article/matertrans1960/7/3/7_3_158/_article.
- Jackson, L.A. et al., 2001. Safety and immunogenicity of varying dosages of trivalent inactivated influenza vaccine administered by needle-free jet injectors. *Vaccine*, 19(32), pp.4703–4709. Available at: <http://linkinghub.elsevier.com/retrieve/pii/S0264410X01002250>.
- Ji, J. et al., 2006. Microfabricated Silicon Microneedle Array for Transdermal Drug Delivery. *Journal of Physics: Conference Series*, 34, pp.1127–1131. Available at: [208](http://stacks.iop.org/1742-</p>
</div>
<div data-bbox=)

6596/34/i=1/a=186?key=crossref.96baf5aaa6f887e6c007eb91a97275c9.

- Jimma, T. et al., 1998. An application of ultrasonic vibration to the deep drawing process. *Journal of Materials Processing Technology*, 80–81, pp.406–412. Available at: <http://linkinghub.elsevier.com/retrieve/pii/S0924013698001952>.
- Kaiser, G. & Pechhold, W., 1969. Dynamic-mechanical investigations for the study of dislocation motion during plastic flow. *Acta Metallurgica*, 17(4), pp.527–537. Available at: <http://linkinghub.elsevier.com/retrieve/pii/0001616069900340>.
- Kalia, Y.N. et al., 2004. Iontophoretic drug delivery. *Advanced Drug Delivery Reviews*, 56(5), pp.619–658. Available at: <http://linkinghub.elsevier.com/retrieve/pii/S0169409X03002424>.
- Kalluri, H. & Banga, A.K., 2011. Formation and closure of microchannels in skin following microporation. *Pharmaceutical Research*, 28(1), pp.82–94.
- Kalluri, H., Kolli, C.S. & Banga, A.K., 2011. Characterization of Microchannels Created by Metal Microneedles: Formation and Closure. *The AAPS Journal*, 13(3), pp.473–481. Available at: <http://www.pubmedcentral.nih.gov/articlerender.fcgi?artid=3160154&tool=pmc&entrez&rendertype=abstract%5Cnhttp://www.ncbi.nlm.nih.gov/pubmed/21732220%5Cnhttp://www.pubmedcentral.nih.gov/articlerender.fcgi?artid=PMC3160154%5Cnhttp://www.springerlink.com/index/10.1>.
- Karande, P. et al., 2005. Design principles of chemical penetration enhancers for transdermal drug delivery. *Proceedings of the National Academy of Sciences*, 102(13), pp.4688–4693. Available at: <http://www.pnas.org/cgi/doi/10.1073/pnas.0501176102>.
- Kaushik, S. et al., 2001. Lack of Pain Associated with Microfabricated Microneedles. *Anesthesia and Analgesia*, 92(2), pp.502–504. Available at: <http://content.wkhealth.com/linkback/openurl?sid=WKPTLP:landingpage&an=00000539-200102000-00041>.
- Kendall, M.A.F. et al., 2004. Measurements of the gas and particle flow within a converging-diverging nozzle for high speed powdered vaccine and drug delivery. *Experiments in Fluids*, 37(1), pp.128–136. Available at: <http://link.springer.com/10.1007/s00348-004-0792-4>.
- Kermici, M., Bodereau, C. & Aubin, G., 1977. Measurement of biochemical parameters in the stratum corneum. *Journal of the Society of Cosmetic Chemists*, 28(4), pp.151–164.
- Kim, Y.C., Park, J.H. & Prausnitz, M.R., 2012. Microneedles for drug and vaccine delivery. *Advanced Drug Delivery Reviews*, 64(14), pp.1547–1568. Available at: <http://dx.doi.org/10.1016/j.addr.2012.04.005>.
- Kirchner, H.O.K. et al., 1984. Plastic deformation under simultaneous cyclic and unidirectional loading at low and ultrasonic frequencies. *Materials Science and*

Engineering, 68(2), pp.197–206.

Kost, J., 1993. Ultrasound induced delivery of peptides. *Journal of Controlled Release*, 24(1–3), pp.247–255. Available at: <http://linkinghub.elsevier.com/retrieve/pii/0168365993901836>.

Kripke, M.L. et al., 1990. Evidence that cutaneous antigen-presenting cells migrate to regional lymph nodes during contact sensitization. *Journal of immunology (Baltimore, Md. : 1950)*, 145(9), pp.2833–8. Available at: <http://www.ncbi.nlm.nih.gov/pubmed/2212665>.

Kupper, T.S. & Fuhlbrigge, R.C., 2004. Immune surveillance in the skin: mechanisms and clinical consequences. *Nature Reviews Immunology*, 4(3), pp.211–222. Available at: <http://www.nature.com/articles/nri1310>.

Langenecker, B., 1966. Effects of Ultrasound on Deformation Characteristics of Metals. *IEEE Transactions on Sonics and Ultrasonics*, 13(1), pp.1–8. Available at: <http://ieeexplore.ieee.org/document/1538364/>.

Langkjær, L. et al., 1998. Iontophoresis of monomeric insulin analogues in vitro: effects of insulin charge and skin pretreatment. *Journal of Controlled Release*, 51(1), pp.47–56. Available at: <http://linkinghub.elsevier.com/retrieve/pii/S0168365997001557>.

Lansdown, A.R., 1999. *Molybdenum Disulphide Lubrication, Volume 35 (Tribology and Interface Engineering)*, Elsevier Science.

Lark, M.R. & Gangarosa, L.P., 1990. Iontophoresis: An Effective Modality for the Treatment of Inflammatory Disorders of the Temporomandibular Joint and Myofascial Pain. *CRANIO®*, 8(2), pp.108–119. Available at: <http://www.tandfonline.com/doi/full/10.1080/08869634.1990.11678305>.

Laurent, P.E. et al., 2010. Safety and efficacy of novel dermal and epidermal microneedle delivery systems for rabies vaccination in healthy adults. *Vaccine*, 28(36), pp.5850–5856. Available at: <http://linkinghub.elsevier.com/retrieve/pii/S0264410X10008844>.

Lavon, I. & Kost, J., 2004. Ultrasound and transdermal drug delivery. *Drug Discovery Today*, 9(15), pp.670–676. Available at: <http://linkinghub.elsevier.com/retrieve/pii/S1359644604031708>.

Li, D. & Soar, R.C., 2008. Plastic flow and work hardening of Al alloy matrices during ultrasonic consolidation fibre embedding process. *Materials Science and Engineering A*, 498(1–2), pp.421–429.

Li, G. et al., 2009. In vitro transdermal delivery of therapeutic antibodies using maltose microneedles. *International Journal of Pharmaceutics*, 368(1–2), pp.109–115. Available at: <http://linkinghub.elsevier.com/retrieve/pii/S0378517308006972>.

Lichtenberger, L.M., 1987. Membranes and barriers: with a focus on the gastric

- mucosal barrier. *Clinical and investigative medicine. Medecine clinique et experimentale*, 10(3), pp.181–8. Available at: <http://www.ncbi.nlm.nih.gov/pubmed/3304749>.
- Lin, L. & Pisano, A.P., 1999. Silicon-processed microneedles. *Journal of Microelectromechanical Systems*, 8(1), pp.78–84. Available at: <http://ieeexplore.ieee.org/document/749406/>.
- Lindberg, M. & Forslind, B., 2003. The Skin as a Barrier. , pp.9–18. Available at: [http://www.scientificspectator.com/documents/personal_care_spectator/The Skin as a Barrier.pdf](http://www.scientificspectator.com/documents/personal_care_spectator/The_Skin_as_a_Barrier.pdf).
- Littmann, W., Storck, H. & Wallaschek, J., 2001. Sliding friction in the presence of ultrasonic oscillations: superposition of longitudinal oscillations. *Archive of Applied Mechanics (Ingenieur Archiv)*, 71(8), pp.549–554. Available at: <http://link.springer.com/10.1007/s004190100160>.
- Liu, J.G. et al., 2011. Influence of size effect on the springback of sheet metal foils in micro-bending. *Computational Materials Science*, 50(9), pp.2604–2614. Available at: <http://linkinghub.elsevier.com/retrieve/pii/S0927025611002114>.
- Lucas, M., 1996. Vibration sensitivity in the design of ultrasonic forming dies. *Ultrasonics*, 34(1), pp.35–41.
- Lucas, M., Gachagan, A. & Cardoni, A., 2009. Research applications and opportunities in power ultrasonics. *Proceedings of the Institution of Mechanical Engineers, Part C: Journal of Mechanical Engineering Science*, 223(12), pp.2949–2965. Available at: <http://www.scopus.com/inward/record.url?eid=2-s2.0-72749121078&partnerID=tZOtx3y1>.
- Lv, Y.-G. et al., 2006. Modeling of transdermal drug delivery with a microneedle array. *Journal of Micromechanics and Microengineering*, 16(11), pp.2492–2501. Available at: <http://stacks.iop.org/0960-1317/16/i=11/a=034?key=crossref.f0c2d77e1cbf8866c86bb72626c92038>.
- Malygin, G. a., 2000. Acoustoplastic effect and the stress superimposition mechanism. *Physics of the Solid State*, 42(1), pp.72–78.
- Markova, N. et al., 1993. Profilaggrin is a major epidermal calcium-binding protein. *Molecular and cellular biology*, 13(1), pp.613–25. Available at: <http://www.pubmedcentral.nih.gov/articlerender.fcgi?artid=358940&tool=pmcentrez&rendertype=abstract>.
- Matriano, J.A. et al., 2002. Macroflux® Microprojection Array Patch Technology: A New and Efficient Approach for Intracutaneous Immunization. *Pharmaceutical Research*, 19(1), pp.63–70. Available at: <http://link.springer.com/10.1023/A:1013607400040>.
- Matteucci, M. et al., 2009. Poly vinyl alcohol re-usable masters for microneedle replication. *Microelectronic Engineering*, 86(4–6), pp.752–756. Available at:

<http://linkinghub.elsevier.com/retrieve/pii/S0167931709001075>.

- May, D.J., Allen, J.S. & Ferrara, K.W., 2002. Dynamics and fragmentation of thick-shelled microbubbles. *IEEE Transactions on Ultrasonics, Ferroelectrics and Frequency Control*, 49(10), pp.1400–1410. Available at: <http://ieeexplore.ieee.org/document/1041081/>.
- McLachlan, D.R.C., 1995. Aluminium and the risk for alzheimer's disease. *Environmetrics*, 6(3), pp.233–275. Available at: <http://doi.wiley.com/10.1002/env.3170060303>.
- Mesiwala, A.H. et al., 2002. High-intensity focused ultrasound selectively disrupts the blood-brain barrier in vivo. *Ultrasound in Medicine & Biology*, 28(3), pp.389–400. Available at: <http://linkinghub.elsevier.com/retrieve/pii/S030156290100521X>.
- Messner, A. et al., 1994. Size effect in the FE-simulation of micro-forming processes. *Journal of Materials Processing Technology*, 45(1–4), pp.371–376. Available at: <http://linkinghub.elsevier.com/retrieve/pii/0924013694903689>.
- Mezei, M. & Gulasekharan, V., 1980. Liposomes - a selective drug delivery system for the topical route of administration I. Lotion dosage form. *Life Sciences*, 26(18), pp.1473–1477. Available at: <http://linkinghub.elsevier.com/retrieve/pii/0024320580902684>.
- Mikszta, J.A. et al., 2002. Improved genetic immunization via micromechanical disruption of skin-barrier function and targeted epidermal delivery. *Nature Medicine*, 8(4), pp.415–419. Available at: <http://www.nature.com/articles/nm0402-415>.
- Mikszta, J.A. et al., 2005. Protective immunization against inhalational anthrax: a comparison of minimally invasive delivery platforms. *The Journal of infectious diseases*, 191(2), pp.278–88. Available at: <http://www.ncbi.nlm.nih.gov/pubmed/15609239>.
- Mitragotri, S., 2006. Current status and future prospects of needle-free liquid jet injectors. *Nature Reviews Drug Discovery*. Available at: <http://www.nature.com/doifinder/10.1038/nrd2076>.
- Mitragotri, S., 2005. Healing sound: the use of ultrasound in drug delivery and other therapeutic applications. *Nature Reviews Drug Discovery*, 4(3), pp.255–260. Available at: <http://www.nature.com/articles/nrd1662>.
- Mitragotri, S., Blankschtein, D. & Langer, R., 1995. Ultrasound-mediated transdermal protein delivery. *Science*, 269(5225), pp.850–853. Available at: <http://www.sciencemag.org/cgi/doi/10.1126/science.7638603>.
- Mitragotri, S. & Lahann, J., 2012. Materials for Drug Delivery: Innovative Solutions to Address Complex Biological Hurdles. *Advanced Materials*, 24(28), pp.3717–3723. Available at: <http://doi.wiley.com/10.1002/adma.201202080>.

- Møller, A.R., 2012. *Hearing: Anatomy, Physiology, and Disorders of the Auditory System* 3rd ed., Abingdon: Plural Publishing.
- Møss, J. & Bundgaard, H., 1990. Prodrugs of peptides. 7. Transdermal delivery of thyrotropin-releasing hormone (TRH) via prodrugs. *International Journal of Pharmaceutics*, 66(1–3), pp.39–45. Available at: <http://linkinghub.elsevier.com/retrieve/pii/037851739090382E>.
- Mousavi, S. a. a. A., Feizi, H. & Madoliat, R., 2007. Investigations on the effects of ultrasonic vibrations in the extrusion process. *Journal of Materials Processing Technology*, 187–188, pp.657–661.
- Narayan, R.J., 2009. *Biomedical Materials* R. Narayan, ed., Boston, MA: Springer US. Available at: <http://link.springer.com/10.1007/978-0-387-84872-3>.
- Obland, G.F., 1958. The Fine Structure of the Interrelationship of Cells in the Human Epidermis. *The Journal of Cell Biology*, 4(5), pp.529–538. Available at: <http://www.jcb.org/cgi/doi/10.1083/jcb.4.5.529>.
- Ohgaku, T. & Takeuchi, N., 1987. The Blaha Effect of Alkali Halide Crystals. *Physica Status Solidi (a)*, 102(1), pp.293–299. Available at: <http://doi.wiley.com/10.1002/pssa.2211020130>.
- Olejniak, L., Presz, W. & Rosochowski, A., 2009. Backward extrusion using micro-blanked aluminium sheet. *International Journal of Material Forming*, 2(Suppl 1), pp.617–620. Available at: <http://link.springer.com/10.1007/s12289-009-0533-6>.
- Olejniak, L. & Rosochowski, A., 2008. Scaled-up ECAP with enhanced productivity. *Steel Research International 79; Special Edition*, 2, pp.439–447. Available at: <https://strathprints.strath.ac.uk/id/eprint/13929>.
- Olejniak, L., Rosochowski, A. & Richert, M., 2008. Incremental ECAP of Plates. *Materials Science Forum*, 584–586, pp.108–113. Available at: <http://www.scientific.net/MSF.584-586.108>.
- Omatsu, T. et al., 2010. Metal microneedle fabrication using twisted light with spin. *Optics Express*, 18(17), p.17967. Available at: <https://www.osapublishing.org/oe/abstract.cfm?uri=oe-18-17-17967>.
- Ovsianikov, A. et al., 2007. Two Photon Polymerization of Polymer?Ceramic Hybrid Materials for Transdermal Drug Delivery. *International Journal of Applied Ceramic Technology*, 4(1), pp.22–29. Available at: <http://doi.wiley.com/10.1111/j.1744-7402.2007.02115.x>.
- Paliwal, S. & Mitragotri, S., 2006. Ultrasound-induced cavitation: applications in drug and gene delivery. *Expert Opinion on Drug Delivery*, 3(6), pp.713–726. Available at: <http://www.tandfonline.com/doi/full/10.1517/17425247.3.6.713>.
- Park, J.-H. et al., 2007. Polymer particle-based micromolding to fabricate novel microstructures. *Biomedical Microdevices*, 9(2), pp.223–234. Available at:

<http://link.springer.com/10.1007/s10544-006-9024-4>.

- Park, J.-H., Allen, M.G. & Prausnitz, M.R., 2005. Biodegradable polymer microneedles: Fabrication, mechanics and transdermal drug delivery. *Journal of Controlled Release*, 104(1), pp.51–66. Available at: <http://linkinghub.elsevier.com/retrieve/pii/S0168365905000568>.
- Park, J.-H. & Prausnitz, M.R., 2010. Analysis of mechanical failure of polymer microneedles by axial force. *Journal of the Korean Physical Society*, 56(4), p.1223.
- Park, Y. et al., 2016. Fabrication and characterization of dissolving microneedle arrays for improving skin permeability of cosmetic ingredients. *Journal of Industrial and Engineering Chemistry*, 39, pp.121–126. Available at: <http://dx.doi.org/10.1016/j.jiec.2016.05.022>.
- Pathan, I. & Setty, C., 2009. Chemical Penetration Enhancers for Transdermal Drug Delivery Systems. *Tropical Journal of Pharmaceutical Research*, 8(2). Available at: <http://www.ajol.info/index.php/tjpr/article/view/44527>.
- Pavlina, E.J. & Van Tyne, C.J., 2008. Correlation of Yield Strength and Tensile Strength with Hardness for Steels. *Journal of Materials Engineering and Performance*, 17(6), pp.888–893. Available at: <http://link.springer.com/10.1007/s11665-008-9225-5>.
- Pellett, M.A., Roberts, M.S. & Hadgraft, J., 1997. Supersaturated solutions evaluated with an in vitro stratum corneum tape stripping technique. *International Journal of Pharmaceutics*, 151(1), pp.91–98. Available at: <http://linkinghub.elsevier.com/retrieve/pii/S0378517397048977>.
- Pelletta, M.A., Davisb, A.F. & Hadgraftc, J., 1994. Effect of supersaturation on membrane transport: 2. Piroxicam. *International Journal of Pharmaceutics*, 111(1), pp.1–6. Available at: <http://linkinghub.elsevier.com/retrieve/pii/0378517394903956>.
- Potts, R.O. & Francoeur, M.L., 1991. The Influence of Stratum Corneum Morphology on Water Permeability. *Journal of Investigative Dermatology*, 96(4), pp.495–499. Available at: <http://linkinghub.elsevier.com/retrieve/pii/S0022202X9190455Y>.
- Potts, R.O. & Guy, R.H., 1992. Predicting Skin Permeability. *Pharmaceutical Research*, 09(5), pp.663–669. Available at: <http://link.springer.com/10.1023/A:1015810312465>.
- Prausnitz, M.R., 2001. Analysis: Overcoming Skin's Barrier: The Search for Effective and User-Friendly Drug Delivery. *Diabetes Technology & Therapeutics*, 3(2), pp.233–236. Available at: <http://online.liebertpub.com/doi/abs/10.1089/152091501300209606>.
- Prausnitz, M.R., Allen, M.G., et al., 2004. Devices and methods for enhanced microneedle penetration of biological barriers - US6743211B1. , pp.1–35.

Available at: <https://patents.google.com/patent/US6743211B1/en>.

- Prausnitz, M.R. et al., 1993. Electroporation of mammalian skin: a mechanism to enhance transdermal drug delivery. *Proceedings of the National Academy of Sciences of the United States of America*, 90(22), pp.10504–8. Available at: <http://www.ncbi.nlm.nih.gov/pubmed/8248137>.
- Prausnitz, M.R. et al., 2009. Microneedle-based vaccines. *Current Topics in Microbiology and Immunology*, 333(1), pp.369–393.
- Prausnitz, M.R., 2004. Microneedles for transdermal drug delivery. *Advanced Drug Delivery Reviews*, 56(5), pp.581–587. Available at: <http://linkinghub.elsevier.com/retrieve/pii/S0169409X03002394>.
- Prausnitz, M.R., 1997. Reversible skin permeabilization for transdermal delivery of macromolecules. *Critical reviews in therapeutic drug carrier systems*, 14(4), pp.455–83. Available at: <http://www.ncbi.nlm.nih.gov/pubmed/9450177>.
- Prausnitz, M.R., Mitragotri, S. & Langer, R., 2004. Current status and future potential of transdermal drug delivery. *Nature Reviews Drug Discovery*, 3(2), pp.115–124. Available at: <http://www.nature.com/doifinder/10.1038/nrd1304>.
- Presz, W. & Andersen, B., 2007. Flexible tooling for vibration-assisted microforming. *Journal of Achievements in Materials ...*, 21(2), pp.61–64. Available at: http://www.wjournalamme.org/papers_vol21_2/1546S.pdf.
- Presz, W. & Rosochowski, A., 2006. The influence of grain size on surface quality of microformed components. In *ESAFORM 2006 Conference, Glasgow*. Glasgow, pp. 587–590.
- Reshetov, A. et al., 2017. The Occurrence of Ideal Plastic State in CP Titanium Processed by Twist Extrusion. *Advanced Engineering Materials*, (January 2018).
- Rosochowska, M., 2003. *The influence of tool excitation on material deformation - PhD Thesis*. University of Strathclyde, Glasgow.
- Rosochowska, M., Rosochowski, A. & Olejnik, L., 2010. FE simulation of micro-extrusion of a conical pin. *International Journal of Material Forming*, 3(S1), pp.423–426. Available at: <http://link.springer.com/10.1007/s12289-010-0797-x>.
- Rosochowski, A. et al., 2006. Compression behaviour of UFG aluminium. *Proc. of the 9th Int. Conference on Material Forming ESAFORM*, pp.26–28. Available at: <https://link.springer.com/article/10.1007/s12289-010-0797-x>.
- Rosochowski, A. et al., 2007. Micro-extrusion of ultra-fine grained aluminium. *The International Journal of Advanced Manufacturing Technology*, 33(1–2), pp.137–146. Available at: <http://link.springer.com/10.1007/s00170-007-0955-6>.
- Rosochowski, A. & Olejnik, L., 2007. FEM simulation of incremental shear. In E. Cueto & F. Chinesta, eds. *Esaform 2007, 10th International Conference on*

Material Forming (American Institute of Physics Proceedings 907),. Zaragoza, Spain, pp. 653–658.

Rosochowski, A. & Olejnik, L., 2011. Incremental Equal Channel Angular Pressing for Grain Refinement. *Materials Science Forum*, 674, pp.19–28. Available at: <http://www.scientific.net/MSF.674.19>.

Rosochowski, A., Olejnik, L. & Richert, M., 2008. Double-Billet Incremental ECAP. *Materials Science Forum*, 584–586, pp.139–144. Available at: <http://www.scientific.net/MSF.584-586.139>.

Sanchez-Salmeron, A.J. et al., 2005. Recent development in micro-handling systems for micro-manufacturing. *Journal of Materials Processing Technology*, 167(2–3), pp.499–507. Available at: <http://linkinghub.elsevier.com/retrieve/pii/S092401360500590X>.

Saotome, Y. & Iwazaki, H., 2001. Superplastic backward microextrusion of microparts for micro-electro-mechanical systems. *Journal of Materials Processing Technology*, 119(1–3), pp.307–311. Available at: <http://linkinghub.elsevier.com/retrieve/pii/S0924013601009578>.

Saotome, Y., Zhang, T. & Inoue, A., 1998. Microforming of Memes Parts with Amorphous Alloys. *MRS Proceedings*, 554, p.385. Available at: http://journals.cambridge.org/abstract_S1946427400176043.

SASAKI, H. et al., 1990. Transdermal delivery of 5-fluorouracil and its alkylcarbamoyl derivatives. *International Journal of Pharmaceutics*, 60(1), pp.1–9. Available at: <http://linkinghub.elsevier.com/retrieve/pii/0378517390901846>.

Scheuplein, R.J., 1976. Permeability Of The Skin: A Review Of Major Concepts And Some New Developments. *Journal of Investigative Dermatology*, 67(5), pp.672–676. Available at: <http://linkinghub.elsevier.com/retrieve/pii/S0022202X15449231>.

Scheuplein, R.J. & Blank, I.H., 1971. Permeability of the skin. *Physiological Reviews*, 51(4), pp.702–747. Available at: <http://www.physiology.org/doi/10.1152/physrev.1971.51.4.702>.

Schramm, J. & Mitragotri, S., 2002. Transdermal drug delivery by jet injectors: energetics of jet formation and penetration. *Pharmaceutical research*, 19(11), pp.1673–9. Available at: <http://www.ncbi.nlm.nih.gov/pubmed/12458673>.

Schwidetzky, O. & Rutherford, N.J., 1944. History of Needles and Syringes. *Anesthesia and Analgesia*, Jan-Feb, pp.34–38.

Segal, V.M., 1995. Materials processing by simple shear. *Materials Science and Engineering: A*, 197(2), pp.157–164. Available at: <http://linkinghub.elsevier.com/retrieve/pii/0921509395097058>.

Segal, V.M. et al., 1981. Plastic Working of Metals by Simple Shear. *Russian*

Metallurgy (Metally), 1, pp.99–105.

- Segal, V.M., 1977. The Method of Material Preparation for Subsequent Working - USSR. Pat, (575892). *Invention Sertificate of the USSR*, p.330.
- Severdenko, V.P., Klubovich, V.V. & Stepanenko, A.V., 1972. *Ultrasonic rolling and drawing of metals*, New York: Consultants Bureau.
- Shikida, M. et al., 2004. Non-photolithographic pattern transfer for fabricating arrayed three-dimensional microstructures by chemical anisotropic etching. *Sensors and Actuators, A: Physical*, 116(2), pp.264–271.
- Sieg, A., Guy, R.. & Delgado-Charro, M.B., 2004. Electroosmosis in Transdermal Iontophoresis: Implications for Noninvasive and Calibration-Free Glucose Monitoring. *Biophys J.*, 87(5), pp.344–3350.
- Siegert, K. & Möck, a., 1996. Wire drawing with ultrasonically oscillating dies. *Journal of Materials Processing Technology*, 60(1–4), pp.657–660.
- Siegert, K. & Ulmer, J., 2001. Influencing the Friction in Metal Forming Processes by Superimposing Ultrasonic Waves. *CIRP Annals - Manufacturing Technology*, 50(1), pp.195–200.
- Singh, T. et al., 2010. Microporation Techniques for Enhanced Delivery of Therapeutic Agents. *Recent Patents on Drug Delivery & Formulation*, 4(1), pp.1–17. Available at: <http://www.eurekaselect.com/openurl/content.php?genre=article&issn=1872-2113&volume=4&issue=1&spage=1>.
- Sklenicka, V. et al., 2012. Equal-Channel Angular Pressing and Creep in Ultrafine-Grained Aluminium and Its Alloys. In P. Z. Ahmad, ed. *Aluminium Alloys - New Trends in Fabrication and Applications*. InTech, pp. 4–45. Available at: <http://www.intechopen.com/books/aluminium-alloys-new-trends-in-fabrication-and-applications/equal-channel-angular-pressing-and-creep-in-ultrafine-grained-aluminium-and-its-alloys>.
- Spierings, E.L.H., Brevard, J.A. & Katz, N.P., 2008. Two-Minute Skin Anesthesia Through Ultrasound Pretreatment and Iontophoretic Delivery of a Topical Anesthetic: A Feasibility Study. *Pain Medicine*, 9(1), pp.55–59. Available at: <https://academic.oup.com/painmedicine/article-lookup/doi/10.1111/j.1526-4637.2007.00281.x>.
- Stachowiak, J.C. et al., 2009. Dynamic control of needle-free jet injection. *Journal of controlled release : official journal of the Controlled Release Society*, 135(2), pp.104–12. Available at: <http://www.ncbi.nlm.nih.gov/pubmed/19284969>.
- Stoeber, B. & Liepmann, D., 2000. Fluid injection through out-of-plane microneedles. In *1st Annual International IEEE-EMBS Special Topic Conference on Microtechnologies in Medicine and Biology - Proceedings 12-14 Oct. 2000*. Lyon, France, pp. 224–228.

- Stoitzner, P., Sparber, F. & Tripp, C.H., 2010. Langerhans cells as targets for immunotherapy against skin cancer. *Immunology and Cell Biology*, 88(4), pp.431–437. Available at: <http://doi.wiley.com/10.1038/icb.2010.31>.
- Sugiyama, S., Khumpuang, S. & Kawaguchi, G., 2004. Plain-pattern to cross-section transfer (PCT) technique for deep x-ray lithography and applications. *Journal of Micromechanics and Microengineering*, 14(10), pp.1399–1404.
- Sullivan, S.P., Murthy, N. & Prausnitz, M.R., 2008. Minimally Invasive Protein Delivery with Rapidly Dissolving Polymer Microneedles. *Advanced Materials*, 20(5), pp.933–938. Available at: <http://doi.wiley.com/10.1002/adma.200701205>.
- Syková, E. & Nicholson, C., 2008. Diffusion in Brain Extracellular Space. *Physiological Reviews*, 88(4), pp.1277–1340. Available at: <http://www.physiology.org/doi/10.1152/physrev.00027.2007>.
- Taberner, A., Hogan, N.C. & Hunter, I.W., 2012. Needle-free jet injection using real-time controlled linear Lorentz-force actuators. *Medical engineering & physics*, 34(9), pp.1228–35. Available at: <http://www.ncbi.nlm.nih.gov/pubmed/22245386>.
- Tabor, D., 1953. Mohs's Hardness Scale - A Physical Interpretation. *Proceedings of the Physical Society. Section B.*, 67, 3, pp.249–257.
- Tamada, J.A. et al., 1999. Noninvasive Glucose Monitoring. *JAMA*, 282(19), p.1839. Available at: <http://jama.jamanetwork.com/article.aspx?doi=10.1001/jama.282.19.1839>.
- Taureza, M., Song, X. & Castagne, S., 2014. On the influence of workpiece material on friction in microforming and lubricant effectiveness. *Journal of Materials Processing Technology*, 214(4), pp.998–1007. Available at: <http://dx.doi.org/10.1016/j.jmatprotec.2013.11.003>.
- Terry, R.D. & Pena, C., 1965. Experimental Production of Neurofibrillary Degeneration: 2. Electron Microscopy, Phosphatase Histochemistry and Electron Prose Analysis. *Journal of Neuropathology and Experimental Neurology*, 24(2), pp.200–210. Available at: <https://academic.oup.com/jnen/article-lookup/doi/10.1097/00005072-196504000-00003>.
- Tiesler, N., 2002. Microforming-size effects in friction and their influence on extrusion processes. *Wire*, 52(1), pp.34–38.
- Tisza, M., 1983a. Deep drawing experiments in ultrasonically vibrating tools. *Banyasz. Kohasz. Lapok(Kohasz.)*, 116(3), pp.104–109.
- Tisza, M., 1983b. The use of superimposed ultrasonic vibrations in deep drawing. *Kohaszat*, 116, pp.104–109.
- Trautmann, A., Ruther, P. & Paul, O., 2003. Microneedle arrays fabricated using suspended etch mask technology combined with fluidic through wafer vias. In

The Sixteenth Annual International Conference on Micro Electro Mechanical Systems, 2003. MEMS-03 Kyoto. IEEE. Kyoto, Japan: IEEE, pp. 682–685. Available at: <http://ieeexplore.ieee.org/document/1189841/>.

- Trichur, R. et al., 2002. Development of Plastic Microneedles for Transdermal Interfacing Using Injection Molding Techniques. In *Micro Total Analysis Systems 2002*. Dordrecht: Springer Netherlands, pp. 395–397. Available at: http://link.springer.com/10.1007/978-94-010-0295-0_132.
- Uchino, K., 2010. *Advanced Piezoelectric Materials Science and Technology*, Oxford: Woodhead Publishing Limited.
- Uhlmann, E., Piltz, S. & Doll, U., 2005. Machining of micro/miniature dies and moulds by electrical discharge machining—Recent development. *Journal of Materials Processing Technology*, 167(2–3), pp.488–493. Available at: <http://linkinghub.elsevier.com/retrieve/pii/S0924013605005881>.
- Valiev, R.Z. et al., 1991. Mössbauer analysis of submicrometer grained iron. *Scripta Metallurgica et Materialia*, 25(12), pp.2717–2722. Available at: <http://linkinghub.elsevier.com/retrieve/pii/0956716X9190145Q>.
- Vandervoort, J. & Ludwig, A., 2008. Microneedles for transdermal drug delivery: a minireview. *Frontiers in bioscience: a journal and virtual library*, 13(13), pp.1711–5. Available at: <http://www.bioscience.org/2008/v13/af/2794/list.htm>.
- Vollertsen, F., 2013. *Micro Metal Forming* F. Vollertsen, ed., Berlin, Heidelberg: Springer Berlin Heidelberg. Available at: <http://link.springer.com/10.1007/978-3-642-30916-8>.
- Vollertsen, F. et al., 2004. State of the art in micro forming and investigations into micro deep drawing. *Journal of Materials Processing Technology*, 151(1–3), pp.70–79. Available at: <http://linkinghub.elsevier.com/retrieve/pii/S0924013604003097>.
- Wang, J. et al., 1993. An investigation of ductility and microstructural evolution in an Al–3% Mg alloy with submicron grain size. *Journal of Materials Research*, 8(11), pp.2810–2818. Available at: http://www.journals.cambridge.org/abstract_S0884291400072022.
- Wang, Y. et al., 1993. Iontophoresis of Hydrocortisone across Hairless Mouse Skin Investigation of Skin Alteration. *Journal of Pharmaceutical Sciences*, 82(11), pp.1140–1144. Available at: <http://linkinghub.elsevier.com/retrieve/pii/S0022354915492615>.
- Wang, Y. et al., 2005. Transdermal iontophoresis: combination strategies to improve transdermal iontophoretic drug delivery. *European Journal of Pharmaceutics and Biopharmaceutics*, 60(2), pp.179–191. Available at: <http://linkinghub.elsevier.com/retrieve/pii/S0939641105000226>.
- Weaver, J.C., Vaughan, T.E. & Chizmadzhev, Y., 1999. Theory of electrical creation

- of aqueous pathways across skin transport barriers. *Advanced Drug Delivery Reviews*, 35(1), pp.21–39. Available at: <http://linkinghub.elsevier.com/retrieve/pii/S0169409X98000611>.
- Weinstein, J. et al., 1979. Liposomes and local hyperthermia: selective delivery of methotrexate to heated tumors. *Science*, 204(4389), pp.188–191. Available at: <http://www.sciencemag.org/cgi/doi/10.1126/science.432641>.
- Weniger, B.G., 2003. Jet injection of vaccines: overview and challenges for mass vaccination with jet injections (JIS). *Innovative Administration Systems for Vaccines*.
- Whitehead, K.A., Langer, R. & Anderson, D.G., 2009. Knocking down barriers: advances in siRNA delivery. *Nature Reviews Drug Discovery*, 8(2), pp.129–138. Available at: <http://www.nature.com/articles/nrd2742>.
- Wilke, N. et al., 2005. Silicon microneedle electrode array with temperature monitoring for electroporation. *Sensors and Actuators, A: Physical*, 123–124, pp.319–325.
- Williams, A.C. & Barry, B.W., 2004. Penetration enhancers. *Advanced Drug Delivery Reviews*, 56(5), pp.603–618. Available at: <http://linkinghub.elsevier.com/retrieve/pii/S0169409X03002412>.
- Winsper, C. & Sansome, D., 1967. A review of the application of oscillatory energy to metals deforming plastically. In *Advances in Machine Tool Design and Research 1967, Proceedings of the 8th International M.T.D.R. Conference, Manchester*. Elsevier, pp. 1349–1360. Available at: <http://linkinghub.elsevier.com/retrieve/pii/B9780080126296500420>.
- World Health Organization, 1997. *Environmental Health Criteria 194*, Geneva: WHO.
- Wu, Y. et al., 2008. Microneedle-based drug delivery: studies on delivery parameters and biocompatibility. *Biomedical Microdevices*, 10(5), pp.601–610. Available at: <http://link.springer.com/10.1007/s10544-008-9171-x>.
- Yoon, Y.-K., Park, J.-H. & Allen, M.G., 2006. Multidirectional UV Lithography for Complex 3-D MEMS Structures. *Journal of Microelectromechanical Systems*, 15(5), pp.1121–1130. Available at: <http://ieeexplore.ieee.org/document/1707771/>.
- Yuzhakov, V. V, 2010. Microneedle array, patch, and applicator for transdermal drug delivery - US 7658728 B2. , pp.1–16. Available at: <https://patents.google.com/patent/US7658728B2/en?q=+US11328813>.
- Zahn, J. et al., 2000. Microfabricated polysilicon microneedles for minimally invasive biomedical devices. *Biomedical Microdevices*, 24, pp.295–303. Available at: <http://link.springer.com/article/10.1023/A:1009907306184>.
- Zhu, D.D. et al., 2016. Acta Biomaterialia Rapidly separating microneedles for

transdermal drug delivery. *Acta Biomaterialia*, 41, pp.312–319. Available at:
<http://dx.doi.org/10.1016/j.actbio.2016.06.005>.

